ROBUSTNESS
OF MOMENT STEEL FRAMES
UNDER COLUMN LOSS SCENARIOS

Teză destinată obţinerii
titlului ştiinţific de doctor inginer
la
Universitatea Politehnica Timişoara
în domeniul Inginerie Civilă
de către

Ioan Mircea Mărginean

Conducător ştiinţific: Acad.prof.univ.dr.ing. Dan Dubină
Referenţi ştiinţifici: prof.univ.dr.ing. Jean-Pierre Jaspart
                           prof.univ.dr.ing. Radu Văcăreanu
                           prof.univ.dr.ing. Florea Dinu

Ziua susţinerii tezei: 10 martie 2017

Seriile Teze de doctorat ale UPT sunt:

1. Automatică
2. Chimie
3. Energetică
4. Ingineria Chimică
5. Inginerie Civilă
6. Inginerie Electrică
7. Inginerie Electronică şi Telecomunicaţii
8. Inginerie Industrială

9. Inginerie Mecanică
10. Ştiinţa Calculatoarelor
11. Ştiinţa şi Ingineria Materialelor
12. Ingineria sistemelor
13. Inginerie energetică
14. Calculatoare şi tehnologia informaţiei
15. Ingineria materialelor
16. Inginerie şi Management

Universitatea Politehnica Timişoara a iniţiat seriile de mai sus în scopul diseminării expertizei, cunoştinţelor şi rezultatelor cercetărilor întreprinse în cadrul Şcolii doctorale a universităţii. Seriile conţin, potrivit H.B.Ex.S Nr. 14 / 14.07.2006, tezele de doctorat susţinute în universitate începând cu 1 octombrie 2006.

Acknowledgement

Mărginean, Ioan-Mircea

Robustness of moment steel frames under column loss scenarios

(Studiul robusteții structurilor în cadre metalice prin aplicarea scenariilor de cedare a stâlpilor)

Abstract:
To save lives and reduce economic losses, multi-story buildings, like other components of the built infrastructure, should be designed and constructed to withstand extreme natural or human-made hazards without collapse. In order to achieve this essential requirement, the structural systems should be able to absorb the local damage that may be caused by the abnormal event and prevent of collapse. Steel frames are widely used for multi-storey buildings, offering the strength, stiffness, and ductility that are required to resist the effects of the gravity, wind, or seismic loads. Considered to produce robust structures, seismic design philosophy has been seen as appropriate for controlling the collapse of structures subjected to other types of extreme hazards, too. However, there are specific issues that should be considered to forestall the localized failures, particularly of columns. The thesis focuses on the evaluation of the structural response of steel frame buildings following extreme actions that are prone to induce local damages in members or their connections. Extensive experimental and numerical studies were used to identify the critical points and to find the structural issues that are required to contain the damage and to prevent the collapse propagation. Four types of beam-to-column joints, which cover most of the joints used in current practice, have been investigated experimentally, and the data was used to validate advanced numerical models. The findings indicated that catenary action substantially improves the capacity of moment resisting frames to resist column loss, but increases the vulnerability of the connection due to high level of axial force. The results showed that bolted connections could fail without allowing for redistribution of loads if not designed for these special loading conditions. Composite action of the slab increases stiffness, yield capacity, and ultimate force but decreases ductility. Parametric studies were performed to improve the ultimate capacity of joints and implicitly the global performance of steel frame building structures in the event of accidental loss of a column, without affecting the seismic performance and design concepts. Based on validated numerical models, an analysis procedure was developed for evaluating the performance of full-scale structures to different column loss scenarios considering dynamic effects and realistic loading patterns. Moreover, a design procedure was proposed for verification of the capacity of beam-to-column connections to resist progressive collapse, including design recommendations for each connection configuration.

Table of contents

List of figures

List of tables

Notations, abbreviations & acronyms

Notations

Chapter 2

Z   scaled distance

Chapter 3

$\dot{\varepsilon}$	strain rate
Ω	overload factor
$\dot{\varepsilon}_0$	strain rate of 10^{-4} s^{-1}
Ω_D	dynamic overload factor
Ω_S	static overload factor
ε_y	yield strain
a_g	peak ground acceleration
A_{gt}	total elongation at maximum stress
C	pseudo-static loading test protocol
CS	strain rate loading test protocol
d_{all}	allowable interstory drift
D_{beam}	beam section height (depth)
D_{column}	column section height (depth)
d_{max}	maximum interstory drift
D_y	yield displacement
e_1	major strain
e_2	minor strain
e_{xy}	shear strain
f_u	ultimate strength
f_{usr}	ultimate strength at strain rate
F_y	yield force
f_y	yield strength
f_{ysr}	yield strength at strain rate
h_{storey}	storey height
I_y	section moment of inertia
M_{max}	maximum bending moment
M_{pl}	bending moment plastic resistance
N_M	expected axial capacity reduced due to bending
$N_M{}^a$	axial capacity reduced due to bending moment
N_{max}	maximum axial force
N_{pl}	axial plastic resistance
q	dynamic behavior factor
T_c	corner period
W_{el}	elastic section modulus
W-V	single bevel but-weld T-stub
W-Y	double bevel but-weld T-stub
W-Δ	fillet weld T-stub
γ	reduction factor for seismic return interval

Chapter 4

ε	strain
ε_{11}	strain on the direction of the beam axis
ε_{true}	true strain
ε_y	yield strain
A	elastic modulus
a_g	peak ground acceleration
A_{gt}	total elongation at maximum stress
B_p	cover plate width
D_{pl}	displacement at which plastic hinge develops
e_1	major strain
e_2	minor strain
e_{xy}	shear strain
f_{ck}	characteristic concrete compressive strength
f_u	ultimate strength
f_{usr}	ultimate strength at strain rate
f_y	yield strength
f_{ysr}	yield strength at strain rate
f_{ysr}	yield strength at strain rate
G	shear modulus
H_h	haunch height
L_p	cover plate length
M_{max}	maximum bending moment
M_{pl}	bending moment plastic resistance
N_{pl}	axial plastic resistance
T_c	corner period
Tp	cover plate thickness
tw	
W-V	single bevel but-weld T-stub
W-Y	double bevel but-weld T-stub
W-Δ	fillet weld T-stub
λ	overload factor
σ	stress
σ_{true}	true stress

Chapter 5

A_{wpl}	area of the cover plate
D	local danmmge
F_{beam}	force in the beam
F_{beam}	force in the beam
F_{con}	force in the connection
F_{con}	force in the connection
$F_{ed,T-stub}$	designedresistance of the T-stub
$F_{rd,T-sub}$	designed force for the T-stub
f_u	ultimate strength
$f_{u,beam}$	ultimate strength of the beam
f_y	yield strength
$f_{y,beam}$	yield strength of the beam
H_i	hazard
M	bending moment
N	axial force
$N_{ed,wp}$	cover plate designed axial force
$N_{rd,wpl}$	cover plate designed axial resistance
PC	progressive collapse
γ_{ov}	overstrength factor

Abbreviations & Acronyms

AEM	Applied Element Method
AISC	American Institute of Steel Construction
ASCE	American Society of Civil Engineers
AVE	Advanced Video Extensometer
CEMSIG	Research Center for Mechanics of Materials and Structural Safety
CMMC	Department of Steel Structures and Structural Mechanics
CODEC	Structural conception and collapse control performance based design of multistory structures under accidental actions
CWP	Welded cover plate
DIC	Digital Image Correlation
DL	dead load
DoD	Department of Defense
ECCS	European Convention for Constructional Steelwork
ELS	Extreme Loading for Structures
EP	Extended end-plate
EPH	Extended end-plate with haunch
FEM	Finite Element Method
FEMA	Federal Emergency Management Agency
FREMEBLAST	Experimental validation of the response of a full scale frame building subjected to blast load
FS	Full strength
GSA	General Service Administration
HSZ	high seismic zone
INSEMEX	National Institute for Research and Development in Mine Safety and Protection to Explosion INSEMEX Petroșani
LL	live load
LLOP	Low level of protection
LSZ	low seismic zone
MSZ	medium seismic zone
NIST	National Institute of Standard and Technology,
PEEQ	equivalent plastic strain
PL	Point Load
PS	Partial strength
RBS	Reduced beam section
UDL	Uniform distributed load
UEFUSCDI	Executive Agency for Higher Education, Research, Development and Innovation Funding
UFC	United Facilities Criteria
UPT	Politehnica University of Timisoara
URBAN-INCERC	National Institute for Research and Development in Construction, Urban Planning and Sustainable Spatial Development
UTCN	Technical University of Cluj-Napoca
TNT	Trinitrotoluene
VIC	Video Image Correlation

REZUMAT

Clădirile, ca de altfel si celelalte tipuri de construcții, trebuie proiectate și construite astfel încât să reziste tuturor încărcărilor care ar putea să acționeze asupra lor pe parcursul duratei lor de viață. In plus, in cazul producerii unor acțiuni extreme, cum ar fi explozii sau impact, integritatea lor structurală trebuie păstrată prin evitarea sau limitarea avariilor.

Pentru a asigura integritatea structurală, trebuie îndeplinițe cerințe specifice în funcție de tipul sistemului structural și de clasa de importanță. În cazul clădirilor în cadre, o astfel de cerință prevede ca structura să rămână stabilă și avariile locale să nu depășească limitele acceptabile in cazul eliminării complete a oricăruia dintre stâlpi (sau a oricărei grinzi care susține un stâlp). Îndeplinirea acestei cerințe poate fi făcută prin diferite mijloace, însă o combinație între capacitate, ductilitate și continuitate la nivelul sistemului structural este probabil capabila să ofere un nivel ridicat de protecție și siguranță împotriva evenimentelor extreme.

Cadrele metalice sunt folosite pe scară largă la realizarea clădirilor multietajate, asigurând rezistența, rigiditatea și ductilitatea necesară să reziste efectelor încărcărilor gravitaționale, a celor seismice sau a celor din vânt. Considerate eficiente in asigurarea unei robusteți ridicate, conceptele folosite in proiectarea antiseismică sunt considerate un model pentru controlul mecanismului de cedare in cazul producerii unor acțiuni extreme, altele decât de cele asociate mișcărilor seismice. Cu toate acestea, pot sa apară anumite probleme specifice care trebuie luate în considerare pentru a limita extinderea cedările locale in cazul cedării stâlpilor.

Teza se axează pe evaluarea răspunsului structural al clădirilor in cadre metalice necontravântuite în urma unor acțiuni extreme care pot produce deteriorări locale în elemente sau in îmbinările acestora. Studiile experimentale si numerice desfășurate au permis dezvoltarea unor noi strategii pentru a identifica punctele slabe și pentru a obține robustețe structurală ridicata, capabila sa limiteze pagubele și sa prevină propagarea colapsului. Patru tipuri de îmbinări grindă-stâlp au fost investigate experimental, acoperind in mare parte tipologiile de îmbinări folosite in mod curent in practica, iar rezultatele experimentale au fost utilizate pentru validarea unor modele numerice avansate. Rezultatele au arătat că acțiunea catenara îmbunătățește în mod substanțial capacitatea cadrelor necontravântuite de a rezista in urma cedării unui stâlp, însă mărește vulnerabilitatea îmbinării din cauza creșterii nivelului forței axiale. Rezultatele au arătat de asemenea ca îmbinările cu placa de capăt si șuruburi pot ceda prematur, fără a permite redistribuirea încărcărilor aferente dacă acestea nu sunt proiectate pentru aceste condiții specifice de utilizare. Influența planșeului (acțiunea compusa) crește rigiditatea și capacitatea ultimă, dar reduce ductilitatea structurii.

Au fost efectuate si studii parametrice pentru a îmbunătăți capacitatea ultimă a îmbinărilor și, implicit, a performanței globale a structurilor în cadre metalice în cazul pierderii unei stâlp, fără a afecta comportarea și principiile antiseismice. Pe baza modelelor numerice validate, a fost elaborată o metoda de analiză pentru evaluarea performanței structurilor la diferite scenarii de cedare a stâlpilor, luând în considerare efectele dinamice și modul real de încărcare. Totodată, a fost propusă o procedură de calcul pentru proiectarea îmbinărilor grindă-stâlp la colaps progresiv, incluzând recomandări de proiectare pentru fiecare tip de îmbinare în parte.

SUMMARY

Buildings, like other components of the built infrastructure, should be designed and constructed to resist all actions that may occur during the service life. When the actions are caused by extreme hazards, such as explosion or impact, the structural integrity should be also maintained by avoiding or limiting the damage. Depending upon the type of structural system and class of importance, specific requirements should be met to ensure the structural integrity is assured. In the case of framed buildings, one such requirement is that after the notional removal of each supporting column (and each beam supporting a column), the building remains stable and any local damage does not exceed a certain acceptable limit. This requirement can be achieved by several means, but a combination of strength, ductility and continuity of structural system is likely to provide a high level of protection and safety against extreme hazards.

Steel frames are widely used for multi-storey buildings, offering the strength, stiffness, and ductility that are required to resist the effects of the gravity, wind, or seismic loads. Considered to produce robust structures, seismic design philosophy has been seen as appropriate for controlling the collapse of structures subjected to other types of extreme hazards, too. However, there are specific issues that should be considered to forestall the localized failures, particularly of columns.

The thesis focuses on the evaluation of the structural response of steel frame buildings following extreme actions that are prone to induce local damages in members or their connections. Extensive experimental and numerical studies were used to identify the critical points and to find the structural issues that are required to contain the damage and to prevent the collapse propagation. Four types of beam-to-column joints, which cover most of the joints used in current practice, have been investigated experimentally, and the data was used to validate advanced numerical models. The findings indicated that catenary action substantially improves the capacity of moment resisting frames to resist column loss, but increases the vulnerability of the connection due to high level of axial force. The results showed that bolted connections could fail without allowing for redistribution of loads if not designed for these special loading conditions. Composite action of the slab increases stiffness, yield capacity, and ultimate force but decreases ductility.

Parametric studies were performed to improve the ultimate capacity of joints and implicitly the global performance of steel frame building structures in the event of accidental loss of a column, without affecting the seismic performance and design concepts. Based on validated numerical models, an analysis procedure was developed for evaluating the performance of full-scale structures to different column loss scenarios considering dynamic effects and realistic loading patterns. Moreover, a design procedure was proposed for verification of the capacity of beam-to-column connections to resist progressive collapse, including design recommendations for each connection configuration.

1 INTRODUCTION

1.1 Motivation

Multi-storey steel frame buildings are subjected during their service life to various types of actions arising from operation conditions. The design shall therefore provide an adequate structural resistance and durability to the structure to sustain these actions. Due to the uncertainties in occupancy or environmental loads but also due to other unforeseen hazards not explicitly considered in the design (accidental actions, e.g. fire, blast, gas explosion, or impact), the structure can be at risk of local damage. In turn, the local damage can lead to a spread of failure to neighboring elements and, in the end, to the collapse of disproportionately large part of the structure (or a complete collapse), known as progressive collapse. Structural robustness is the capacity of the structure to survive local damages caused by unforseen events (exceptional loading and indeterminate frequency) preventing dammage propagation.

The concern of the professional community on the progressive collapse caused by a local damage started in 1968 with the collapse of the Ronan Point apartment building in the United Kingdom, due to a gas explosion. The event led to the development of the first studies regarding the progressive collapse and means to avoid it and to the introduction of first requirements in codes and standards. Many other similar events, involving the progressive collapse of multi-storey buildings, produced in the next decades worldwide, a history that culminated in the total collapse of World Trade Center Tower in 2001, following a terrorist attack (see Figure 1.1).
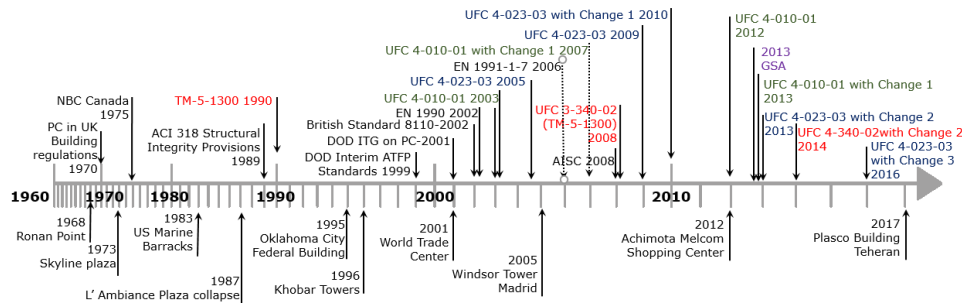
Figure 1.1 Timeline of progressive collapse events and development of design provisions (adapted from[1] and [2])

After more than four decades, the knowledge and practice are still limited, and therefore particular attention should be paid if comprehensive design guidelines are to be developed and issued in the future. In parallel with an increased frequency and intensity of natural hazards, terrorist bombing has emerged at the global scale (the globalization of terrorist actions, the increased scale of regional conflicts with high fatalities and destruction in populated regions). Such threats can have a severe impact on the integrity of buildings and therefore require structures to be designed to withstand such effects with minimum losses.

Local strengthening of members and connections can enhance the global response and reduce the vulnerability to progressive collapse (which pose the main risk to occupants) - the ability of a structure to withstand extreme events without being damaged to an extent disproportionate to the original cause is called *structural robustness* (EN 1991-1-7 [3]). A robust structure is characterized by high redundancy, which can be achieved by proper design (conception and detailing, a good balance between stiffness, overstrength and ductility of its components). Such a design should provide multiple routes for force transfer, secure plastic capacity in structural members and sufficient strength for structural members to prevent collapse. Therefore, redundancy may be defined as the property of structure to ensure safe alternate load transfer paths in case of a localized failure [4]. Structural robustness, including redundancy and prompt recovery, is essential, for ensuring structural resilience. Structural robustness also enhances structural reliability (structural safety), represented by very low probability levels for failure to occur or for exceeding specific criteria [5].

These principles are already implemented in modern seismic design, such that in case of severe earthquakes, ductile components in the dissipate zones undergo plastic deformation, while overstrengthened components designed to remain predominantly elastic. Structural collapse of dissipative structures is prevented due to the capacity to transfer stresses in the adjacent zones.

Seismic designed structural systems are certified to possess ductility, stress redistribution capacity and energy absorbing properties in case of oligocyclic bending moment loading state associated to seismic activity, but their performance is not validated for axial force-bending moment interaction corresponding to large vertical displacements of columns, as catenary action can develop in case of column loss deformation state. Beam-to column connections can be particularly vulnerable for these internal forces interactions, with their vulnerability transferring to the structure itself.

In this context, the thesis' aims are to investigate the response of multi-storey steel frame buildings in case of extreme loading events and to test and validate new or improved beam-to-column connection typologies to resist progressive collapse. Due to the complexity of the behavior, the local and global response was first investigated using experimental tests on connection macro-components and assemblies. The experimental data were used to validate complex numerical models and to perform extensive numerical parametric simulations. Finally, recommendations for detailing beam-to-column connections to provide resistance to column loss scenarios were provided.

Figure 1.2 Main of research activities of the thesis

1.2   Objectives

Multistorey steel frame structures may be subjected during their lifetime to unforeseen loads types or intensities, capable of significant local damage. The capacity of the structural system to redistribute the load is essential for protecting human life and minimizing economic losses due to progressive collapse. The redistribution capacity within structural members is limited also by the capacity of the connections to transfer the loads developed in such conditions.

The main purpose of the thesis is to evaluate the performance of seismic designed beam-to-column connections in mitigating progressive collapse caused by exceptional loading.

A major thesis objective is to obtain consistent experimental results from an integrated experimental framework with relevant experimental specimens and test set-up. The design of realistic boundary conditions is essential for the development of internal forces interaction (bending moment and overlapped axial force due to catenary action). Instrumentation and design of experimental tests must provide insight on the performance of seismic designed beam-to-column connections subjected to column loss and provide sufficient data to allow model calibration.

The second major objective of the thesis is to develop and calibrate numerical models capable of replicating the complex behavior of steel frame structures under column removal. The use of modeling tools has to be optimized to allow the performance assessment on full-scale structures subjected to accidental action within a reasonable computational effort.

Experimental and numerical investigation must be performed to reach specific objectives of the thesis, as assessment of the importance of some issues in the structural robustness of steel frame structures:
- strain rate effect
- loading distribution influence
- and composite effect
- dynamic increase factors

The third major objective of the thesis is the development design approaches and procedures suitable for assessing and improve seismic steel beam-to-column

connections for ensuring adequate performance when subjected to exceptional loading causing the loss of a structural member. Design optimizations or verifications for specific configurations of steel beam-to-column connections should be recommended in order to improve the structural robustness by enhancing the connection robustness.

1.3   Thesis outline

Chapter 2 presents a state of art of existing studies in the field of progressive collapse of steel frames and introduces the main gaps and needs for the development of the knowledge. An overview of existing design codes is given. Experimental testing methods on connection components, 2D and 3D assemblies and full scale structures are presented.

Chapter 3 provides detailed information about the experimental program. Based on conventional design rules and requirements and without taking into account the special conditions associated with the accidental design situations, several steel frame building structures were designed for low and high seismicity conditions, considering various lateral resisting systems. One structure was selected for detailed experimental investigations, i.e. tests on full-scale joints, connection macro-components, and weld details, as well as full-scale frame assemblies. The structure selected for detailed investigations was tested preliminarily for several column loss scenarios within a full-scale simulation using Applied Element Method (AEM) [9]. The numerical model was calibrated using experimental data available in the literature. Four types of connections were designed and detailed for the experimental program on joints, i.e. bolted and welded joints, respectively. From these joints, connection macro-components and weld details were tested using different loading rates and temperature conditions. Static push-down tests were performed to evaluate the full response of 3D frame structures in case of an internal accidental column removal, starting with first yielding, plastic mechanism, and failure mode.

Chapter 4 presents the numerical simulations program. Experimental data obtained in Chapter 3 were used for validating the numerical models. For weld details and connection macro-components, finite element models were constructed and validated to determine the response. Finite element analyses were performed for optimizing the response and improve the ultimate capacity. For joints and 3D assemblies, both finite element models and applied element models were constructed and validated. Several case study buildings were used in the numerical program to get insights into the response of multi-storey steel frames in the event of column loss and to develop strategies to mitigate the progressive collapse.

Chapter 5 provides a methodology and recommendations for designing steel frame buildings with improved robustness and resistance against progressive collapse, and in general for cases when accidental actions can lead to severe local damage (partial or complete loss of some members). The recommendations address mainly the design and detailing of beam-to-column joints, but also the selection of structural analysis techniques (static, dynamic), and of structural systems, and load pattern consideration when progressive collapse resistance is addressed.

Chapter 6 presents the results and main contributions and maps the direction for future research works. The extensive experimental program, coupled with advanced numerical simulations allowed the development of beam-to-column connections with improved robustness for extreme loading conditions. The application of refined nonlinear models to case study buildings demonstrated the efficiency of the solutions compared to existing knowledge and practice.

References contain thesis, journal and conference papers, research and other reports, and standards that contain information presented in the thesis. Other technical information sources, computer program software and grant details are also presented here.

Annexes give specific definitions. detailed information and results regarding the experimental and numerical program.

2 SELECTED AND CRITICAL REVIEW OF EXISTING RESEARCH AND SCIENTIFIC PAPERS

2.1 Introduction

To prevent progressive collapse, structures should be designed and constructed to be robust. According to EN 1990 (2002) [8] requirements, the robustness can be ensured by one of the following measures:
- Avoiding, eliminating or reducing the hazards to which the structure can be subjected;
- Selecting a structural form which has low sensitivity to the hazards considered;
- Selecting a structural form and design that can survive adequately the accidental removal of an individual member or a limited part of the structure, or the occurrence of acceptable localized damage;
- Avoiding as far as possible structural systems that can collapse without warning;
- Tying the structural members together.

All these requirements aim at providing the structure with enough capacity to survive (avoid progressive collapse) the effects of any type of loading condition the structure was designed for and beyond. The main problems arise from the difficulties in verifying the efficacy of the measures listed above with a reasonable degree of confidence.

Considering the different features of possible actions on buildings, it is reasonable to expect that the design of a building structure to withstand a specific load may be ineffective for other loads. However, some design conditions, for example, the design philosophy employed in seismic design codes, produce more robust structures by virtue of the explicit consideration of the strength ratio between members, failure mechanism, redistribution capacity, and ductility requirements. This assumption is supported by the FEMA 277 report (1996) [9], which concluded that, if the Murrah Building (see Oklahoma City Bombing, 1995) had been designed to resist seismic action, its progressive collapse would have been precluded. Thus, to achieve a design that is both safe and economical, it is necessary to determine the structural features that may produce an adequate response in the event of extreme loading [10]. This may be done by using the alternate path (AP) method to ascertain the capacity of a structure to resist the loss of one or more critical load-bearing elements without causing disproportionate collapse (DoD)[11]. The AP method, with its emphasis on continuity and ductility, is similar to current seismic resistant design practice (NISTIR) [12]. However, although the seismic design philosophy may be considered as a model for controlling the collapse of structures subjected to extreme events other than earthquakes [4], there are specific issues that should be considered to forestall localized failures, particularly of columns. For example, the development of catenary forces in the girders and floor slab and the admissibility criteria should be considered in the design of beam-to-column connections, taking into account the interaction between bending and axial loads.

2.2   Design Guidelines

2.2.1   *Europe*

2.2.1.1 UK

Following the collapse of an entire corner of the Ronan Point building, in 1968, London, UK, due to a gas explosion (see Figure 2.1), first studies about progressive collapse were initiated. UK research efforts commenced shortly after the Ronan Point collapse, and first standards have been approved in 1970. Other provisions entered the British Standards in 1974. In 1976, the design provisions have been released in a new edition (Statutory Instrument, HMSO, 1976 [13]). The efficacy of the provisions was confirmed by the performance of structures subjected to accidental actions, including explosion, impact, etc. since the introduction of the disproportionate collapse rules, in 1976. One example is Exchequer Court, St Mary's Axe, London, a modern construction at that time that consisted of a steel frame, concrete floors acting compositely and designed to resist lateral wind loads by a system of braced steel bays. In April 1992, a bomb exploded in the vicinity of the building. The explosion caused damage to a number of buildings. Although the building suffered considerable damage to both its non-structural and structural members, the building remained intact (Figure 2.2). Furthermore, the type of explosion at St. Mary's Axe was of an entirely different nature to the internal gas explosions which were the principal cause for the disproportionate collapse rules given in the Building Regulations and the material Codes ([14]). The continuous research efforts led to the upgrading of the design provisions, and the new version of the Guidelines has been released in 1992 (Approved Documents A, 1992 [15]), followed by 2004 and 2010 editions. The requirements of these standards are considered to produce more robust structures which are more resistant to disproportionate failure due to various causes, such as impact as well as to gas explosions ([14]). The most recent version of the Approved Documents, released in 2010, has fourteen technical "Parts" and refers, among other to structural safety (progressive collapse) and fire safety.

Figure 2.1 Ronan Point Collapse, 1968, London, UK [16]

a) damage to composite floors   b) ground floor steel columns
Figure 2.2 Exchequer Court bombing, St Mary's Axe, London 1992 [14]

Apart from the UK, early studies about progressive collapse have also been performed by Granstrom in Sweden (1970) [17] and Hanson and Olesen in Denmark (1969) [18], but also in Germany, Netherlands, and France. The cooperative effort across Europe and the provisions from various national standards led to the development of the Eurocodes.

2.2.1.2 Eurocodes

In Europe, EN 1991-1-7 [3], in the Annex A "Design for consequences of localized failure in buildings from an unspecified cause", specifies that a structure should be designed such that it would not be damaged by events such as fire, explosions, impact, or the consequences of human errors to an extent disproportionate to the original cause. The recommended strategies depend on the consequence classes, i.e. low, medium and high Consequences Classes. For buildings in Consequences Class 1, provided the building is designed and constructed in accordance with EN1992 to EN1999 standards (considering therefore that stability in normal use is satisfied), no further consideration is necessary with regard to accidental actions from unidentified causes while for buildings in Consequences Class 2L (Lower Risk Group), the use of a system of ties is considered sufficient to provide the required structural integrity. For buildings that are categorized as Consequences Class 2U (Upper-Risk Group) buildings, the use of a system of ties is still required but, additionally, the design should check that the structure can resist the notional removal of a column. For Consequences Class 3 (important buildings, buildings with large area or number of storeys), a systematic risk assessment of the building should be undertaken. However, for the detailed progressive collapse assessments (Class 2U and class 3 buildings), the design procedures are very prescriptive and therefore, difficult to apply. Also, they do not deal with specific design cases such as for different types of constructions or external explosions. As a result, significant contributions to the development of comprehensive robustness design guidelines are still necessary.

2.2.2   U.S. approach

The first studies about progressive collapse were initiated in the 1970s, following the collapse of Ronan Point building, and focused on the vulnerability of precast concrete structures in case of internal gas explosions. First requirements for general structural integrity to provide resistance to progressive collapse have been incorporated in 1972 (ANSI A58.1 [19]). The studies have been revived by terrorist attacks that affected US facilities (on US soil or worldwide): Beirut barracks bombings, 1983; US embassy bombing, Nairobi, 1998; WTC, 1993; Murah Building, Oklahoma,

1995; WTC & Pentagon, 2001, etc. As a result, several federal agencies developed their own design requirements for mitigation the risk associated with the progressive collapse under extreme load events. The most important design requirements have been developed by General Services Administration (GSA) and the Department of Defense (DOD UFC). GSA Progressive Collapse Guidelines are used by the US General Services Administration for the design of new federal buildings and for evaluation of existing buildings. The main method is based on the assessment of the structural integrity after some primary members are lost, also called "alternate load path" method. The UFC applies for buildings belonging to Department of Defense but can also be used by other federal agencies as well as organizations with role in creating or implementing design codes for constructions. UFC applies to new and existing buildings. Other documents, e.g. TM 5-1300 (1990) [20], were specifically developed to be used for direct evaluation of blast and explosion effects on buildings or other structures.

2.2.2.1 TM 5-1300: Structures to Resist the Effects of Accidental Explosions

A widely used technical manual for not only for military but also for civilian applications, TM 5-1300 [20] manual, has been developed by U.S. Departments of the Army, Navy, and Air Force, in 1990. The manual contains analysis and design procedures, with detailed information specific for the blast and explosions, as actions definition (blast, fragment, and shock-loading), dynamic analysis principles, design of reinforced and structural steel structures, and special design considerations (e.g. information on tolerances and fragility, shock isolation). For example, Figure 2.3 plots the positive phase pressures, impulses, durations, and other parameters of the shock wave caused by a spherical TNT explosion, versus the scaled distance, Z.
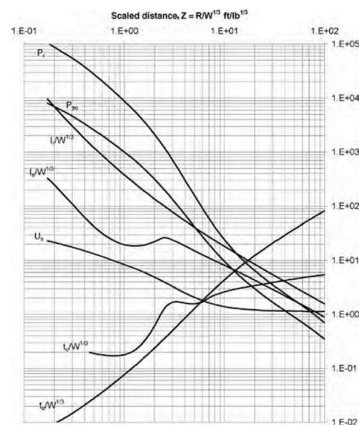
Figure 2.3 Positive phase shock wave parameters for a spherical TNT explosion in free air at sea level, [20]

2.2.2.2 UFC 3-340-02: Unified Facilities Criteria (UFC). Structures to resist the effects of accidental explosions [21]

This document, which superseded the TM 5-1300 Manual [20], presents methods of design for protective construction used in facilities for, among others, development, testing, storage, maintenance, and disposal of explosive materials. It establishes design procedures and construction techniques whereby propagation of

explosion or mass detonation can be prevented, and protect personnel and valuable equipment.

2.2.2.3 UFC 4-023-03: Unified Facilities Criteria (UFC). Design of buildings to resist progressive collapse

This document, which was first released in 2005 [22], provided the design requirements that are necessary to reduce the potential of progressive collapse for new and existing constructions that experience localized structural damage due to unforeseen events. Four levels of protection, equivalent to classes of consequences from EN 1993-1-7[3], were used to categorize the buildings, i.e. very low level of protection (VLLOP), low level of protection (LLOP), medium level of protection (MLOP), and high level of protection (HLOP). UFC 4-023-03 also adopted two approaches for verifying the progressive collapse design requirements, i.e. tie forces and alternate load path (AP) method. Tie forces (Figure 2.4) are typically provided by the existing structural elements and connections that are designed using conventional design procedures to carry the standard loads imposed upon the structure ([23]). When the vertical ties are not capable of resisting the required strength or the structure requires MLOP or HLOP, then the AP method must be applied considering the notional removal of vertical load-bearing elements (i.e. columns in case of frame structures). When AP method is used, there are three allowable analysis procedures, i.e. Linear Static, Nonlinear Static, and Nonlinear Dynamic.

Following some significant developments in the knowledge, the document suffered important updates in 2009[11] (with further changes in 2010 [24], 2013 [25], and lastly in 2016 [26]). The main important changes refer to:
- Replacement of levels of protection with Risk categories (I, II, III and IV);
- Revision of the Tie Force method;
- Inclusion of Load Increase Factors for Linear Static models and Dynamic Increase Factors for Nonlinear Static models;
- Adoption of modeling parameters and acceptance criteria from ASCE 41 [27] Seismic Rehabilitation of Existing Buildings.

Concerning the last change adopted in 2009 [11] edition, i.e. the data adopted for modeling and the acceptance criteria based on seismic conditions, it should be noted that these requirements are based on cyclic performance. It is questionable if the limits that are set for seismic conditions (ASCE 41 [27]), where the catenary action is not considered, should be also adopted for column loss scenarios, where catenary action can increase the capacity to resist the applied load. More important, the limits that are set for seismic conditions assume cyclic performance, while column loss event assumes monotonic performance. The difference between the two is about half, based on many experimental tests [28].
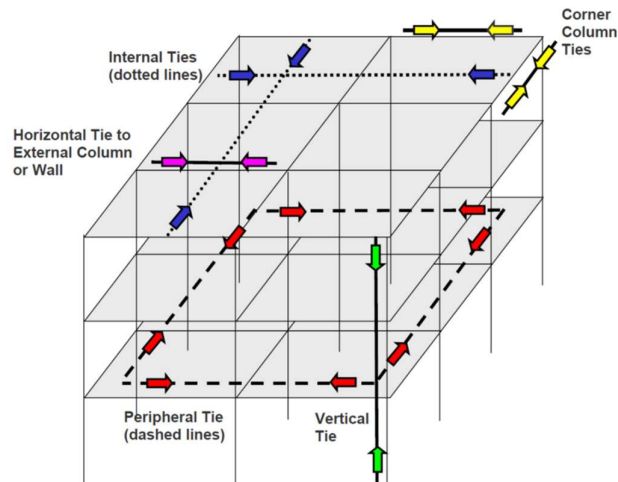
Figure 2.4 Different types of ties incorporated to provide structural integrity, [22]

2.2.2.4 GSA General Services Administration Guidelines

First GSA document, "Progressive Collapse Analysis and Design Guidelines for New Federal Office Buildings and Major Modernization Projects" [29], was published in 2000 and revised in 2013 [30]. The guidelines, based on the alternate load path (AP) method and removal of vertical load carrying members, were adopted by the US General Services Administration for the design of new federal buildings and for evaluation of existing buildings. The application of the guidelines was function of the level of protection or function of the number of stories (4 stories or greater), with some buildings exempted base on several factors (e.g. type of use, type of the facility, or structural features such as seismic design). While in the 2000 edition only linear elastic static and non-linear dynamic analyses were used to check the structural members in the alternate path structure, in the 2003 edition also inelastic static method was incorporated, using an amplification factor to allow for the dynamic effects associated with the loss of a column.

In 2013, new Guidelines were released to replace the 2003 document. The new document, entitled "General Services Administration. Alternate Path Analysis and Design Guidelines for Progressive Collapse Resistance" [30], provides a new, threat-dependent methodology for minimizing the potential for progressive collapse that utilizes the alternate path (AP) analysis procedures of UFC 4-023-03, Design of Buildings to Resist Progressive Collapse [25] and ASCE-41 Seismic Rehabilitation of Existing Buildings [27]. The design procedures employed by 2013 Guidelines aim to reduce the potential for progressive collapse by bridging over the loss of a structural element, limiting the extent of damage to a localized area (Alternate Path) and providing a redundant and balanced structural system along the height of the building. It also focuses on mitigating progressive collapse due to man-made explosive threats only. This is reflected by limiting column removal scenarios to the ground level and high-risk public areas, where structural elements are most vulnerable to explosive effects due to their proximity to potential vehicle and package threats.

2.3   Literature review

A review of research on the progressive collapse of steel and composite frame buildings has been performed, focusing on three main directions, i.e. experimental testing, numerical simulations, and analytical developments. The experimental research developed worldwide followed several directions, ranging from small scale connection components (bolted T-stubs, bolted angle connections, bolted web cleat connections) to large scale (full-scale) assemblies, with or without the presence of a concrete slab. However, experimental testing, especially when it involves assembly or sub-assembly testing, is expensive, difficult and time-consuming. Therefore, numerical simulations are preferred, which require much less effort and are less expensive than experimental testing. The accuracy of numerical modeling of progressive collapse depends on the constitutive models used for materials and loading condition, and, in most cases, validation against experimental (or theoretical) data is required. In fact, in many cases, studies involving experimental testing also included numerical model validation and other numerical simulations. Therefore, in the next section they will be summarised together. Analytical approaches have also been developed for evaluating the potential for progressive collapse, but they often have limitations and difficulties in practical applications.

2.3.1   Experimental and numerical studies

Several large European projects and intergovernmental frameworks aimed to improve the knowledge and design procedures for enhancing the robustness of building structures and bring important contributions to risk assessment.

RFSR-CT-2008-00036 – ROBUSTFIRE - *Robustness of car parks against localised fire* [31] (2008-2012) developed and validated numerical and analytical models of fire response of critical structural components of car parks subject to localized fire. Relevant and practical design guidance for a robustness assessment approach was developed for composite car parks under fire. RFCS N°RFSR-CT-2012-00029 – ROBUSTIMPACT - *Robust impact design of steel and composite building structures* (2012-2015) aims to ensure a better resistance against progressive collapse of steel/composite structures using guidelines and tools that consider a Residual Strength Method – a combination between residual strength and the alternate load path method [32, 33]. The aim of another project, RFCS N°RFS-CR-04046 – ROBUSTNESS - Robust structures by joint ductility (2004-2007) [34], was to define general requirements to increase the system performance of joints with large ductility, if subjected to accidental loading. Increasing the performance of High strength steel tubular structures, reducing weight of the structure and reducing operating costs of the construction were the targets of RFCS N°RFSR-CT-2008-00035 – HITUBES - Design and integrity assessment of high strength tubular structures for extreme loading conditions (2008-2011) [35].

The project RFSR-CT-2010-00030 – ADBLAST – *Advanced design methods for blast loaded steel structures* (2010-2013) [36] developed fundamental design guidance for steel structures under external blast loads including risk assessment and benchmark examples defining safety and performance requirements. RFSR-CT-2013-00020 – BASIS – Blast Actions on Structures in Steel (2013-2017) [37] aims to develop more accurate and practical fire assessment tool for class 4 Steel members with H or I shape. Advanced and simplified design approaches are proposed in- RFCS N°RFSR-CT-2004-00047 - COSIMB – Composite column and wall systems for impact

and blast resistance (2004-2007) [38] based on the experimental and analytical results.

COST C26 Action - Urban Habitat Constructions under Catastrophic Events [39] connected specialists with interests in the aftermath of catastrophic events (earthquakes, fi re, wind, impact, explosions etc.) regarding the behavior urban habitat, preventing premature collapse due to Infrequent Loading Conditions. The main objective of COST TU0601 Action – Robustness of structures [40] was to provide the main framework, methods and strategies to ensure the desired level of structural robustness demanded by the relation between function, exposure, life-safety requirements, environment and economy.

Xu & Ellingwood [41] investigated the performance of steel frames with partially restrained connections fabricated from bolted T-stubs following damage to load-bearing columns. They reported that frames with strong T-stub connections could resist collapse in damage scenarios involving notional removal of one column, while the robustness of the frames with weak T-stub connections is questionable. In a similar study, Gong [42] conducted tests on bolted double angle connections under pure tension load. The results showed that to ensure a ductile behavior as required for developing a catenary action, the capacity design philosophy should be followed in the robustness design of connections ([43]). Abidelah et al. [44] investigated the influence of the bolt bending on the behavior of the T-stubs. The numerical study showed that the presence of the bending moment in the bolt could modify the failure mode of the T-stub (failure mode 1 changes to failure mode 2). There is also a decrease in the values of the ultimate capacity of the T-stubs by almost 30% when the bending of the bolts is considered. Ribeiro et al. [45] investigated T-stub models under dynamic loading conditions to predict the response in case of accidental loading. The analytical results were compared with 3D Finite Element predictions and experimental results ([46]). Bo and Kang's [47] experimental results showed that the ultimate performance of the bolted-angle assembly is not predictable by the initial part up to the yielding. Tests focused on the influence of strain rate on T-stubs modeling a flush end-plate beam-to column bolted connection were performed at the University of Trento [48]. Results showed a potential influence of strain rate on the ultimate load in case of stiff T-stub configurations, but no significant influence on the ductility. In the experimental and numerical tests on connections under quasi-static and dynamic loading, performed by Rahbari et all [49], it was observed that the failure mode of web cleat connections is not influenced by the loading rate due to the flexibility of the connection.

Astaneh-Asl, Jones, Zhao, and Hwa [50] experimentally studied the ability of a typical steel structure to resist progressive collapse in the event of the loss of a column and attempted to establish the failure modes. Their findings suggested that a retrofit scheme in which cables are added to the side of beams could be used to develop catenary action with a higher factor of safety (see Figure 2.5). The increase in capacity achieved by this scheme was confirmed by a different test in which horizontal cables were placed in the floors and on the top flange of the girders along the exterior column line [51]). Yu, Zha, and Ye [52] used numerical simulations to study the progressive collapse of steel frames with composite slabs and proposed effective retrofitting techniques for existing building using pre-stressed steel cables.
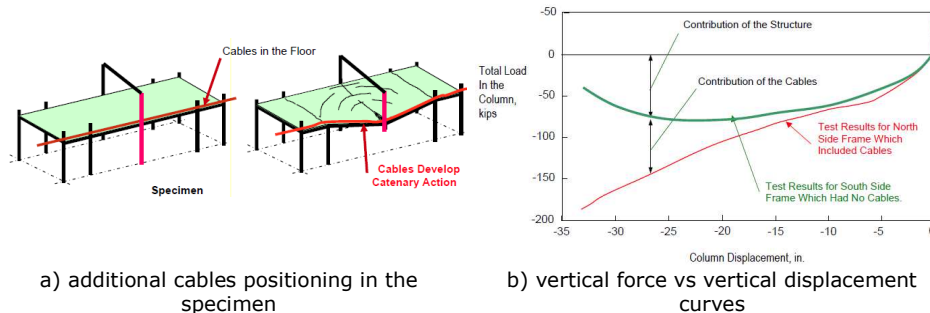
a) additional cables positioning in the specimen

b) vertical force vs vertical displacement curves

Figure 2.5 Column loss experimental results at the University of California, Berkeley [50]

The robustness of a typical concrete deck–steel beam composite floor system with simple shear connections was investigated by Sadek, El-Tawil, and Lew [53] in the event of a central column removal. Their observations suggested that a composite floor system with simple shear connections was potentially vulnerable to the loss of a central column ([10]).

Alashker, El-Tawil, and Sadek [54] investigated the progressive collapse resistance of steel-concrete composite floors in which steel beams were attached to columns through shear tabs. The simulation results showed that the greater part of the collapse resistance was provided by the steel deck and that increasing the connection strength by increasing the number of bolts might not be beneficial to increasing the overall collapse strength. Based on a modified version of the model developed by Sadek et al. , Alashker and El-Tawil [54] proposed a design-oriented model for computing the load-resisting capacity of composite steel-concrete floors subjected to an interior column loss. The model can be used to determine the effect of the main variables on collapse resistance, although there are limitations to its application in terms of the type of beam-to-column connections, failure condition, or deformation of the beams ([10, 43]).

Demonceau and Jaspart [55] experimentally tested for column loss scenario a two-dimensional (2D) composite frame (composite beams, steel columns, and partial strength composite joints). In order to observe the development of catenary action in a composite frame following column removal, a 4-span full-scale frame was experimentally tested at the Liege University. Initial uniform distributed load (UDL) was applied to the structure while having a middle column simulated by blocked jacks (Figure 2.6.a). The jacks were released until "0" force was obtained in the column simulated by the jacks. Afterward, vertical displacement was applied to the column until failure was attained. The test was a "premiere" in Europe indicating that large axial forces can develop if the frame if laterally restrained - see Figure 2.7. The system showed very high ductility reaching almost 190 mrad. The results indicated ductile behavior of the tested configuration, with significant contribution from the catenary action that developed in the beams.
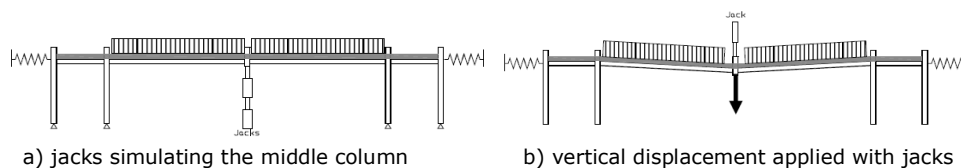
a) jacks simulating the middle column

b) vertical displacement applied with jacks

Figure 2.6 Frame specimen loading[55]

a) vertical force – vertical displacement curve   b) specimen at end of test
Figure 2.7 Experimental results on 2D composite frame [55]
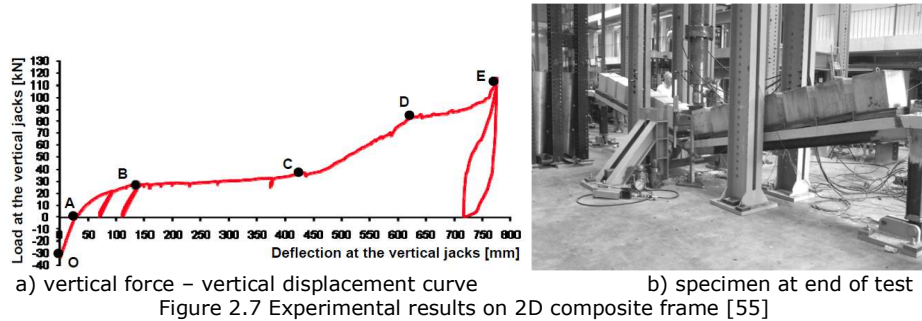
Similar steel–concrete composite frame was tested with 2 m inter-column distance and rigid beam-to-column connections by Guo et all. [56]. Results indicate that while arching effect is beneficial to the load resistance of composite frame in the early stage of column loss, at advanced vertical displacements, catenary action enhances the structural capacity, see Figure 2.8.a. Parametrization of calibrated models points out that increase of rebar ratio in slabs would not significantly improve the resistance of the structure, but increasing of depth of steel beam dramatically improves the structural behavior. Horizontal restraining stiffness has noteworthy influence in the into catenary stage, but none at all in the flexural stage.

a) vertical force – vertical displacement curve   b) specimen at the end of test
Figure 2.8 Experimental results on 2D composite frame [56]
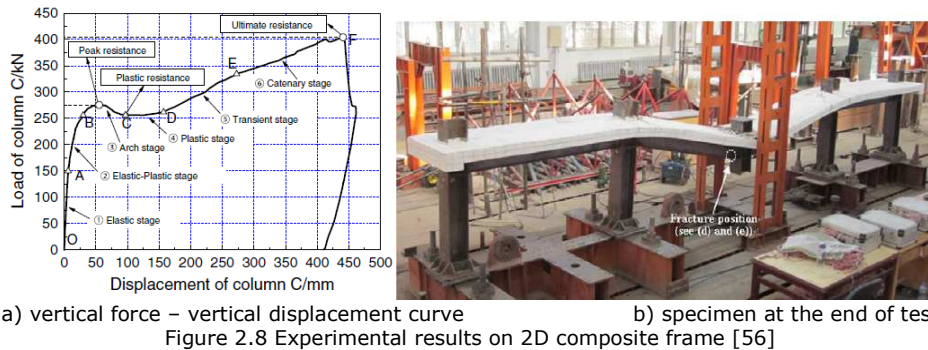
The experimental performance of a welded unreinforced flange bolted web connection and of a reduced beam section connection was investigated under middle vertical column displacement by Lew et all. [57], see Figure 2.9.a for test set-up. Flexure behavior was dominant in the early stage of the loading, succeeded by catenary action indicated by axial tension developed in the beams. The first connection failure started with top flanges local buckling of the central connections, followed by shear-tab bolt failure in shear, and finally, the bottom flange fractured near the weld. RBS connection failure occurred due to fracture of the bottom flange in the reduced section of a central connection. Failure propagated through the web (Figure 2.9.b). The ultimate capacity of the connections in both assemblies was limited to the connection resistance of combined axial and flexural stresses associated with increasing axial tension in the beams, see Figure 2.10. The experimental rotational capacities of both connections under monotonic column displacement were approximately twice as large as those based on seismic test data.

a) experimental set-up (top) and upper floor restraining(bottom) [58]

b) experimental [57] and numerical failure of RBS specimen [58]
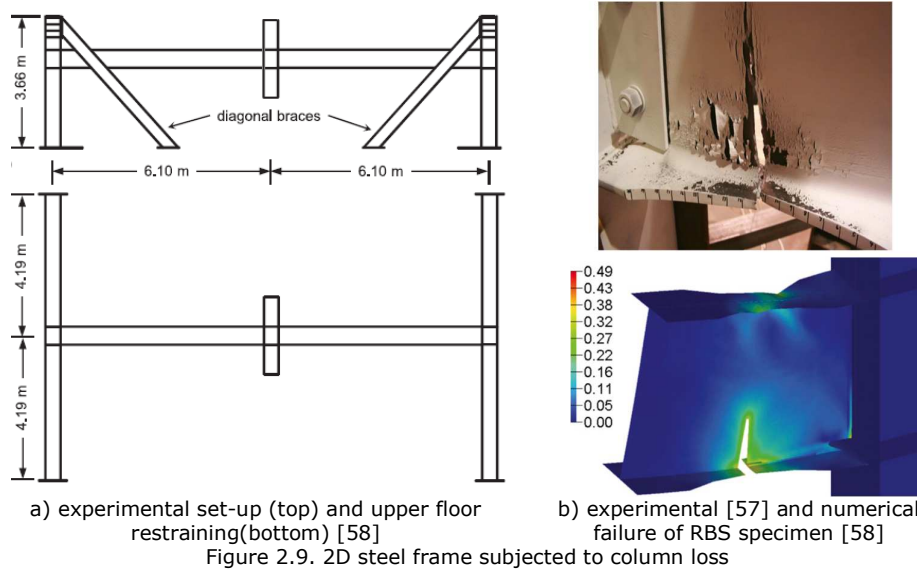
Figure 2.9. 2D steel frame subjected to column loss

The results of detailed solid models with a large number of elements were compared to reduced models with a limited number beam and spring elements obtaining similar results [58]. The simple model can be used for assessing the behavior of full-scale multi-storey structures. Also, detailed model numerical results showed that the testing set-up with diagonal braces gives very similar results (see Figure 2.10). to full-length columns also restrained at the level of the upper floor – conditions similar to restraints within the structure.

a) experimental set-up (top) and upper floor restraining(bottom) [58]

b) experimental [57] and numerical failure of RBS specimen
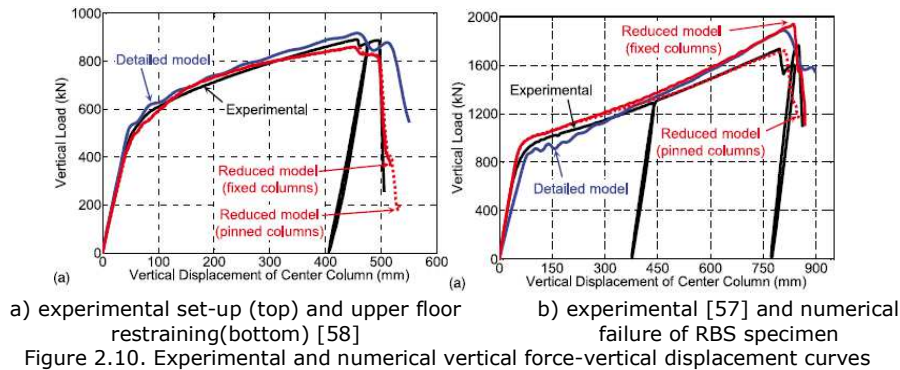
Figure 2.10. Experimental and numerical vertical force-vertical displacement curves

A series of full-scale laboratory experiment was conducted at Tongji University, Shanghai, to investigate the behavior of steel beam-to-column moment connections under column removal scenario. The specimens consist of middle column and two half beams pinned at the end which are laterally restrained, see Figure 2.11.a. Li et all. [59] tested welded and a bolted web connection steel beam-to-tubular column moment connections with an outer diaphragm. At the early stage, both specimens transferred the load to the end supports primarily by the flexural action, the end of the flexural action stage was marked by the fracture of the bottom flanges

at a chord rotation in the range of 0.08–0.1 rad. In the case of the welded web connection specimen (Specimen CO-W), the crack immediately propagated deep into the web plate, dramatically reducing the effective beam section. Though the specimen was still capable of load-bearing to some extent, the resistance capacity never recovered, and no meaningful catenary action developed (Figure 2.12.a). Failure in the bolted connection started with fracture at the bottom flange, but the presence of the bolts interrupted fracture propagation. With significant portion of active area of the section, catenary action effectively developed. The vertical resistance in the specimen recovered and exceeded the maximum bearing capacity before fracture due to large axial forces. The beam chord rotation exceeded 170 mrad.

Another experimental study [60] compared the performance of welded unreinforced flange bolted web connections with two types of bolt configurations: (1: SI-WB) all four bolts at the connection arranged in a single row across the beam web; and (2: SI-WB-2) with the bolts arranged in two rows around the middle portion of the beam web. The SI-WB specimen was able to engage the beam web into action more effectively after the bottom flange failure, allowing for a smoother transition into the centenary action phase than the case with the two-row layout of the bolts (SI-WB-2), see Figure 2.12.b. Further study of the failure modes of the bolted connections was performed with detailed finite element numerical simulations. Study of the local failure patterns indicates that further improvements may be achieved in both cases by enhancing the local connection details.

Column wall failure was examined using the same experimental set-up and RBS connection specimen [61]. Firstly, separation occurred between the inner diaphragm and the inside wall, the column wall crack and extended fully across the width of the beam's bottom flange and through the thickness. At this point, the flexural mechanism is replaced by the catenary mechanism (Figure 2.12.c). FEM results indicate that if properly welded, the beam would fail in the reduced section. The paper suggests that even though column failures are not preferred in seismic structural designs, in frame structures comprising tubular columns, under the column removal scenario, the column wall failure mode is more desirable than the beam-end or beam-section continuous failure, because of the column failure mode's ability to develop an effective catenary mechanism. Authors highlight, though, the necessity of substantial additional studies in the context of progressive collapse.

In another study, which was performed by Wang et al. [62], three tests were performed on double-span frames with circular hollow sections subjected to column removal. The types of connections used were the welded flange-weld web connection with internal diaphragms, the welded flange-bolted web connection with internal diaphragms, and the welded flange-bolted web connection with short through diaphragms. Based on the results of the study, it was concluded that, during a sudden-column-loss scenario, progressive collapse could be triggered upon the initial fracturing of the bottom beam flange; this was true for all the specimens tested

A conventional and a reinforced welded flange-bolted web connection under a central-column-removal scenario was experimentally tested by Qin et all. [63] displaying different failure modes. At a relatively small imposed vertical displacement, the beam bottom flange fractures for the typical welded flange-bolted web connection specimen (Figure 2.12.d), while for the specimen with the reinforced welded flange-bolted web connection, the beam bottom flange can continue to transfer force even after the failure of the bottom welded connection. The reinforced connection develops a load resistance that is double compared to the conventional connection. "Full plastic strength of the beams can be achieved under the large deformation stages for the assembly with the reinforced welded flange-bolted web connection." [63]

The set-up was also used by Wang et all. [64] to assess the behavior of two composite subassemblies under a column removal scenario (Figure 2.11.b). One specimen was tested by pushing down the central column, while the other by pulling up the central column, to obtain both sagging and hogging behavior. The experimental showed that the composite subassemblies with slab increased their capacity by over 63% more load than the pure steel subassemblies.
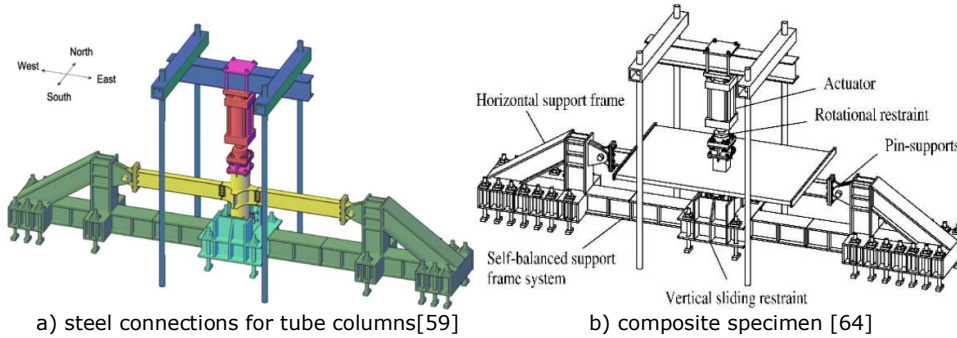
a) steel connections for tube columns[59]   b) composite specimen [64]

Figure 2.11 Test set-up at Tongji University

a) steel connections for circular tube columns [59]

b) welded unreinforced flange bolted web connections [60]
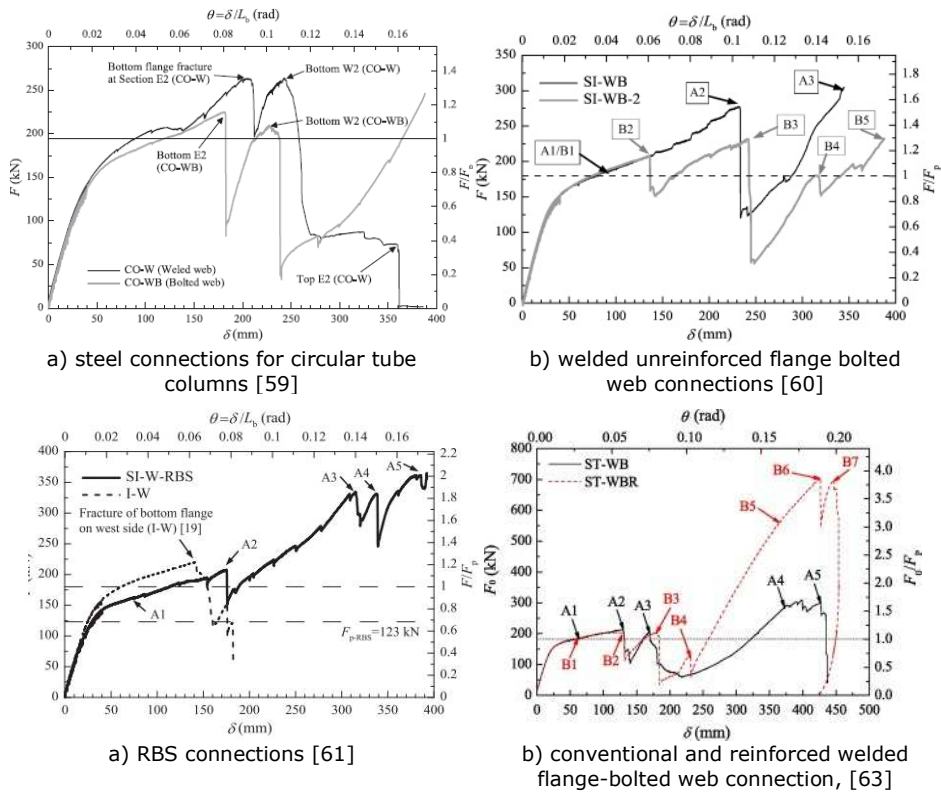
a) RBS connections [61]

b) conventional and reinforced welded flange-bolted web connection, [63]

Figure 2.12 steel connections experimentally tested

Using a 2-D frame experimental set-up (Figure 2.13) consisting of a vertical actuator on top of a column connected to two half beams pinned to rigid lateral restraints, the response of bolted angle connections in case of column loss was experimentally evaluated in Nanyang Technological University, Singapore. FEM results were more accurate in case of using a static solver, rather than a dynamic one, but the same conclusions can be drown using both sets of results, and a greater convergence was found for the dynamic solver [65].

Yang and Tan's [66] experimentally tests on common types of bolted-steel beam-to-column joints performance under central column loss, showed that the tensile capacity of beam-to-column joints after large rotations usually determines the failure mode and the development of catenary action ([43]).

A component-based model was deployed for parametrization, showing that the increase of the angle thickness in some configurations, even though it improved the axial stiffness, there were deformation capacities reduction. Hence, there is a high sensitivity of components [67].
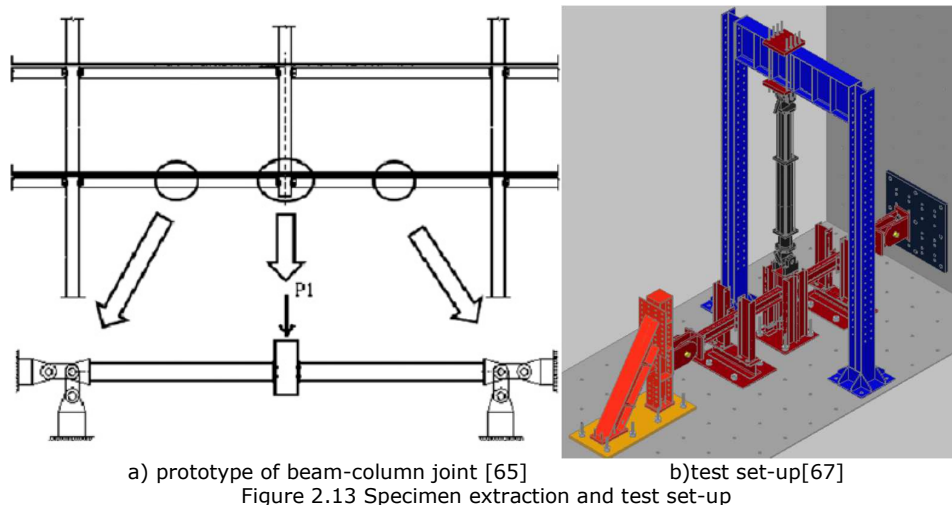
a) prototype of beam-column joint [65]   b)test set-up[67]
Figure 2.13 Specimen extraction and test set-up

The same test set-up was used by Liu et all. [68] for dynamic testing with uniformly distributed load suspended on the beams and a quick release mechanism. A FEM model was calibrated taking into consideration the dynamic effect, but not the strain rate, as the maximum strain rate during the test was about 5^{-s} (based on the conclusion that strain rate effects become significant for steel for strain rates ranging from 50 to 1000 s^{-1}[69]). The effect of the release time was studied ranging from 1 ms to 1000 ms. Figure 2.14. shows a very small variance of results between 1 ms and 2 ms and important differences for 1000 ms, 5000 ms, and 200 ms. Extrapolating, we can conclude that sudden release results are very close to results obtained for 1 ms support removal time. Figure 2.14.b shows the static and dynamic response of the same structure. Dynamic increase factors can be computed based on this data. Displacement based DIF_D reached values of 2.8, while force based DIF_F values ranged between 1.1 and 1.5.
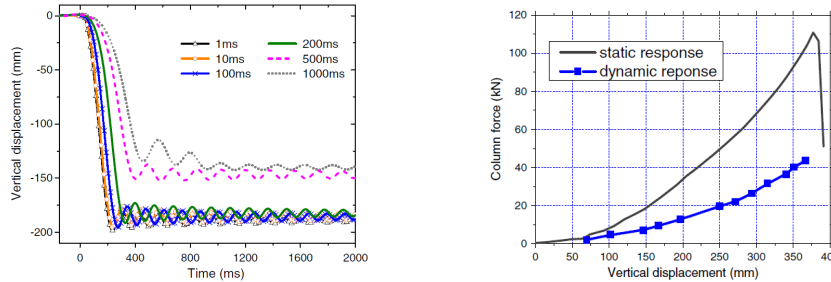
a) Comparison of the dynamic response under different load release time

b) Comparison of the maximum dynamic response with static response

Figure 2.14 Dynamic results for column loos [68]

A very interesting study was made by comparing the effect of the distribution of loads on the force-displacement relationship with the calibrated model. The two loading systems, and also testing methods, are presented Figure 2.15.a: (1) gradually increasing the point load at the middle column (test procedure is also known as concentrated load–displacement control approach) and (2) applying an initial uniform distributed force (UDL) and reducing the column support force to zero (force-release test method). Figure 2.15.b shows almost identical results for the two testing methods.
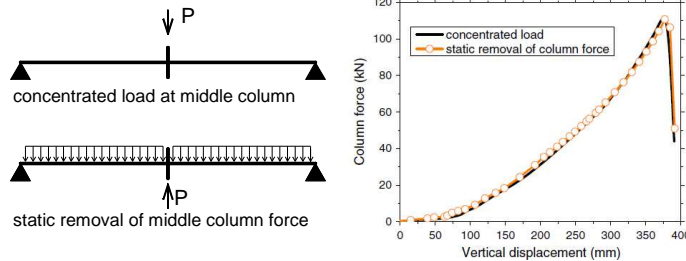
a) The two different static loading methods

b) relationship between the vertical column displacement with horizontal force

Figure 2.15 Column removal with explosive charges [68]

Furthermore, using the same testing set-up, composite joints were tested to sagging moment (connections adjacent to the central column and by reversing the specimen – slab bellow the steel beam – hogging moment (connections near the undamaged columns). Results showed that the catenary contributes to the ductility and load resistance of the specimens. Capacity improvement for composite joints can be seen in Figure 2.16, where the pure steel specimen is compared with the composite specimens subjected to sagging and respectively to hogging. The computed internal forces shoed that the applied load was resisted initially by flexural action, while at the large deformation stage, the load was resisted by catenary action [70].

a) web cleat connections   b) flush end-plate connections
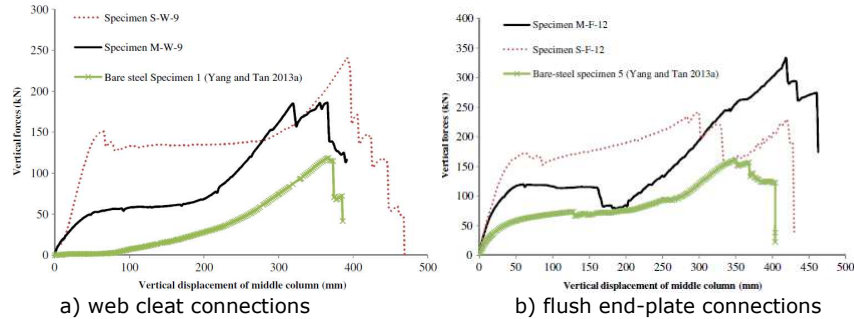
Figure 2.16 Effect of composite slab for connections

A similar type of test set-up was used by Hayes et all. [71] to investigate the performance of flexible (simple) shear connections under quasi-dynamic load (63mm/sec column vertical deformation rate for the 4.477 m span). Experimental results show loading rate can affect the ductility of the bolts, but not consistently.

Hoffmann and Kuhlmann [72] also used a double-hinge set-up to assess the behavior of a composite joints to column loss scenario by inducing vertical downward displacement on the column to evaluate sagging performance and flipping the specimen (reinforced concrete slab on the bottom) to evaluate hogging performance. Another test set-up used that takes into account the performance to sagging and hogging simultaneously, similar with the one in Liege [55], was used to asses column loss for two flush end-plate connection configuration of composite joints. Simple changes in the connection configuration can lead to significant capacity increase.

Two reinforced concrete beam-column assemblies representing parts of moment resisting frames of two ten-story reference building were tested under a simulated column removal scenario, as part of a NIST research program. The behavior can be summarized as a three-stage process: (1) an arching action stage (compressive arching forces due to beam ends horizontally); (2) a plastic hinging stage (flexural bending caused yielding of reinforcement in tension and concrete softening and crushing in compression); and (3) a catenary action stage (development of tensile catenary forces after center column deflection exceeded the beam depth). Arching and catenary stages have larger capacities than the plastic hinge stage (Figure 2.17.a), as they mobilize lateral forces to increase the resistance [73].

a) specimen after the test   b) vertical force vs. vertical displacement
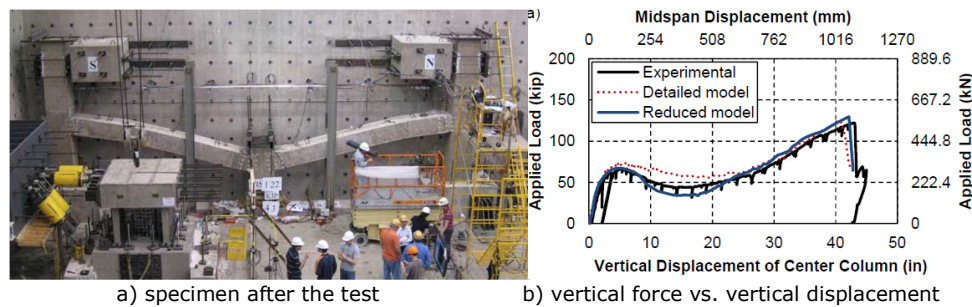
Figure 2.17 Experimental results on 2D [73]

Other 2D experimentally tested frames [74] showed an increase of capacity and decrease of ductility due to composite specimen.

A Nanyang Technological University study assessed the dynamic load redistribution performance of RC substructures following predefined initial damage [75]. Results from testing equivalent beam-corner column substructure with suitable boundary conditions showed that the span length has a major influence on progressive collapse resistance. The influence of the slab was not assessed.

The influence of concrete slabs on the resistance of steel moment-frame buildings was experimentally investigated for a 2 storey substructure by sudden removal of a perimeter column at Tongji University, Shanghai [76]. Results show that considering composite beam theory according to the effective flange width, the role of the composite slab is underestimated.

A first floor substructure was tested at University of Trento [77] by gradually removing the column under distributed load (see Figure 2.19) to assess the floor system redundancy contribution. Failure initiated with bolt fracture in the bottom row of the central column connection.

Reinforced concrete slab-beam assemblies have been tested for center and façade penultimate columns, see Figure 2.20.b. The load was applied with a 9-point system, see Figure 2.20.a. In the central column loss experimental test Dat and Tan [78] reported that collapse resulted from failure of the perimeter compressive ring as shown, rather than from fractures of tension reinforcement in the central region. The failure of the compressive ring is caused by rupture of flexible perimeter beams, or by compressive failure of slab corners. For external column removal [79] it was observed that until the half-compressive ring failed at a displacement of 10% of a span length, the load capacities of the three tested structures were able to maintain at least 90% of the corresponding peak values.

Figure 2.18 Experimental specimen subjected to sudden perimetral column loss [76]

| a) specimen at the end of the test | b) Slab crack pattern |

Figure 2.19 Experimental results on symmetric 3D specimen [77]
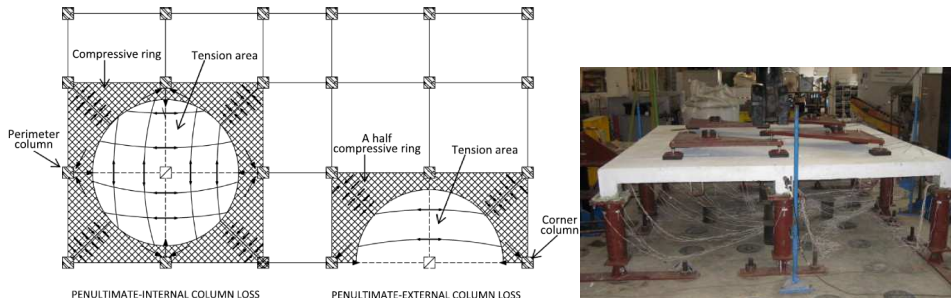
a) Reinforced concrete floor of structures subjected to column loss [79]   b) typical setup for beam-slab systems under the PI column loss scenario. [80]

Figure 2.20 Experimenta testing of slab 3D systems

In an experimental investigation of one-way RC beam-slab substructures against progressive collapse, Ren et all. [81] discovered great slab contribution for flexural behavior and also catenary action (cracks mainly perpendicular on the restrained beam direction). For perimetral column loss [82], the slab significantly enhanced the resistance due to catenary action and membrane effect (cracks show the formation of compression rings).

Test were performed by Lu et all. [82] on 1/3-scaled substructure specimens to investigate the progressive collapse resistance RC beam-slab structures under an edge-column-removal scenario. The contribution of the slabs improves significantly the progressive collapse resistance of the beam-slab substructures under an edge-column-removal scenario: 146% resistance increase under flexural mechanism and respectively 98%under the catenary mechanism (Figure 2.21.a).
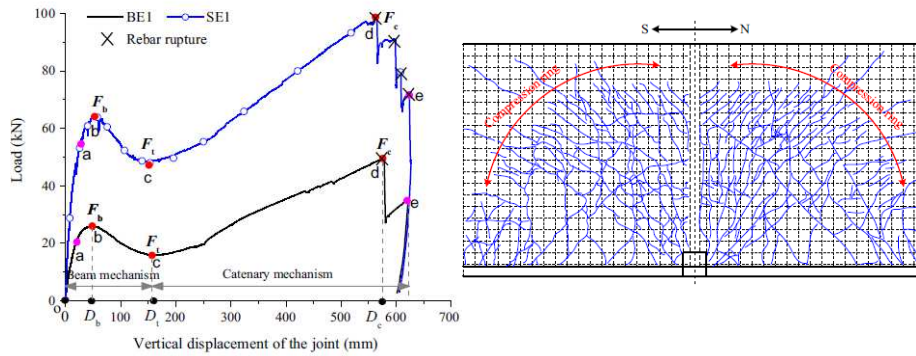
a) vertical force-vertical displacement curve   b) bottom slab cracks
Figure 2.21 Edge column loss experimental results [82]

Wang et all. [83] tested a 3x2 bays two story reinforced concrete frame structure to middle façade column removal, and replicated the results using the FEM software OpenSees.

A 2-bay by 2-bay steel gravity frame structure with a composite floor system, of about 10mx8.5m, was specially built to be tested, see Figure 2.22. Results reported by Hull [84] suggest that steel gravity frame structures may mobilized significant reserve strength in cases of interior column loss. After interior column removal, the test specimen deflection was only 1/40 of the total initial span length, for a 1.2DL + 1.6LL loading combination.

Figure 2.22 Tested specimen - before and after of the test [84]

A half-scale steel-concrete composite floor system, designed for efficient gravity load transfer, was studied experimentally by Johnson et all. [85] to evaluate its structural integrity under column loss scenarios. The 3x3 bay test specimen was subjected to four separate column removal scenarios: corner column, column with spandrel beams, edge column with spandrel girders, interior column. Distributed load was incrementally applied filling containers that were placed on top of the slab with water, see Figure 2.23.

Modifications to typical steel-concrete composite floor systems used in commercial buildings appear necessary, as the capacities are below the extreme event load combination of 1.2DL+0.5LL commonly used when designing to prevent progressive collapse.

Figure 2.23 Edge column removal final equilibrium point [85]

A large scaled test was performed by Kai [86] et all. to study the behavior of a reinforced concrete frame-core tube structure under static column removal. The seismic response after column loss was analyzed using a shaking table.

| a) tested frame-core tube structure | b) structure after static column removal | c) removed column structure after shake-table test |

Figure 2.24 Experimental tests on multi-storey structure [86]

Baciu [87] positioned explosive charges inside several boreholes of a ground level column (Figure 2.25.a) of an 80's old chemical plant building with a mixes prefabricated and cast in place reinforced concrete structure. The blast removed the capacity of the column almost immediately, but did not affect the rest of the structure. A model of the structure was created in ELS (Figure 2.25.b) and AEM simulation of instant column removal was performed. The numerical and experimental results are very similar, as seen in Figure 2.25.c, indicating an extremely good approximation of the AEM model.

a) removed column, before   b) ELS model of the   c) vertical displacement
    and after blast   structure   vs time
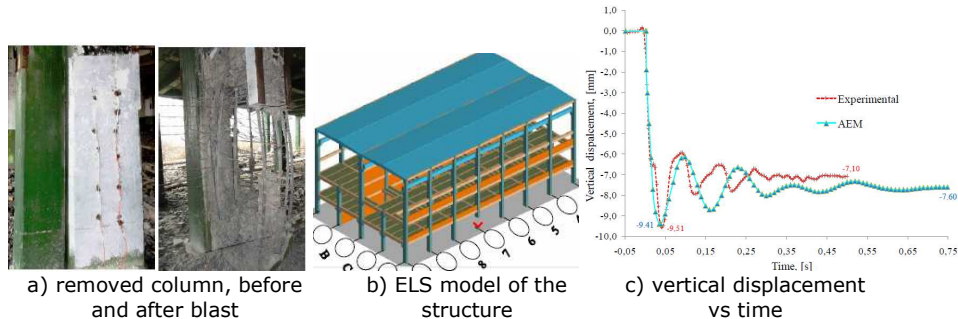
Figure 2.25 Column removal with explosive charges [87]

Existing steel frame buildings, were tested by physically removing four first-story columns prior to the scheduled demolition of the buildings [88], see Figure 2.26. Results were compared to models of the structure created in a commercially available software – SAP2000, showing that the 3-D model was more accurate than 2-D model. Column removal was performed either by pulling after flame cutting [89], as presented in Figure 2.27.a, or using blast loading in the case of Hotel San Diego building [90] - Figure 2.27.b. Numerical simulations using fiber hinges, accounted for axial and flexural interaction in beams closely estimated local and global experimental data for the Crowne Plaza Hotel column removal tests [91]. Design methodologies and simplified analysis procedures recommended in design guidelines were evaluated using the experimental data [89]. Another conclusion is that more reliable results are obtained if the actual material properties and connections of the building are considered in the analytical models [92].

Botez [93] studied modeling techniques for reinforced concrete structures for progressive collapse analysis employing FEM and EAM numerical procedures. Bredean [94] successfully calibrated a FEM detailed solid model with truss elements for reinforcement and a simplified bar element model in commercially available software reproducing the behavior of reinforced concrete structures.

a) Ohio Union building, 2007   b) Bankers Life and Casualty Company, 2008

Figure 2.26 Buildings with exposed columns to be sequentially removed before testing [88]

| a₁) Torching the column [89] | a₂) column ready to be pulled out [89] | a₃) removal of the column [89] | b) blast loading [90] |

Figure 2.27 Column removal procedure
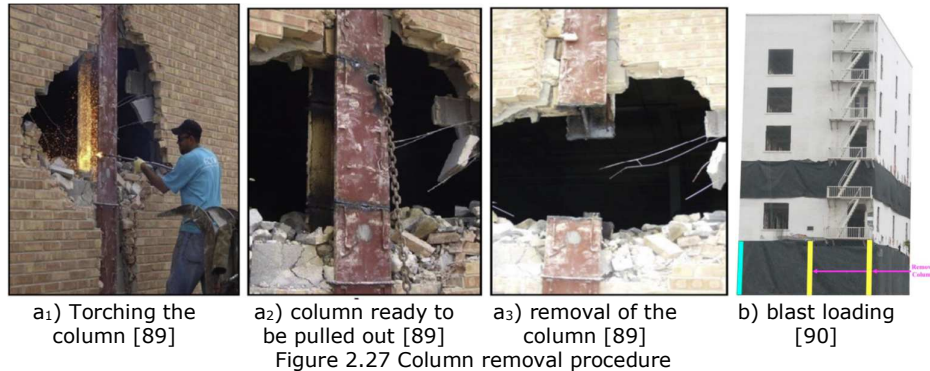
2.3.2 Analytical developments

Izzuddin, Vlassis, Elghazouli, and Nethercot [95, 96] developed a simplified framework for assessing the progressive collapse of multi-story buildings within a design scenario considering the sudden loss of an column. The static push-down curve is transformed in a pseudo-dynamic capacity curve by considering an energy balance principle. For each value of the vertical displacement of the column, the strain energy absorbed by the system must be equivalent to the work performed by the loads. The simplified design-oriented method for progressive collapse assessment of multi-storey buildings was applied for a peripheral and a corner column removal scenario in a typical steel-framed composite building. Results showed that fin plates, due to the increased flexibility and reduced strength, were much less adequate than flexible end-plates and should, therefore, be carefully reviewed from the standpoint of a robust design. Based on this multi-level progressive collapse assessment framework, Balance Energy method was extensively used in research studies to evaluate the dynamic performance of a structure subjected to column loss using static push-down data. [62, 64, 68, 97-99]. Also analytical formulation for the estimation of dynamic response amplification have been developed and applied for experimental and numerical studies of column removal scenarios [100-102].

A complete analytical method to predict the response of a 2D frame subjected to column removal was presented by Huvelle, Hoang, Jaspart, and Demonceau [103], considering the rigidity given by the entire frame and the joint yielding due to axial force – bending moment interaction. The method is compared to experimental and numerical data to validate the capacity to predict the behavior for of the structural elements and connections after the formation of plastic hinges.

Chen et all. [104] proposed a simplified beam damage model and adopted a probabilistic assessment approach depending on probability of hazard occurrence. For structural robustness performance level evaluation, a robustness index is also proposed based on the acceptable probability of global failure and structural collapse probability.

Due to the extremely reduced likelihood an extreme event to cause the complete failure of only one element, and that the affected damage area will most probably include more than one elements, Gerasimidis and Sideri [105] introduces a method for progressive collapse analysis considering partial distribution damage scenarios. The results show that notional column removal used in the Alternate Path

Method can be less conservative and predict other types of collapse mechanism than using the proposed partial distributed damage method.

2.3.3   Notional columns removal vs. close range blasts effects

The effects of direct blast load can result in the loss of bearing capacity of a column, or other primary structural member. Besides the influence of charge, standoff distance, there is also an influence of the charge shape as well [106]. Many studies do not consider for modeling, assessing, etc. the load that would cause the failure of the structural member, but only its main effect – the loss of that column modeled as element removal. On the other hand, the direct effect of the extreme event can have significant other effects.

Jahromi and Izzudin [107] discovered that upward lift of beams due to direct blast pressure increases the dynamic increase factor, with regards to column removal. The pressure wave can "unload" the beams, or even change the sigh of the bending moment in the blast phase. The part of the structure subjected to free fall has the same mass for the inertia forces as in the case of notional removal, but also additional forces due to the rebound from the blast pressure.

In the framework of the CODEC research project two 3D specimens were tested under direct blast effects inside a bunker. Due to space restrictions of the bunker, specimens extracted from a typical building were scaled down, considering aspects detailed in section 3.2.3.4.

The specimens include a façade column, two half-span façade longitudinal beams and one half-span transverse beam. The difference between the specimens consists in the column axis, as the blast placed in front of the column "outside of the structure" induces deformations in the major axis direction of the column for one specimen and respectively the minor direction, for the other specimen.

Experimental results and model calibration is presented in detail in a dedicated paper [108]. The variation of blast pressure with time and distance has been evaluated for bunker test conditions with several TNT charges – up to 1815 g. The results showed that charges located at close distance can produce large damages in the members, with complete fracture of the section walls. Thus, for the specimen loaded against the strong axis (charge normal to the column flange), the blast caused severe local bending of the external flange, and fracture of the web on the flange common line. In the case of specimen loaded against the weak axis (charge normal to the column web), punching, or shear-type failure developed, with the web completely separated for a length of 600 mm, before structural element to be able to respond in bending. The comparison between experimental results and the numeric calibration is presented in Figure 2.28.

a) blast load on column major axis   b) blast load on column minor axis
Figure 2.28 Deformed shape blast results: Numerical vs. experimental [108]
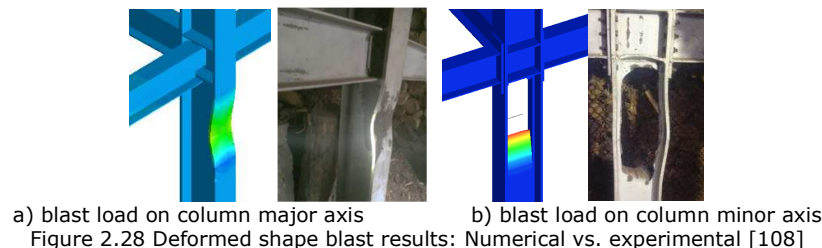
The case of web direct affected by blast (specimen II) is critical, especially for buildings with perimeter steel moment resisting frames and interior gravity frames.

In the test, the complete failure of the column was prevented only due to the absence of any gravity loads. Test based calibrated numerical models indicated a very good agreement, giving the possibility to extend the research to full-scale structures, using different blast loading conditions. Another paper studies the structural response of multi-storey steel building frames exposed to external blast loading conditions [109], using the calibrated models to analyze full-scale structures. An analysis was made between the notional removal of a column and blast loading causing column loss in terms of structural response. Figure 2.29 presents the vertical displacement in time for notional removal of the column and for blast loading of 100 kg of TNT at 0.2 m distance from the column. Due to blast effects on the other elements of the structure and altered dynamic amplification, the vertical displacement of the structure subjected to direct blast is 25% larger than the vertical displacement resulting for notional removal.

Although the notional removal of a column may not always be conservative, due to infinite possibilities of loading scenarios (charge distances, materials, and quantity) for standard comparison of structural systems in column loss events, notional removal is a more practical analysis scenario, with results that are not very different from real case blast conditions.
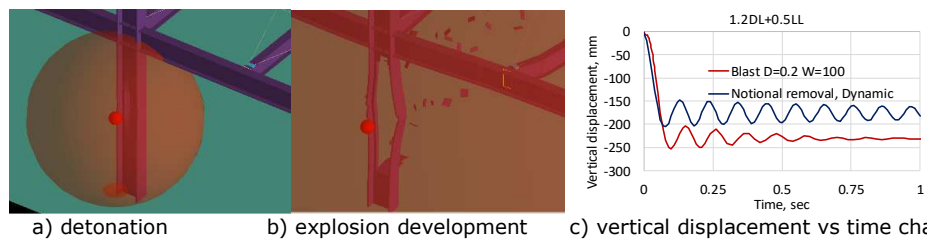
a) detonation   b) explosion development   c) vertical displacement vs time chart
Figure 2.29 Notional removal of columns vs. blast loading [109]

2.4   Conclusions and recommendations: Needs for future research

The large number of projects that deal with the development of guidelines, methodology and recommendations for arresting progressive collapse, many of them very recent or undergoing, show the major interest of investigators, structural engineers involved in design and governmental agencies (funding agencies and regulatory agencies). Current experimental research aiming to evaluate progressive collapse resistance of frame structures comprises a substantial number of experimental tests on details, 2D and 3D structural assemblies or full structures.

The variation of experimental investigations methods (static/dynamic, loading distribution, boundary conditions, etc) is derived from the advantages and disadvantages offered by each testing technique, and also because slight configuration changes for the same type of test can lead to significant behavior changes, while there are dissimilar performances for distinct typologies of connections.

In both 2D [55-73] and 3D [50, 51, 75, 76, 78-86] subassemblies tests, the most common experimental approach for evaluating the capacity of a structure to resist progressive collapse is notional column removal. The procedure can assess the behavior of the structural in case of accidental loading, regardless of the initial cause of the structural element damage, by considering complete removal of the damaged

structural member – the column. Due to its simplicity regarding action modeling and relatively safe implementation, this method was also used for experimental research of 2D and 3D frames studied in this thesis.

The result of column removal, considering that the main part of the beam is in elastic, is large displacement imposed on T-stubs. This is the premises for tests on connection macro-components (T-stubs) subjected to large displacement up to failure. Connection macro-component tests are concentrated on bolted T-stubs [42, 47, 67], but there is no data for the performance of weld type at large deformation under dynamic loading. Dynamic experimental tests on flexible T-stubs have concluded that, due to their flexibility, strain rate does not influence the performance of the T-stub and hence, of the connection [71]. Seismic connections T-stubs are stiffer, and due to this reason strain rate may have an incresed impact of their behavior in dynamic loading. As, plastic deformations concentrate mainly in T-subs, therefore also strain-rates, dynamic testing of the connection macro-components is relevant and also less difficult and safer than dynamic testing of the subassemblies.

Dynamic testing [68, 75, 76, 102, 110] [85] of a specimen undergoing plastic deformation can give experimental information for a single load value and configuration. However, these investigation techniques give accurate results regarding dynamic effects. These investigations are more facile to be performed numerically, as the distinct load values can be used for each separate analysis. Static testing, on the other hand, can give detailed information of the system response, with the possibility to identify different resisting stages (e.g. arching stage, flexural stage, hinge stage, catenary stage, membrane stage). The entire behavior, especially ultimate capacity, can be observed and easily recorded.

When considering the direct effect of impact or blast, strain-rate is very important for local damage development, but due to the flexibility of some connection details, the dynamic effect induced by the free fall of a column does not induce high strain rates in the connection [68, 99]. Other studies considered an overall 10% hardening of the material [51]. Behavior of the concrete, however, in such loading rates, is positively affected [21], resulting in large improvements [111]. Seismic designed connections of moment resistant frames are generally stiff, as they are desired to control inter-storey drifts. A higher stiffness could lead to larger strain-rate influences, therefore investigations for strain-rate influence on seismic designed connections should be performed. Strain-rate effect may be range also on the type of details used in the connection's configuration (macro-component deformability, weld type).

The restraining system proved to have a direct influence on the development of catenary action [72, 112]. Experimental set-ups should be designed to be capable of providing sufficient lateral stiffness such that catenary action would be activated realistically.

The influence of composite effect on connection performance [64, 70] (capacity increase and ductility decrease) was mainly studied on 2D frames, but in many cases, there is a membrane effect [79], therefore the study of the influence of the composite interaction should be performed on a 3D structure. The same system should be tested without the floor slab.

The necessity of robustness related experimental evaluations is highlighted by a major number of thesis, research publication and reports. In the thesis "The integrity of steel gravity framing system connections subjected to column removal loading" [113], Weigand recommends connection component tests (T-stubs) for evaluation of the performance of bolted connections under large deformations. The

lack of dynamic test results on welded and bolted connection macro-component corresponding to seismic designed beam-to-column connections should be addressed, in order to identify if for these specific connections. Selvarajah suggests at the end of his Ph.D. thesis "Robustness analysis and design of steel-concrete composite buildings" [111] that experimental tests are necessary for assessing the connection behavior on axial force- bending moment interaction loading conditions. The same conclusion is reached by Vidalis in "Improving the resistance to progressive collapse of steel and composite frames", his Ph.D. thesis [114]. Progressive collapse dedicated reviews [115] also recommend experimental tests, some insisting on dynamic experimental testing to assess the dynamic effects on the column loss process [2]. Although there is an appreciable number of experimental research on steel structures for evaluating progressive collapse resistance, ranging from T-stub experimental study for large deformation, 2D or 3D substructure testing, or even tests on existing structures, there are very few experimental results for seismic designed beam-to-column connections. Such connections are certified in extensive experimental and numerical tests for providing structural integrity just for the case of seismic action. As they are intently use in seismic areas, the evaluation of their performance in case of accidental actions resulting in column loss is essential for assessing the robustness of seismic resistant MRF structures. To conclude, experimental tests are necessary for evaluation of steel seismic beam-to-column connections subjected to column loss scenarios or related loading conditions. Such tests should evaluate the performance of connection from macro-component level, to connection type, and finally for interaction with the floor system.

Numerical models are essential to be calibrated on the resulted experimental data, for completing the results and for expanding the obtained data for other configurations. Therefore, a numerical program must be developed based on the experimental results, in such a manner that results can be obtained for other configurations, but also for full-scale structures under dynamic loading conditions associated with column loss. Such a tool would allow the robustness assessment of structures and to develop strengthening strategies.

Code provisions recommend design approaches, but do not provide consistent methodologies and give informative data regarding to design of structures to resist severe local damages. The prescriptive lack of comprehensive design guides and consistent set of recommendations should be addressed by developing a design approach for multi-storey structures to prevent progressive collapse due to accidental actions. Furthermore, if the design approach indicates inadequate performance of connection subjected to column loss, improvements should be recommended for the connection's configuration. These improvements must not alter the connection capacity to seismic loading states, and therefore the seismic design philosophy should not be modified or infringed.

Additionally, there is a major necessity for studies regarding risk assessment, in order to define performance levels acceptance criteria, coupled with possible scenarios for total/ partial damage of elements. This data is essential for a relevantly assessment of the structural capacity to resist extreme events, and also could influence the application of mitigation strategies. Due to the complexity of these issues, they are not directly approached in this thesis, but will be the subject of further research activities.

3 EXPERIMENTAL PROGRAM

3.1 Introduction

This chapter presents the experimental tests, which were performed to investigate the ressponse of structural components of steel frame structures in case of large deformation demands associated with the removal of a column. Small connection macro-components (T-stubs, weld details) as well as 3D assembly frame specimens were tested under different loading conditions to capture the main response parameters, e.g. elastic and ultimate capacity, failure modes, and differences compared with the usual gravity and seismic response. Obtaining consistent experimental results from an integrated experimental framework with relevant experimental specimens and test set-up for robustness evaluation of seismic connections is the first major objective of the thesis. For allowing comparisons and interpretations, all specimens were extracted from the same reference steel frame structure. In addition, at fabrication, same material properties were used for fabrication of similar specimens. When necessary, reference to current code provissions saw done. All experimental tests that will be detailed in the next sections were performed considering notional column removal (with different durations), without taking into account any other possible direct effects of extreme loading.

The effect of temperature and the duration for column removal were also considered for connection macro-components. The beam-to-column connections sub-assembly specimens were tested in quasi-static loading conditions (push-down tests assuming removal of a column) and were similar for all connection types. For system testing (on 3D sub-structures), the same structural system was tested in two different configurations, i.e. with and without beam-concrete floor interaction, also in cvasi-static loading conditions.

All tests were performed within CODEC research project. A detailed description of the test program and interactions between different test configurations performed to achieve the thesis objectives are shown in Figure 3.1. Within this framework, tests at room temperature are performed on bolted and welded connection macro-components under static and dynamic loading, and steel frames with different configurations of beam-to-column connections are tested to column loss, as well as 3D subassemblies with and without reinforced concrete slab. The testing facilities used for performing the experimental program are part of the research infrastructure of partners involved in the project. T-stub macro-components were tested with the 1000 kN capacity Instron universal testing machine available at the CEMSIG laboratory, UPT (see Figure 3.2.a). The joints with different types of connections tested under column loss scenario were also tested in the CEMSIG laboratory, using the reaction wall (5.0x6.2 m) and strong concrete slab (5.0x9.5 m), see Figure 3.2.b. The tests on 3D sub-assembles were carried out in the Laboratory of URBAN INCERC Cluj-Napoca Branch (see Figure 3.2.c).
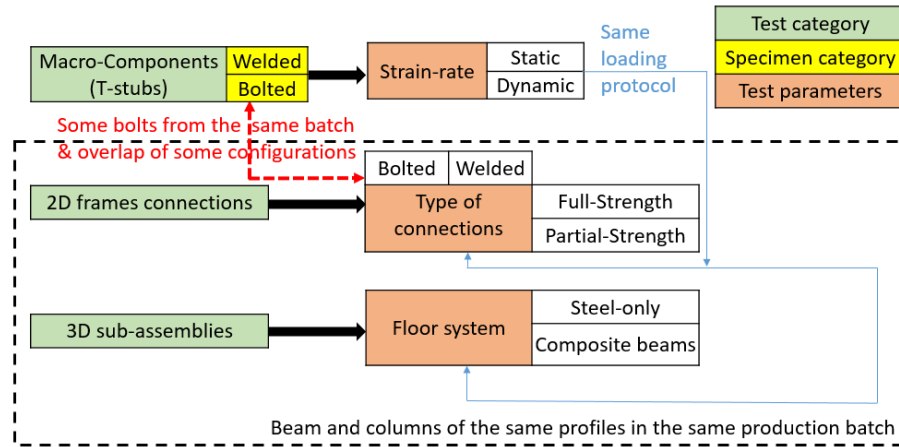
Figure 3.1. experimental testing program

a) INSTRON-   b) reaction wall and strong slab-   c) reaction wall and strong slab

Figure 3.2. Experimental infrastructure

3.2   Design of experimental program

3.2.1   Preliminary studies and design of reference structure

For allowing comparisons and interpretations of results, all experimental specimens were extracted from the same reference steel frame building. The reference building is an office building with three-bay, four-span and six-stories. Bays and spans measure 8.0m each, and all stories are 4.0m high. The structural type is a moment resisting frame on both transverse and longitudinal direction. The secondary beams are placed parallel to transverse frames, at intervals of 2.66 m. The geometry of the multi-story frame building is shown in Figure 3.3. The design of the structure was performed using Eurocodes, and considered two design situations, i.e. permanent and seismic, without any accidental design situation. The gravity loads (permanent and variable actions) and the lateral loads (wind and seismic) were calculated using specific provisions ([8, 116-119]). Dead and live loads amount 4.0 kN/m^2 each, while reference wind pressure is 0.5 kN/m^2.

For evaluating the importance of seismic requirements, two seismic zones were used in design, i.e. low and high seismicity, respectively. For the low seismicity case, the reference peak ground acceleration is a_{gR}=0.1 g and the ground type is stiff

(corner period T_c=0.7 s), while for high seismicity case a_{gR}=0.4 g and ground type is medium-stiff (corner period T_c=1.0 s. The seismic hazard was taken from the Romanian Seismic Code, P100-1, released in 2013 [120]. In addition, two types of beam-to-column connections were used, i.e. rigid and full strength, noted as *FS*, and semi-rigid (0.8 rigidity ratio with respect to a full rigid connection) and partial-strength (0.8 strength ratio with respect to a full-strength connection), noted as PS. Frames with partial strength connections would dissipate the seismic energy in the connection, rather than in the beam, which is the case for FS frames
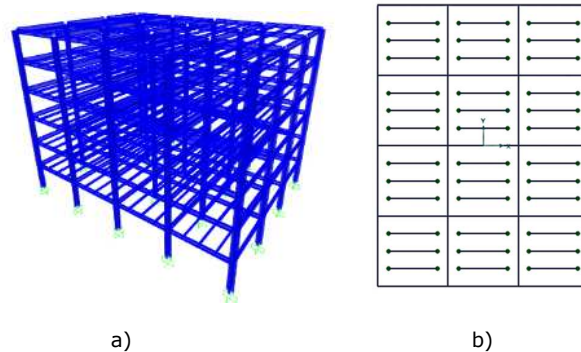
a)   b)
Figure 3.3. Views of the reference structure: a) isometric view; b) floor plan

Beams and columns were made from hot rolled profiles and steel grade S355. A behavior factor $q = 6.5$, corresponding to high ductility class, was considered in the seismic design. SAP2000 finite element analysis software [121] was used for the structural analysis and using 3D models.

For serviceability requirements, the interstory drift computed as:

$$q \cdot d_{\max} \cdot \gamma \tag{3.1}$$

was compared with the allowable limit (P100-1/2013 limit [120]):

$$d_{all} = 0.0075 \cdot h_{storey} \tag{3.2}$$

where $\gamma = 0.5$ is the reduction factor accounting for the seismic return interval associated with SLS.

Table 3.1 presents the details about the size of cross-section, type of connection, and the location (seismic zone) of each structure considered in the preliminary design. Due to lateral stiffness demands (the two equations above), the structure with partial strength connections located in HSZ was not considered for the preliminary study.

Two structures were further selected for preliminary sizing of the experimental specimens, i.e FS-LSZ and FS-LSZ. The two structures are similar (see Figure 3.4), excepting the type of connections.

Table 3.1. Structures used in the preliminary design

Structure name	Main beam	Secondary beam	Column	Connection	Seismic zone
FS-LSZ	IPE400	IPE 330	2xHEB450	FS	Low seismicity
FS-HSZ	IPE600	IPE 330	2xHEB900	FS	High seismicity
PS-LSZ	IPE400	IPE 330	2xHEB450	PS	Low seismicity
PS-HSZ*	N/A	N/A	N/A	PS	High seismicity
* structural system cannot fulfill seismic lateral stiffness demands					
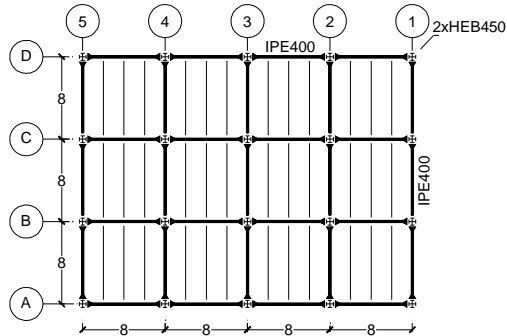
Figure 3.4 The configuration of FS-LSZ/PS-LSZ structure. [10]

The full strength (FS) and partial strength (PS) beam-to-column connections are extended end-plate bolted connections. The difference between the two types of connections is the end-plate thickness and bolt diameter (Figure 3.5). According to EN1993-1-8 [122], there are three possible failure modes for such types of connections. Mode 1 is characterized by a complete yielding of the flange; Mode 2 is characterized by bolt failure with yielding of the flange, while in the case of Mode 3 the connection fails due to the failure of the bolt. FS connection has a strength ratio (compared to beam) of 1.0 and fails in Mode 2, while PS connection has a strength ratio of 0.8 and fails in Mode 1, see Figure 3.6. However, according to EN 1998-1 [117], both connections are classified as partially restrained.

The influence of the interaction between the reinforced concrete slab and the steel beam on the behavior of beam-to-column connections is presented in detail in a dedicated paper [123].
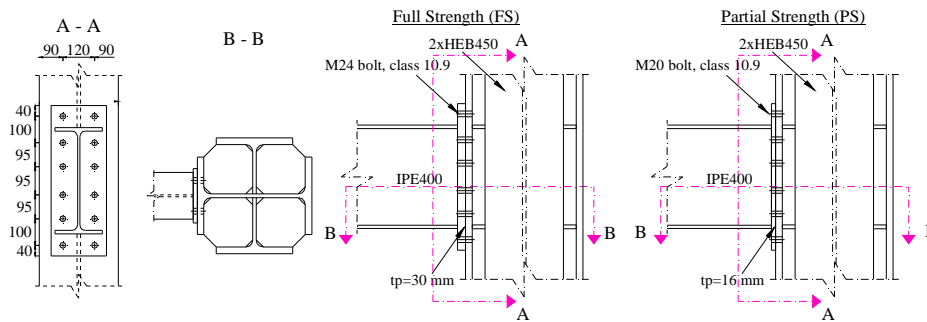
Figure 3.5 Details of the beam-to-column connections[10]
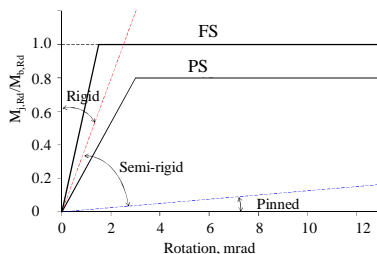
Figure 3.6 Moment-rotation characteristics for connections[10]

3.2.2   *Preliminary evaluation of column-loss structural performance*

3.2.2.1 Scenarios

The structural response has been studied for several scenarios including for one or two columns removal situations with nonlinear analyses performed in ELS software. All of the studied scenarios imply the complete and instant damage of ground floor columns. Five column loss scenarios have been investigated: corner column loss scenario – column A1, antepenultimate column loss scenario – column A3, central column loss scenario – column B2, corner and penultimate column loss scenario – columns A1+A2, penultimate, and antepenultimate column loss scenario – columns A1+A2. For the scenarios with two columns removed, both columns were removed in the same time, the hypothesis with the highest dynamic amplification. The locations of the removed columns are described in Figure 3.7.

Because the structures designed for the low seismic zone (LSZ) share the same beam profile (IPE400), the analysis of the partial strength and full strength connection structures can indicate the connection configuration influence on the progressive collapse resistance. The analysis labels are listed in Table 3.2, where S-FS-A1 defines a full strength connection (FS) structure with corner column (A1) removal.
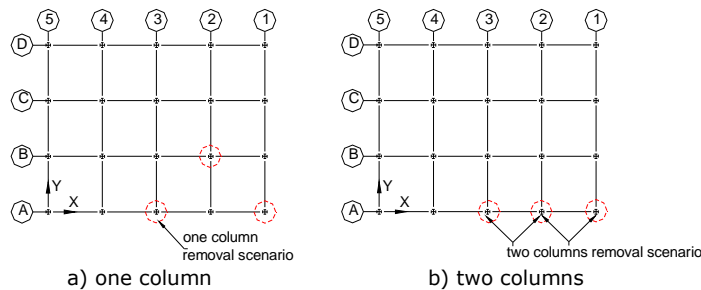
a) one column   b) two columns
Figure 3.7 Column removal scenarios [10]

Table 3.2. Column loss scenarios

Scenario	Column removed	Type of connection
S-FS-A1	A1	
S-FS-A3	A3	
S-FS-B2	B2	Rigid connection FS
S-FS-A12	A1 + A2	
S-FS-A23	A2 + A3	
S-PS-A1	A1	
S-PS-A3	A3	
S-PS-B2	B2	Semi-rigid connection PS
S-PS-A12	A1+A2	
S-PS-A23	A2+A3	

3.2.2.2 Analysis procedure

The analyses of the column loss scenarios have been performed in Extreme Loading for Structures (ELS) software [124] using an AEM solver, presented in detail in section 4.1.2.2.

The entire structure has been modeled in the ELS software to obtain its global response, allowing the simulation of tying forces of the undamaged bays acting on

the bays adjacent to the removed column (columns), or the redistribution of forces between the different stories.

The material models have been defined by their main characteristics: elastic properties, yielding limit, maximum allowable stress, maximum allowable elongation, separation elongation, etc. Structural steel S355 was assigned for the beams, columns, and end-plates. Class 10.9 bolts were used for connections. Nominal values have been used for all materl models.

Columns have been defined as vertical elements with a constant built-up cross-section made from two I section (Figure 3.8.a). Beams (both main and secondary beams) were also modeled as elements with constant cross-sections (Figure 3.8.b). In order to reduce the computational cost, beams were divided into different numbers of elements, number which was increased in the bays near the removed column (columns). Beams with no expected plastic deformations have been divided into 7 elements per length and beams in the adjacent bays of the removed columns have been divided into 20 elements. Beam end-plates were modeled using 8 nodes (solid parallelograms) in direct contact with the beam end, and were considered welded on the common surface (Figure 3.8.c).

The secondary beams were connected to the main beams with 3 bolts, modeled trough three reinforcement bars made of bolt material and with the adequate cross-section (Ø16), placed at the interface between the secondary and main beam. These reinforcement bars would generate corresponding springs. The ends of the secondary beam were elongated up to the main beam web. To make possible the rotation of the secondary beam, a special element, called *region,* was assigned at the shared area between the main and secondary beam (Figure 3.8.e). A spring controller was assigned for all of matrix springs in the region (sprigs generated between objects – this excludes reinforcement) changing the material of the spring into a material with very low compression and tension strength, therefore allowing rotations of the elements around the bolts.

To simulate the contact between the end-plate and the column, a region was created in that area (Figure 3.9.a) to change the material of matrix springs from the default steel to a material that has no tension resistance, but transferring only compression. The bolts were modeled with reinforcement bars of bolt material and specific cross-section for each connection design type. Since the spring generated from reinforcement would, in fact, transfer a point load to just one element of the end-plate, it is possible to have a punching effect by pulling out the element connected to the spring. As this is not a realistic case, additional reinforcement springs have been provided in the interior of the end-plate transferring the force to a wider surface equivalent to the surface of the head of the bolt (Figure 3.9.b).

| a) generated column springs | b) generated beam springs | c) end-plate-beam connection | d) end-plate mesh | e) pinned connection |
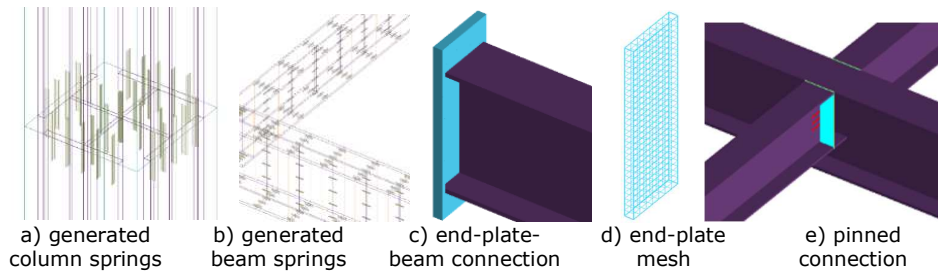
Figure 3.8. Element modeling

a) contact region   b) bolt modelled as reinforcement   c) generated bolt springs
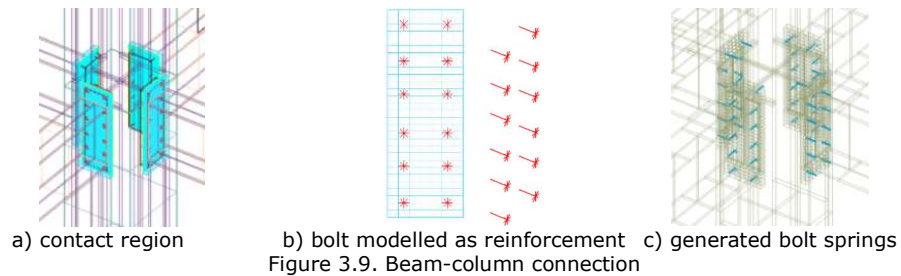
Figure 3.9. Beam-column connection

The external boundary conditions of the structure include a rigid surface beneath the ground level, which was simulated by a concrete interface bellow the entire building on which falling debris can bounce. The column bases were modeled as rigid.

3.2.2.3 Model calibration

In order to improve the accuracy of the numerical analyses for column loss scenarios, models were calibrated and validated against experimental data available in the literature. First issue is the influence of axial force on the moment capacity and ductility of the beam-to-column connections. The catenary action, which develops in the beams at large deflections need to be transferred through the beam end connections, thus significant tension forces develop. Most of existing experimental data on beam-to-column connections are generally related to moment capacity, in the absence of axial forces, which is a common assumption for the seismic field. A set of experimental tests which investigated the influence of axial force on the connection response, carried out at the University of Coimbra, Portugal, were used as reference [125]. The experimental program included 9 experimental tests on flush end-plate configurations (Figure 3.10). Several combinations of bending moment and axial forces were considered during testing. In the initial stage, a fixed level of axial tension or compression was applied, after that, the bending moment was applied incrementally up to the failure attainment in the connection. Figure 3.11.a presents the experimental set-up. The calibration of the model is detailed in [126]. Based on these tests, a numerical model was constructed, using the same loading principles, boundary conditions, and material properties. The beam (IPE240) and column (HEB240) were created with objects of constant cross-section, while the end-plate was made using an 8-node object, all from S275 steel. The column is fixed at both ends allowing only the rotation around Y axis. Details of the mesh are presented in Figure 3.11.b. The bolts were modeled with reinforcement bar elements using bolt material (class 10.9) with the same area of M20 bolts used in the test.

The numerical testing procedure follows the same loading protocol used in the experimental test. Initially, a specific tension force was applied at the end of the beam. This tension force would remain constant during the entire testing duration. After this initial loading, a vertical displacement was applied incrementally at the end of the beam in a nonlinear analysis, until the connection reached its ultimate capacity. The model was calibrated to two different levels of axial force, i.e. zero axial force and 20% plastic capacity of the beam section in tension, respectively. The experimental and numerical bending moment-rotation curves are shown in Figure 3.12.a, with a good agreement. The model was further used to evaluate the moment capacity of the joint for all levels of axial force, resulting in the interaction curve presented in Figure

3.12.b. Continuous degradation of moment capacity with the increase of tensile axial force can be observed.
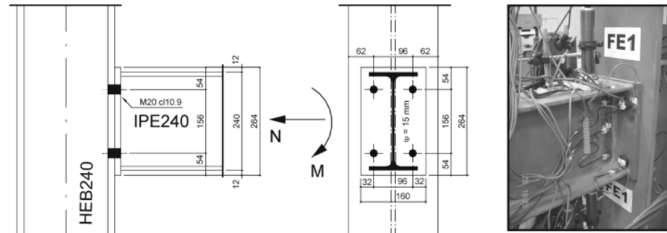
Figure 3.10. Experimental flush end-plate configuration [125]
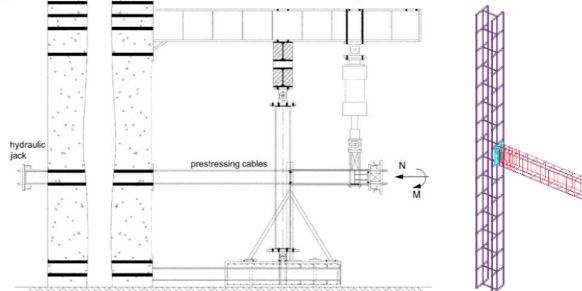
a) Experimental setup [125]   b) mesh view of numerical model
Figure 3.11. Beam-to-column connections subjected to bending moment and axial force
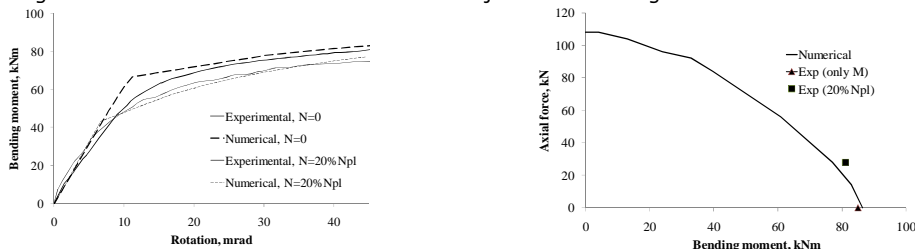
a) Moment-rotation curves   b) Bending moment – axial force interaction
Figure 3.12. Calibrated model versus the experimental data[126]

For the evaluation of the frame behavior in case of column loss, with the development of catenary action and influence of progressive tension axial force on the connections and elements moment capacity, another set of experimental data, obtained by J.-P. Jaspart and J.-F. Demonceau at the University of Liège in the framework of the *Robust structures by joint ductility* research program (2004-2007) [34] was used to refine the calibration of the numerical model. The substructure configuration is shown in Figure 3.13. The principles of beam-to-column connection modeling were the same as in the previously calibrated model. Reinforcement, concrete and headed shear studs were also modeled using the data provided in the experimental test [55]. Details of the calibration are presented in [10]. The selected experimental frame, which includes reinforced concrete slab and shear studs, was used to determine the behavior of structures with reinforced concrete slab and composite beams in column loss scenarios [10].

The central column was initially blocked. The experimental specimen was loaded with concrete blocks equivalent with 10kN/m. The same initial gravity load was

assigned through point loads in the numerical model. The horizontal restraints are assigned in the numerical model with the properties of the calibrated jacks used in the experimental tests. The central column is gradually displaced downwards, passing the point where the reaction force becomes zero (and tension initiates), up to the failure of the specimen.

The behavior of the numerical model was close to that of the tested specimen. Plasticity occurred in the same areas with a very similar overall deformed shape (Figure 3.14).

a) detailed drawing [34]
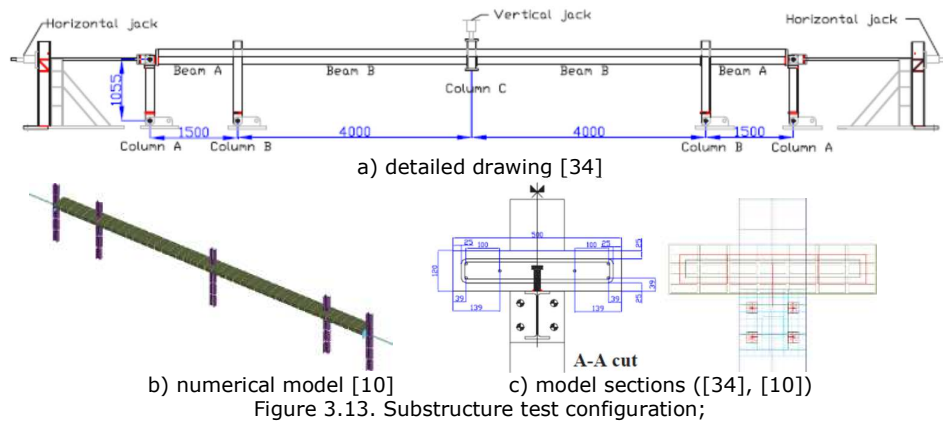
b) numerical model [10]   c) model sections ([34], [10])
Figure 3.13. Substructure test configuration;

The very good agreement between the experimental test data and the numerical simulation can be seen in Figure 3.15. All major phenomena observed in the test (elastic behavior, plasticity due to the crushing of concrete, initiation of catenary force, etc.) can be identified at similar forces and displacements in the numerical model.
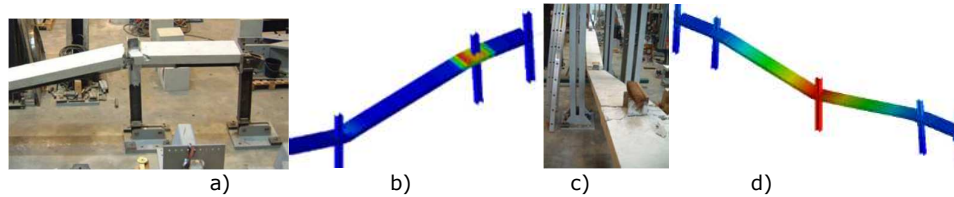
a)   b)   c)   d)
Figure 3.14. Plastic deformations in concrete [34] and [10]: a) experimental test [34];
b) numerical model; and specimen displacements: c) experimental test; d) numerical model;
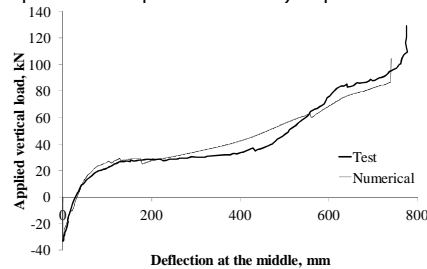
Figure 3.15. Force – vertical displacement curve: Test vs. Numerical [10]

3.2.2.4 Column loss scenarios results for nominal loads

The first assessment of the structural behavior in case of column loss was performed using scenarios A1, A3, B2, A12, and A23, and with rigid or semi-rigid beam-to-column connections. The analysis procedure was nonlinear dynamic analysis, using a load combination characteristic for accidental design situation (1.0DL+0.5LL).

One of the most important indicators of this analysis is the vertical displacement of the column above the removed column part. The variation in time of this vertical displacement is given in Figure 3.16. The phenomenon of progressive collapse did not occur in any of the dynamic analyses when nominal gravity loads were used.

The maximum vertical displacement is highlighted in Figure 3.17.a, where the largest values for both types of connections are reached for scenario A12, followed by scenario A23 - both scenarios are with two columns lost. From the single column loss scenarios, the central column loss scenario B2 has the highest vertical displacement. Frames with stronger connections (FS) lead to less vertical displacements for all scenarios.

The influence of the connection properties can be seen also in Figure 3.17.b, where the vertical displacement ratios are obtained by dividing the vertical displacement of the structure with PS connection to the vertical displacement of the structure with FS connection for each scenario.

Other observed parameters have been the plastic deformations in structural elements, see maximum strains in Table 3.3. FS structures have slighlty reduced plastic strain in the beam, but dramatic reduction of plastic strain in the connection.

For the undamaged part of the structure, a tendency can be observed of elements or part of the structure to be pulled to the damaged zone when catenary action develops. This effect may induce damages to other parts of the structure (i.e. buckling of columns due to out-of-plane deformations). Mutually, the development of catenary action strongly depends on the lateral restraint provided by the rest of the structure.
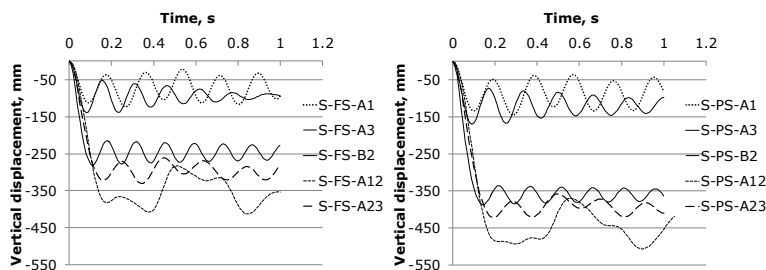
a) full strength connections structure   b) partial strength connections structure

Figure 3.16. Vertical displacement vs time
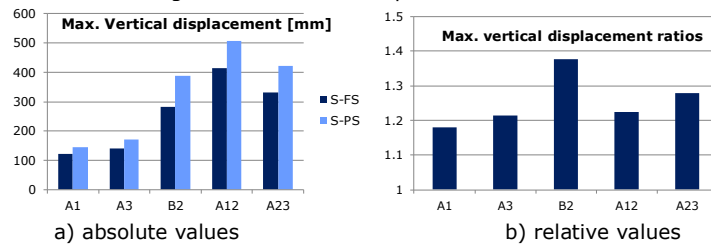
a) absolute values   b) relative values

Figure 3.17. Maximum vertical displacement from non-linear dynamic analysis

Table 3.3 Maximum strain in the structures

Scenario	Steel beam	Beam-to-column connection	Scenario	Steel beam	Beam-to-column connection
S-FS-A1	0.005	0.010	S-PS-A1	0.0055	0.0181
S-FS-A3	0.009	0.013	S-PS-A3	0.011	0.024
S-FS-B2	0.025	0.024	S-PS-B2	0.029	partial fracture
S-FS-A12	0.023	0.029	S-PS-A12	0.028	0.053
S-FS-A23	0.024	0.034	S-PS-A23	0.027	partial fracture
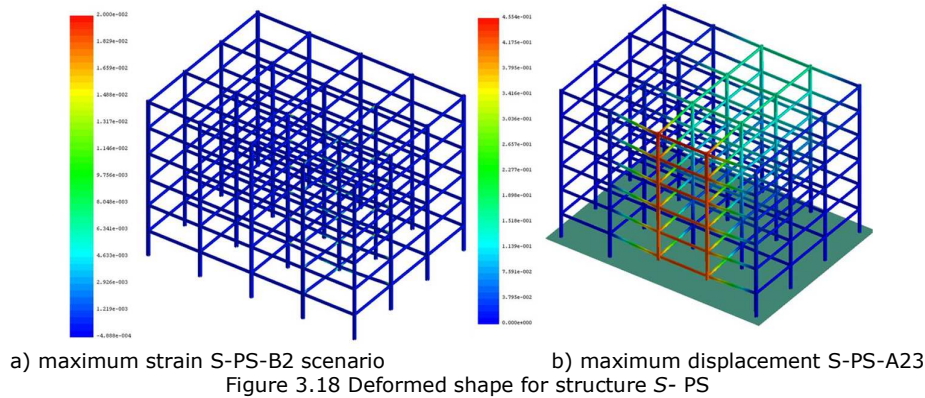
a) maximum strain S-PS-B2 scenario   b) maximum displacement S-PS-A23
Figure 3.18 Deformed shape for structure *S*- PS

For the first floor beam, at the end opposite end to the adjacent removed column, moment and axial forces have been monitored for both. As it can be seen in Figure 3.19.b, the moment capacity of the connection in cases S-PS-B2 and S-PS-A23 is reduced due to the axial force that develops in the beams (see Figure 3.20.b). The fracture of the top side bolt row in S-PS-B2 can be identified by a sudden loss of capacity. The capacity of the beam analyzed for scenario B2 is an intermediate frame beam, while all other beams are marginal frame beams, therefore it is more loaded in the initial static analysis, where no rotations occur. Tension axial forces appear only for scenarios that can develop catenary action (A3, B2, A23).
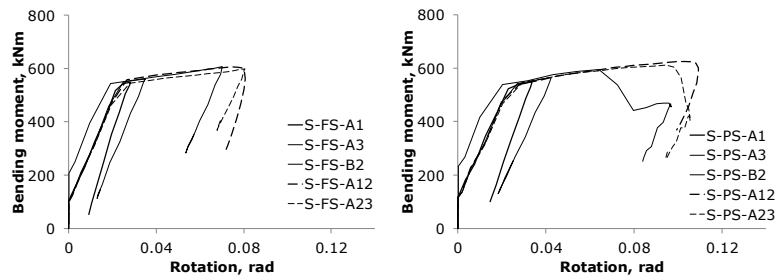
a) structure with rigid connections   b) structure with semi-rigid connection
Figure 3.19 Bending moment vs. rotation at maximum vertical displacement [126]
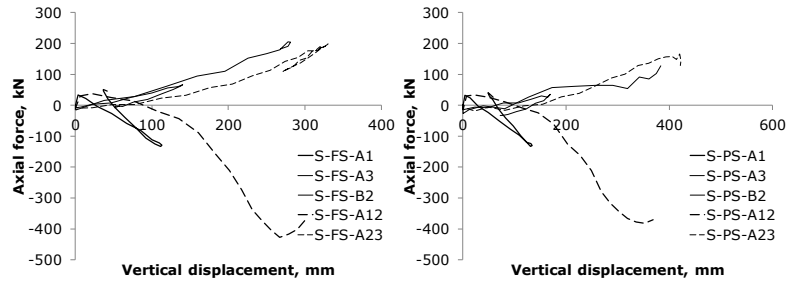
| a) structure with rigid connections | b) structure with semi-rigid connections |

Figure 3.20 Axial force vs. vertical displacement [126]

3.2.2.5 Ultimate capacity for column loss scenarios results

In order to identify the critical components in resisting the progressive collapse, the structures were further analyzed under increasing gravity loads until the collapse is reached, using both static and dynamic nonlinear analysis procedures. Gravity loads applied on the bays adjacent to the lost column have been incremented until progressive collapse is reached. The ratio of the value of gravity load that trigger the progressive collapse related to nominal gravity loads (*DL+0.5LL*) is actually a robustness index, also known as the overload factor, Ω [127]:

$$\text{Overload factor}\,(\Omega) = \frac{\text{Failure load}}{\text{Nominal gravity load}} \tag{3.3}$$

Column loss using static nonlinear analysis was performed by removing the damaged column, then followed by an increase of gravity loads on all floors above the adjacent bays to the removed element. This step by step load increment approach takes into account also the second order effects. The progressive collapse state was considered to be reached when the total vertical base reaction decreased in relation to the applied gravity load (the structure was not able to withstand further gravity loads).

The column loss dynamic nonlinear analysis required distinct analyses for the same column loss scenario, with incremented initial gravity loading. In the first stage, all columns have their full bearing capacity, and gravitation loads are applied in a static procedure. Afterward, the damaged column is removed instantaneously in a time history analysis, in which the time step is 0.001 seconds. This analysis takes into account the inertial effects caused by the weights of the modeled elements and applied loads. If the results indicate that, for a specific gravity load, the structure is able to redistribute the forces and reach the equilibrium, the process is repeated with higher initial gravity loads, up to triggering progressive collapse.

The displacement-based dynamic increase factor (DIF) relates to the increase of gravity loads values in the static analysis to the extent of obtaining the same results (maximum vertical displacement) as in the dynamic analysis. In this case, the DIF represents the ratio of static versus dynamic analysis load values for initiating disproportionate collapse (ultimate loading capacity).

Table 3.4 gives a summary of the overload factors from the static analysis (Ω_S) and dynamic analysis (Ω_D), and also the resulting dynamic increase factors (DIF).

The minimum level of robustness for pure steel structure with semi-rigid connections (PS) is $\Omega_D = 1.05$ and is obtained for one internal column removal (S-PS-B2), with similar results for two column removal cases, S-PS-A12 and S-PS-A23. The structure is much less affected by one edge column removal (A1 and A3) resulting in the largest overload factors.

The influence of connection rigidity in the decrease of the DIF, see Figure 3.21, is explained by the fact that structures with semi-rigid connections have larger flexibility in the initial phase of column loss, therefore inertial forces are higher.

The dynamic increase factor, DIF, calculated for all scenarios, shows values less than 1.5 and is in agreement with other similar studies performed in the last years [110, 128-130].

The evolution of internal forces at beam-ends was examined in detail, particularly in S-FS-A23. Figure 3.22.b reveals three distinct stages of behavior on the bending moment and axial force at first-floor beam (section 1) versus column vertical displacement. The first stage (0-I) representing the elastic behavior and is characterized by a combined state of compression (arching) and bending. The external loads are resisted entirely by the bending action. At the end of this stage, plastic hinges develop at the beam ends. The second stage (I-II) represents the flexural mode and is characterized by plastic rotations and increasing axial forces. The external loads are resisted both by flexure and axial tension. The third stage (II-III) represents the catenary stage and is characterized by a drastic reduction of the flexural capacity at the plastic hinges while the catenary action continues to increase. The external loads are now mostly resisted by axial tension until the capacity is reached and the collapse is initiated.

Catenary action does not activate in the same extent on all floors. The floor immediate above the removed columns develops the highest level of axial force in the beams (Figure 3.22). The beams in the top floor are actually subjected to compression due to the inward displacement of the adjacent columns of the lost column. These columns are pulled inward by the catenary action developed in the beam. Thus, the assessment of structural performance in case of column loss events, must be performed on the entire structure.

Axial load in columns above the removed elements are very low, indicating that the loads on each floor are generally transferred by main beams they act upon. Lods are not transferred through the column.

Table 3.4 Overload factor from static dynamic analysis and dynamic increase factor

Scenario	(Ultimate) Overload factor, Ω		Dynamic increase factor
	Static analysis, Ω_S	Dynamic analysis, Ω_D	DIF=Ω_S / Ω_D
S-FS-A1	2.88	2.3	1.25
S-FS-A3	2.35	1.8	1.31
S-FS-B2	1.55	1.2	1.29
S-FS-A12	1.5	1.2	1.25
S-FS-A23	1.58	1.15	1.37
S-PS-A1	2.7	2.05	1.32
S-PS-A3	2.2	1.6	1.38
S-PS-B2	1.4	1.05	1.33
S-PS-A12	1.45	1.1	1.32
S-PS-A23	1.5	1.15	1.3
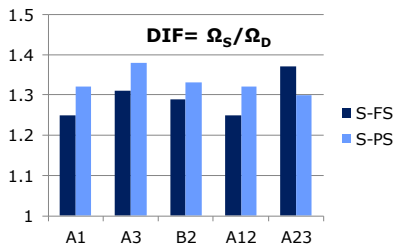
Figure 3.21. Dynamic increase factor
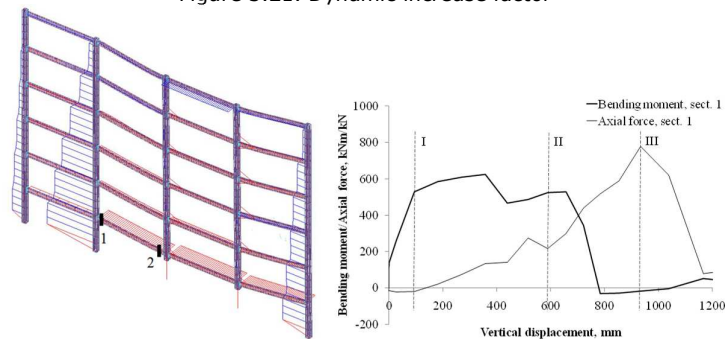
a) axial force diagram on deformed shape   b) bending moment and axial force

Figure 3.22. Scenario A-23 (frame A) [126]

3.2.3   Factors affecting column loss resistance

3.2.3.1 Column loss testing: static vs dynamic

Full-scale testing of column loss events in building structures is expensive and technically demanding. An exception would be the old buildings that are planned for demolition, which may be instrumented and tested before demolition. A great disadvantage would persist regarding the dynamic testing: only one initial load can be tested due to the plastic deformations that appear during testing. This issue makes the determination of the ultimate capacity of the structure in dynamic testing very difficult to achieve, unless several identical structures are tested under different initial gravity loads. This approach, even at acceptable costs, would be rather difficult to employ to study in detail the post-elastic behavior of the structure or the progression of damage in the structural components during the test.

Quasi-static testing, conducted using a gradual increase of the load, allows a detailed study of the components, and data are gathered for the entire post-yielding response until failure, using a single specimen.

Two main aspects cannot be investigated in a quasi-static column loss testing, namely the inertia forces (dynamic increase factor) and the strain rate effect on the material. In our studies, reported in previous sections, **the dynamic increase factor** ranges between 1.25 to 1.38, but for elastic or nearly elastic behavior these values could go up to 2. This factor can be taken into consideration in numerical analysis, without major calibration efforts for this specific aspect, as long as the damping of the structure is estimated correctly. Loading rate (or **Strain rate)** affects only material that undergoes plastic deformations. The areas with plasticized material are isolated near the connection and in beam plastic hinges. The material in such areas

can be changed considering such factors described in section 3.2.3.2. If, however, strain-rate would not be considered, the results for column loss scenarios are generally conservative.

3.2.3.2 Strain-rate influence

As mentioned in the previous section, the removal of a column, e.g. due to a blast, can have a duration on the order of milliseconds, which means is short enough to induce dynamic effects in the response of the material. For the scenario with highest plastic deformations and nominal loads (scenario S-PS-A23), maximum displacement and maximum strains are reached at 0.19 seconds after column removal, see Figure 3.23. A gross estimation of the deformation rate could consider a quasilinear linear deformation path. Therefore, a rough estimation of the strain rate could be obtained by dividing the maximum strains to the time interval up to reaching the maximum deformation.
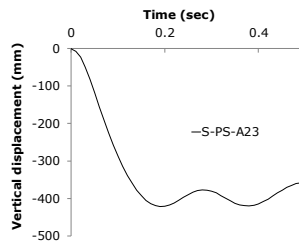
Figure 3.23. Vertical displacement in time for scenario S-PS-A23

For the beam, the average strain rate in the plastic hinge is 0.147 s^{-1} (at a strain of 0.028), while the average strain rate in the connection (mainly in the T-stub) is 0.279 s^{-1} (at a strain of 0.053). Considerable lower values are obtained for A1 and A3 scenarios. For S-PS-A3 for example, the maximum strain rate is 0.0267 s^{-1}.

For tensile material tests with a calibrated length of 150 mm, the loading rate necessary to obtain an average strain rate of 0.0267 s^{-1} is 4 mm/ sec, while for 0.279 s^{-1} is 42 mm/sec.

In the numerical analysis, the influence of the strain rate on the material properties (yield and ultimate strength) was approximated using the following equations [131]:

$$\frac{f_{ysr}}{f_y} = 1 + \frac{21}{f_y}\log\frac{\dot{\varepsilon}}{\dot{\varepsilon}_0} \tag{3.4}$$

$$\frac{f_{usr}}{f_u} = 1 + \frac{7.4}{f_y}\log\frac{\dot{\varepsilon}}{\dot{\varepsilon}_0} \tag{3.5}$$

$where: \dot{\varepsilon} = strain\ rate,\ \dot{\varepsilon}_0 = 10^{-4}$

$f_y, f_u = yield\ and\ tensile\ strength\ in\ quasi-static\ conditions, \dot{\varepsilon}_0 = 10^{-4}$

$f_{ysr}, f_{usr} = yield\ and\ tensile\ strength\ at\ strain\ rate\ \dot{\varepsilon}$

Using the equations (3.4) and (3.5), the strain rate influence at several loading rates have been computed for the S355 specimen with 150 mm calibrated length. Results are presented in Table 3.5. As seen in Table 3.5, for an increase of loading rate from 10 mm/s to 40 mm/s, the estimated results show a small difference, i.e. less than 0.9% for ultimate strength and around 3% for yield strength. Therefore,

also due to some limitations of the experimental facility, a low loading rate of 10 mm/s was planned for the experimental tests on T-stubs and weld details.

Table 3.5 Load rate influence on material properties

loading rate	$\dot{\varepsilon}$	f_{ysr} / f_y	f_{usr} / f_u
4 *mm/s*	0.027	1.144	1.036
10 *mm/s*	**0.067**	**1.167**	**1.042**
20 *mm/s*	0.133	1.185	1.047
40 *mm/s*	0.267	1.203	1.051
80 *mm/s*	0.533	1.220	1.055

3.2.3.3 Influence of beam-to-column connection type

Assumed in design or resulting from detailing and execution process, the connection characteristics may differ from those of a fully rigid and fully resistant connection [132]. The performance of connection impacts the response to column loss, see Figure 3.17.b. Thus, in a column loss scenario, frame structures with semi-rigid connections may undergo vertical displacements 20% to 40% higher than similar structures with rigid connections.

Most of connections used today in practice are either bolted or welded. The decision to adopt one solution or the other depends on the cost, experience of the steelwork contractors, specific limitations or conditions on site or of the system. As welding on site may be technically difficult - weather conditions, alignments, member support, difficult welding positions, in many cases bolted connections are preferred. Aesthetics may also be part of the design decision [133].

Extended end-plate bolted connections are used on a large scale, at least in Europe. These types of connections may fail by bolt fracture, end-plate or column flange yielding, shear failure of the column web panel, or by fracture of material in the beam or other components of the connection. Welded connections are sensitive to the detailing as well as quality of execution, but may fail also in the vicinity of the welds - heat affected zone. As each type of connection has several possible failure modes, to assess the critical failure mode (smallest resistance of all possible failure modes for that specific connection [134]), each type must be tested separately.

To cover a wide range of connection typologies, bolted and welded, and respectively, connections that are stronger or weaker than the beam, four types of specimens were chosen for the experimental tests, based on the matrix presented in Table 3.6. Frames with Cover Plate (CP), Extended End-Plate with Haunches (EPH), Reduced Beam Section (RBS), and Extended End-Plate (EP) connections will be experimentally tested for column loss scenarios. To compare the performance of the structure in case of a column loss, the same beams were used for the structures and only the connections were different [135]. Although the same beam was used, the performance of the connection led to different ultimate capacities, especially in case of a central column loss, or two columns loss scenarios, as these are scenarios where axial forces develop in the connections due to catenary action. The testing set-up was therefore designed to allow the development of catenary action in beams.

Table 3.6 Types of connections used in the experimental program

Connection type	Welded	Bolted
Rigid	Cover Plate (CP)	Extended end-Plate with Haunch (EPH)
Semi-rigid	Reduced Beam Section (RBS)	Extended end-Plate (EP)

3.2.3.4 Scale down vs. full scale specimens

The beams from moment resisting frames with full-strength connections range from IPE 400 to IPE 600, thus resulting in beam length over depth ratios (L/d) from 13.33 to 20. The maximum allowable space to test a full 3D structure (at INCERC Cluj-Napoca Laboratory) was 6.0 m by 6.0 m. Therefore, for a two-way double span structure to be tested, the span was limited to 3.0 m. For this beam length, in order to maintain the same L/d ratio interval, the height of the beam can vary from 225 mm to 150 mm. Hot rolled European profiles were considered for use. In order to allow the arrangement of at least three bolts rows inside the beam flanges for the connection, and to minimize the scale effect on the rotation capacity of beams, IPE220 section profiles were used for the beams.

Since the structure is a MRF on both directions, a solution for the columns was to use cruciform sections (hot rolled profiles - 2 x HEB). In order to allow the access for longitudinal welding of the two profiles, it was necessary to cut out the flanges of HEB260 profiles along both sides. In this way, the width of the profiles was reduced from 260 to 160 mm (50 mm from each side of the flange). The profile, marked as HEB260*, has wide/depth ratio close to the one of a HEB450. Some of the reasons for choosing this specific configuration can be explained using data from Table 3.7. Elements from the MRF structures designed for HSZ and LSZ are given as reference. Stiffness, resistance and geometric ratios between the beams and columns of the structures are computed and compared to ratios for the elements of the scaled down structure. The ratios of $W_{el,beam}/W_{el,column}$ and $I_{y,beam}/I_{y,column}$ for the scaled-down specimen are slightly higher (less than 10%) than the interval given by the two full-scale structures, but cutting less from the flanges (increasing column properties) would make difficult the welding of the two profiles.

Table 3.7 Types of connections used in the experimental program

Struct	element	profile	I_y [mm⁴]	W_{el} [mm⁴]	profile height	L [mm]	$W_{el,beam}/W_{el,column}$	$I_{y,beam}/I_{y,column}$	D_{beam}/D_{column}	L/D_{beam}
FS-HSZ	beam	IPE600	9.21E+08	3.07E+06	600	8000	0.185	0.278	0.667	13.33
	column	2xHEB900	4.97E+09	1.10E+07	900					
FS-LSZ	beam	IPE400	2.31E+08	1.16E+06	400	8000	0.258	0.291	0.889	20.00
	column	2xHEB450	8.98E+08	3.97E+06	450					
scaled-down	beam	IPE220	2.77E+07	2.52E+05	220	3000	0.267	0.315	0.846	13.64
	column	2xHEB260*	1.04E+08	7.99E+05	260					

For the 2D frame tests (joint tests), the reference structural system is an one way MRF system. For these tests, the scaled down column is a single HEB260 profile also with the flanges reduced by cutting out to 160 mm, as reference structure columns are individual profiles. In case of 3D frames tested experimentally, the cruciform columns are made from HEB260* profile, as the reference structure is considered a 2-way MRF with cruciform columns.

3.2.3.5 3D vs. 2D testing

3D testing is certainly more realistic than 2D testing, but more difficult and requires higher costs . For pure steel structures, in case of central column loss with perfect symmetry conditions, a 3D steel frame response capacity would be the sum of the capacities of the 2D frames connected to the central column (ideal behavior transfers half the force in each direction), therefore 2D tests may be performed

instead. However, a reason for choosing 3D instead of 2D, even for pure-steel structures, is the evaluation of the ultimate capacity in the catenary stage. 2D or 3D test or analysis may lead to different conclusions and the ideal behavior that transfers half the force in each direction may not be valid. Thus, at failure, the system is more a "serial" system and not a "parallel" system. On the other hand, if the floor system is interacting with the steel frame, 2D tests are not able to provide an accurate prediction of the structural response in case of column loss, as they will not take into account the membrane response of the floor system and other complex interactions. For such tests, a 3D structure is recomended. The experimental program on 3D structures contains three different types of floor systems.

For assessing the behavior of different types of connections, 2D tests with appropriate boundary conditions would provide necessary information, and would be more economic and also practical, due to simplified structures with fewer parameters and less calibration difficulties.

3.2.3.6 Testing methods and boundary conditions for 2D and 3D tests

Distributed gravity loads on the floors is the most common arrangement of permanent and live loads in design. The experimental tests for column loss scenario with uniform load distribution are performed by applying a distributed load (UDL) along the beam in an initial stage, followed by the release of the support at the lost column, either quasi-static or dynamic (UDL method). An alternative to this method is to gradually increase a point load (PL) at the missing column location, with or without distributed loads along the beam (PL method). Liu et al. [68] investigated the differences between these two methods for low forces (maximum 22% of the system capacity) and proved almost identic behavior in case of the two loading methods. In the 2D and 3D tests that were performed in this study, the second method has been adopted, i.e. gradually increase of a point load at the missing column location, without any additional distributed load on the beams.

A specific attention was given to the restraints of the specimens against lateral and vertical displacements in order to create similar conditions to those in the reference structure. For example, the development of the catenary action in the beams that are adjacent to the lost column depends, among other factors, on the restraining effect provided by the adjoining structure [112]. Therefore, preliminary simulations were performed to calibrate the position, size, and local detailing of the restraining system to fulfil these conditions.

3.2.4   Overview of the experimental program

The experimental program has three main sections, which are presented in separate sections, i.e. tests on connection macro-components under different loading conditions, 2D frames against column loss, and 3D frames against column loss.

The connection macro-components were tested at room and elevated temperatures at different loading rates in order to assess the influence of the strain rate for different types of bolted and welded connection macro-components.

The two span 2D frames were subjected to a quasi-static vertical loading, applied at the middle column, to investigate the performance of different connection typologies and the effects of bending moment - axial force interaction on the ultimate resistance, deformation capacity, and failure mode.

The two span and two bay 3D frames were also subjected to a quasi-static vertical loading, applied at the internal column, to investigate the contribution of the

concrete floor slab to the performance of steel frames in case of column loss. Results on pure steel frame were also used to compare 3D test with 2D test.

3.2.4.1 Material of tested structures

The beams, column, plates and diagonals were specified as S235, S275 and S355. Bolts were specified as 8.8 and 10.9 class. The concrete used for the slab in the 3D test was normal weight concrete class C20/25. The shear connectors used also in the 3D test were specified as S235J2+C450. Material tests were performed prior each type of testing. The concrete tests were performed both at 28 days and in the day prior to testing.

Three coupons were fabricated from each type of steel elements according to ISO 6892-1:2009 [136] and tested at room temperature with the INSTRON universal testing machine at the UPT-CMMC laboratory (INSTRON Fast track 8805). A typical coupon specimen dimensions is shown in Figure 3.24. The compressive strength tests on concrete specimens were performed at INCERC Cluj-Napoca laboratory.

The results of tests on materials were used for preliminary numerical analysis of the models, in order to design and detail the test set-up (actuator capacity – stroke and force, restraining system – if any) and the instrumentation (position and type of displacement transducers).
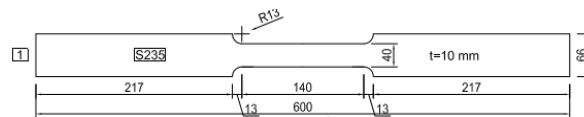
Figure 3.24 Coupon specimen

The tensile tests were performed at the *Research Center for Mechanics of Materials and Structural Safety* – CEMSIG Laboratory of Politehnica University Timisoara, Romania on an INSTRON and a UTS universal testing machine and the elongations were measured using a video extensometer module. Two points at each end of the calibrated length of the coupons were visually monitored during the tensile test with an Advanced Video Extensometer (AVE - see Figure 3.25) in order to get an accurate relative displacement, avoiding errors such as grip slippage and influence of the elasticity of the machine itself.

Detailed information regarding the test results for each material are given in sections corresponding to testing of the three categories of specimens, for the material related coupons.

Figure 3.25. Tensile test in progress

3.3   Tests on connection macro-components

The first experimental program focused on the behavior of connection components, i.e. bolted T-stubs and welded connections, at large deformation stage. The main objectives of the research were:

- to evaluate the ultimate capacity and the failure mode of bolted T-stub components under large deformation demands;

- to investigate the capacity of Eurocode provisions (EN 1993-1-8) to predict the response of bolted T-stub components under large deformation demands;

- to investigate the main parameters that affect the response of bolted T-stub components and to propose new recommendations for the design of beam-to-column connections that are subjected to large deformations and catenary action;

- to evaluate the capacity of common welding details and procedures to allow the development of large plastic deformations in the base material without fracture in the weld.

The loading was applied in quasi-static and dynamic conditions. In addition, to simulate the effect of fire, specimens were tested at room temperature (20 ºC) and elevated temperature (542 ºC), respectively. However, in the thesis only the results at room temperature are reported. The experimental results at elevated temperature are presented elsewhere ([137],[138]).

3.3.1   Test set-up and loading protocol

The universal testing machine INSTRON (INSTRON Fast track 8805) was used for the tests, see Figure 3.26.

Specimens (bolted T-stubs, welded details) are double symmetrical. The specimens are fixed at the top end in the hydraulic grips, while at the lower end are fixed using bolts.
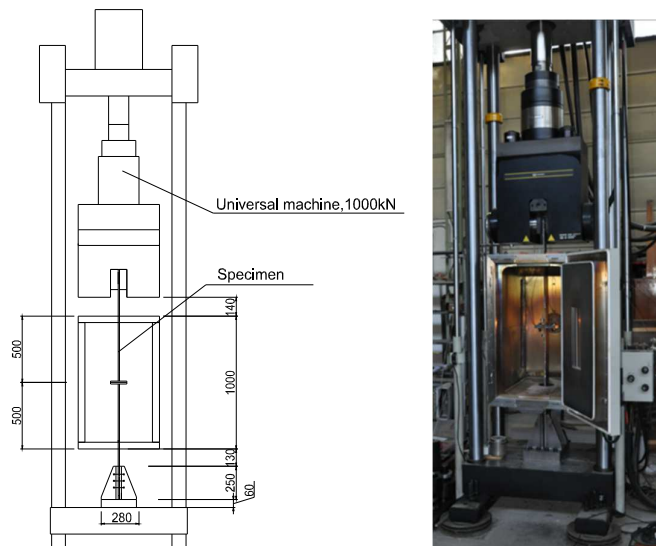
Figure 3.26 Conceptual scheme and illustration of test set-up

The loading rates were 0.05 mm/s for quasi-static loading and 10 mm/s for dynamic (strain-rate) loading. In the initial position, the upper hydraulic grips are closed after calibrating the machine to zero force. Fixing the upper end of the specimen usually induces external forces in the specimen, therefore the track is manually moved up to a zero force is obtained. For strain rate loading, an initial loading at 0.05mm/s is applied for two seconds, afterward the imposed displacement is done at a rate of 10mm/second. T-stub loading conditions and the name of each series of tests are presented in Table 3.8 T-stub loading conditions labels (in bold are the test reported in the thesis).

Table 3.8 T-stub loading conditions labels

Loading conditions		Low strain rate "Static" 0.05 mm/ s	High strain-rate "Dynamic" 10 mm/ s
Normal temperature:	**+20° C**	**C**	**CS**
Elevated temperature:	+542° C	T	TS
Low temperature:	-35° C	L	LS

3.3.2   Instrumentation

The force was applied directly from the testing machine, using a displacement control. Preliminary tests (Figure 3.27.a) showed that for the bolted T-stubs, the displacement between the two end-plates is identical with the imposed displacement. This is due to the high axial rigidity of the web in comparison with the flexural rigidity of the end-plate. Thus, for assessing the deformation of the T-stub, besides the testing machine track displacement transducer no other displacement transducers were used. This was very convenient for tests at other temperature.

For the welded T-stub, two displacement transducers were used to measure the absolute displacement of the upper and lower ends of the calibrated (reduced) zones, see Figure 3.27.b. The deformation of the calibrated zone is therefore obtained as the difference between these two measurements (external transducers / machine track displacement transducers).

a) bolted T-stub preliminary tests   b) welded T-stub instrumentation
Figure 3.27 test instrumentation tests
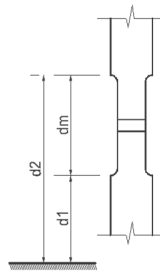
In addition, for the welded T-stub, strains and displacements on one of the two calibrated zones were measured using a digital image correlation device DIC, called VIC-3D [139]. DIC is an optical method which measures deformations on object's surface [140] using two photo cameras, see Figure 3.28.a. The images, one before and one after deformation, are recorded, digitized and compared to detect displacements. The comparison is done by searching a matched point from one image to another. Because it is difficult to find the matched point using a single pixel, an

area with multiple pixel points, called subset, is used to perform matching process. The subset has a unique distribution of light intensity (gray level). The displacement of the subset is found by searching the area of same gray level distribution in the two images taken before and after the deformation. To achieve sub-pixel accuracy, the correlation algorithms use gray value interpolation, representing a field of discrete gray levels as a continuous spline. The DIC system used had a point-to-point strain accuracy of 0.02%.

The trigger for stereo image acquisition is set at a rate of 5 seconds for static loading protocol (at a deformation rate of 0.25 mm) and respectively at a rate of 0.25 seconds (4 frames / s) for dynamic loading protocol (at a deformation rate of 2.5 mm / s).
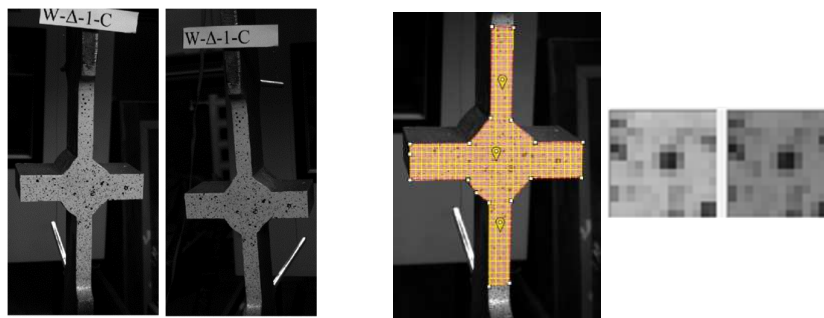
a) left and right view of cameras   b) subset size with tracking for both cameras
Figure 3.28. Specimen instrumented for testing

3.3.3   *Experimental specimens*

3.3.3.1 Welded T-stub specimens

Three types of weld specimens were designed and fabricated, i.e. fillet weld (Δ), single bevel but-weld (V) and double bevel but-weld (Y), see Figure 3.29.a. Two identic specimens were tested for each condition (quasi-static loading, strain rate loading). The entire set of specimen is presented in Table 3.9.

Table 3.9. T-stub welded test specimen label description

test	Weld type	Loading rate
W-Δ-C-test1	fillet weld (Δ)	0.05 mm/s (-)
W-Δ-C-test2		
W-Δ-CS-test1		10 mm/s (S)
W-Δ-CS-test2		
W-V-C-test1	single bevel but-weld (V)	0.05 mm/s (-)
W-V-C-test2		
W-V-CS-test1		10 mm/s (S)
W-V-CS-test2		
W-Y-C-test1	double bevel but-weld (Y)	0.05 mm/s (-)
W-Y-C-test2		
W-Y-CS-test1		10 mm/s (-S)
W-Y-CS-test2		

The components of the welded T-stubs were made from two 15 mm thick plates (web) welded on a perpendicular 25 mm thick plate (end-plate). The total length of the specimens is 1645 mm, see Figure 3.29.b. To assure the properties of

the steel components are identical in all specimens, similar components were fabricated from the same steel plate.

Metal inert gas (MIG) process and 1.2 mm wire were used for welding. In order to obtain a continuous weld with uniform properties in the fabrication of specimens with the same weld type, the entire plates of the webs and end-plates were welded in an initial phase. Afterward, the specimens were cut/machined (the entire web-end-plate connection macro-component), and no other welding was necessary.

The width of the webs was reduced near the end-plate to ensure that the plastic deformation is concentrated near the welds.
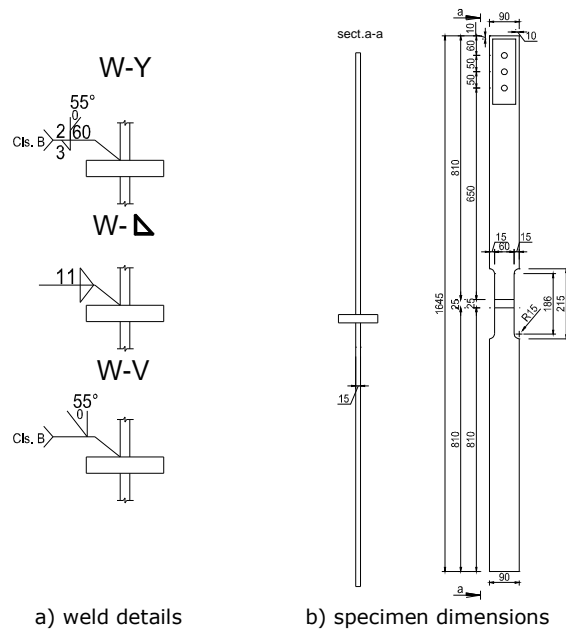
a) weld details   b) specimen dimensions
Figure 3.29 Welded T-stubs and specimens

3.3.3.2 Bolted T-stub specimens

The bolted T-stub configurations have been designed to fail in mode 1 and 2. From the different possible configurations, the following typologies have been selected for the experimental program: T-10-16-100; T-10-16-120; T-10-16-140; T-12-16-100; T-12-16-120; T-12-16-140. The first letter represents the bolted T-stub, the second term represents the thickness of the end-plate, followed by the diameter of the bolt and the distance between the bolts, all in mm ([46, 141] [137, 138]).

The steel grades were S235 for end-plates, S355 for webs, and M16 class 10.9 for bolts. The bolts were normally tightened (no controlled preloading was applied).

As in the case of welded T-stubs, components of the specimens with the same thickness and steel grade were fabricated from the same steel plate, to assure the same material properties.

T-stubs were fabricated using fillet weld, with a 7 mm throat thickness, and using metal inert gas (MIG) process and 1.2 mm wire. In order to obtain a continuous weld with uniform properties, in the fabrication of specimens with the same bolt

distance (including specimens to be tested at elevated temperature) the entire plates of the webs and end-plates were welded in an initial phase. Afterward, the specimens were cut (web-end-plate macro-component), and no other weld were necessary.

Each test was performed by connecting two identical T-stubs using two bolts M16, class 10.9. The nominal dimensions of a T-stub are presented in Figure 3.30 and detailed in Table 3.10.
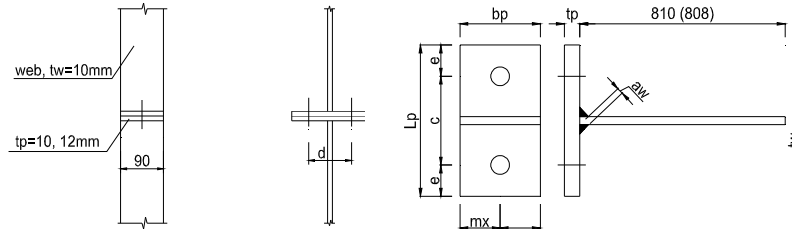
Figure 3.30 Bolted T-stub geometry

Table 3.10. Bolted T-stub specimens [mm]

Specimen	Dimensions in mm, Figure 3.29								Loading rate
	a_w	t_w	t_p	b_p	L_p	c	e	m_x	
T-10-16-100-C	7	10	10	90	160	100	30	45	0.05 mm/s (-)
T-10-16-100-CS	7	10	10	90	160	100	30	45	10 mm/s (S)
T-10-16-120-C	7	10	10	90	180	120	30	45	0.05 mm/s (-)
T-10-16-120-CS	7	10	10	90	180	120	30	45	10 mm/s (S)
T-10-16-140-C	7	10	10	90	200	140	30	45	0.05 mm/s (-)
T-10-16-140-CS	7	10	10	90	200	140	30	45	10 mm/s (S)
T-12-16-100-C	7	10	12	90	160	100	30	45	0.05 mm/s (-)
T-12-16-100-CS	7	10	12	90	160	100	30	45	10 mm/s (S)
T-12-16-120-C	7	10	12	90	180	120	30	45	0.05 mm/s (-)
T-12-16-120-CS	7	10	12	90	180	120	30	45	10 mm/s (S)
T-12-16-140-C	7	10	12	90	200	140	30	45	0.05 mm/s (-)
T-12-16-140-CS	7	10	12	90	200	140	30	45	10 mm/s (S)

3.3.4 Experimental results

The results of the tensile test on steel plate components and bolts are given in Table 3.11 and Table 3.12.

Table 3.11 Average characteristic values for the steel plates of welded T-stubs

Element	f_y	f_u	A_{gt}	A_t
	N/mm²	N/mm²	%	%
Welded T-stub detail web, t = 15 mm	299	402	15.71	24.11
Welded T-stub detail end-plate, t = 25 mm	261	441	16.43	22.92

Table 3.12 Average characteristic values for the steel plates and bolts of bolted T-stubs

Element		f_y	f_u	A_{gt}	A_t
		N/mm²	N/mm²	%	%
Bolted T-stub web, t = 10 mm		390	569	18.7	26.5
Bolted T-stub end-plate	t = 10 mm	310	408	22.5	34.7
	t = 12 mm	305	445	23.3	32.7
Bolt, M16		965	1080	5.0	6.5

3.3.4.1 Welded T-stubs

The geometric measurements of the specimens before the test are presented in Table C.1 from ANNEX C, with the notations of the geometrical lengths presented in Figure C.2. The geometric properties of the T-stubs are close to the nominal ones.

For welded T-stub tests, the monitored deformation was measured using as reference the length of the reduced section – the calibrated length. Figure 3.31 presents the force-displacement curves for the welded specimens, tested under static and dynamic loading. The maximum force is higher for specimens tested under dynamic loading, and in most cases is accompanied by a small decrease of the ductility.

All specimens, before fracture, developed necking in two zones of the reduced section of the web (at the bottom and top of the welded end-pate), see Figure 3.31. No damage could be observed in the heat affected zone. Views of the reduced area at failure are presented in Figure 3.32.

The yield strength (f_y) increases from 20% to 33%, while the maximum strength (f_u) increase does not exceed 10%. The highest reduction of ductility is obtained for W-Δ tests, respectively 22%, but is not a generalized phenomenon.

Detailed views with the welds for all specimens before and after the test are shown in Figure C.3. Although in some cases small cracks developed in the weld, they did not influence the ultimate capacity (strength and deformation) of the T-stub, as the failure and deformability were governed by the material properties of the web. For specimens tested at high strain rate, the extent of cracking in the welds was, in most cases, higher than for the specimens tested at low strain-rate.
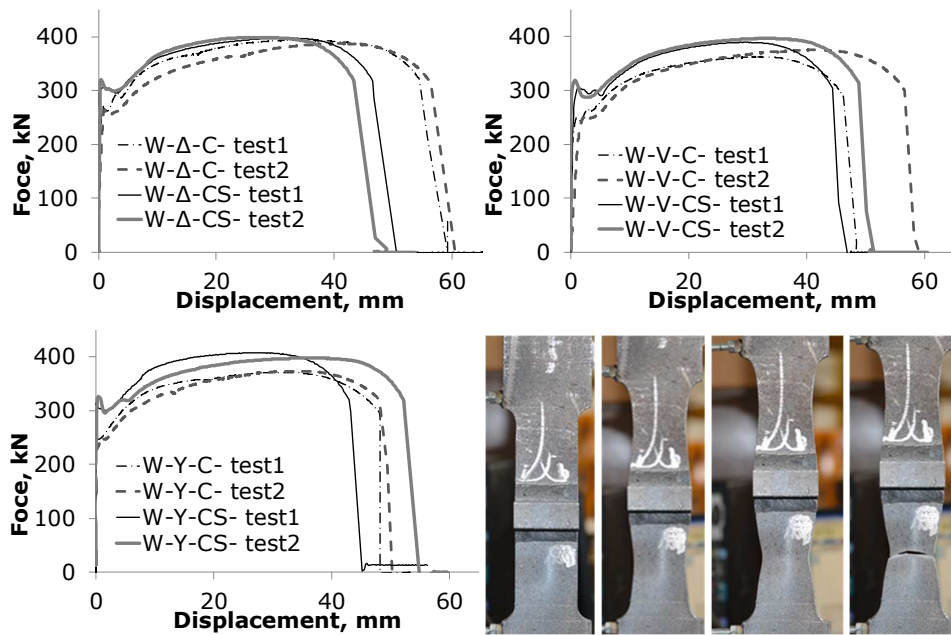
Figure 3.31. Force-displacement curves for welded T-Stubs
and failure development of welded T-Stub W-Δ-C-test1 (bottom-right) [142]

Specimens have been monitored using advanced image correlation (VIC [139]) in order to obtain a map of average specific deformations. The surface of the specimen was prepared as described in section 3.3.2. The system was calibrated by taking gray stereo photos with both cameras for the same position of a target with a calibration grid. The system can recognize the dot grid on the target, see colored dots in Figure 3.33, and computes the relative position and angle of the cameras and the distance between the cameras and the calibrated zone. Before the test, a stereo image of the speckled surface is taken and processed with the dedicated software to verify the calibration, the focus of the cameras, and quality of the random speckle pattern on the monitored surface. The plane irregularity (surface roughness) of the monitored surface before the test is presented in Figure 3.33 (left).

Data obtained from VIC measurements are given in ANNEX C (Figure C.4 to Figure C.14). The pictures are taken just before fracture, when T-stubs are still in tension, therefore the strain values include plastic strain and elastic strain. Maximum values are given in Table 3.13, where e_1 [%] is the major strain, e_2 [%] is the minor strain and e_{xy} [%] is the shear strain. These are Lagrangian finite strain tensors, therefore finite strain measures with gradients defined in terms of the original configuration. To note that the Lagrangian strain can become much larger than the engineering strain and is commonly used for materials that undergo large strains [143].
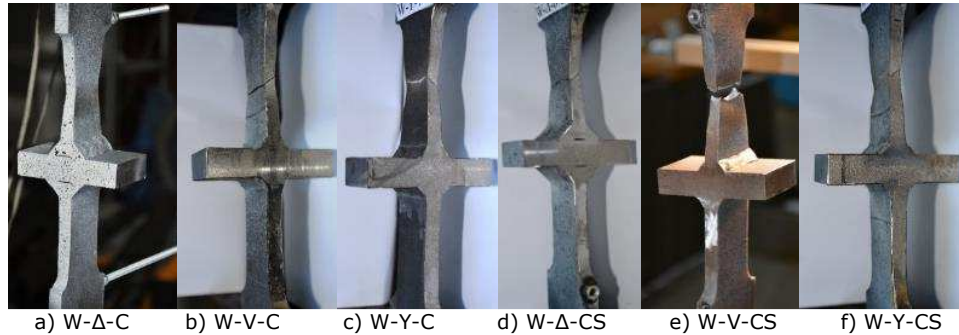
a) W-Δ-C   b) W-V-C   c) W-Y-C   d) W-Δ-CS   e) W-V-CS   f) W-Y-CS
Figure 3.32 Reduced zone of welded T-stubs at failure

Table 3.13. Welded T-stub test maximum strain

	e_1 [%]		e_2 [%]		e_{xy} [%]	
test	min	max	min	max	min	max
W-Δ-C-test1	-0.5	96.5	-21.4	0.3	-4.65	4.4
W-Δ-C-test2	0	100	-22.4	0.1	-4.1	2.95
W-Δ-CS-test1	0	40.4	-13.4	0.1	-2.26	2.12
W-Δ-CS-test2	-0.4	43.4	-12.3	0.3	-3.85	3.65
W-V-C-test1	-0.5	96.5	-25.8	4	-2.18	1.5
W-V-C-test2	-0.5	88	-20.8	0.1	-3.7	1.3
W-V-CS-test1	-0.5	59.5	-17.1	0	-0.87	0.48
W-V-CS-test2	-0.5	74.5	-17.7	0.1	-1.78	1.34
W-Y-C-test1	n.a	n.a	n.a	n.a	n.a	n.a
W-Y-C-test2	-0.5	74.5	-18.6	0.4	-3.72	1.12
W-Y-CS-test1	-0.4	29.4	-10.5	0.25	-0.64	3.58
W-Y-CS-test2	-0.5	59	-19.9	0.1	-0.32	1.42

The principal strain may reach 100% (1) in the failure zone for the static tests, while in the dynamic tests the average is approximately 51% (0.51). This reduction

is also due to the fact that in the dynamic tests, it is much more unlikely to get a stereo image of the specimen near failure as the trigger per deformation rate is 10 times lower, see 3.3.2. Due to the same reason, also in the failure zone, the minimum secondary strain is about -21% for static loaded specimens and about -15% for the dynamic loaded specimens. No principal strains appear in the welding, as they are concentrated in the reduced zones of the web due to necking. The shear tensor in the monitored surface plane, on the other hand, is concentrated only in the welds, reaching about ±2%. However, comparing the measurements from *Table C.2. Welded T-stubs dimensions measured before test* and *Table C.3. Welded T-stubs dimensions measured after test, an average* 24.1% elongation for the entire calibrated zone resulted from low loading rate tests, while the average elongation for high loading rate tests was reduced just with 2.23% related to the initial calibrated length.

The good quality of the welds prevented failure in the weld, therefore no difference could be observed between the three types of welds in terms of performance.
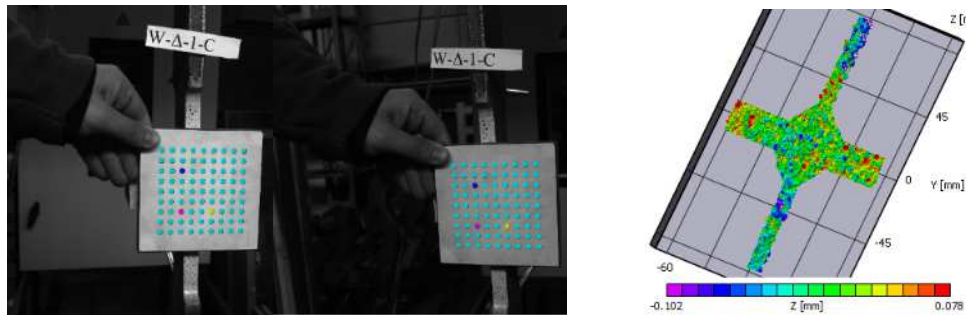
Figure 3.33 VIC calibration

3.3.4.2 Bolted T-stub

Figure 3.34 shows the force-displacement curves for static and dynamic tests on bolted T-stubs. It may be seen that the increase of the end-plate thickness increases the resistance but reduces the ultimate deformation capacity. When the distance between bolt rows increases from 100 to 120 mm, there is a reduction of the resistance, but the deformation capacity increases. When bolt row distance increases from 120 mm to 140 mm, the deformation capacity increases without a reduction of the ultimate resistance. The failure is ultimately attained due to the fracture of the bolts in all cases, see Figure 3.35.

No failure of the welding has been observed, even though for the most ductile specimens (with 140 mm bolt row distance) some cracks developed near the welding toe, in the heat affected zone, see Figure 3.36. There is a small influence of the loading rate, in terms of ultimate resistance, deformation capacity and failure mode ([141, 142]).

a) 10 mm thick end-plate   b) 12 mm thick end-plate
Figure 3.34. Force-displacement curves for bolted T-stubs [142]

a) T-10-16-100-C   b) T-10-16-120-C   c) T-10-16-140-C

d) T-10-16-100-CS   e) T-10-16-120-CS   f) T-10-16-140-CS

g) T-12-16-100-C   h) T-12-16-120-C   i) T-12-16-140-C

j) T-12-16-100-C   k) T-12-16-120-C   l) T-12-16-140-C
Figure 3.35 Bolted T-stub specimens after failure [46]
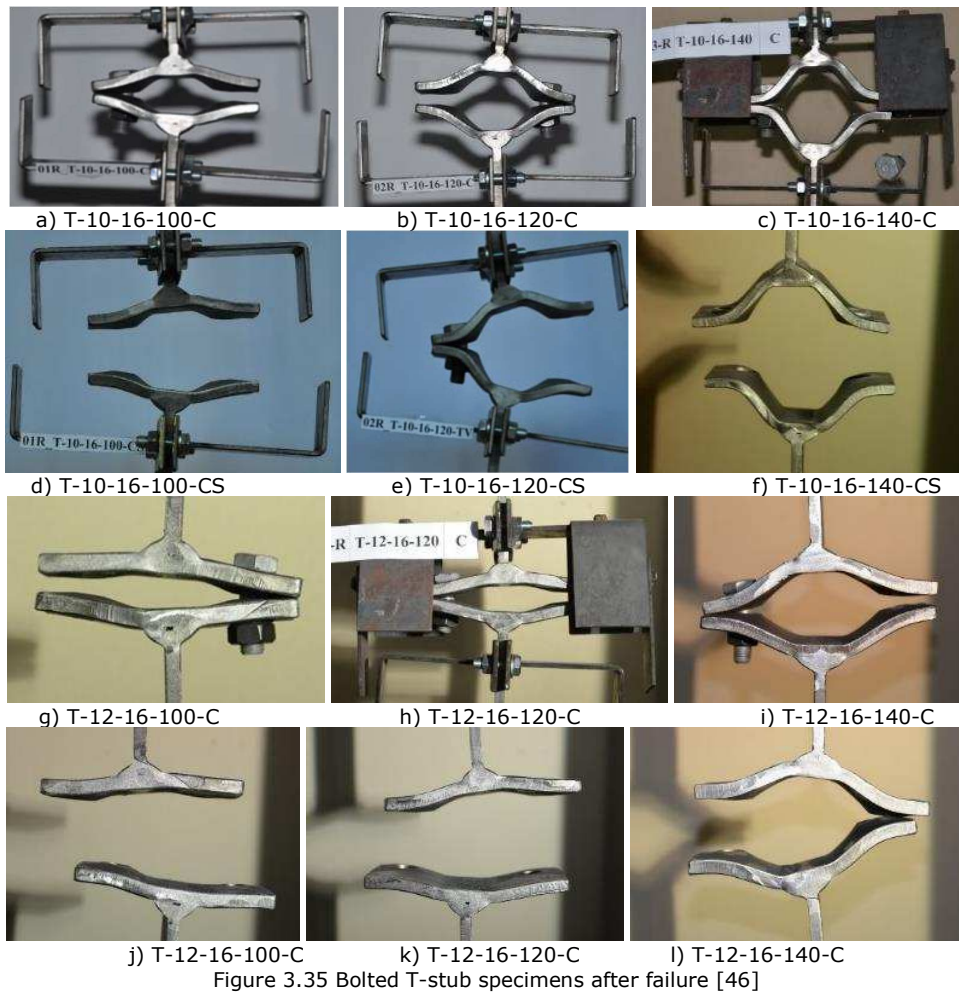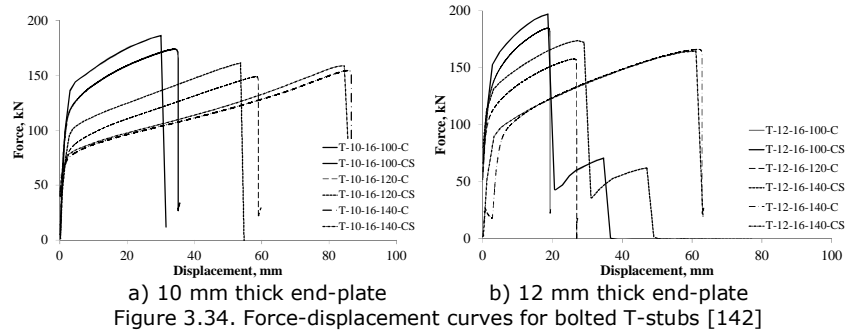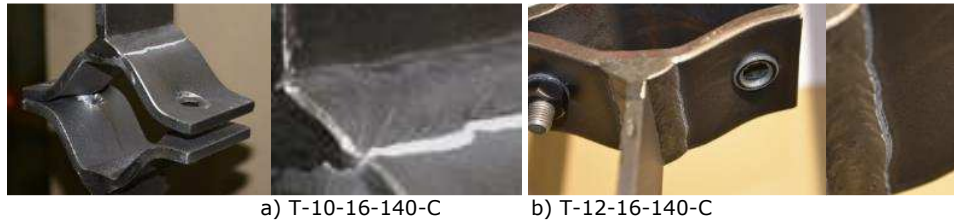
a) T-10-16-140-C   b) T-12-16-140-C
Figure 3.36 Cracks near the welding for the specimens with largest deformations: [142]

3.3.5   Comments related to connection macro-component test results

The experimental results on the welded connection macro-components showed no important changes in the performance and failure mode of the three types of weld. If loading rate increases from 0.05 mm/s to 10 mm/s, there is a moderate increase in ultimate resistance capacity, while the deformation capacity reduces with a similar ratio. Proper welding prevents dammage in the weld or heat affected zone.

The interaction between end-plate thickness, bolt diameter, and bolt distance can be used to identify the best ratio between strength and deformation capacity that is required for collumn loss scenarios. The design based on EN 1993-1-8 provisions cannot be used for such situations, as the post yielding capacity for mode 1 and mode 2 T-stubs is ignored. The increase of the T-stub flexibility increases the deformation capacity but induces additional effects on the bolts, i.e. increase of prying forces and reduction of capacity due to N-M interaction. The effect of strain rate decreases as the distance between bolts increases (end-plate flexibility).

3.4   2D frame tested for column removal

The planar frame systems selected for experimental testing were extracted from a moment resisting frame at the first floor of a reference building presented in the 2013 CODEC research report [144]. The tests were performed in the CEMSIG Laboratory of UPT.

In order to allow a planar testing configuration, out of plane beam-to-column connections were released. The stability of the structure was provided by vertical braces in perimeter frames. Figure 3.37 shows the plan layout of the full-scale structure with moment resisting frames on transversal direction and braces on longitudinal direction. The bays and spans each measure 8.0 m. The highlighted area indicates the perimeter frame extracted for investigation. Due to space limitation in the laboratory, the frame was scaled down from 8.0 m span to 3.0 m span as presented in section 3.2.3.4. Four specimens were constructed, each with a different type of beam-to-column connection, see section 3.2.3.3.
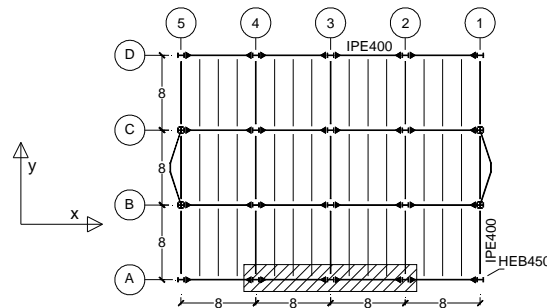
Figure 3.37: Reference building layout plan with position of extracted specimens for testing

3.4.1   Test set-up and loading protocol

The test specimen consists of two steel beams and three columns, and have two spans of 3.0 m each (between the centerlines of the columns).

The boundary conditions that resemble the constraints in the reference structure are provided using a strong reaction wall, on one side (left) and a brace system, on the other side (right). To simulate the central column removal, the specimen is loaded vertically on top of the middle column by a 1000 kN actuator (Figure 3.38). The vertical force is applied using a displacement control until complete failure of the specimen. The displacement is gradually increased at a rate of 2 mm/min) to ensure a quasi-static response.
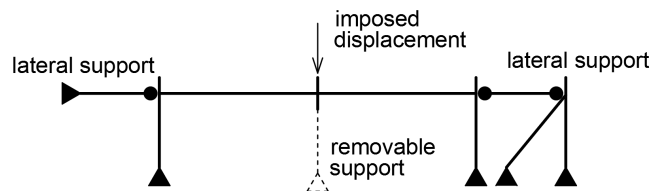
Figure 3.38 Boundary conditions and application of loading

The development of the catenary action in the beams after a column loss depends very much on the lateral stiffness of the system. Without lateral restraint, the structural system resists the vertical loads only by flexural action. In case of steel frame structures, the lateral stiffness can be insufficient to prevent in plane displacements after a column loss, for example in case of a penultimate column loss. The floor system may increase this capacity through the diaphragm effect.

For the design of the in-plane lateral restraining system, double-hinged elements were used to transfer lateral forces from the specimen to the reaction wall and the strong slab, respectively. From the preliminary numeric analysis, the maximum force transferred in the catenary stage was measured and used to design the double-hinged elements (*links*). The West link, connected directly to the reaction wall, has an axial rigidity of 1.31mm/1000 kN, and resembles the stiffness of a braced span in the equivalent scaled structure. The East link, connected to a triangular assembly that is connected to the rigid beam on the strong slab, has a stiffness of 8.03mm/1000 kN, very similar to a moment resisting frame span in the equivalent scaled structure. The two pins that connect the links are made from 60 mm diameter steel rods. This asymmetry of the in-plane restraining system is more a rule than a particularity, as even for symmetric structures, unsymmetrical conditions arise in case of a column loss.

To avoid out of plane displacements of the specimen during testing, lateral supports were used along the beam span and at the central column. These supports also prevent the lateral torsional buckling of the beam and allow the beam to reach plastic moment capacity. For reducing the friction with the specimen, contact plates made from low friction materials (i.e. Teflon) were used. Even it obstructs the visibility during testing, the lateral restraining system at the central column is very important, especially for large deflections stages, as out-of-plain instability is expected to occur [145]. To note that in plane rotations of the central column are not prevented.

Figure 3.39 shows the specimen and test set-up, with the position of the in-plane and out of plane restraining elements.
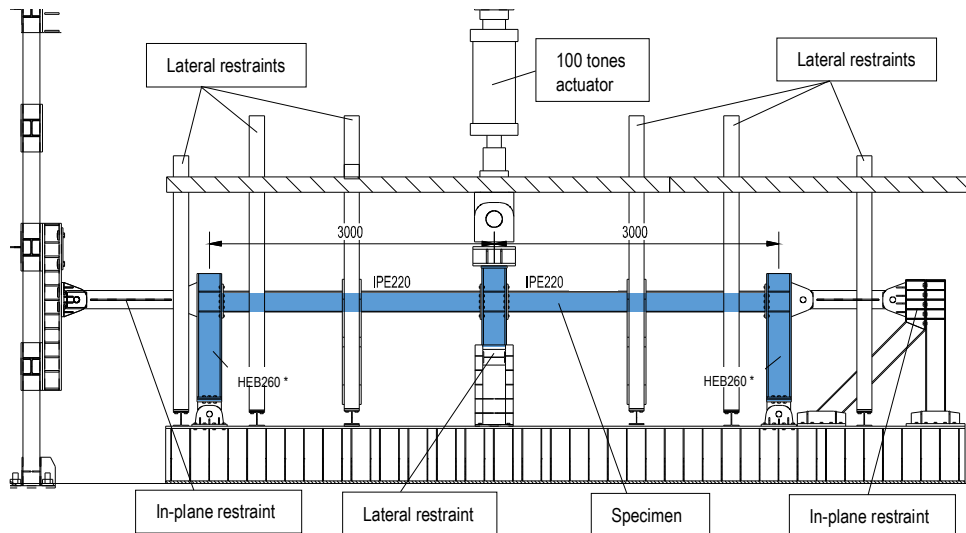
Figure 3.39 Detailed view of the test set-up

Figure 3.40 presents an isometric views of the assembly specimen-test set-up and the notations used for geometrical characteristics and instrumentation. In the figure, the right is East (E), the left is West, the upper direction is top (T) and the downward direction is bottom (B). Perpendicular on the plane, behind is North (N) and front is South (S). The connections are numbered from West to Est from 1 to 4, connection 2 and 3 being the ones on the West and respectively the East sides of the central column.

Figure 3.41 shows a view from the laboratory with the specimen ready for testing.
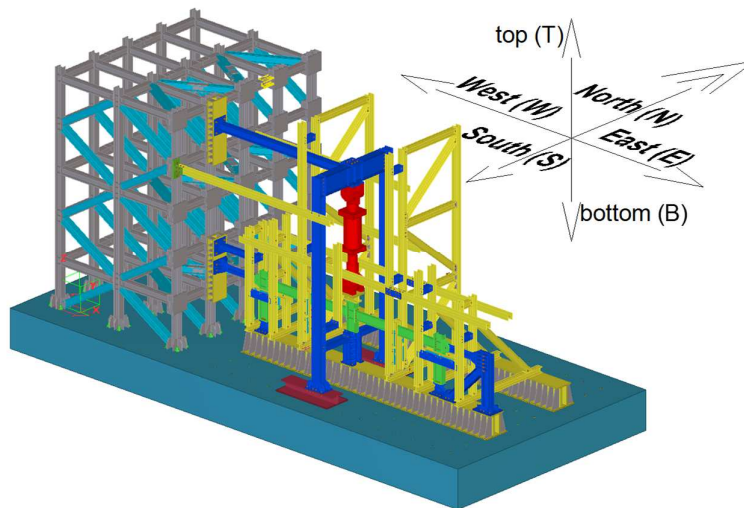
Figure 3.40 Isometric view of the assembly specimen-test set-up
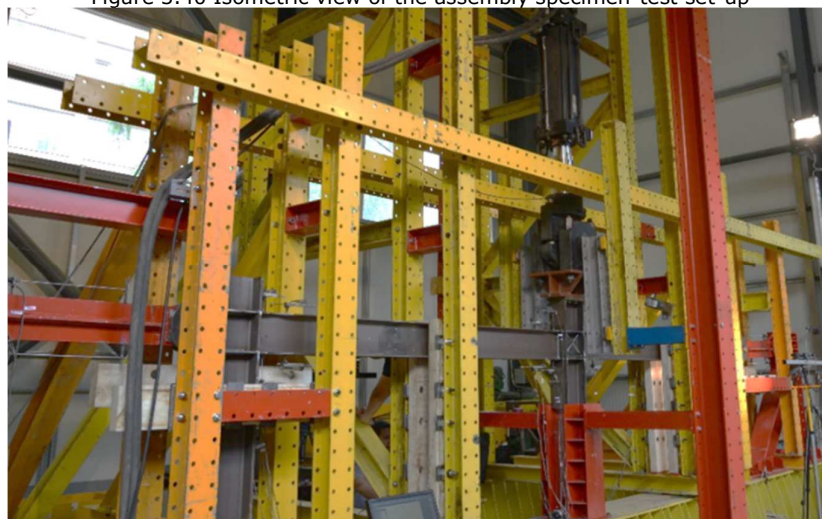
Figure 3.41. View with a specimen ready for testing

3.4.2   Experimental specimens

To allow direct comparisons between results, all beams and columns were fabricated from the same profiles, i.e. IPE 220 for beams and HEB260* for columns, respectively. Surface of the specimens was treated using sand blasting. Welds (and non-destructive testing) were made in the workshop while bolted specimens were assembled in the laboratory using site bolting.

In the next sections, detailed information about each specimen are provided.

3.4.2.1 Cover plate specimen (CWP)

The cover plate welded connection was designed according to *section 3.5.4 "Welded Flange Plate Connections"* from chapter *3 "CONNECTION QUALIFICATION"* of FEMA 350 [146]. The top and bottom cover plates are 12 mm thick, with 130 mm width and 150 mm length. Cover plates are welded to the column flange using complete joint penetration CJP groove welds and with fillet welds to the top and bottom beam flanges. Beam web is connected using a shear tab and two M16 class 10.9 bolts, reinforced with filet welds. Figure 3.42 shows a detailed view of the connection and a view of the central joint before testing.
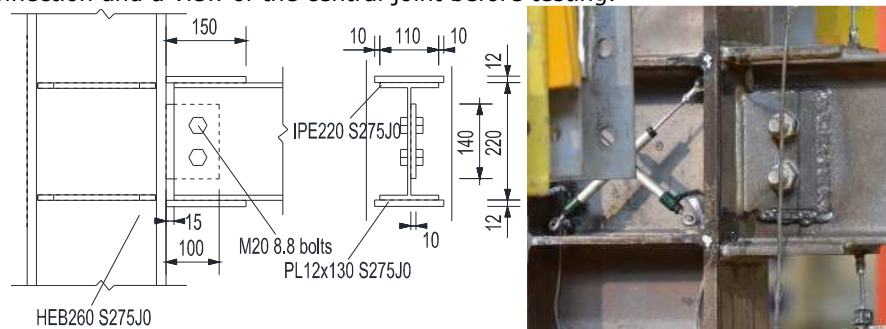
Figure 3.42. Details of CWP specimen (dimensions in mm)

3.4.2.2 Extended end-plate with haunch specimen (EPH)

The extended end-plate with bottom haunch (EPH) bolted connection was designed using EN 1993-1-8 [147] for a resistance capacity 1.375 times higher than the beam. The overstrength requirement was taken according to EN 1998-1 [117]. The characteristics of the connection were calculated using *STeel CONnection* [148] commercial software. The 20 mm thick end-plate is connected to the column flange using six bolt rows M20 class 10.9. The bolts were normally tightened (no controlled preloading was applied). The height of the haunch is 110 mm while the length is 150 mm (same length as for cover plates in CWP). Full penetration welds connect beam flanges to the end-plate. Figure 3.43 presents the dimensions of the EPH specimen and a view of the central joint before testing.
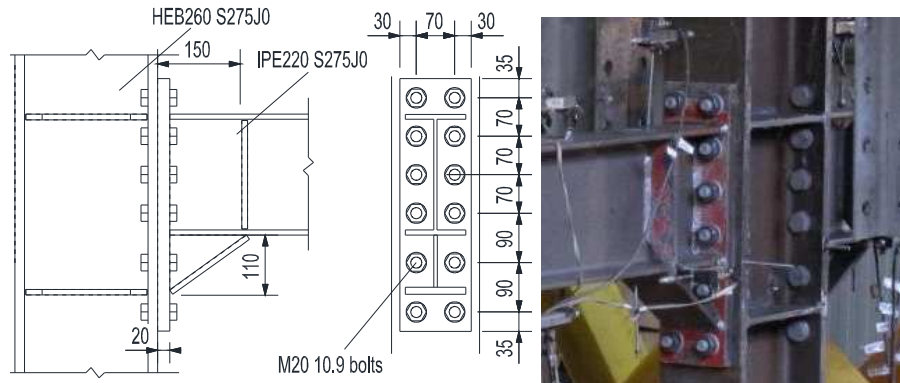
Figure 3.43. Details of EPH specimen (dimensions in mm)

3.4.2.3 Reduced beam section specimen (RBS)

The reduced beam section (RBS) connection has circular radius cuts in both top and bottom flanges of the beam. Dimensions of the reduced zones, calculated according to chapter 5 "*Reduced beam section (RBS) moment connection*" from ANSI/AISC 358-10 [149], are a=66 mm, b=150 mm and c=22 mm. Welds of beam flanges to the column are CJP groove welds and web is connected using fillet welds. Figure 3.44 presents the dimensions of the EPH specimen and a view of the central joint before testing.
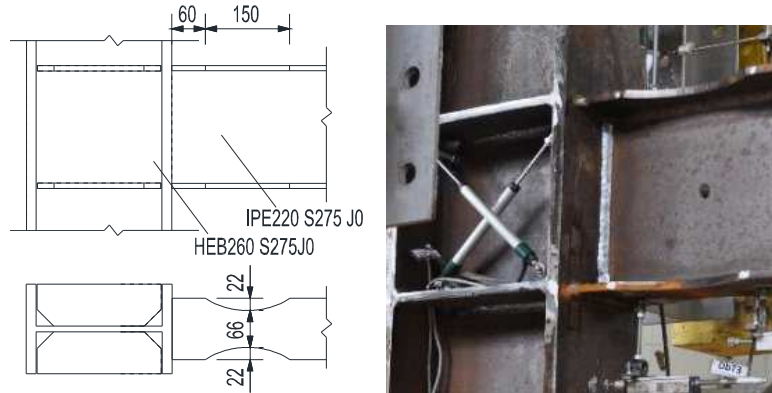
Figure 3.44. Details of RBS specimen (dimensions in mm)

3.4.2.4 Extended end-plate specimen (EP)

The unstiffened extended end-plate bolted connection was designed using EN 1993-1-8 [147] considering a minimum resistance ratio of 0.8 compared to the beam according to EN 1998-1 requirements [117]). The characteristics of the connection were calculated using *STeel CONnection* [148] commercial software. The 16 mm thick end-plate is fixed with five rows of bolts M16 class 10.9. The bolts were normally tightened (no controlled preloading was applied). Full penetration welds connect beam flanges to the end-plate. Figure 3.45 presents the dimensions of the EPH specimen and a view of the connection before testing.
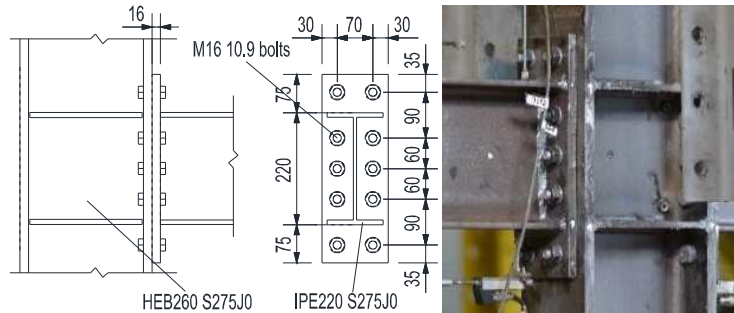
Figure 3.45. Details of EP specimen (dimensions in mm)

Figure 3.46 shows the moment-rotation characteristics of the connections and the classification according to EN 1993-1-8 [147].
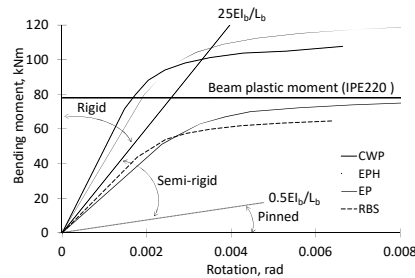
Figure 3.46. Moment-rotation characteristics of the connections [150]

3.4.3   Instrumentation

Figure 3.47 and Figure 3.48 show the instrumentation used in the four tests. The displacements were measured with displacement transducers (Figure 3.47). Stringpot transducers DVW and DVE were used to measure the vertical displacement of the central column bottom. The difference between DHW and DHE PT101 stringpot transducers represents the horizontal displacement of the central column at the level of the connection with the actuator. DLW and DLE position transducer with return spring (TR-TRS) track the absolute (horizontal) displacement of the top of the marginal columns.

TR-TRS type transducers are also used to determine vertical and horizontal displacement of the lower ends of the marginal columns, near the support, see Figure 3.48.a, d.

For estimating the axial force in beams, additional transducers were placed on horizontal elements of the in-plane restraining system. As these elements remain elastic and are subjected to axial forces only, the intensity of the axial force in the restraining system can be estimated during the test based on the elastic elongation. LWT, LWB, LET, and LEB are inductive displacement transducers (Novotechnik - Series F 200 g) with an "almost infinite resolution" [151] monitoring the displacement of 2 points 500 mm apart on a constant cross-section segment of the doubled-pined link. The transducer is fixed at one point and has the free head attached to a steel rod that is fixed at 500 mm distance, see Figure 3.48.a, b. With the exception of these transducers, all the others are potentiometric transducers.
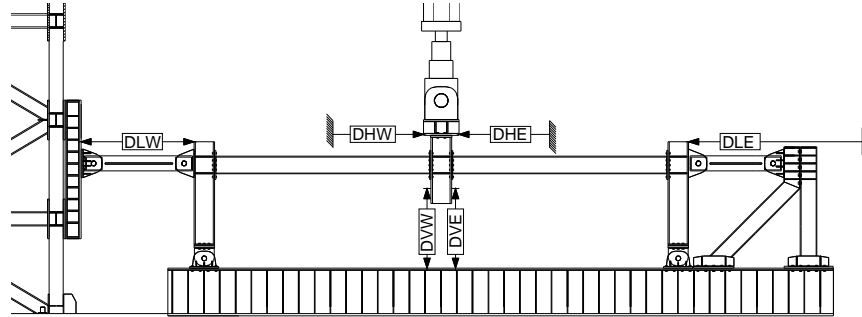
Figure 3.47. Displacement transducers for measuring absolute displacements
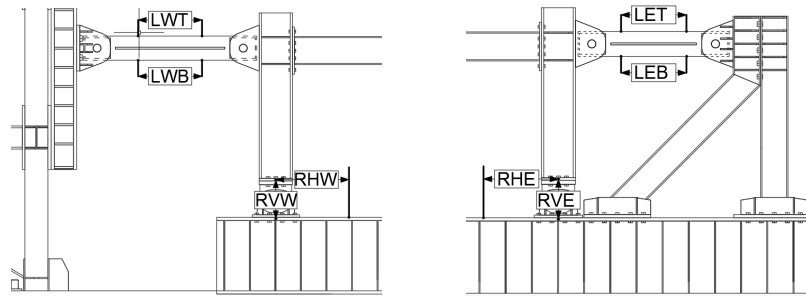
a) conceptual scheme - West side and East side

b) LWT&LWB   c) LET&LEB   d) RVE&RHE

Figure 3.48. Link (inductive) and column support (potentiometric) displacement transducers

        To measure the rotations in the connections 1, 2 and 3 for each specimen, TR-TRS were placed on the flanges or T-stub in the potential plastic zones. Data from these displacement transducers were used to compute the joint rotations R1, R2 and R3, see Figure 3.49. The schematic representation for each type of connection is shown in Figure 3.50. A general view with these transducers is shown in Figure 3.51. MD1 and MD2 potentiometric position transducers with pivot head mounting (TX2) are used to determine the deformation of the web panel in the welded connections.
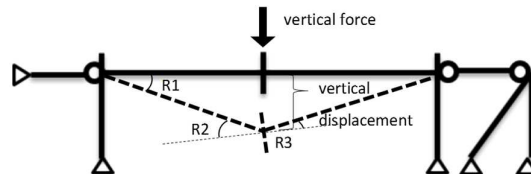
Figure 3.49 Schematic representation of the experimental setup and notations for beam rotation [150]
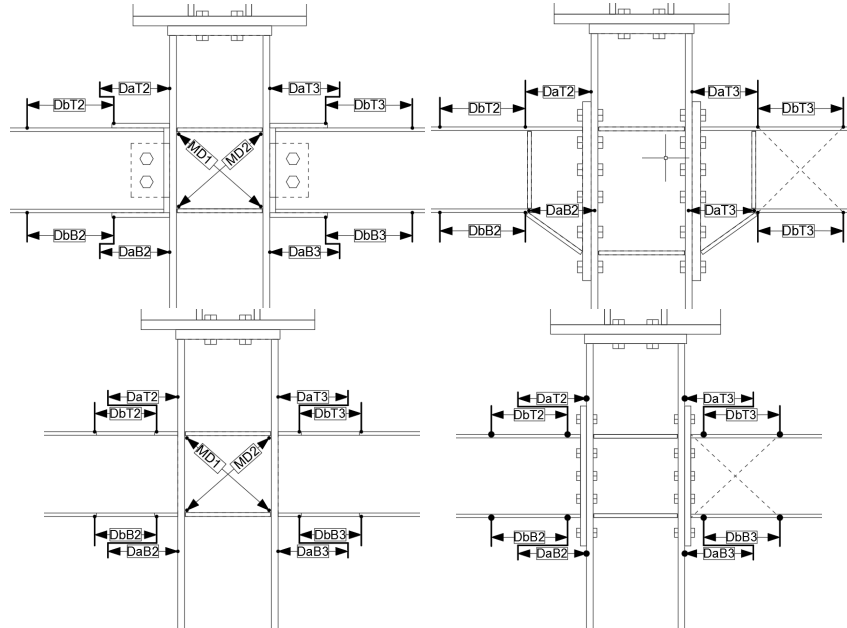
Figure 3.50. Schematic representation of displacement transducers on the connections

Figure 3.51. Overall view with positon of the transducers on a specimen

The strains on the web of the beam and column for connection 4 (East) was measured using a digital image correlation technique VIC-3D [139]. The system is presented in detail in section 3.3.2. The system simultaneous takes a set of two pictures of the same region, but from different angles. In order to have clear unobstructed images of the connection, displacement transducers have not been mounted on that region (connection 4). Random dots of black paint are sprayed and used as marks for post-processing the images in DIC. These marks are used to identify small regions (subsets) on both cameras, see Figure 3.52. A total station was also used to track the vertical displacements along the beams.
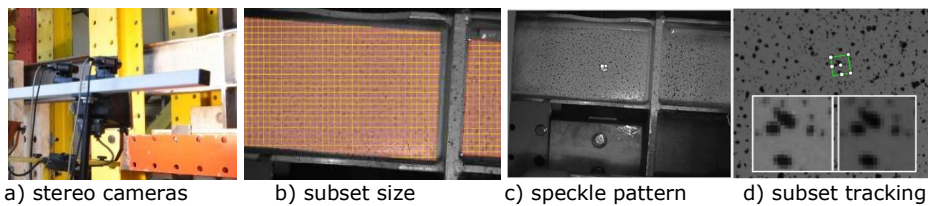
a) stereo cameras   b) subset size   c) speckle pattern   d) subset tracking
Figure 3.52. Preparation of the surface for DIC measurements

3.4.4   Experimental results

Results for coupon tests corresponding to materials used for the fabrication of the 2D frame specimens are presented in Table 3.14.

Before each specimen was tested, nondestructive examination (using Olympus EPOCH 600 ultrasonic flaw detector) did not show any defects. The quality of the welds was confirmed during testing, and there were no cracks or fractures in the welds.

Table 3.14 Average characteristic values for steel profiles, plates, and bolts from connections

Element	f_y (N/mm²)	f_u (N/mm²)	ε_y (%)	A_{gt} (%)
Beam web IPE220, t = 5.9 mm	370	497	0.18	15.0
Beam flange IPE220, t = 9.2 mm	351	498	0.17	15.0
Column web HEB 260, t = 10 mm	402	583	0.19	12.9
Column flange HEB 260, t = 17.5 mm	393	589	0.19	13.3
End-plate, t = 16 mm	305	417	0.15	17.1
End-plate, t = 20 mm	279	430	0.13	12.7
Cover plate, t = 12 mm	315	455	0.15	16.3
Shear tab, t = 10 mm	314	416	0.15	16.7
Bolt, M20 class 10.9	920*	1085	1.75*	12.2
Bolt, M16 class 10.9	965*	1080	1.76*	12.0
Bolt, M20 class 8.8	672*	825	1.78*	12.3
* 0.2% offset yield point				

3.4.4.1 Cover plate specimen (CWP)

Figure 3.53.a shows the vertical force vs. middle column displacement for specimen CWP. Three stages can be identified on the curve, i.e. elastic, flexural and catenary, without a clear point of demarcation but with some zones of interaction. At the initial loading stage, the specimen was in elastic range and the applied load increased almost linearly because the connection was stiff and no slippages were possible in the connection components. The local buckling of the top flange of the right beam, near the connection with the central column, indicated the initiation of yielding and, at this point, the displacement was 35 mm while the applied force reached 147 kN.

After yielding started, the second stage was initiated and the flexural stiffness started to decrease. The maximum applied force at the pure flexural stage was 201 kN and the corresponding vertical displacement was 115 mm. To note that up to 115 mm vertical displacement, the beams were in compression (axial force was negative), with a maximum compressive force of 17 kN, indicating a very low arching behavior in the structure, see Figure 3.53.b.

Up to a vertical displacement of 210 mm, most of the applied load was still resisted by the flexural capacity but the catenary action continues to increase, and the axial force in beams increased from zero to 214 kN. At the end of this stage, which can be called flexural-catenary stage, the bending moment reached the maximum value, i.e. 153 kNm, Figure 3.53.b. After this point, the flexural resistance started to decrease while the catenary action became more predominant. The stiffness continued to increase until the vertical displacement and applied force reached 519 mm and 603 kN, respectively. At this point, due to large tensile force in beams, the end connection of the right beam (near the central column) started to fracture, first in the bottom cover plate, which completely separated from the column flange, followed immediately by a large fracture in the shear tab. This fracture was

accompanied by a large drop in the applied force. The axial force in beams reached a maximum value of 1230 kN, then started to decrease, see Figure 3.53.b. Because the fracture was quite violent, the test was halted and the transducers located near the central column were detached for safety reasons. The test was then resumed and the applied load started to increase again until the top cover plate fractured and the beam was completely separated from the column, see Figure 3.53.d. When the test was stopped, the ultimate vertical displacement reached 586 mm. Figure 3.53.c shows the rotation in sections R1, R2, and R3. It may be seen that up to a vertical displacement of 210 mm (end of the flexural-catenary stage), the rotations were almost identical. After this point, due to the rotation of the central column, the two beam ends connected to the central column recorded different rotations, i.e. R2 and R3. At the peak applied load, the maximum rotation recorded in the connections was R3=0.193 rad ([150]).

| a) vertical force vs. vertical displacement | b) bending moment, axial force vs. vertical displacement | c) beam end rotation vs. vertical displacement |
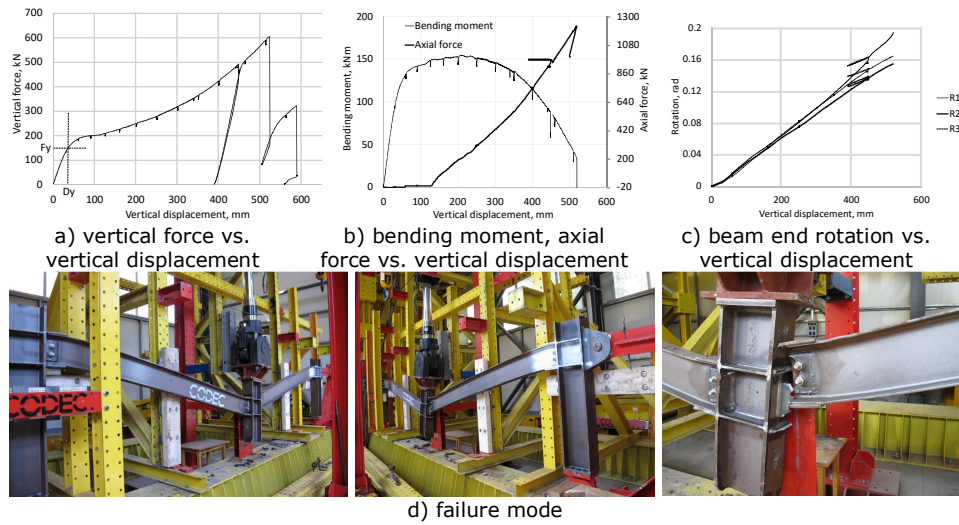
d) failure mode
Figure 3.53. Experimental results for CWP specimen [150]

3.4.4.2 Extended end-plate with haunch specimen (EPH)

Figure 3.54.a shows the vertical force vs. middle column displacement for specimen EPH. As in the case of specimen CWP, three stages can be identified on the curve, i.e. elastic, flexural and catenary.

At the initial loading stage, the specimen was in elastic and the applied load increased almost linearly because the connection is rigid and there was virtually no slippage in the connection. The local buckling of the top flange of the right beam, near the connection with the central column, indicated the initiation of yielding and, at this point, the displacement was 37 mm while the applied force reached 147 kN. After yielding started, the second stage was initiated and the flexural stiffness started to decrease. The maximum applied force at the pure flexural stage was 212 kN and the corresponding vertical displacement was 110 mm. To note that up to 110 mm vertical displacement, the axial force in beams was nearly zero, indicating there is no arching behavior in the structure, see Figure 3.54.b. Up to a vertical displacement of 171 mm, most of the applied load was still resisted by the flexural capacity but the catenary action continues to increase, and the axial force in beams increased from zero to 235

kN. At the end of this stage, which can be called flexural-catenary stage, the bending moment reached the maximum value, i.e. 156 kNm, see Figure 3.54.b. After this point, the flexural resistance started to decrease while the catenary action became more predominant. The stiffness continued to increase until the vertical displacement and applied force reached 440 mm and 477 kN, respectively. At this point, due to large tensile force in beams, the right connection of the right beam failed due to the fracture of first three bolt rows in tension, see Figure 3.54.e. Next, two bolt rows also suffered plastic deformations but did not fracture because the test was stopped due to safety reasons. The axial force in beams reached a maximum value of 1035 kN, see Figure 3.54.b. Figure 3.54.c shows the rotation in sections R1, R2, and R3. It may be seen that up to a vertical displacement of 171 mm (end of the flexural-catenary stage), the three rotations were very similar. After this point, due to the rotation of the central column, the two beam ends connected to the central column recorded different rotations. At the peak applied load, the maximum rotation recorded in the connections was R1 = 0.150 rad. To note that when the right connection of the right beam failed due to fracture of the bolts, the beams connections to the central column showed no visible damages, see Figure 3.54.d. The reason for this behavior is the non-symmetrical arrangement of the connection. Thus, under sagging bending, the connection has more capacity in tension because more bolt rows are engaged. In the case of hogging bending, there are fewer bolt rows active in tension. Therefore, even the connection was designed with overstrength compared to the beam, the axial capacity was not enough to resist the full development of the beam axial capacity in tension ([150]).

a) vertical force vs. vertical displacement

b) bending moment, axial force vs. vertical displacement

c) beam end rotation vs. vertical displacement
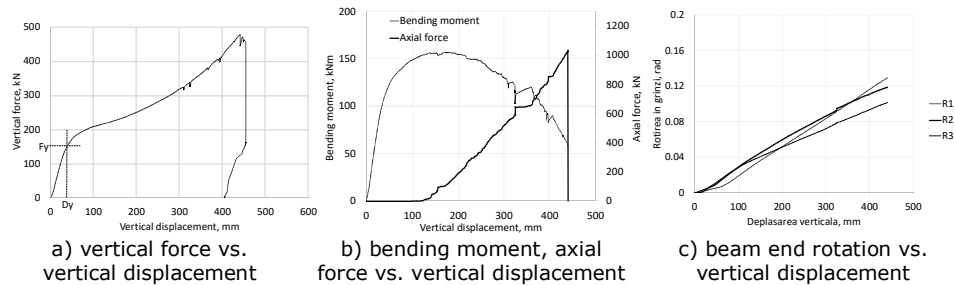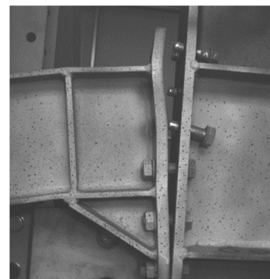
d) central column joint after the test   e) marginal column joint after the test

Figure 3.54. Experimental results for EPH specimen [150]

3.4.4.3 Reduced beam section specimen (RBS)

The vertical force vs. middle column displacement for specimen RBS is shown in Figure 3.55.a. Three stages can be identified on the curve, i.e. elastic, flexural and

catenary. At the initial loading stage, the specimen was in elastic and the applied load increased almost linearly because the connection was stiff and no slippages were possible in the connection components. The yielding initiated at a vertical displacement of was 33 mm, while the applied force amounted 110 kN. After yielding started, the second stage was initiated and the flexural stiffness started to decrease. The maximum applied force at pure flexural stage (no tensile axial force in beams) was 195 kN and the corresponding vertical displacement was 200 mm. To note that up to this point the axial force in beams was nearly zero, indicating no arching behavior in the structure, see Figure 3.55.b. Up to a vertical displacement of 250 mm, most of the applied load was still resisted by the flexural capacity, but the catenary action continues to increase, and the axial force in beams increased from zero to 100 kN. At the end of this stage, which can be called flexural-catenary stage, the bending moment reached the maximum value, i.e. 147 kNm, see Figure 3.55.b. After this point, the flexural resistance started to decrease while the catenary action became more predominant. The stiffness continued to increase until the vertical displacement and applied force reached 480 mm and 401 kN, respectively. At this point, due to large tensile forces in beams, a crack was initiated in the top flange of the reduced beam zone, at the end away from the central column. The fracture then propagated in the web (see Figure 3.55.d) and the test was stopped due to safety reasons because the rupture was quite violent. The maximum axial force recorded in the beams was 753 kN, see Figure 3.55.b. Figure 3.55c shows the rotation in sections R1, R2, and R3. It may be seen that the three rotations were almost identical up to the end of the test indicating that the rotation of the central column was negligible. At the peak applied load, the maximum rotation recorded in the connections was R3 = 0.172 rad ([150]).

a) vertical force vs. vertical displacement (VD)   b) bending moment, axial force vs. DV

c) beam end rotation vs. vertical displacement   d) failure mode
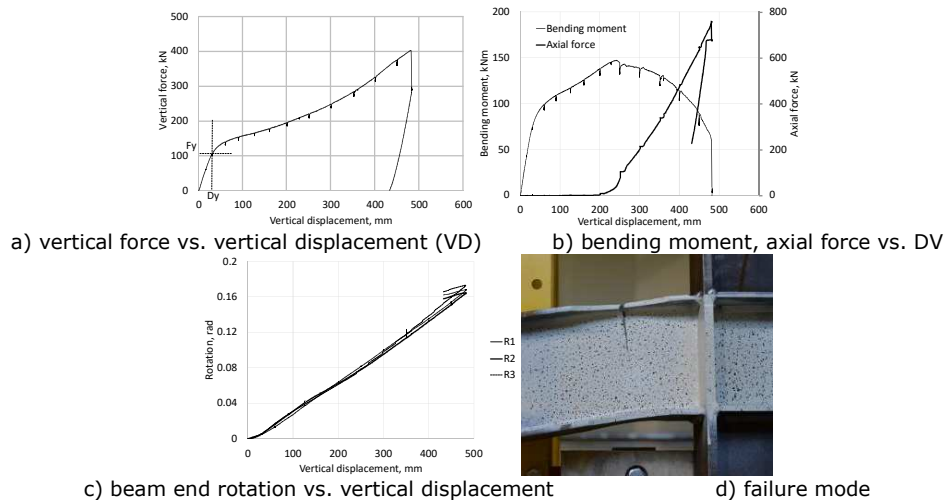
Figure 3.55. Experimental results for RBS specimen [150]

3.4.4.4 Extended end-plate specimen (EP)

Figure 3.56.a shows the vertical force vs. middle column displacement for specimen EP. Compared to the full strength specimens CWP and EPH, this specimen did not show distinctive catenary behavior. At the initial loading stage, the specimen was in elastic and the applied load increased nonlinearly because the connection was

semi-rigid and thus more flexible than CWP and EPH. The initiation of yielding was due to bending in the end-plate of the right beam, near the connection with the central column, at a vertical displacement of 39 mm and an applied force of 117 kN. After yielding started, the second stage was initiated and the flexural stiffness started to decrease. The maximum applied force at pure flexural stage (no tensile force in beams) was 175 kN and the corresponding vertical displacement was 154 mm. To note that up to 154 mm vertical displacement, the axial force in beams was nearly zero, indicating there is no arching behavior in the structure, see Figure 3.56.b. At a maximum applied force of 182 kN and a corresponding vertical displacement of 194 mm the specimen suffered the first failure due to the fracture of the bottom external bolt row of the right beam connection near the central column. The fracture was caused by the flexural action, with a minor contribution from the axial load. The test continued and the failure propagated to second bolt rows within the same connection. In the same time, also the top second bolt row of the right beam connection away from the central column failed due to excessive tensile forces. The specimen finally failed when three bolt rows from left and right connections of the right beam, and two bolt rows from the left connection of the left beam were fractured. Even at this final stage, the axial force in beams reached 571 kN, the specimen failed without developing significant catenary action. The main cause is the insufficient tying resistance of the connection which led to an insufficient rotation capacity that is required to develop catenary action. Figure 3.56.d shows the rotation in sections R1, R2, and R3. It may be seen that up to a vertical displacement of 175 mm, the rotations R2 and R3 were almost identical, suggesting the central column remained on vertical position. After this point, due to the rotation of the central column, the rotation concentrated in the right connection R3, while R2 started to reduce. At the peak applied load, the rotation recorded in the connections was R3 = 0.079rad. The rotations beyond this point cannot be considered acceptable, because the resistance started to decrease, indicating the progressive collapse is imminent. ([150])

a) vertical force vs. vertical displacement

b) bending moment, axial force vs. vertical displacement

c) beam end rotation vs. vertical displacement
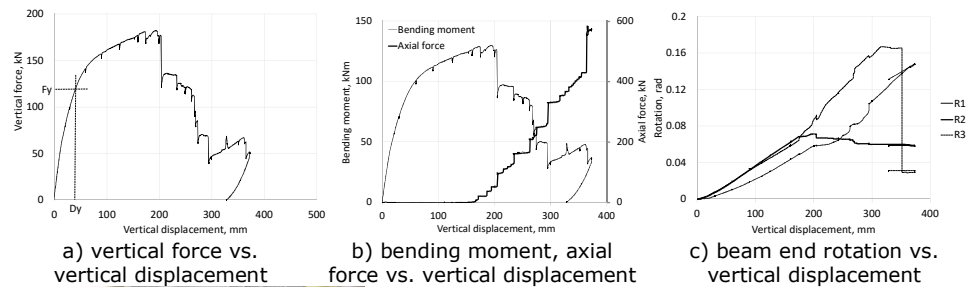
joint after the test: d) central column   e) West column   f) East column

Figure 3.56. Experimental results for EP specimen [150]

3.4.4.5 Comparative analysis of experimental results on 2D frame tests

Table 3.15 and Figure 3.57 compare the response parameters of all four types of connections. The ratio N_{max}/N_M presented in Table 3.15 relates the maximum axial force resisted by the connection, N_{max}, and the axial strength of the beam (reduced due to the bending moment). Value less than one indicate the failure takes place in the connection and not in the beam. The connection capable of resisting the largest vertical load applied at the missing column is CWP, which also has the largest deformation capacity (it attains the largest vertical displacement and joint rotation, respectively). The axial strength of the connection is sufficient to allow the development of large catenary forces in beams, but the failure occurs because of the fracture in the connection and not in the beam, i.e. $N_{max}/N_M < 1$. This could be explained by the fact that, even the connection was designed with flexural overstrength compared to the beam, the axial overstrength is not directly assured. It is also possible that relatively weak shear tab, which is susceptible to net section fracture, to have initiated and weakenedd the connection and thus causing the failure. Similar conclusions were drawn by Khandelwal and El-Tawil [127].

The second largest capacity was attained by the EPH specimen. The failure occurs in the connection, i.e. $N_{max}/N_M < 1$, even the connection is designed with flexural overstrength compared to the beam. A possible solution for improving the axial resistance of the connection is to use stronger bolts or to stiffen the top side of the connection (where the hogging bending is more demanding than the sagging bending).

First partial strength connection specimen, EP, exhibited the lowest resiatnce against column loss, due to the premature fracture of the bolts produced before the development of significant catenary forces in beams. The ratio $N_{max}/N_M << 1$ indicates a very low axial strength compared to the beam. Therefore, this type of connection requires specific attention is design, particularly with respect to the design of bolts for larger axial forces than those resulted from current flexural-based design.

A very good response was provided by the second partial strength connection specimen, RBS, which failed in tension due to the fracture of the beam in the reduced area, but after developing large catenary forces ($N_{max}/N_M =1$). It is, therefore, worth to note that, when properly designed and detailed, RBS connections can be a cost-effective solution for providing resistance to collapse, compared to the stronger, but costlier connections CWSP or EPH.

With the exception of the EP specimen, which showed limited rotation capacity, the other three specimens demonstrated that rotational capacities are much higher that actually reported in UFC 023 [25] (Figure 3.57.c)., which are based on ASCE 41 Provisions for Seismic Design [27]. It is also worthwhile to mention that, with the exception of EP specimen, for which the contribution from catenary action in resisting the vertical load is negligible, for the other three specimens the catenary action significantly increased this capacity, see Figure 3.58. [152]

Table 3.15. Test results for specimens

Test	Maximum applied force F_u [kN]	Maximum rotation in beams [rad]	Maximum axial force in beams N_{max} [kN]	Maximum bending moment in beams M_{max} [kNm]	Axial capacity reduced due to bending N_M^a [kN]	N_{max}/N_M
CWP	603	0.193	1230	154	1323	0.93
EPH	477	0.150	1035	156	1060	0.98
RBS	401	0.172	760	147	757	1.00
EP	182	0.079	571	130	1066	0.54
[a] - N_M - calculated using linear interaction relationship $N_M = N_{pl}[1-M/M_{pl}]$, where N_{pl} is axial plastic resistance, M_{pl} is plastic moment resistance						

a) vertical force vs. vertical displacement (VD)

b) axial force in beams vs. VD

c) bending moment in beams vs. VD

d) rotation in beams vs. VD
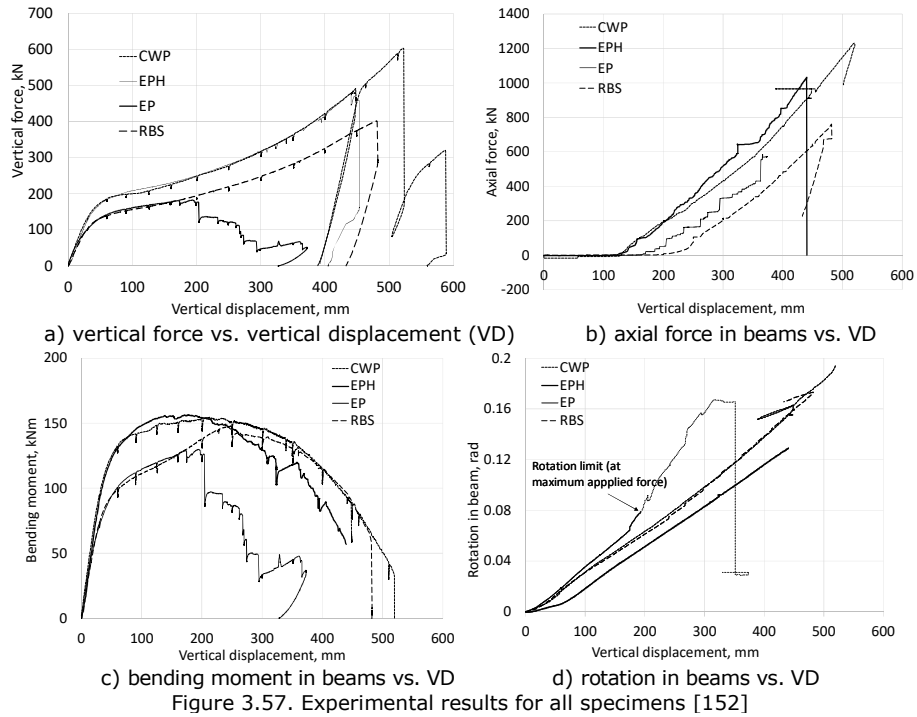
Figure 3.57. Experimental results for all specimens [152]

a) CWP

b) RBS

c) EP

d) EPH
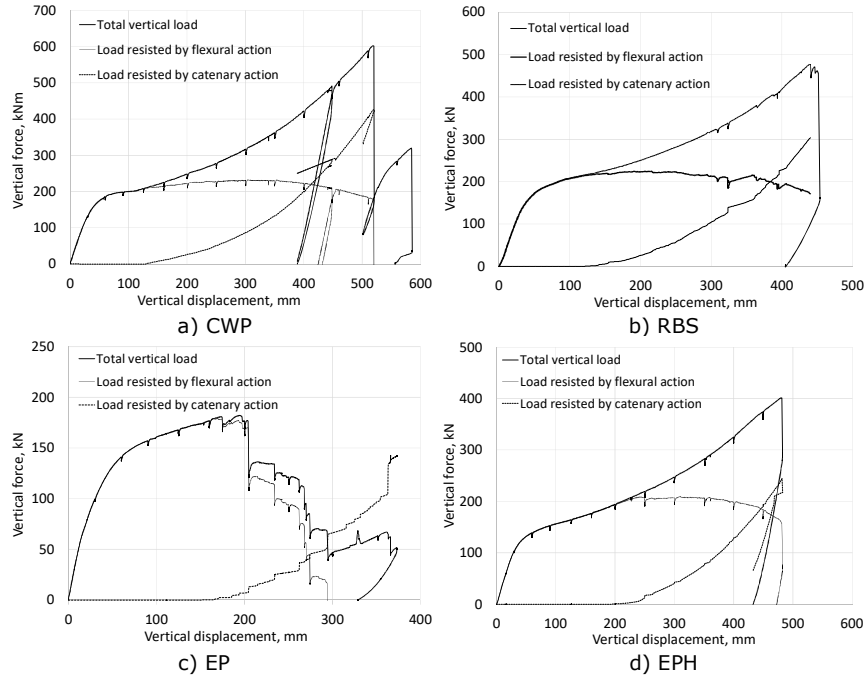
Figure 3.58. Force-displacement curves of specimens [152]

The evolution of strains in webs of beams, from initiation of yielding to the ultimate stage before failure, obtained with VIC-3D software is presented in detail in ANNEX D. The principal strain maps are shown as an overlay to the actual deformation state of the specimens during testing. The labels of figures include the notations D_y (yield vertical displacement), N_i (displacement at which catenary action initiates), or either F_u (maximum vertical force) or D_u (maximum vertical displacement) followed by the corresponding vertical displacement and the type of output: e_1 (principal maximum strain), e_{xx} (strain in the beam axis direction), gamma (the principal strain angle,), or rad (absolute rotation).

For CWP specimen (Figure D.15), the ultimate recorded data indicates strain concentrations (in excess of 0.08) at top flange in tension, near the cover plate. To note that, even the specimen failed due to fracture of the connection (cover plate followed by shear tab), there were also large cracks in the top flange, exactly at the position indicated by the strain concentrations mentioned above. For the CWP specimens, no data are available after 488 mm vertical displacement.

For RBS specimen, the ultimate strains indicated in Figure D.16 (equal to 0.2860) are actually the tensile failure strains, because the measurements covered exactly the crack opening and development zone. The rotation at failure reaches 170 mrad (23 mrad column rotation subtracted from 193 mrad beam rotation).

For EPH and EP, the strains indicated in Figure D.17 and Figure D.18 are not actually the ultimate strains that govern the failure, because they failed due to bolt fracture, where the strains were not measured. If for EPH the rotation at maximum force reached 143 mrad, for the EP specimen the rotation was 66 mrad.

3.5 3D assembly frame tested for column removal

The 3D assembly frame models were extracted from a four-bay, four-span, and six-story steel structure with moment frames in both directions, see Figure 3.59.a. Bays and spans measure 8.0 m each, and all stories are 4.0 m high. The structure (geometry, sections of elements, detailing) are identical to the three-bay, four-span and six story structure designed for high seismic conditions and full strength connections (see details about FS-HSZ in section 3.2.1). The specimens have the same profiles and materials as the 2D assemblies presented in previous sub-chapter. In total, three models were tested in the frame of CODEC project, see Table 3.16.

In order to evaluate the influence of reinforced concrete slab on the response of steel frames, apart from the pure steel-solution (Ans-M), two similar specimens with two different types of floor were studied. First, is a composite beam system (Ans-C), while the second is realized with composite beams and a composite floor (metal steel deck designed in interaction with concrete slab). All three models have the same steel elements and connections. For the composite specimens, the reinforced concrete slab was connected to the beams with Nelson shear studs. In the thesis, only the first two specimens are reported.

The beam-to-column connections were extended end-plate connections (EP). This type of connection is largely used in Europe for realizing moment resisting frames with site bolting connections. In order to avoid premature failure of the connection (see results on 2D frames subjected to column loss, section 3.4.4), bolts diameter was increased from 16 mm to 20 mm, and the end-plate thickness was increased from 16 mm to 20 mm. The bolt layout and weld details were the same as for the EP connection tested experimetally (see sections 3.4.2.4 and 3.4.4.4). The performance of the improved configuration was verified using numerical simulations on full scale 3D models and models extracted from the full scale structure.

Table 3.16 3D MRF specimen types

Specimen label	Floor system
Ans-M	Steel MRF with secondary beam
Ans-C	Identic with Ans-M with reinforced concrete slab with Nelson studs
Ans-SD	Identic with Ans-M with r. c. slab with Nelson studs and metal steel deck

3.5.1 Test set-up and loading protocol

The 3D assembly frame selected for the test is located at the corner of the first floor of the structure (Figure 3.59.a) and has two spans and two bays (Figure 3.59.b). Laboratory restrictions imposed a downscale from the 16.0 m by 16.0 m assembly to a 6.0 m by 6.0 m specimen. Besides the design criteria presented in section 3.2.3.4, the demand-capacity ratio (DCR) for members and connections was computed for both reference and scaled down structure using a static analysis. The DCR was calculated using nominal material properties of the steel components and un-factored vertical loads and capacity, respectively. In the computation, structural steel S275 (yield strength of 275 N/mm^2) was used for beams and S355 (yield strength of 355 N/mm^2) for columns. In these preliminary analyses, maximum demand-capacity of columns for the reference structure ratio was 0.24, while for the scaled structure, the ratio was equal to 0.27 [43].

The force was applied vertically on top of the central column using a displacement control protocol. The displacement was increased using a low loading rate to ensure a quasi-static response. At several specific vertical displacements of

the central column, the loading was paused and the specimen was investigated. Loading was then resumed and continued until failure of the specimen was reached.
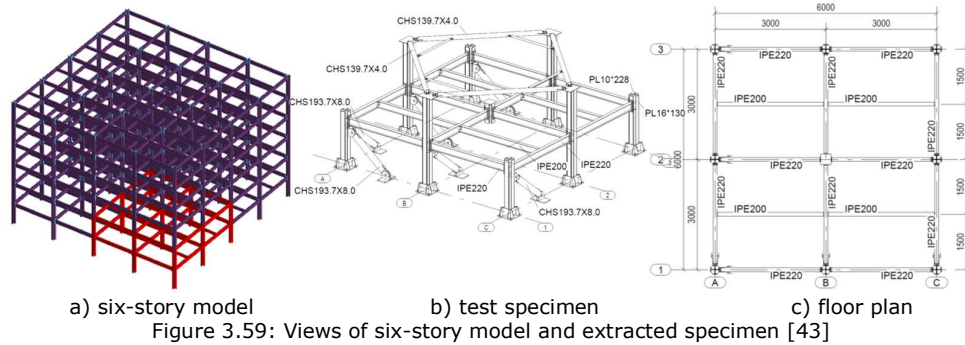
a) six-story model   b) test specimen   c) floor plan

Figure 3.59: Views of six-story model and extracted specimen [43]

3.5.1.1 Boundary conditions for 3D frames

Based on pre-test simulations performed using ELS, the forces that develop in the lateral restraining system were estimated and further used to design the members. Two sets of constraints made from tubular sections were used to simulate the interaction with the original building structure. The first set of constraints is located at the top of the middle perimeter columns and compensates for the frame effect of the floor at second level. The second set of constraints is mounted in the columns located along the two sides that separate the specimen from the original structure, i.e., column line 1 and column line A, simulating the lateral restraint provided by the adjacent structure. The effectiveness of the proposed restraining system was verified using ELS for both Ans-M and Ans-C specimens. Thus, the behavior of the structures, i.e. the isolated specimen and the entire structure, were simulated under the same loading conditions, i.e. removal of one internal column and subsequent application of a force to the top of the missing column until failure. The force–displacement curves plotted in Figure 3.60 show a very good agreement in terms of stiffness, strength, and ultimate capacity. The model isolated from the structure can therefore be studied independently without altering the real behavior and 3D effects that develop within the entire full-scale model. Column bases were modeled as rigid and detailed accordingly.

a) Ans-M [43]   b) Ans-C
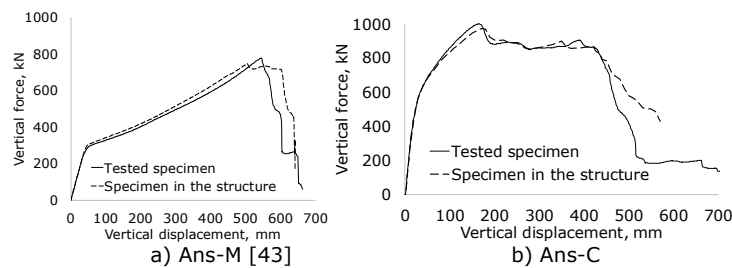
Figure 3.60: Numerical simulation of column loss scenario and resulting force–displacement curves for entire model and test model

Given the reasons described in section 3.4.1, and the fact that the constraints on both directions are not symmetrical, no additional restraints were considered for the central column (removed column).

3.5.2 Instrumentation

The specimen was instrumented with strain gauges and displacement transducers. To monitor the level of the axial force, strain gauges were installed at the mid-length of each of the four main beams that are connected to the central column. Four displacement transducers were used to measure the vertical displacement of the removed column. These four transducers were aligned in two perpendicular directions to capture the possible spatial displacement of the column. Four other transducers were used to measure the horizontal displacements at the mid-height (beam floor level) of the middle perimeter columns. Apart from the vertical displacement below the removed column, chord rotation is very useful for characterizing the deformation capacity of the structure (Figure 3.61.a) ([43]).

A total station with a 1 mm accuracy was mounted at high elevation to monitor displacements of several points on beams and columns. Due to several obstructions, some points were not fully accessible during the entire testing. Apart from the central main beams, top and mid-height displacements of each column were also monitored. Besides points on the line of the central main beams, additional points were marked on top of the slab on the diagonals of the Ans-C specimen.

a) perimetral column joint   b) central column joint   d) column horizontal deflection
Figure 3.61: Displacement transducers [43, 153]

3.5.3 Experimental specimens

3.5.3.1 Pure steel specimen (Ans-M)

The tested system included both main and secondary beams. Figure 3.62 shows the framing plan with the dimensions, types and sizes of element cross sections, and the types of connections used for beams and columns.

The extended end-plate bolted beam-to-column connections were designed as full strength and full rigid connections. Figure 3.63 shows views of the specimen and test setup.

The final configuration of the specimen and the test set-up were adjusted considering pre-test simulations using FEM and AEM models [154, 155]. Stiffeners were used to strengthen the columns at the connection with the braces to avoid concentration of stresses and possible development of local plastic deformations.

a) moment-rotation characteristic curve and details of beam-to-column joint   b) secondary beam-to-main beam connection details
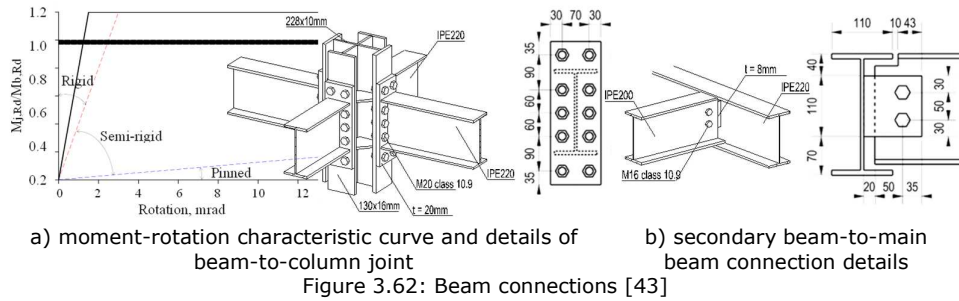
Figure 3.62: Beam connections [43]

Figure 3.63: Views of specimen, test setup, and instrumentation [43]

3.5.3.2 Composite beams specimen (Ans-C)

Steel columns, beams, and connections of the Ans-C specimen are identical with the ones in Ans-M specimen.

The concrete slab is 8 cm thick and C20/25 class. The reinforcement is made of 6 mm steel bars (S235) at 150 mm spacing on both directions for both top and bottom meshes (see Figure 3.64). Additional 1650 mm length Ø8 (S355) shear reinforcement is provided near the central column (see Figure 3.65). Six more bars were introduced in both directions at top and bottom meshes, three at each side of the central column. The role of these reinforcements is to assure shear force transfer from connectors to the slab.
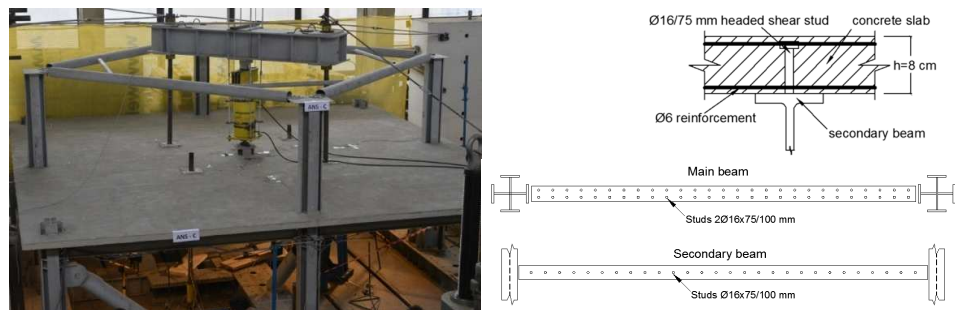
a) view of the Ans-C specimen   b) secondary beam section and distribution of shear studs

Figure 3.64: Views and details of the Ans-C specimen [153]
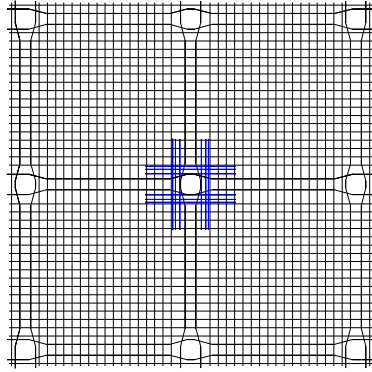
a) schematic representation   b) illustration of the bottom reinforcement mesh [153]
Figure 3.65. Reinforcement plan

3.5.4   *Experimental results*

Before the test, bolts and elements (beams, columns, and end-plates) were tested to evaluate the mechanical characteristics of the materials, see Table 3.17. The characteristic cube compressive strength, f_{ck}, at 28 days was 32.0 N/mm².

Table 3.17 Average characteristic values for steel plates and bolts for 3D structure

Element	f_y N/mm² yield strength	f_u N/mm² ultimate strength	ε_y (%) yield strain	A_{gt} (%) elongation at maximum stress
Web, main beam IPE220, t = 9.2 mm	345	464	0.16	28.0
Flange, main beam IPE220, t = 5.9 mm	353	463	0.17	30.4
Web column, t = 10 mm	407	539	0.19	27.0
Flange column, t = 17.5 mm	420	529	0.20	27.0
End-plate, t = 20 mm	408	535	0.19	24.4
Web, secondary beam IPE220, t = 5.9 mm	350	460	0.20	24.1
Flange, sec. beam IPE220, t = 9.2 mm	355	465	0.19	23.2
Fin plate, t = 8 mm	375	480	0.19	23.3
Bolt, M20 class 10.9	905 *	1081	1.77 *	12.0
Bolt, M16 class 10.9	908 *	1083	1.76 *	12.0
Reinforcement ϕ6 mm	346	480	0.16	30.0
Reinforcement ϕ8 mm	399	588	0.18	29.0
Note: * 0.2% offset yield point				

3.5.4.1 Pure steel specimen Ans-M

The vertical force versus vertical displacement curve for the central column is shown in Figure 3.66.a. Vertical displacements at different sections along the interior beams located on column lines 2 and B are shown Figure 3.66.b. Several pauses were made to allow the inspection of the specimen, to make relevant notes, and to read the position of monitored points with the total station. These pauses can be identified by the spikes visible in the force–displacement curve. Because insufficient stroke length of a hydraulic jack, two stops were made at 285 and 450 mm to allow mounting

of extension elements. During these stops, the force was reduced to zero (Figure 3.66.a).

The yield displacement, D_y, and yield force, F_y, were 30 mm and 233.5 kN, respectively (point A on the curve in Figure 3.66.a), and were calculated according to the ECCS method [156]. Thus, F_y may be defined as the point of intersection between the initial stiffness line at the origin of the force–displacement curve from a monotonic test and the tangent line to the force–displacement curve having a slope of 10% of the initial stiffness. At a column displacement of 569 mm and a vertical force of 732 kN (point B on the curve in Figure 3.66), the bottom tension flange of the B2-B3 beam ruptured near the beam-to-column connection. The corresponding rotation of the beam was θ=206 mrad, the fracture continued to propagate and the test was paused due to safety concerns. After inspection of the specimen, the test was resumed and continued until the fracture reached the upper flange. Then, the test was stopped because of large rotations in the central column and difficulties in applying the force. The ultimate displacement recorded was 617 mm, while the force dropped to 645.5 kN. The corresponding rotation of the beam was θ=220 mrad [43].

a) vertical force evolution   b) vertical displacement of beams
Figure 3.66. Vertical displacement results [43]
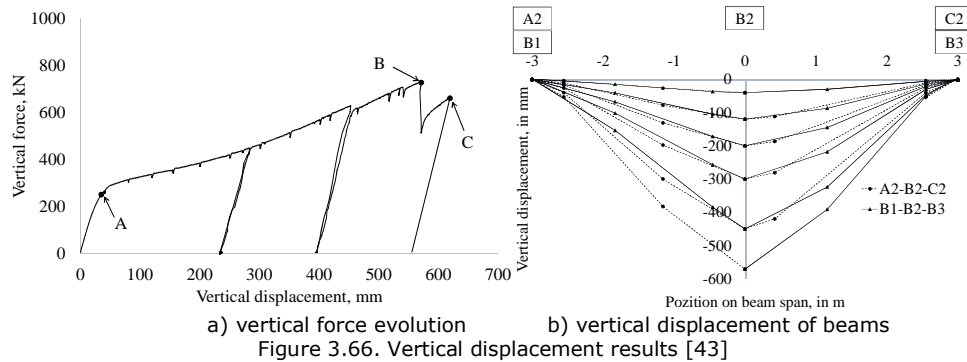
Figure 3.67.a shows the failure mode of beam B2-B3 near internal end B2, and Figure 3.68 shows close-ups of the connections with the perimeter columns, at different stages of the test. General views of the specimen at the end of the test are presented in Figure 3.67.b.

a) first failure   b) Specimen at end of test
Figure 3.67. Failure of specimen Ans-M

a) end B1 of B1-B2 beam
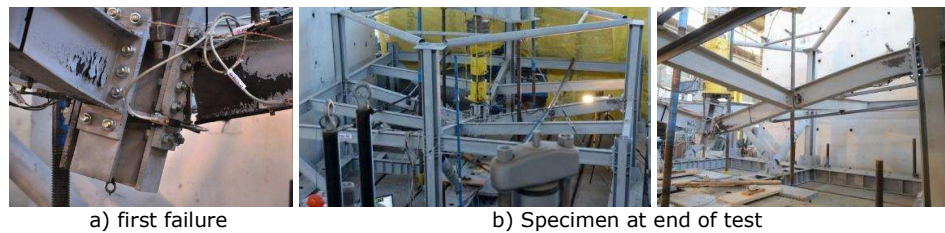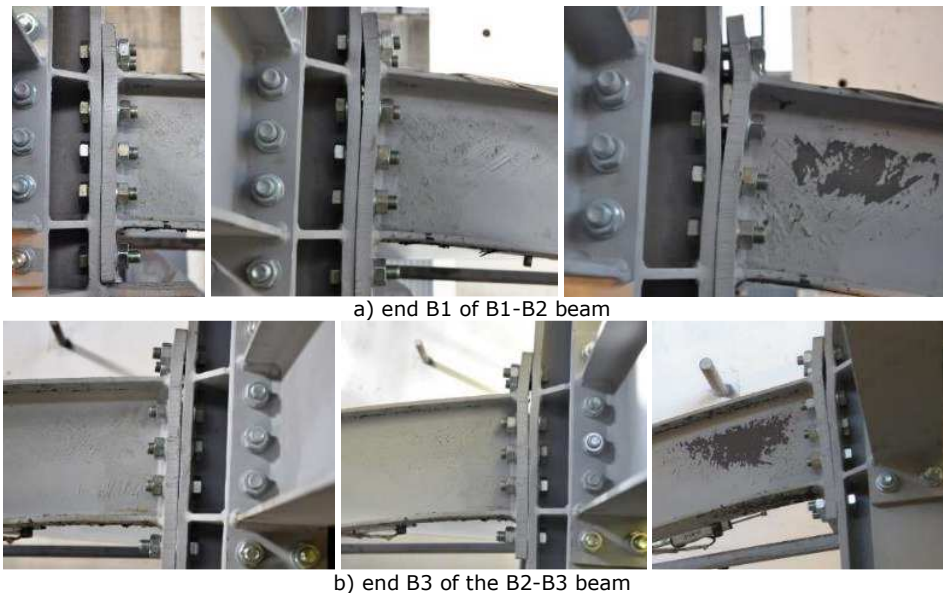
b) end B3 of the B2-B3 beam
Figure 3.68. Connections at 300 mm, 450 mm and 600 mm vertical displacements

Figure 3.69 displays the axial force, and respectively the bending moment in beams B1-B2 and B2-C2 versus the vertical displacement. Axial forces were calculated using data obtained from strain gauges mounted on the mid-height and mid-length of internal beams, while bending moments were calculated at ends B1 and C2, by subtracting the contribution of axial forces. As can be seen from Figure 3.69, after the vertical displacements reached 230 mm, the axial force in the beams began to increase more rapidly, whereas the bending moment started to decrease. The maximum axial force was 778 kN (or 0.67 N_{pl}, where N_{pl} is the beam's plastic axial capacity).

Plastic deformations developed mainly in the beams, even though due to tension in the T-stubs local plastic deformations were also observed after the vertical displacement reached 300 mm (see Figure 3.68). These T-stub deformations are not caused by the bending moment in the flexural stage, as the bending moment started to decrease after 300 mm, but by the high axial forces in beams added to the tension resulted from the bending moment (see Figure 3.69).

Figure 3.70 shows the beam end rotation versus the vertical displacement. Note that columns A2 and B1, named "restrained columns," represent internal columns in the original (reference) structure and have particularly designed horizontal constraints to prevent free displacement at the floor level, taking into account the lateral restraint provided by the adjacent structure. Columns C2 and B3, named "free edge columns," represent penultimate perimeter (facade) columns in the original structure and, therefore, have no other lateral constraints preventing horizontal displacement at the floor level, except their own flexural rigidity.

In case of beams on column line 2 (Figure 3.70.a), up to a vertical displacement of 420 mm, the rotations at the external ends (away from the central column) were very similar. After this step, the rotation at beam end C2 increased with a slower rate than that at the opposite end A2 because of the difference in the flexibilities of columns A2 and C2. Rotations at the internal ends (close to the central column) were

very different because of the rotation of the central column. The maximum rotation was 148 mrad and was measured at end B2.

In case of column line B, the rotations at the external ends followed similar trends as in the case of the beams on column line 2. However, for the internal ends, the two rotations were very different because of the large rotation of the central column. Note that the central column had no additional restraints for preventing lateral displacements and rotations of the free ends. This rotation caused the concentration of the rotations at end B2, which ultimately led to beam failure because of excessive deformations.

a) axial force   b) bending moment
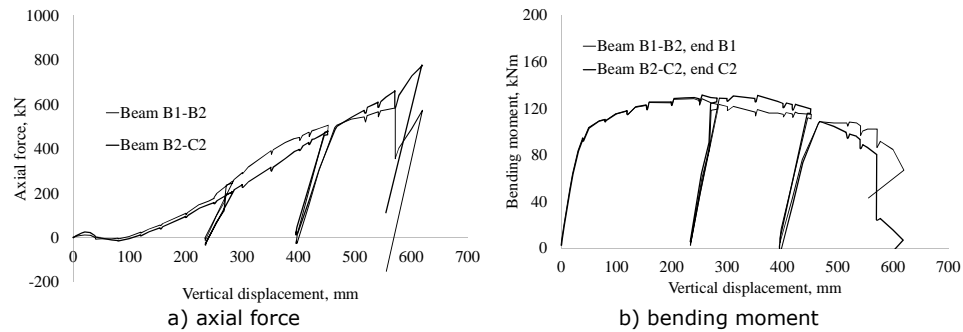
Figure 3.69. Axial force and bending moment in beams versus vertical displacement

a) column line 2   b) column line B
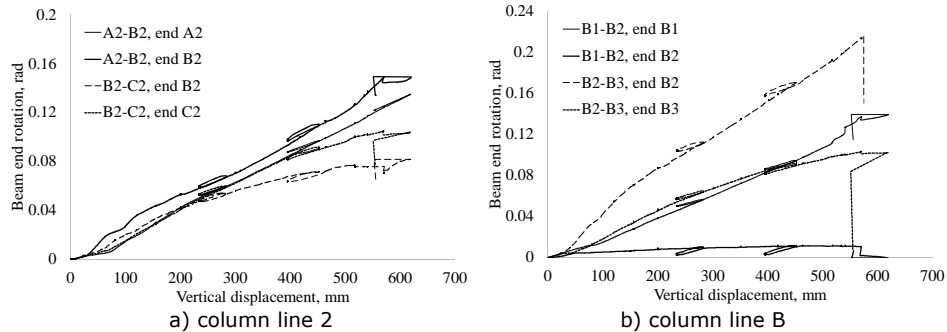
Figure 3.70. Beam end rotations versus vertical displacement [43]

Figure 3.71 shows the graph of the horizontal displacement at the floor level in middle perimeter columns versus the vertical displacement below the removed column. Deformation toward the interior was defined as positive. As can be seen, restrained columns A2 and B1 had low horizontal deflections at the floor level because of the additional restraint provided by the vertical braces. The catenary forces that developed in beams were mainly transferred to the braces and did not affect the column bending. However, in the case of free edge columns, the development of the catenary forces led to inward bowing amounting to 68 mm for column B3 and 58 mm for column C2. These deflections caused plastic deformations in the columns. In a real scenario, the presence of gravity loads in columns might induce column buckling and possible failure of free edge columns. These observations suggest that the development of catenary forces in beams, following the removal of a column, depends on whether or not the adjacent structure has the capacity to support these forces. If the beam is connected to a strong structure, e.g., stiff interior structural framing, the

tying resistance of the connection should be checked. If the beam is connected to a weak structure, e.g., edge columns, the capacity of the column to resist the catenary forces in beams should be checked.
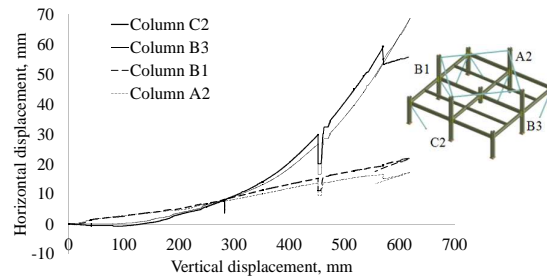
Figure 3.71. Horizontal displacement at the level of the floor in middle perimeter columns versus vertical displacement below removed column [43]

3.5.4.2 Composite beams specimen Ans-C

Figure 3.72.a shows the vertical force versus vertical displacement curve for the central column. To allow the inspection of the specimen, to make relevant notes, and to read the position of monitored points with the total station, several pauses were made which can be identified by the spikes in the force–displacement curve. The force was reduced to zero two times to allow mounting of extension elements to compensate for the limited stroke length.

First cracks in the concrete floor were observed on the top surface, at a vertical displacement of about 30 mm, and followed a circular pattern in the region near the middle perimeter columns (Figure 3.72.b). More cracks started to develop afterward, spreading in and out from the first visible crack line. As seen from the vertical force vs. vertical displacement curve (Figure 3.72.a), the maximum applied force was 910 kN, and the corresponding displacement was 279 mm. After the attainment of peak force, the capacity slightly decreased to 899 kN, when the beam B2-B3 fractured at end B2, near the connection with the central column (point A in Figure 3.72.b), see Figure 3.73.a. The corresponding vertical displacement was 291 mm. The fracture was initiated at the bottom flange and then extended in the web for approximately 120 mm, causing a significant drop in the force. Full depth cracks developed within the floor in the central region, around the removed column. The test continued, and the force started to increase from 674 kN to 759 kN, until the beam A2-B2 also fractured at end B2, near the connection with the central column (point B in Figure 3.72.a). The corresponding vertical displacement was 348 mm. To note that, at this point, the beam B2-B3 suffered complete failure (the beam separated from the end-plate). The concrete was completely crushed and started to detach from the top flanges of the beams.

No permanent deformations were visible in the end-plate bolted connections of the main beams to the perimeter columns or to the central column, respectively. The test continued until the concrete floor completely separated from the steel beams in the central region surrounding the removed column (see Figure 3.73.b); after that, the test was stopped (point C in Figure 3.72.a). As can be seen from Figure 3.72.a crack development followed an almost circular pattern. At failure, the concrete slab failed in shear and completely separated from the beams. After the test, the specimen

was dismantled and the concrete slab has been removed from the supporting beams. This unveiled that the shear studs did not suffer any visible plastic deformations.
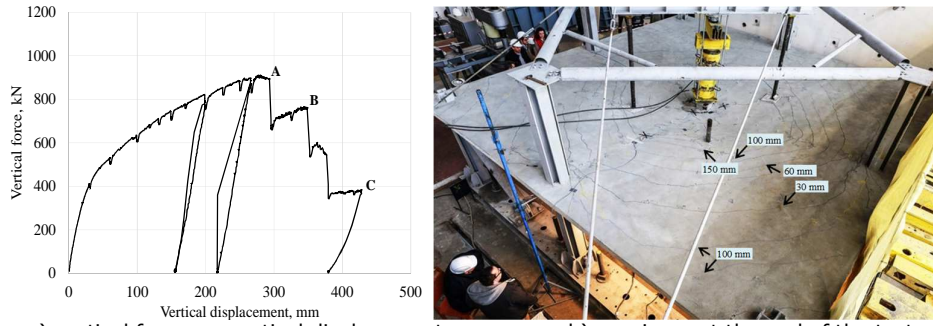
a) vertical force vs. vertical displacement   b) specimen at the end of the test
Figure 3.72. Ans-C results [153]

a) fracture at beam B2-B3   b)complete beam fracture   c) Column B1 connection at point B
Figure 3.73. Detailed views of the connection [153]

The plastic deformations at beam-ends that withstood hogging moments (on the perimeter) were much smaller than those measured at internal beam ends under sagging moments, see Figure 3.73 and Figure 3.74. Thus, Figure 3.74 shows the rotation in main beams at both ends. In point A (first fracture in beams), the ultimate rotation in beam B2-B3 at end B2N amounted 121 mrad. In the beams located in the other direction, the rotation continued to increase, until, at point B, beam A2-B2 also failed in section B2W, at an ultimate rotation of 0.160 mrad.
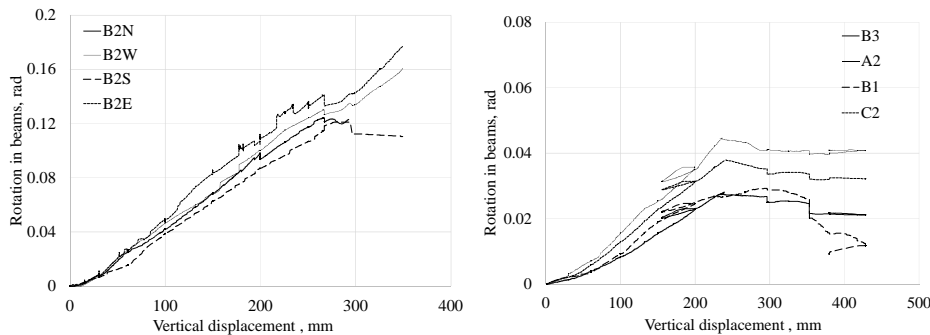
a) beam ends near central column (sagging)   b) beam ends near marginal columns (hogging)
Figure 3.74. Rotation in beams (for notation of sections, see Figure 3.64.b)
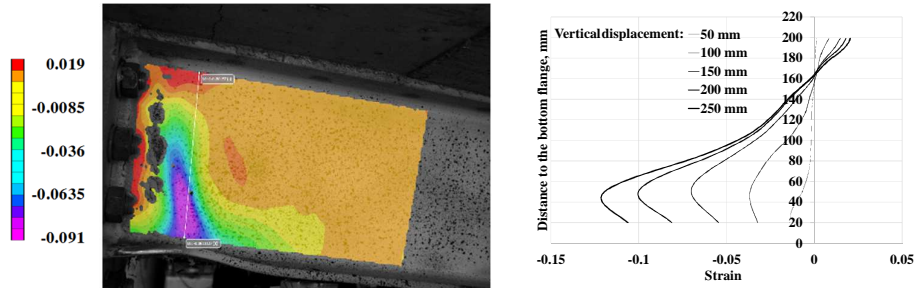
a) strain map at 200 mm vertical displacement   b) strain evolution at 70 mm from beam end
Figure 3.75: Optical strain measurements in beam end C2 (using VIC-3D system) [153]

Figure 3.76 shows the displacement profile of the floor slab along the main beams and diagonals, at different load levels. Before the applied force reached 408 kN, the beams are in elastic and exhibit a typical flexural behavior, with the inflection point at the middle of the span (center column), see Figure 3.76.a. After this load level, the plastic deformations initiate at beam ends and the deflection profile changes, each beam showing distinct inflection points located around the mid-span of each individual beam. As the beam ends under sagging moment exhibit larger plastic deformations compared with the beam ends under hogging moment, beyond 747 kN, the deflection profile of each beam changed and became shaped like a cantilever, almost straight to the tip (central column). A similar behavior was observed for the concrete floor diagonals, with the observation that, at the same relative position to the center of the floor, the displacements measured smaller values when compared with the slab on top of the beams.
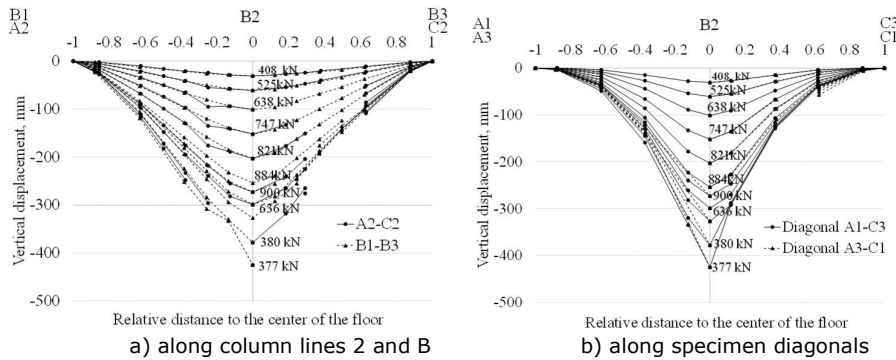
a) along column lines 2 and B   b) along specimen diagonals
Figure 3.76. Slab vertical displacement [153]

3.5.4.3 Comments related to assembly experimental results

The value of the ultimate rotation of the pure steel structure ANS-M is in good agreement with DoD (2005) [22] recommendations, where for beams with seismic cross section (plastic section), the ultimate rotation for a low level of protection LLOP, θ_f, should be taken as 210 mrad. However, the values of the deformation limits in the latest editions of DoD (2013, 2016) [25] [26] are different than those indicated in DoD (2005) [22]. In DoD (2013) [25], the acceptance criteria for nonlinear modeling of steel beams subjected to flexure plus axial tension should be taken from 2013 version of ASCE 41) [27], using the value corresponding to Collapse Prevention Limit

State (CPLS). According to these requirements, for beams with seismic section, the deformation limit for the primary element (at CPLS) is $8 \times \theta_y$, where θ_y is the yield rotation. For the system tested in this study (beam cross section IPE220, beam length L_b = 3.0 m, yield strength of 355 N/mm^2), this deformation limit amounts 68 mrad. However, mobilization of catenary action in beams usually requires rotations of 70 mrad or more ([157]; [158]), with the condition that beams are strongly connected to the columns. More important, the limits that are set in ASCE 41 [27] are mainly applicable for the seismic rehabilitation of buildings, and implicitly assume cyclic behavior, while column loss event implies monotonic behavior. The difference between monotonic and cyclic deformation capacity is about double and is based on many experimental tests [28]. Therefore, if the cyclic limit specified in DoD (2013) [25] is translated into monotonic capacity, the ultimate allowable rotation for our system is approximately 140 mrad. Thus, it is questionable if the limits that are set in ASCE 41, where the catenary action is not considered, should be also adopted for column loss scenarios, where catenary action can increase the capacity to resist the applied load ([43]).

Due to the composite action with the floor slab, the peak force of the ANS-C specimen was 24% larger than that corresponding to bare steel specimen, while the ultimate rotation of beams reduced correspondingly (see Figure 3.77.a). The beam-to-column connections showed very good behavior and had sufficient strength to allow the development of plastic hinges in the beams. Although the rotation capacity of the composite specimen is fairly limited with respect to the pure steel one, the amount of dissipated energy is comparable, due to the higher initial rigidity and ultimate capacity. As it can be seen Figure 3.77.b, the level of dissipation energy for the ANS-C maintains higher values (mostly double) up to a vertical displacement of 300 mm.

a) vertical force vs. vertical displacement   b) energy dissipation
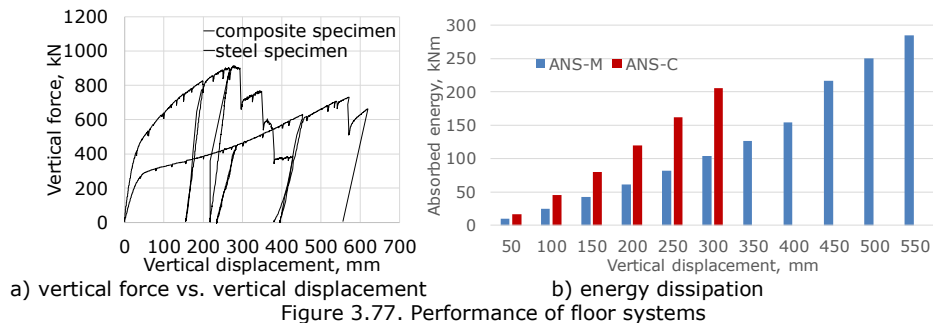
Figure 3.77. Performance of floor systems

3.5.4.4 2D vs 3D test of steel frames under column loss

Figure 3.78 compares the result for pure steel 3D assembly specimen and 2D frames subjected to column loss. The force for the Ans-M assembly is divided by 2, since the two frames (line B and line 2) share in common the applied force. The initial stiffness, yield force, and flexural behavior of the Ans-M specimen are almost identical to the EP and RBS specimens. The ultimate capacity ratio is 1.94, while the ductility ratio is 2.8 when comparing the Ans-M specimen to the of EP specimen, even though the only differences between the two are the thickness of the end-plate (20 mm / 16 mm) and the diameter of the bolts (20 mm / 16 mm). When compared to the RBS specimen, after a vertical displacement of 220 mm, the Ans-M specimen is less rigid, because at this stage, catenary action starts to be significant, and the two systems have different lateral stiffness. The 2D frames are restrained at both ends, while the

3D assembly has a perimeter column in each frame line. Detailed numerical investigations are required to assess the contribution of EP strengthening in 2D and 3D similar numerical models.
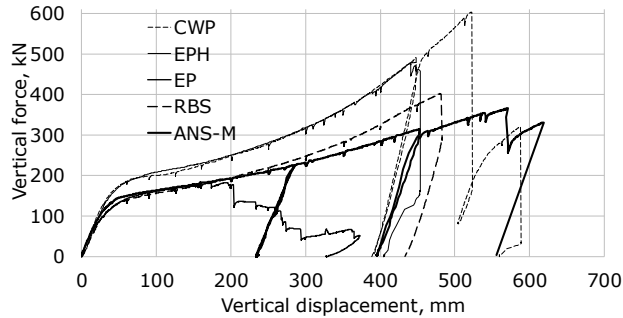
Figure 3.78. MRF subjected to column loss experimental comparison

3.6   Concluding remarks

A large experimental program was designed taking into consideration the requirements for each type of test (boundary conditions, loading protocol, instrumentation, detailing). The design of the experimental program was based on preliminary analyses of full scale structures subjected to static and dynamic column removal for several scenarios using a numerical model validated against relevant experimental data. Specimen scale-down is performed uniformly for the experimental program, and the restraining system was carefully calibrated to simulate the rest of the structure. As the complexity of the testing increased, the number of parameters included in the test program diminished. For small connection components (T-stubs, weld details), several configurations (thickness, bolt distance, weld type) and two loading conditions were employed, i.e. static and dynamic. The results indicated that thin end-plates may be prone to failure before reaching the forces necessary to carry the loads by catenary action. Therefore, thicker plates were considered for EP specimen. In addition, the loading rate showed small influence and was not further considered for the 2D tests. Also, results on weld details showed fillet weld can perform well and was adopted for the frame tests.

In 2D tests, four connection typologies were tested, all under same quasi-static conditions and for the same element sections. The pairs of rigid connection specimens and semi-rigid ones showed almost identical behavior, with the exception of EP specimen, which failed before developing catenary forces in beams. The other three specimens allowed the development of large post flexural capacities, which was one of the main objective of the study. Failure occurred in the tensioned flange of the beam only for the RBS specimen, where the flange fractured in the reduced zone, while bolts fractured in the case of bolted connections, and the welded cover plate failed for the CWP connection.

For 3D assembly tests, only one connection was adopted, i.e. EP connection but with some improvements due to the unsatisfactory behavior of EP specimen in the 2D frame experimental assessment. Thus, the end-plate thickens was increased, together with the bolt diameter. Same beams were used as in case of 2D frame tests, and also similar columns, with the observation that cruciform sections were employed instead of H sections. Three systems were tested for central column loss, one with

pure steel elements, and two with concrete slab in interaction with the beams (second concrete specimen, with corrugated sheeting, is not reported here). The results showed a higher ultimate capacity of concrete specimen but a large reduction in the deformation capacity. As the vertical loads do not decrease if a column is accidentally lost, the main indicator of the progressive collapse resistance is given by the maximum force that is supported by the structure. This maximum capacity can be improved either by strengthening of the system (for example by using composite beams in interaction with the concrete floor) or by improving the deformation capacity and thus to allow the development of catenary forces. In such cases, the connections should be designed considering the development of axial forces in beams with or without interaction with the bending moment. The performance of the strengthened EP connection improved considerably, both in terms of strength and ductility, when compared to the 2D tested EP connection. The slab restrains the displacement of free edge columns pulled inwards by catenary action, thus reduces the risk of buckling.

Lateral restraining system influences the beam axial force contribution to column removal scenarios, as in the catenary phase, the 3D assembly (near penultimate column removal) is less rigid than the tested 2D frames that developed catenary action (intermediate column removal).

The validity of the experimental results is limited to the configurations and loading scenarios covered in the experimental program. Therefore, more studies were necessary to extend and validate the findings, i.e. full scale frame structures, larger scale elements, different connection configurations, and different loading conditions. Numerical models were therefore validated against experimental data and used in parametric studies. The next section presents in detail the construction and validation of numerical models for each type of specimen, the full scale models that integrated component/frame/assembly models and the results of the parametric studies.

4 NUMERICAL PROGRAM

4.1 Introduction

4.1.1 Numerical program framework

Numerical simulation is an efficient and reliable toll for investigating the complex behavior of building structures under extreme events (e.g. accidental loss of a column). Difficulties associated with the experimental testing are well known and does not require further justification. As a result, a numerical program has been designed from the start of the study to follow and supplement the experimental program. The development and calibration of numerical models capable of replicating the complex behavior of steel frame structures under column removal is the second major objective of the thesis. Three main environments were employed in the numerical program. First, SAP2000 program [121] for preliminary analysis of reference structures and design of specimens and test-set-up. Second, FEM based program Abaqus [159] was used for detailed investigations on components and 2D and 3D frames. Third, AEM based program ELS [124] for full scale numerical investigations. ELS, which is mostly oriented to analyze complex structure interactions and effects of extreme loading conditions, can assess the response of large building models with reasonable efforts and computing resources.

The framework of the numerical program is detailed in Figure 4.1. Calibrations presented in the thesis take into account the loading rate and strain rate effect, material damage, performance of different configurations of beam-to-column connections, different materials interaction, and 3D effects. The models, validated against experimental data, were used to identify the distribution/redistribution of stresses in the elements, the development and propagation of failure, and to provide a better understanding of the phenomena by allowing the extraction/collection of results that are difficult to obtain from experimental testing.
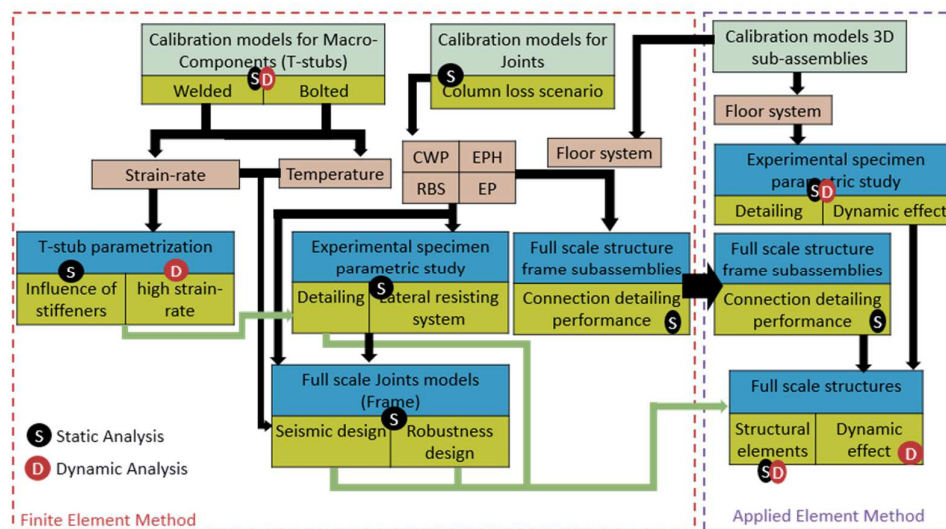
Figure 4.1 Numerical program framework [160]

Some models that were used in the preliminary analysis were continuously updated until final validation against experimental data. Some issues that were initially disregarded, but that proved to have significant contributions to the performance of the specimens, were progressively added. Considering this evolution, it also expected that other improvements can be made such that the models can be used to obtain new data or refine the ones already available.

4.1.2   Numerical modelling

4.1.2.1 FEM with Abaqus/CAE

A very common numerical technique is the Finite Element Method (FEM). Finite element analysis solves partial differential equations for finding approximate solutions to boundary value problems [161]. Complex problems/systems are subdivided into smaller, simpler parts, called finite elements that can be modeled with simple equations, but solved after assembling, giving an approximate result for the entire problem/system.

A widespread FEM platform, with a large amount of available documentation and discussion services, is the Abaqus/CAE software. "Part of the Abaqus FEA product suite, Abaqus/CAE is a complete solution for finite element modeling, visualization, and process automation. This tool covers a vast spectrum of applications offering powerful solutions for routine and sophisticated engineering problems." [162]

A large number of researchers use Abaqus for computer simulations. Such studies mentioned in this thesis are: [45, 46, 49, 56, 60, 61, 63-65, 67-69, 99, 111, 112, 142, 145, 154, 155, 163]

Thanks to the fidelity in simulating complex material behavior (post-elastic, strain-rate effect, propagation of failure, etc.), and to the possibility to model complex geometric behavior in static/dynamic loading conditions or at elevated temperatures, Abaqus/CAE was employed for detailed modeling of coupon tests, connection macro-components, 2D frame tests, and pure steel 3D assembly test.

Tensile tests and connection macro-components

ABAQUS allows the use of complex material properties when creating the models. In order to calibrate the material laws for base material (plates) and other components (welds, bolts), different models that replicate the experimental tests on coupons and T-stubs need to be created. The material properties, like post-elastic strengthening or softening, strain-rate influence, for a given range of modeling attributes (e.g. mesh size) can be identified in order to obtain the same results as in the experimental cases.

2D frames subjected to column loss

The models used the material characteristics calibrated on coupons and connection macro-components, and included the specific boundary conditions and geometry of the specimens of the 2D frames subjected to column loss. For each type of connection, a separate model was constructed.

Pure steel 3D specimen subjected to column loss

The 3D effect of the assembly can be assesed by modeling the column loss on the pure steel assembly ANS-M. At the construction of the model, information and assumptions from 2D frame and macro-component models were used. The model can be used to get detailed information otherwise difficult to obtain in the experimental test, e.g. stress and strain maps on each region or component, at different loading phases.

4.1.2.2 AEM with ELS

One of the most well-known Applied Element Method software is Extreme Loading® for Structures, ELS. This advanced non-linear structural analysis software assesses the structural behavior at various load stages and under different load types (static, dynamic, blast, seismic, impact, progressive collapse, etc). ELS, which uses a non-linear solver based on the Applied Element Method (AEM) [164-166], allows to automatically detect and analyse yielding, hardening, failure of materials, separation of elements, generation of plastic deformations or contacts, buckling/post-buckling, crack propagation, membrane action, and P-Delta effect [167].

Simulation of complex transient-dynamic response of material behavior is difficult due to material fracture and localised fragmentation behaviours [168]. On this purpose, the mathematical approach employed in ELS allows modeling and analysis of element separation and kinematic element interaction (contact at impact) for a considerable reduced computational cost. The elements are not linked through common nodes, but by connectivity between 3D volumetric elements, defined as normal and shear springs between common surfaces (Figure 4.2.a). These springs have the property of the volume of material represented by the interface spring tributary surface and distance between the centroids of the elements (Figure 4.2.c).

The discretization in AEM is not limited to the number of elements, but it also allows controlling the number of springs generated on the surface, thus effectively simulating moment effects between two elements. Plastic deformation can occur at any interface between two elements, although elements behave as rigid bodies. The internal deformations within elements are estimated using spring deformations around each element. Relative displacements between two adjacent elements cause stresses in springs that share common element faces [113].

For elements through which pass reinforcement bars, the effect of reinforcement is simulated by an additional spring at the location of the reinforcement, see Figure 4.2.e. This spring has the properties of the reinforcement bar (length, area, and material), while the matrix spring generated between the two surfaces have the properties of the main material, i.e. concrete.

Springs inherit the nonlinear properties of the modelled material. The spring properties include material characteristics like elasticity, plasticity, hardening, cyclic behavior and failure (Figure 4.3).

Contact between separated elements is simulated by generating contact springs at the surface of elements that are forced towards each other, see Figure 4.4.

ELS has some features that makes it attractive over other programs. First is the computational cost in terms of analysis duration. ELS requires considerably less analysis time than other programs for similar problems. This becomes important when large models are investigated (e.g. full-scale multi-story frame models), especially for composite steel-concrete systems, with several types of materials and several types of interactions. Second, ELS has special analysis options for the loss of an element (e.g. column), progressive collapse, and other types of accidental situations (blast, impact, fire). ELS software allows to model the direct blast pressure created by different types of explosive materials, and also reflecting waves. Calibrating the model with blast experimental testing results allows simulations on the effect of internal or external blast charges for full scale structures.

Considering complexity of future possible features of the research program development (i.e. tests on small components - material, welding, T-stubs, at different strain rates and different temperatures, blast loading on sub-assemblies using explosives, 2D systems under column loss and finally 3D systems with different floor

slabs), the decision was to validate all these tests and then to integrate them into a single global model.

a) Partial connectivity   b) Element generation   c) Spring distribution and influence area

d) connectivity matrix spring   e) reinforcement spring
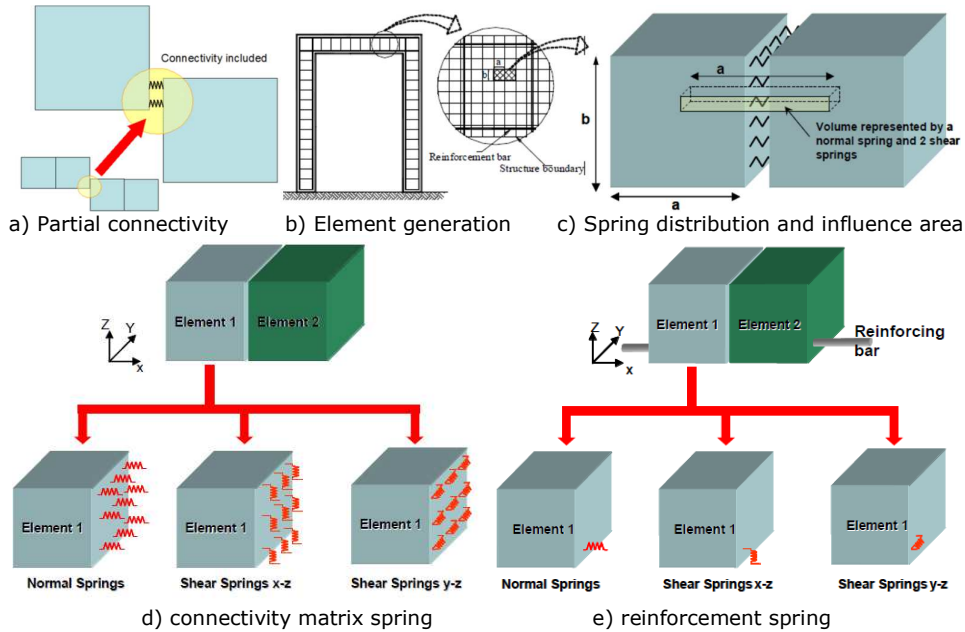
Figure 4.2 Modeling connectivity with AEM: spring generation on element faces [169]

a) concrete compression   b) concrete tension   c) steel tension   d)steel cyclic
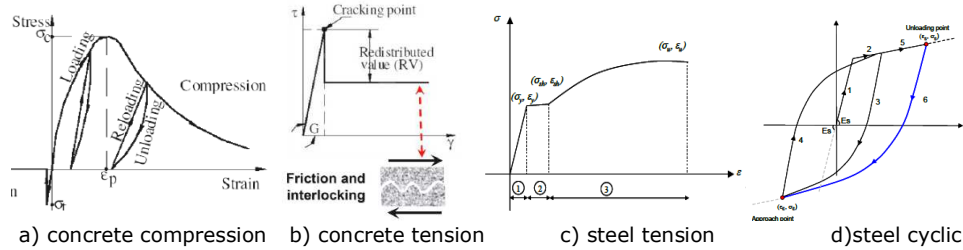
Figure 4.3 Material properties in ELS [169]

a) initial position   b) Matrix spring under tension   c) separation strain reached

d) elements forced towards each other (loading)   e) contact spring activated
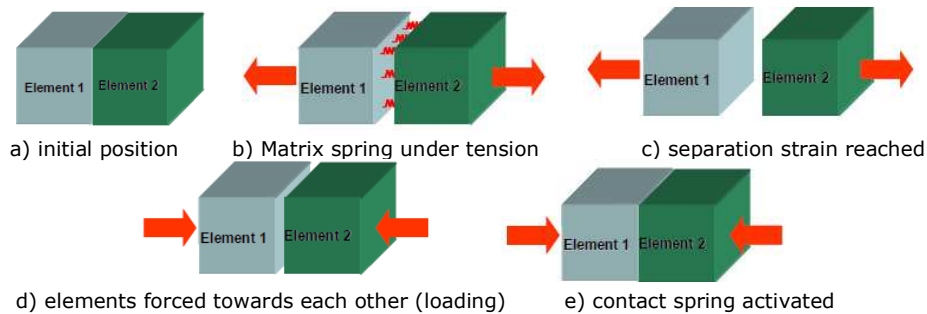
Figure 4.4 Elements separate and re-contact again

4.1.3   AEM vs. FEM modeling (combined method)

FEM and AEM modeling and simulations have specific and complementary advantages. The behavior of steel components and details, material degradation, loss of stability, and, if needed, strain-rate effect, can be represented with high fidelity in Abaqus models (presented in chapter 4.2). For large scale models, however, this detailed modeling increases the size of the input file and require many hours to complete the analysis. Therefore, the advantages given by ELS (AEM) modeling and solving should be employed. Advantages of AEM analysis over FEM analysis for models are presented in Figure 4.5. The disadvantage of using ELS is that ductility is very much dependent on the meshing, and performance of details should be checked and corrected using experimental data.
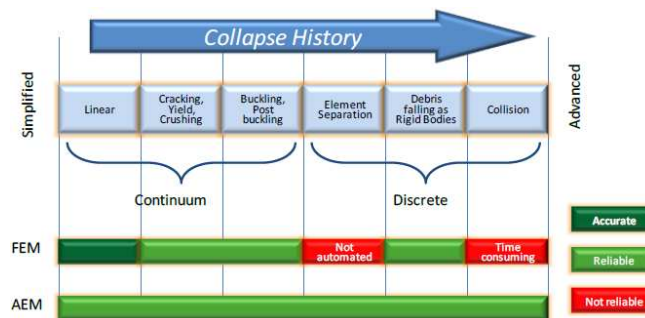
Figure 4.5 Analysis domain of AEM compared to FEM [169]

For evaluating the performance of a specific connection configuration, the following steps were followed in modeling and analysis:

0. Calibrate the FEM against experimental data (see chapter 4.2)
1. Select a representative sub-assembly with the adequate boundary conditions in order to preserve the lateral stiffness in the structure. If a structure has different connection types/ beams, sub-assemblies should be extracted for each beam-to-column connection type and for each of them perform step 1 to 3.
2. Model the sub-assembly frame in the FEM calibrated environment and perform a column loss scenario on the frame
3. Model the same sub-assembly and boundary conditions as in the previous point in AEM, calibrating the model to the FEM results
4. Build the AEM model of the structure using the calibration considerations from the previous point. Static and dynamic analyses can be performed on the structure to obtain reliable results.

A schematization of this process is presented in Figure 4.6.
In this manner, structural analyses (static and dynamic) on global models could be performed using AEM models derived from calibrated FEM models. The AEM models give also the possibility to directly model accidental actions (direct effect of blast, impact, etc.). By modeling these action, the analysis can provide results for the performance of the structure with damaged columns that may still have some residual capacity or evaluate the structural response considering the partial damage of other elements (others than lost column). This type of analysis is more realistic when compared to notional removal of columns.
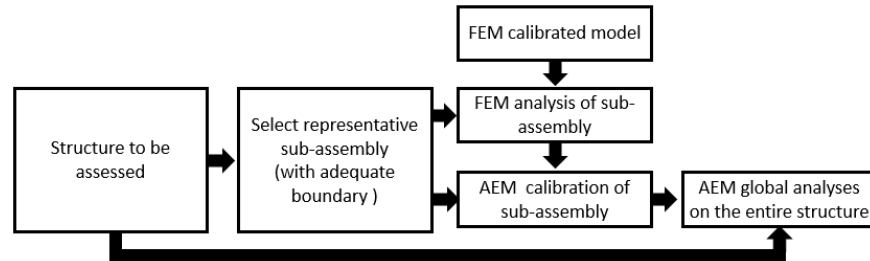
Figure 4.6. Combining FEM and AEM modeling to maximize efficiency for structural analyses

4.2   FEM model calibration

4.2.1   Material model calibration

The material model is based on tensile tests performed on coupons extracted from the same steel plates and profiles that were used to manufacture the specimens.

As the engineering stress-strain curves for coupons in the same batch were very similar, only one curve for each material was selected and processed. The engineering stress-strain curve extracted from the test was transformed in a true stress - true strain curve up to the ultimate force with equations (4.1) and (4.2) from EN 1993-1-5 [170]. After the maximum load is reached, due to necking, the material seems to soften, while it is actually hardening [171]. The material curve for true stress - true strain beyond the maximum load of the engineering stress-strain curve was considered ascending with a parabolic shape. This shape was obtained through iterations by comparing the FEM model results with the coupon experimental results

$$\sigma_{true} = \sigma(1 + \varepsilon) \tag{4.1}$$

$$\varepsilon_{true} = \ln(1 + \varepsilon) \tag{4.2}$$

where: σ_{true} is the true material stress; ε_{true} is the true material strain; σ is the engineering material stress (applied load/ specimen area); ε is the engineering material strain (specimen deformation/ initial length)

Finite element models were created in Abaqus [159] for the tensile test on coupons, using the actual dimensions of the specimens. Only the coupon outside the grip was modeled (Figure 4.7.a), assigning kinematic restraints to the ends of the coupon linking them to reference points. One reference point was fixed in all degrees of freedom (the static grip), while to the other a longitudinal displacement was imposed in a dynamic explicit step (the moving grip). The monitored displacement in the FEM analysis was between points located in the same zone as the points monitored with the video extensometer (highlighted points in red in Figure 4.7.a). The mesh considered for this specimen was the equivalent size of the mesh in the joint models (2D frames) in the potential plastic zones.

The analysis was performed in dynamic explicit step, using mass scaling in order to obtain a reasonable computational time. Thus, the ratio of kinematic energy and external work was monitored and maintained less than 1% to assure a quasi-static response.

Apart from the true stress-plastic strain curve, material density (7.85 10^{-9} tons/mm^3), Young's modulus (210000N/mm^2) and the 0.3 Poisson's ratio, the

material model consists also of a ductile damage characterized fracture strain and stress triaxiality [172]. Also, the sub-option of damage evolution was introduced – displacement type, linear softening and maximum degradation regarding displacement at failure. It is very important to note that coefficients for ductile damage and damage evolution options are directly related to the mesh size and shape. Therefore, for each material, changes of fracture strain and elongation at failure have been performed in order to have the same breaking point as in the experimental tests. Also, changes to the polynomial parameters for the true stress - true strain relationship after the maximum force were made in order to match the descending shape of the engineering stress-strain curve Figure 4.7.c exemplifies the stress - true strain curves for materials.

With the same procedure, the bolt assembly has been calibrated using assembly numerical tensile tests on identical bolts to experimental tests (bolt, nut, washer subjected to axial tension). The nut was considered welded to the bolt shank by modelling it from the same part. The modeled diameter of the shank was the one reduced due to the thread.

| a) FEM coupon model | b) test and FEM engineering stress-strain curve for EP material | b) true strain stress for the for EP connection material |
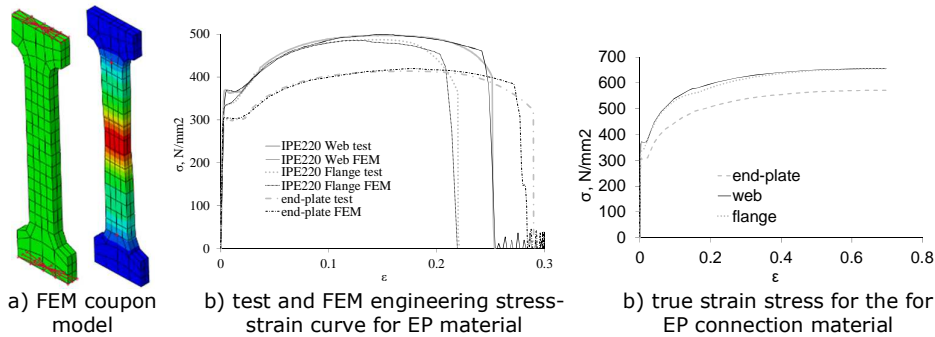
Figure 4.7. Coupon test calibration

4.2.2 *Influence of strain-rate*

Numerical models for T-stub components were created using ABAQUS program, see Figure 4.8. The geometry of the models was based on the precise measurements of the specimens that were made before testing (see Table C.1 and Table C.2 from ANNEX C). Material properties (plates and bolts) are in accordance with the results of the tests on materials (see the previous section).

4.2.2.1 Quasi-static analysis

The analysis was performed in a dynamic explicit step, to take advantage for simpler contact definitions and reasonable computational time. Mass scaling was used to reduce the inertia forces and prevent dynamic effects. Sensitivity analysis was performed for each type of model in order to set the target time increment mass-scaling that allows a cost-effective computational process with a small influence of the dynamic effect. To ensure a quasi-static response, the results were accepted only after the ratio between the kinetic energy and the external work/internal energy was less than 2%([163] recommends 5%). The energy transfer was closely monitored in order to avert numerical errors. Particular attention was given to artificial energy and the mesh was adjusted accordingly.

4.2.2.2 General FEM Analysis parameters

For all T-stub components, the type of finite element was solid element C3D8R (8-node linear brick, reduced integration). The mesh of the elements was done using linear hexahedral elements. For circular elements (e.g. bolts) the circle was divided into minimum 12-sided polygons.

The general contact type was used between elements: the tangential component is defined by frictionless formulation while the normal component is defined by a "hard" contact pressure-overclosure. Based on the observations on failure modes, no special requirements for weld were necessary and the fillet weld was modeled using the same properties as the base material. Loading was applied in displacement control protocol, similar with the test ([46, 141]).
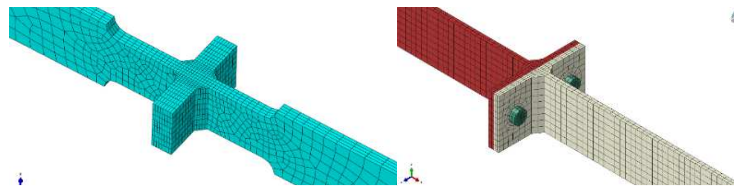
Figure 4.8. Numerical FE model of the T-stubs [109]

4.2.2.3 Strain rate modeling

Method 1: The influence of strain rate on the material properties was computed using Kaneko's equations (3.4) and (3.5), considering an average strain rate derived from a preliminary static analysis. The maximum strain is divided to the loading time in order to get the average strain rate to be used in the formulas and to modify accordingly the material strain-stress curves. The stress in the stress-strain curve of the material is formulated analytically in terms of f_y and f_u. Using the same formulation but with the values for the at $f_{y,sr}$ (yield material stress when subjected to strain rate) and $f_{u, sr}$ (ultimate material stress when subjected to strain rate), the characteristic strain-stress curve for the material influenced by strain rate was obtained.

For each type of material, properties for the entire end-plate or web were modified based on this average value in the zone where maximum strain-rate is localized. This method can be used only if the yielding sequences/ zones share the same strain-rate. For the material that does not undergo plastic deformations, this increase of capacity does not affect the elastic response. Strain-rate in the analysis should be compared to the strain-rate from the preliminary analysis used to evaluate the increase of material capacity, and if differences are observed, iterations should be made by modifying the materials according to the new strain-rate.

As this method is simple to put in practice for small models with few yielding zones, it may be inadequate for complex systems, where yielding sequence may reorder due to strain effects. It may also be laborious for complex models with a large number of plastic zones, requiring several iterations and verifications.

Method 2: A second method, more complex but more reliable has been also used [173]. Using (3.4) and (3.5) and based on values from the stress-strain curve, but computing the increase factors for yield and ultimate strength for a large set of strain-rates values (from 10^{-4} s^{-1} to 10 s^{-1}), data points for strain-stress rate curves at different levels of strain rate were obtained. For strain-rate values higher than 10 s^{-1} (not the case in these analysis) research data from UFC 3-340-01 [174] is used. Method has been developed using c# programming to create a code (Dynamic

Material generator [175]) that can generate the material properties (stress-strain points that form the curve) for a multitude of strain rates in a data format that can be imported in Abaqus. The analysis has to be performed in a dynamic stage, as it computes the strain rate for each element individually based on the deformation rate. This kind of analysis is more expensive from a computational point of view, with very close results to the results obtained with the first/ simple method.

4.2.2.4 Numerical results

Figure 4.9. plots the experimental and numerical force-displacement curves for welded T-stub series W-Y, while Figure 4.10. plots the curves for T-stub series T-10-16. The strain-rate results are obtained using *method 1*. Figure 4.11. shows the deformed shape with equivalent plastic strain map (numerical model) and the deformed shape before failure obtained in the test, for specimen T-10-16-120. It can be seen the FE model follows with high accuracy the actual behavior of the specimen. The type of failure (i.e. mode 1) was also very well replicated.
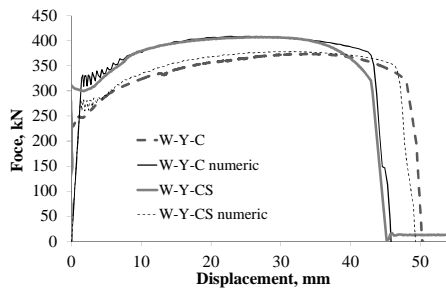
Figure 4.9. Experimental vs numerical force-displacement curves for welded T-stubs

a) static   b) dynamic
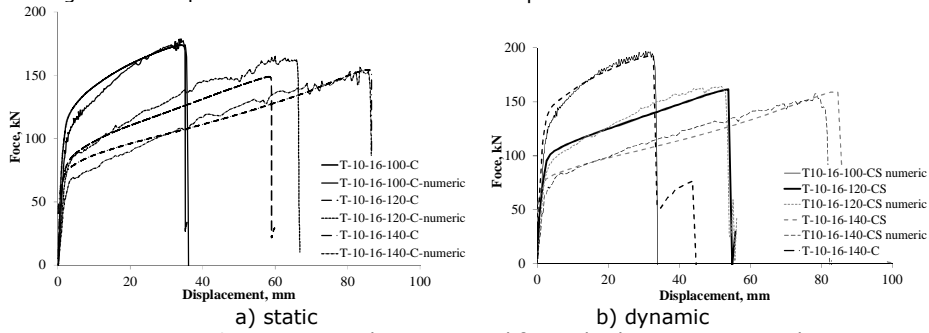
Figure 4.10. Experimental vs numerical force-displacement curves, low
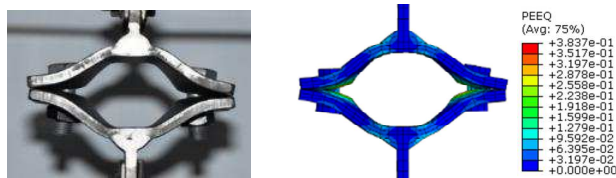
Figure 4.11. Deformed shape before failure, experimental (left) and numerical (right) (the equivalent plastic strain PEEQ)

There is also a good correlation between the FEM results and the data obtained from 3D image monitoring system with respect to specific strain maps. Figure 4.12. displays the maximum strain and vertical displacement obtained from numerical analysis, which matches the data from VIC 3D system.

a) max. strain (C)   b) vert. displacement (C)   c) max. strain (CS)   d) vert displacement (CS)
Figure 4.12. Numerical model and DIC data before failure for W-Y-C and W-Y-CS
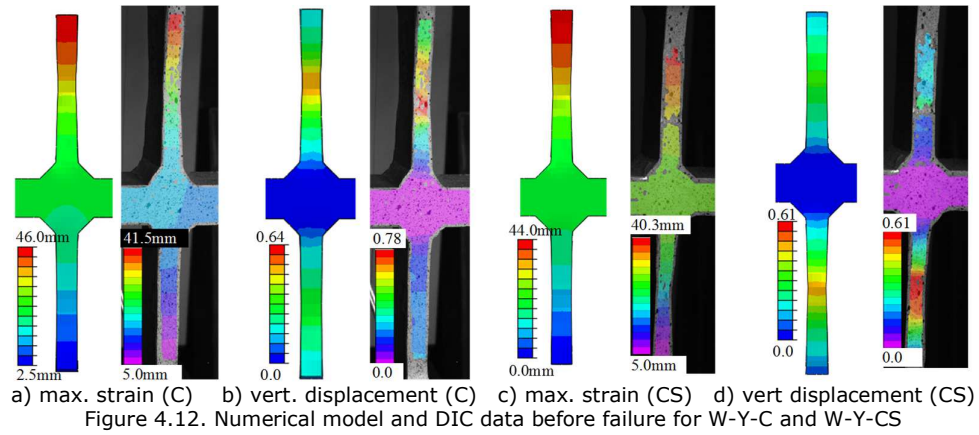
For the specimen with 10 mm thick end-plate and 140 mm bolt row distance (T-10-16-140-C), the force-displacement curve indicates an increased stiffness. Figure 4.13 plots the normal stress (on the direction of the web) for the web and the direction of the bolt line in the end-plate of the T-stub. After large deformations are attained (> 60 mm), flexural resistance decreases while catenary forces start to develop in the end-plate, thus increasing the capacity. Both parts of the end-plate between the bolt and the web are entirely in tension reaching normal strains higher than 125 N/mm^2.
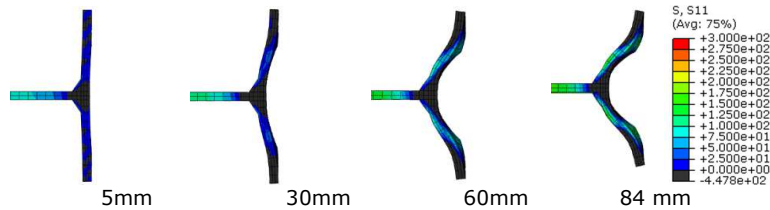
          5mm   30mm   60mm   84 mm
Figure 4.13. Evolution of normal stresses with the total displacement, for model T-10-16-140

The calibrated bolt assembly (based on the T-stub tests) was used to create bending moment-axial force interaction curves by subjecting the bolt to several constant levels of axial forces and increasing the applied bending moment until the failure is attained. The values at failure were normalized to the ultimate capacity and then plotted as M-N interaction curve, see Figure 4.14.a. The evolution of normalized bending moment with respect to normalized axial force in bolts for the most/ least ductile T-stubs (T-10-16-140/ T-12-16-100) was also plotted on this figure. The M-N relation is mostly linear until the limit points on the interaction curve are reached, and is followed by an increase of axial force and a reduction of the bending moment up to the bolt failure ([46]). The point of failure for all T-stubs are marked on the M-N interaction curve in Figure 4.14.b. Failure of all configurations was mainly due to axial force in bolts, as all bolts reached values higher than 70% of their capacity. The bolts

in the 12 mm thick end-plate T-stubs fail at the same level of internal axial force and bending moment, but the T-stubs have different capacities. In order to detail the behavior, the forces in the bolts were normalized to the applied load (F_{bolt}/F_{T-stub}) and monitored in respect to the imposed displacement of the T-stub (see Figure 4.14.c). The ratio F_{bolt}/F_{T-stub} increases with the distance between bolts. The ratios are always larger than 1 and may reach values close or higher than 2 due to the prying effect. The resultant force from the contact pressure between the end-plates has a corresponding amplitude tension force in the bolts which is added to the forces derived directly from the load applied on the T-stub.

| a) bolt interaction curve and M-N evolution | b) bolt interaction curve and bolt failure | c) ratio between forces in bolts and applied force |
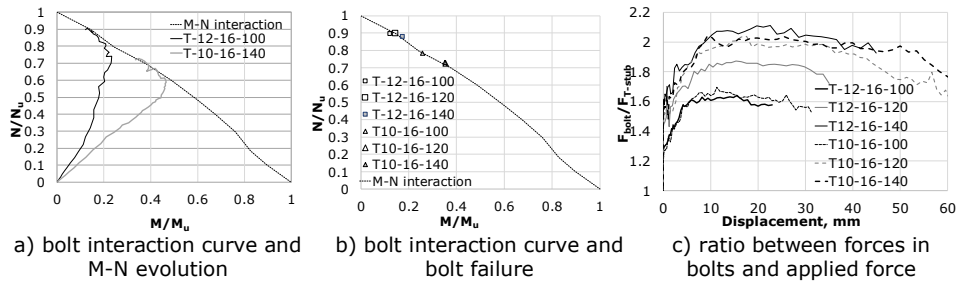
Figure 4.14. Forces in T-stub bolts [46]

Strain-rate results obtained with method 2 ([173]) are presented in Figure 4.15. The numerical data are in good agreement with the experimental results, but no substantial improvements can be observed with respect to method 1.
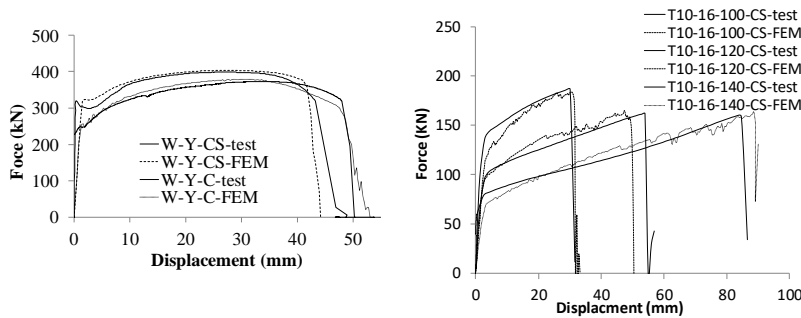
Figure 4.15 Experimental vs numerical curves for T-stubs using Method 2 [173]

Forces from the numeric results show higher prying effects in the more flexible configurations (mode 1) than in the more rigid configurations (mode 2). Therefore the mode 2 configurations can reach higher forces. On the other hand, flexible T-stubs can sustain larger deformations that would engage catenary action in the end-plate and therefore increase the resistance beyond the flexural one.

4.2.2.5 Loading rates in case of column loss scenarios

From the incremental dynamic analysis of structure S-FS-A-3 presented in section 3.2.2.5, the vertical displacement vs. time curve was studied for the smallest load that induces progressive collapse. In 0.43 seconds, the column descends 1.77 m. Using a simple computation, if all deformation were consumed in the T-stub, the average displacement of the T-stub would be around 200 mm/ second, see Figure

4.16. The 200 mm/ second loading rate would be the highest loading rate that can be measured in the T-stub.
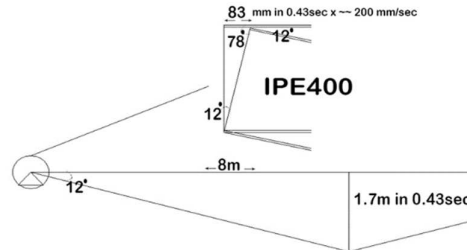
Figure 4.16 T-stubs deformation related to beam rotation [173]

Using **method 2,** [173], the effect of a 200 mm/second loading rate was assessed. Figure 4.17 show the force-displacement curves for the models T-10-16-100 and T-10-16-140, and for three loading rates, i.e. quasi-static, 10 mm/sec and 200mm/ sec, respectively. There are small differences in the ultimate force, as it depends mostly on the maximum capacity of the bolt (High resistance steel class 10.9 is less influenced by strain rate compared with mild carbon steel) [21]

Figure 4.18 shows the variation of strain-rate in specific locations of the T-stub, indicating a very high complexity of strain-rate dependency on the plasticity of the zone and also on the time/ imposed displacement. Since numerical simulations considering the effect of strain-rate with method 2 are computationally very demanding, and results do not show significant loading-rate effects, strain-rate will not be considered in full scale frame models.
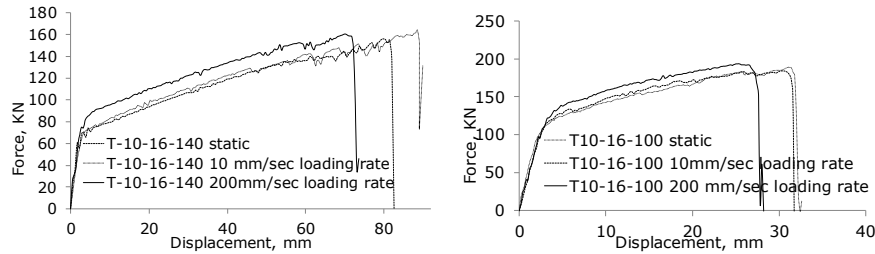
Figure 4.17 Numerical T-stub curves for different loading rates [173]
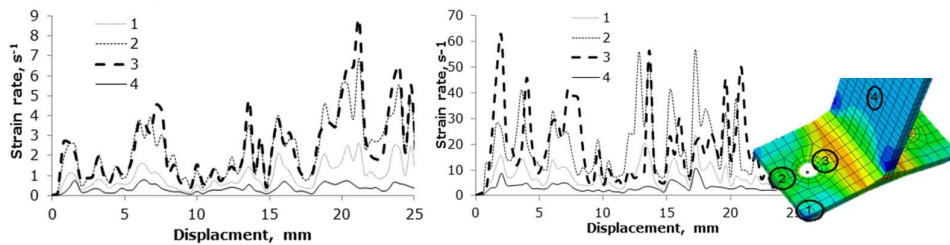
a) 10 mm/ second loading rate   b) 200 mm/ second loading rate
Figure 4.18 Strain rate values vs T-stub displacemet, in various locations of T-10-16-100 [173]

4.2.3   Calibration of 2D frame models under column removal

The principles, methods and parameters from sections 4.2.2.1 and 4.2.2.2 are used to define the analysis environment.

Nominal geometry was used to create the models for each experimental specimen, as initial measurements indicated very small deviations from nominal geometry (Figure 4.19.). The models included lateral restraining system which reproduced in detail the test set-up for the in-plane and out-of-plane restraining systems. The Est lateral restraining system was modelled with solid elements, even for the lateral and bottom fixing bolts, as some slippage occurred at high axial loads due to catenary action.

The horizontal links and reaction structures were modeled as beam parts and were meshed with B31 elements (2-node linear beam in space). C3D8R and C3D8I (8-node linear brick and incompatible modes) finite elements were used to mesh the solid parts in a sweep or structural technique using local seed constraints for refined meshes in critical zones (see Figure 4.20). The mesh size of the plastic zones has the same shape and size as the mesh of FEM models for material calibration of coupon tests. Properties of the materials were defined based on coupon tests results presented in Table 3.14.

The root radius of the hot rolled steel beam profile was modeled in detail, because initial results that disregarded this issue showed significant differences from the experimental data obtained.

The interaction between nodes was also modeled (some are presented in Figure 4.21). Welds were either modeled as ties, linking all degrees of freedom between points of two different solid parts, or directly modeled as continuous material of the solid part. Kinematic constraints connected nodes from a surface to a reference point to which boundary conditions are imposed (the hinge under the edge columns, or the loading point above the central column). Small imperfections were assumed by the asymmetry of the mesh and vibrations in the dynamic loading.

The load was applied with a smooth step amplitude in displacement control at the top of the central column until the failure is attained.
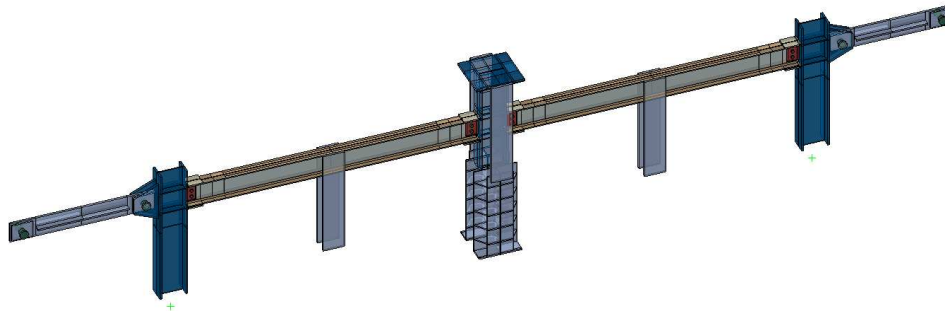
Figure 4.19. General view of the FEM model with types of material
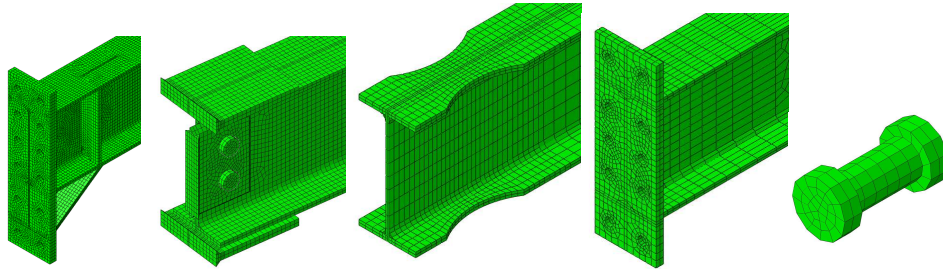
Figure 4.20. Detailed views of beam ends and bolts meshing
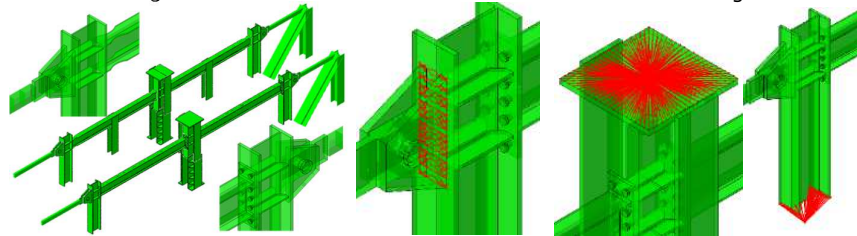
Figure 4.21. FE model of joints (in red- ties or constraints)

Figure 4.22. presents comparatively the experimental and numerical vertical load vs. vertical displacement curves. As can be seen, the results agree very well for each specimen, with good approximation of the peak force and the ultimate displacement. Also, the failure modes and failure sequence of the specimens were very well simulated, see Figure 4.23 to Figure 4.27. In the figures, PEEQ represents the equivalent plastic strain for elements while von Mises stresses in bolts are given in N/mm^2.
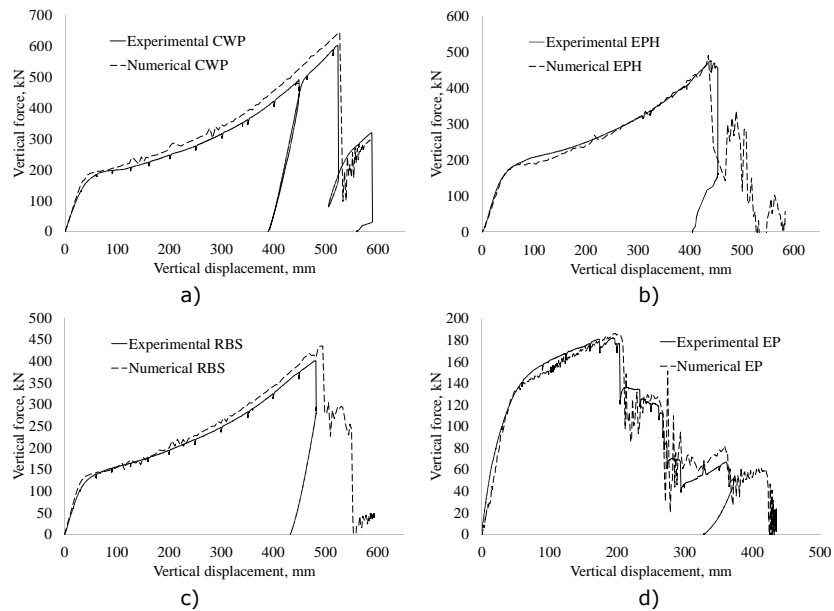
Figure 4.22. Vertical force vs. vertical displacement, experimental and numerical

For CWP model, the failure was initiated after the fracture of the bottom plate in tension near the middle column weld, before the beam weld (Figure 4.23.a). The fracture propagated in the shear tab along the bolt line (Figure 4.23.b), and finally, the beam completely separated from the column (Figure 4.23.c).

In the case of EPH model, due to the asymmetry caused by the bottom haunch, the performance of the connection in hogging (Figure 4.24) was different than in sagging (Figure 4.24). Three bolt rows from the right end of the beam (under hogging) fractured. First bolts that fractured were from the second row, soon followed by first and third rows. Although there is no indication of failure at the beams connections to the central column (end in sagging) at the point of maximum load, the results of the numerical simulation indicate the development of significant stresses in the bottom bolt rows (maximum stress of 1042 N/mm^2).

RBS failure consisted of the fracture in the middle zone of the reduced area at the top flange (Figure 4.26), which then propagated in the web.

For EP specimen, the sequence of failure started with fracture of the first bolt row (after the development of large deformations in the end-plate), followed by second and third bolt rows, respectively, see Figure 4.27.

Columns did not undergo significant plastic deformations. In the case of the central column, as both right and left bending moments are sagging moments, tension forces from the bottom flange from one side is balanced by a tension force from the bottom flange from the other side. The same is with compression forces in the top flange. Therefore, no significant shear is acting on the column web panel, while the continuity plates are subjected to tension (bottom) and compression (top).

a) fracture initiation - bottom cover plate	b) propagation of fracture in shear tabs	c) complete beam separation

Figure 4.23 Failure mode of specimen CWP: numerical simulation (top) and experimental (bottom)

a) large deformation of end-plate and bending of bolts owing to prying

b) three bolt rows fracture simultaneously
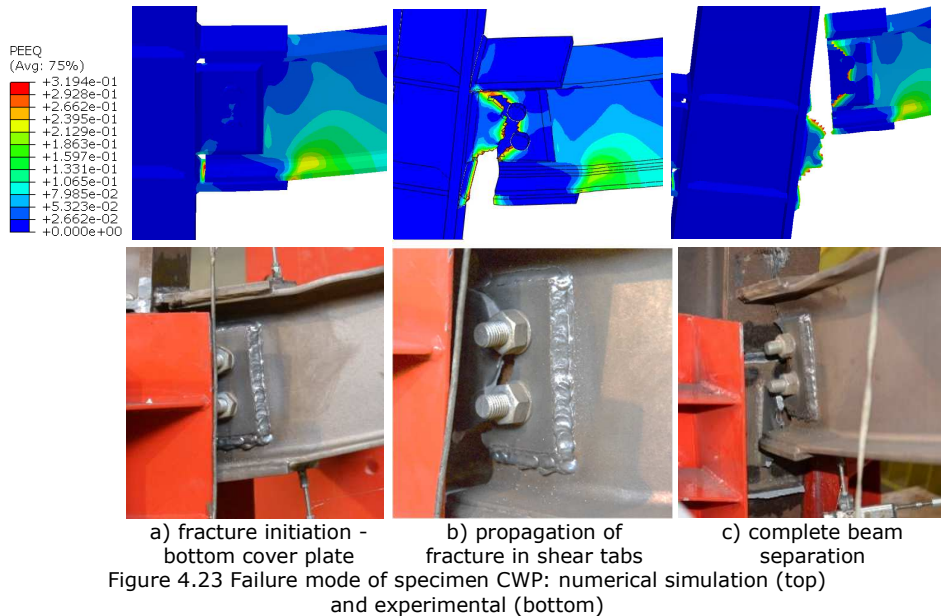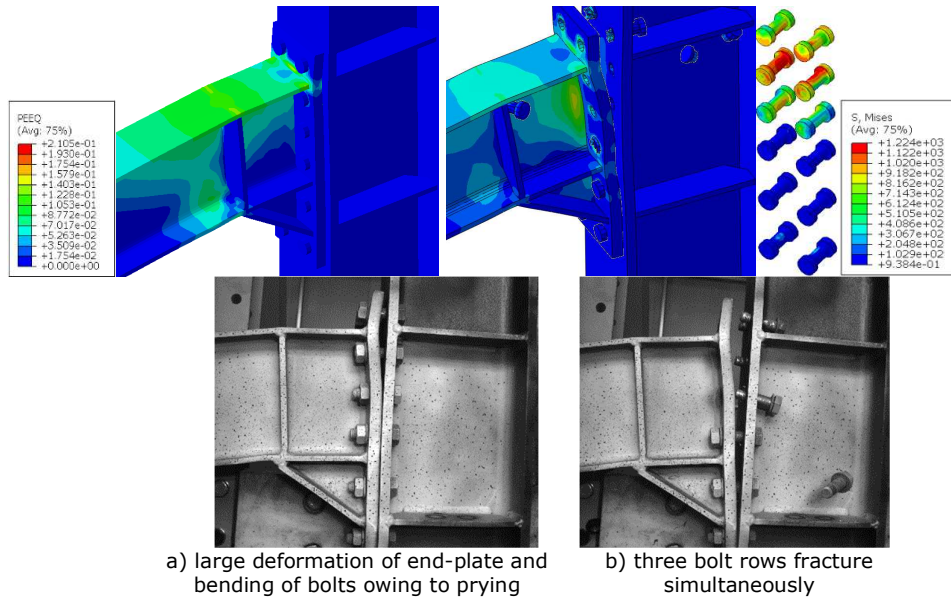
Figure 4.24. Failure mode of specimen EPH (hogging beam end): numerical simulation (top) and experimental (bottom)
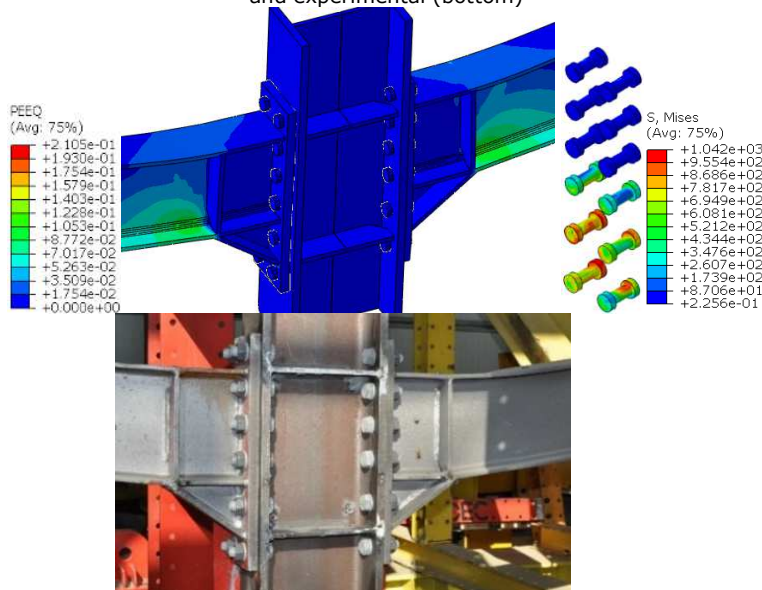
Figure 4.25. Deformation state at sagging beam end after failure of specimen EPH: numerical simulation and experimental

Although connections with over-strength failed in connection components, cover plate in tension and respectively bolts in tension, large parts of the beam outside the strengthened zone undergo plastic deformations that exceeded 10% strain. These deformations concentrate mostly in the beam flanges in tension.
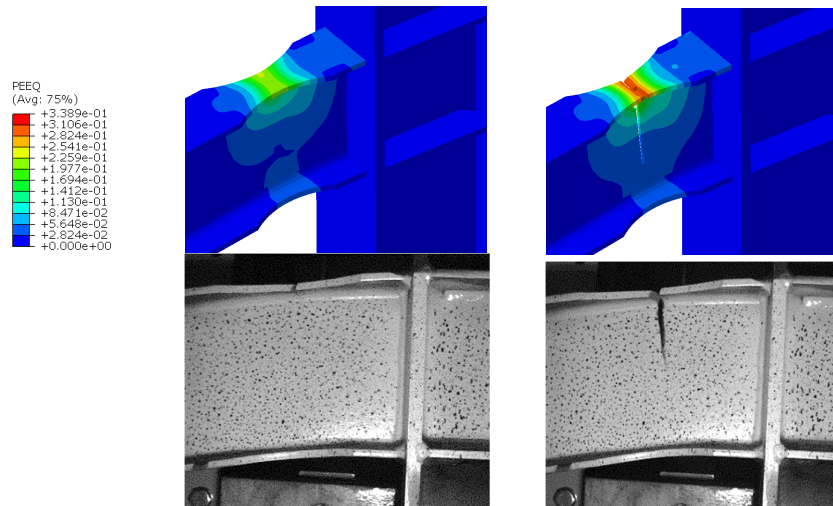
Figure 4.26. Failure mode of specimen RBS: numerical simulation (top) and experimental (bottom)
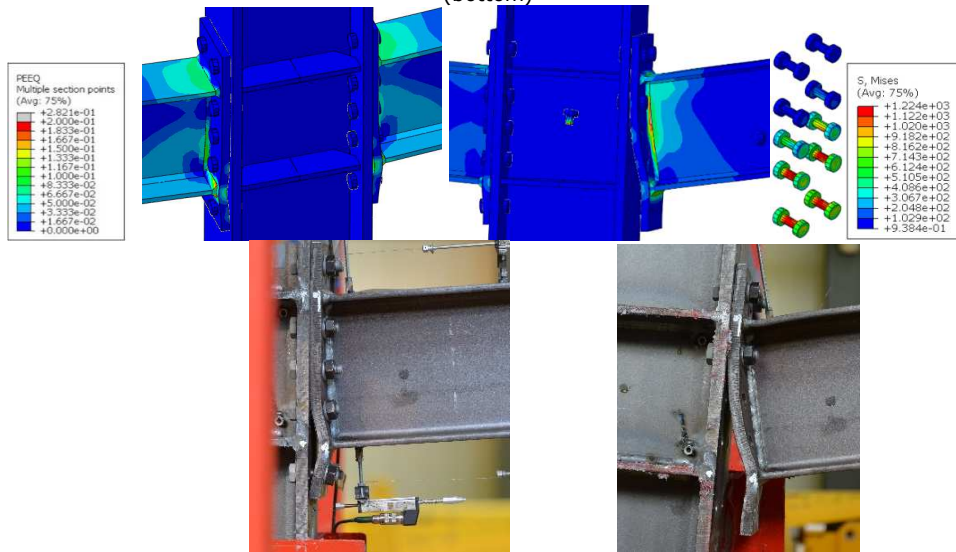
Figure 4.27. Failure mode of specimen EP as determined through numerical simulation (top) and experimental (bottom)

Figure 4.28 plots comparatively, from yielding to fracture, the normal strain distribution ε_{11} at the external end of right beams (connection 4), obtained in the test (and measured with VIC-3D) and the numerical simulations. The section for which the surface tension is plotted is located at 110 mm distance from the strengthened zones of CWP and EPH, at the most reduced section for RBS and at 50 mm from the end-plate for EP specimen. At the early loading stage, the beam sections exhibit flexural behavior, with the neutral axis close to the mid-height of the beam. For specimens developing significant catenary action (CWP, EPH, and RBS), the transition from the flexural to the catenary stage is given by the shift of the neutral axis from the mid-

height down to the flange in compression. For EP specimen, the strains indicate elastic flexural bending for almost entire loading process because the plastic deformations are localized in the connection. The deviation from the linear form is due a slight out-of-plane deformation of the web in the direction of the cameras, therefore the surface strains from the local buckling (parabolic and with variation in the thickness of the web) are added to the strains from the bending moment on the section (linear and constant on the thickness of the web).
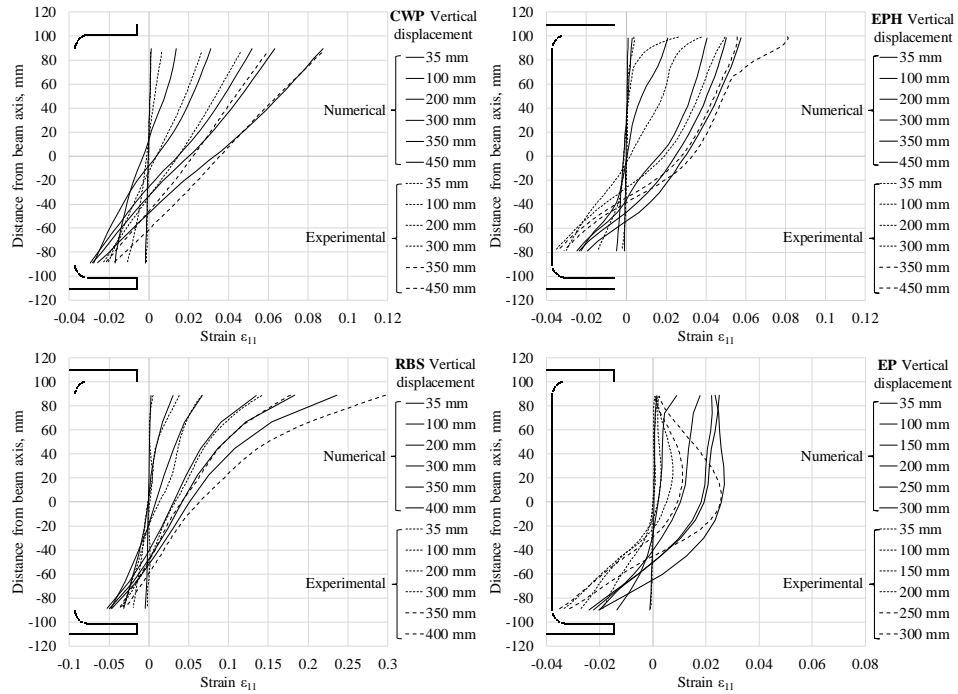
Figure 4.28. Strain ε_{11} distribution in beam, experimental (VIC-3D) vs. numerical

4.2.4   Calibration 3D MRF assembly under column removal

The principles, methods and parameters from sections 4.2.2.1 are used to define the modeling and analysis. Meshing techniques and other modeling parameters are very similar to the ones presented in section 4.2.3.

Nominal geometry was used to create the model for each experimental specimen, as initial measurements indicated slight deviations from nominal geometry (Figure 4.29).

The circular hollow section elements used for restraining the system were modeled as beam elements using B31 (2-node linear beam in space) mesh elements. Steel constitutive response of members and bolts was modeled using a true stress vs true strain relationship, within a significant strain formulation, and material characteristics based on the experimental values presented in Table 3.17.

The perimeter columns have rigid supports at the base. For the bottom ends of the vertical circular hollow section braces, designed and detailed as pinned connections, the 3 linear displacement degrees of freedom were blocked. The load was applied at a reference point located on the top of the central column connected through a kinematic coupling to the top surface of the column.

a) general view   b) central column details
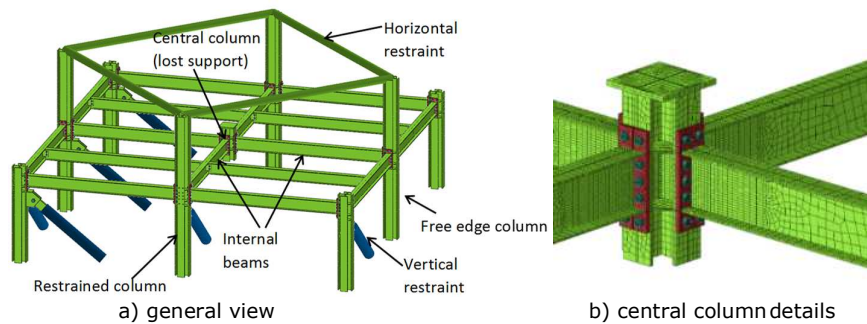
Figure 4.29: Finite element model of 3D specimen:

The force-displacement curve obtained from FE analysis is compared with the one obtained in the test, see Figure 4.30.

Figure 4.31 shows the deformed shape and equivalent plastic strain (PEEQ) at maximum force. Figure 4.32 and Figure 4.33 show in detail the distribution of equivalent plastic strains at the peak load in three different beam-to-column joints and connecting bolts.
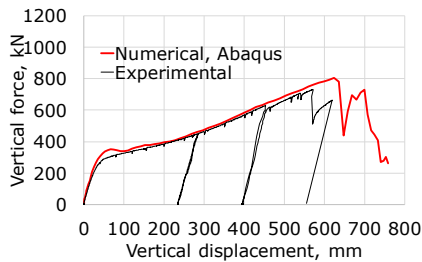
Figure 4.30 Experimental and numerical vertical force–vertical displacement curves
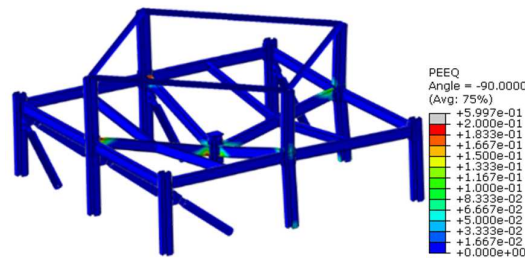
Figure 4.31 Deformed shape and equivalent plastic strain (PEEQ) at failure

a) central column   b) restrained column B1   c) free edge column B3

Figure 4.32: Closed view of deformed shape and equivalent plastic strain (PEEQ) at peak load

a) central column   b) restrained column B1   c) free edge column B3

Figure 4.33: Equivalent plastic strain (PEEQ) in bolts at peak load
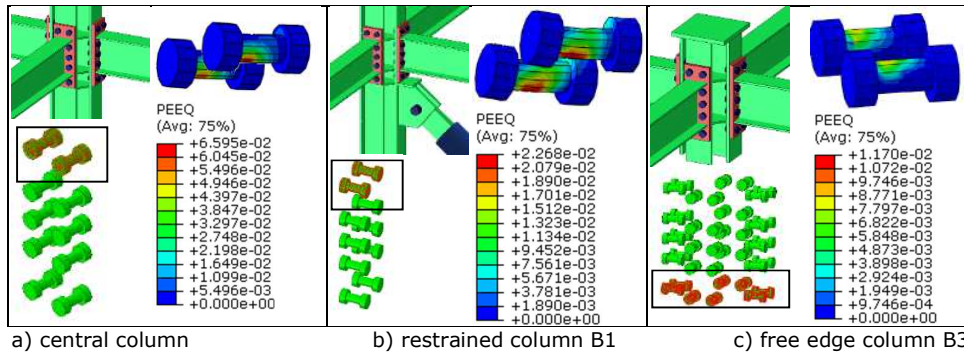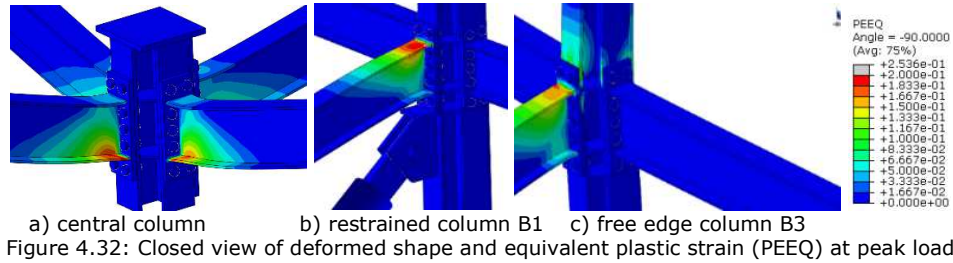
The FE model predicted with accuracy the force-deformation response and also the failure mode. However, the peak load and ultimate deformation are over-estimated. This shortcoming in the FE modeling is mainly caused by the imperfections in load application and geometrical/material imperfections, which were not considered in the numerical model. In the experimental model, the rotation of the central column leads to concentrations of plastic deformations and failure in one beam. This rotation was not very significant in the FE model because the eccentricities were ignored ([176]).

Figure 4.34 shows the axial force in internal main beams and the bending moment in internal beams at ends away from the central column versus vertical displacement.
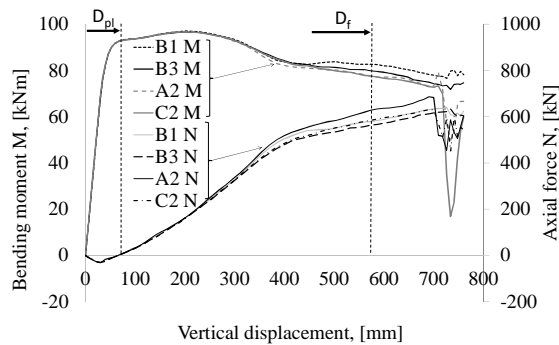
Figure 4.34: Axial force and bending moment in beams versus vertical displacement [176]

The plastic hinge develops at the beam end section (see Figure 4.34.) at a vertical displacement of about 70 mm (D_{pl}) where the value of the plastic moment is M_{pl}=93.2 kNm. The bending moment in beams reaches the maximum, M_{max}= 96.5kNm, at a vertical displacement of 226 mm. The corresponding axial force is 202 kN, or approximately 0.18 N_{pl}, where N_{pl} represents the beam axial capacity. When the bending moment decreases up to 0.85 of M_{max}, the corresponding vertical displacement of the central column is 400 mm and the axial force is 519 kN, respectively 0.48 N_{pl}. Although the bending moment decreases, the axial forces in the beams develop due to catenary action, increasing the overall capacity of the system to resist vertical loads. At a vertical displacement D_f = 570 mm (or a chord rotation of 12°), the internal forces and moments are 0.83 M_{pl} and 0.52 N_{pl}. As the level of axial force is high, an analytical approach for evaluating the section at this phase must be based on the interaction between the bending moment and axial force.

The internal forces show the identical behavior of the four beams, except the failure, see Figure 4.34. Therefore, it can be concluded that each of the two perpendicular main frames is loaded for each value of vertical displacement with the same amount of force, up to the point of the first failure that occurs in the beam. Hence, to describe the vertical force - vertical displacement on each frame direction, the total force imposed to the system can be divided by two. Catenary action induces large axial forces in the beam, which are transferred to the columns. Free edge columns (with no lateral restraints) resist the forces trough flexural capacity. In Figure 4.32.c, the plastic deformation of the column can be observed as it is pulled inwards. The level of deformations are not high, but they can induce a bow deformation of the column and reduce the buckling resistance of the columns under gravity loads ([176]).

4.2.5 *Performance of EP connections*

The bolted extended end-plate connection performance was experimentally tested for different configurations, within different test set-ups. Several numerical models have been developed for a detailed investigation of its behavior. The calibrated models used for this study are the partial strength connection experimental test in a 2D set-up from Timisoara presented in section 3.4.4.4 with calibration detailed in section 4.2.3, and the improved configuration experimental test in the 3D test set-up from Cluj-Napoca, see section 3.5.4.1, with the calibration presented in section 4.2.4.

It should be noted that the development of catenary action in the two experimental test set-ups is different due to different lateral stiffness of the restraining systems. The 3D set-up is calibrated for a near penultimate column removal, as the subassembly is extracted from the corner of the structure with the removed column adjacent to edge columns on both directions (see removed column D2 from Figure 4.35.a). Thus, for each of the perpendicular frames containing the removed column, one adjacent column is located in the façade (D1; E2) with no restraining for in-plane lateral forces. The calibration of the restraining system was performed in ELS software, presented in Figure 3.60, and is valid for both steel only and composite specimens.

The 2D test set-up is calibrated for an intermediate column loss (see Figure 4.35.c). In plane rigidity for the structure and set-up was analyzed with SAP2000 in linear static analysis and is given in section 3.4.1. The influence of the perpendicular system is considered by torsional rotation restraining in the location of secondary by preventing the frame from out of plane deformation beams, but resistance contribution is not considered. The 2D test set-up is stiffer than the 3D one, allowing for the development of higher axial forces resulting from catenary action at the same

columns vertical displacements. Therefore, to assess the difference between 2D and 3D performance of frames with EP connections, an additionally test set-up was used, derived from the 3D set-up (composed of two perpendicular frames subjected to penultimate column loss), but containing just one 2D frame with the same lateral rigidity as in the case of a 3D system frame. Also in this case, only stability influence of lateral system is considered (out of plane restraining). The names of the numerical models are given in Table 4.1, function of the connection type and test set-up. All numerical testes followed the experimental test loading protocol, by imposing vertical displacement in the middle column up to failure was reached.

Table 4.1 EP numerical model labels for 3D and 2D tests

| | 2D frame set-up | | 3D frame set-up |
	Central column loss - CC	Penultimate column loss - PC	Near penultimate column loss PC
Partial strength connection configuration	EP-2D-CC: (also experimentally tested Timisoara)	EP-2D-PC	EP-3D-PC
Improved connection configuration	iEP-2D-CC	iEP-2D-PC	iEP-3D-PC (also experimentally tested in Cluj-Napoca)

a) 3D Specimen extraction

3D PC - near penultimate column loss set-up

b) 3D test set-up

a) 2D Specimen extraction

2D CC - Central column loss set-up
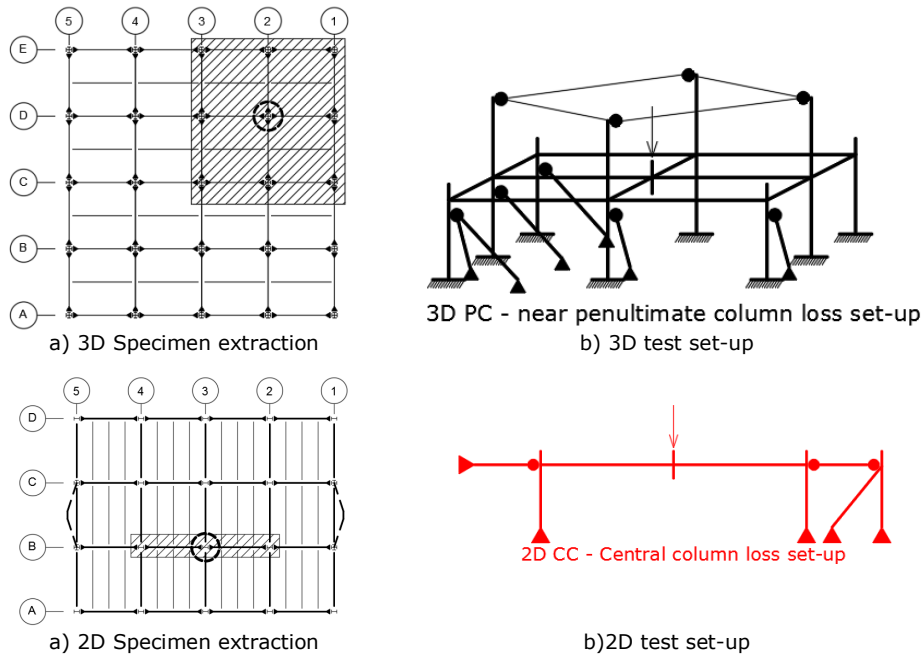
b)2D test set-up

Figure 4.35: 2D and 3D test specimen extraction and set-up

Figure 4.36.a shows the vertical force-vertical displacement results for both EP connections (partial strength and improved) and for both test set-ups used in the experimental program (2D with central column loss and 3D with penultimate column loss). In order to enable the comparison in terms of forces and to obtain the resistance for one frame, the vertical force corresponding to 3D set-up was divided by 2.

Failure of the partial strength EP connections tested in the 3D test set-up initiates at bolts near tension flanges of the central column connection, and occurs simultaneously in both directions (see Figure 4.36.b). The slightly higher ductility of the connection in the 3D configuration is given by reduced amount of axial force due to less lateral stiffness of the system. Therefore, a comparison between 2D and 3D ductility and strength of the connections should be addressed by using in both cases column loss scenarios with the same lateral rigidity.

a) vertical force – vertical displacement curves   b) Failure of EP-3D-PC
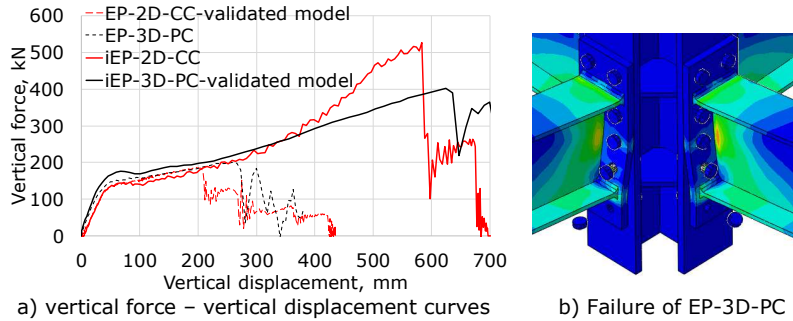
Figure 4.36: Numerical EP and iEP connection configurations tested in 2D and 3D test set-ups

Tests on 2D and 3D numerical models with the same lateral rigidity (PC – penultimate column loss/ near penultimate column loss) are performed for both strengthened and unstrengthened connections. To assess the influence of boundary conditions given by the undamaged structure on the performance of frames in column loss events, the same sets of tests are performed without modelling the restraining system that simulates the rest of the structure. The labels of the tests with no consideration of the rest of the structure restraining are marked with an *f (free)* suffix.

The vertical force vertical displacement curves for these numerical model are given in Figure 4.37.a and Figure 4.37.b for the 2D and 3D frame systems considering penultimate and respectively near penultimate column loss. Some ductility increase can be identified in the partial strength connections in case of lack of restraining from the structure, but the strength is the same. For the improved iEP connection, on the other hand, lack of restraining reduces considerably the capacity to resist vertical loads, as resistance from catenary action is diminished. Ductility demands are also influenced by boundary conditions given by the structure. Consequently, boundary conditions simulation in accordance to the stiffness provided by the entire structure is essential for correct evaluation of frames in column loss for ductility and strength alike, in 3D and 2D structural assemblies.

For all test set-ups configurations, partial-strength connection did not allow the development of catenary action, while the strengthened EP connection (iEP) has a ductile behavior, with enough capacity to shift the failure into the beam (fracture of the beam tensioned flange of the central connection) and allow the development of catenary action. In the case of the partial strength EP connection, the strength and ductility is almost identic for penultimate /near penultimate column removal when comparing 2D results with 3D results.

a) 2D numerical tests, with and without restraining

b) 3D numerical tests, with and without restraining

c) iEP numerical tests, with and without restraining

d) 2D and 3D restrained numerical test set-ups and specimen extraction from structure
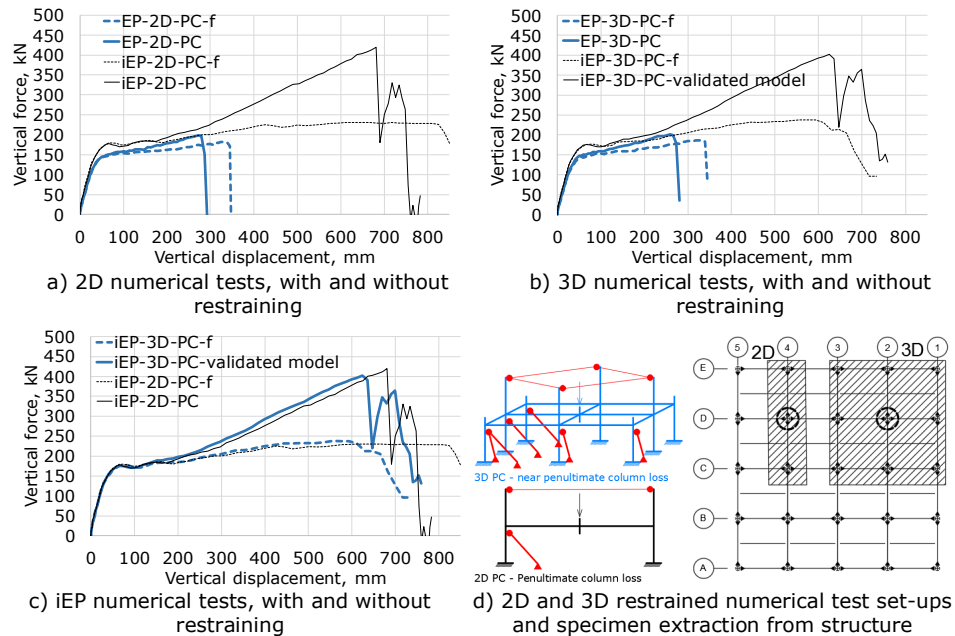
Figure 4.37: Numerical EP and iEP connection configurations tested for column loss in 2D and 3D with and without modelling the restraints from the structure

Results on strengthened iEP connection in 2D and 3D tests with and without boundary conditions determined by the entire structure are compared in Figure 4.37.c. Ductility increase can be seen in the case of the 2D assemblies versus 3D assemblies. This can be explained by the out of plane restraining of the 2D test set-up that does not allow torsional effects to appear, while in the 3D test set-up all rotations are free, consequently small torsional effects can lead to a slight acceleration of fracture initiation. Therefore, 2D numerical investigations do not account for all possible phenomena, resulting in unconservative evaluations. The 3D effect for pure steel specimens with unstrengthened EP connection was insignificant, while some influences were identified in case of strengthened iEP connection. However substantial 3D contributions may appear in case of assemblies with concrete slab.

4.2.6   FEM calibration summary

The FEM modeling and simulations using Abaqus environment allowed the development of complex material laws, which are necessary for simulation of the material degradation and failure of the components. The investigations included, apart from material calibration (elastic and plastic properties, ultimate strength, and degradation), detailed information about bolt assembly behavior, strain rate, geometry and contact, component sensibility, to 3D behavior in an integrated simulation environment. This calibrated tool completes and extend the information about the experimental results, as it delivers more data related to internal forces, local strain and stress maps, and other data that could not (or are difficult) be gathered through experimental procedures alone.

The performance of the initial and strengthened EP connection was assessed using the calibrated models for 2D and 3D test set-up configurations for column removal scenario. The calibrated models can be used not only to extend the data to other configurations but also to obtain results for different loading configurations (uniform distributed load) or testing conditions (thermal effects can also be added in order to get results for different temperature conditions) and evaluate the parameters and conditions that have an impact on the column loss resistance of frame.

4.3   AEM model calibration

4.3.1   Calibration 3D MRF assembly under column removal

The pure steel 3D MRF assembly, calibrated with FEM in section 4.2.4, was calibrated also using AEM (ELS software).

A view of the ELS model, including the steel elements and connections, is shown in Figure 4.38. For the steel members and bolts, the fully nonlinear path-dependent constitutive model described in section 4.1.2.2 was adopted. The material characteristics are based on the experimental values presented in Table 3.17. Note that the model geometry (dimensions, cross-sections, and local details), support conditions, and material characteristics are in full agreement with the tested specimen. Columns, beams, and end-plates were modeled as solid elements and could undergo deformations at the interface between the discretized elements. The constraints, made of tubular steel sections, were modeled as nonlinear axial link elements. The bolts were modeled using individual springs: one for normal stresses and two for shear stresses. Modeling technique is also briefly described in section 3.2.2.2. The column bases were considered fixed, and all displacements and rotations were prevented.

The ultimate vertical load capacity of the model for the central column loss scenario was obtained by performing a displacement controlled dynamic pushdown analysis, but with a low speed, similar to the experimental one (quasi-static).

The overall relationship between the vertical force and the vertical displacement below the central column is shown in Figure 4.39. The results show a very good correlation with the experimental data. All the phenomena that occurred during the test can also be traced on the numerical force–displacement curve, i.e., elastic behavior, plasticity, initiation of catenary force, and failure. The maximum vertical force was 764 kN, and the corresponding displacement was 550 mm, which are very close to the experimental values, i.e., 732 kN and 569 mm, respectively.

Figure 4.40. shows the tensile strains in members, just before failure. Up to the peak load, the model showed the development of plastic hinges in beams but no local failures. At the peak load, the normal springs in the most stressed part of the beam flange (B2-B3 beam end near the central column) reached the separation strain, which implies that they are removed from the model, resulting in less capacity of the section in tension. With the imposed displacement increasing, more and more springs failed, until the complete separation of the beam along the fracture line and the analysis was stopped. Note that the visualization of the gap in the bottom flange is not due to element separation but due to the large elongation of the springs.

Figure 4.41.a and Figure 4.41.b show the bending moment and axial force in beam B1-B2. The curves indicate a very good approximation of the maximum capacity, even though there are some differences between experimental and numerical results. For the axial force, the most importance difference is in the initial phase, up to a vertical displacement of 250 mm. The lack of arching action in the

experimental curve (axial compressive forces) is caused by the slip that occurs within the bolted connections ([43]).
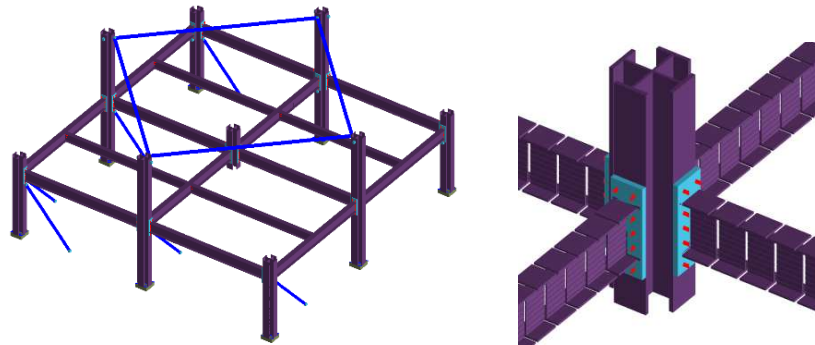
a) overview of model   b) detailed view of beam-to-column connections
Figure 4.38 Applied element model -AEM - of 3D specimen
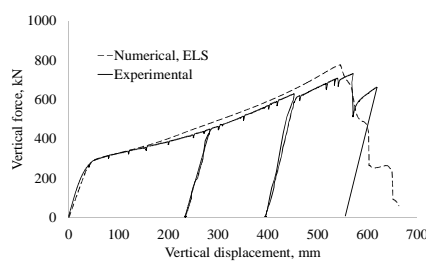
Figure 4.39. Experimental vs. numerical vertical force-vertical displacement
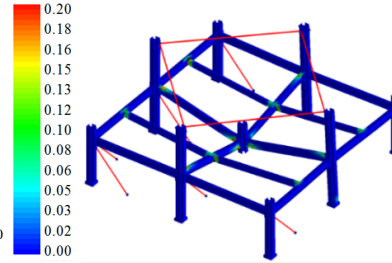
Figure 4.40.Tensile strains in structure at D = 550 mm
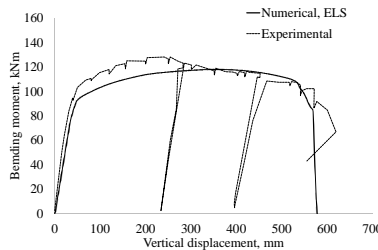
a) Bending moment, beam B1-B2   b)Axial force, beam B1-B2
Figure 4.41. Experimental vs. axial force and bending moment in beams [43]
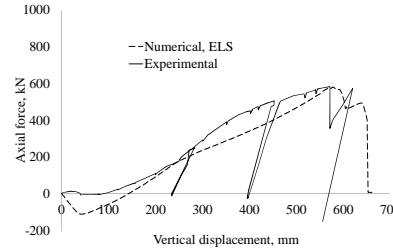
For the development of catenary action in beams, beam-to-column connections must be able to sustain large rotations and large axial forces. It is therefore of interest to see the variation of forces in beams and bolts with the vertical displacement. Note that for the external beam ends, the first bolt row is above the top flange, whereas for the inner ends, the first bolt row is beneath the bottom flange (Figure 4.42.a). Figure 4.42.b–d show the variation of the axial force in bolts with an increase in the vertical displacement. The yield and ultimate force of the bolts, F_{yb} and F_{ub}, are marked on the graphs using dashed lines and are taken from the experimental tests. In all of the cases, the bolts are within the elastic range, except the second bolt row. In that case, two bolts enter into the inelastic range but the tensile strength is not exceeded. Note that bolts did not experience fractures during the test. The first bolt

row has lower axial forces because of the larger flexibility of the end-plate. As shown in Figure 4.42.b–e, three stages can be noticed in the force–displacement curves. In the first stage, the quasi-linear increase in the force in the bolts corresponds to the elastic behavior of the model. The upper limit of the first stage corresponds to the attainment of yielding in beams at a vertical displacement of approximately 30 mm. The second stage ranges between 30 and 215 mm and shows a slow increase in the axial force in the bolts. This stage corresponds to the elastoplastic behavior of the model. After 215 mm, the catenary stage initiates in the beams and axial forces in the bolts increase at higher rates, ultimately reaching the maximum values when the vertical displacement reaches 550 mm. When failure initiates, the corresponding axial force in the bolts starts to reduce ([43]).

a) numbering of bolt rows at beam-to-column connections

b) beam B1-B2, end B1

c) beam B1-B2, end B2

d) beam B2-C2, end C2

e) beam B2-C2, end B2

Figure 4.42. Axial forces in bolts versus vertical displacement [43]
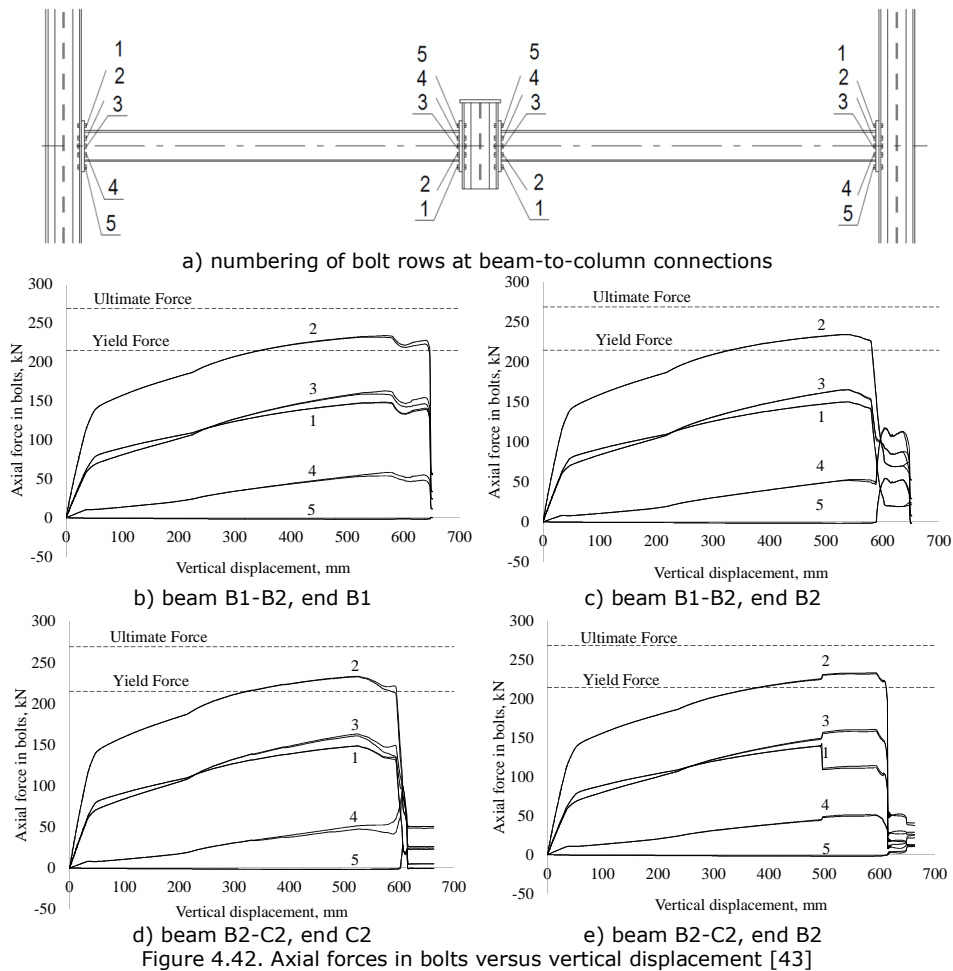
4.3.2   Influence of loading distribution on the ductility of the structure

Structural response in column loss situations is typically investigated either by gradually increasing the vertical point load on the missing column (PL method), or by applying a distributed load along the beams, most common using uniformly distributed load (UDL method), then releasing the column support. PL method is less challenging to apply and control, while the later, also called column release method, represents more faithfully the response regarding internal forces distribution [68]. To compare the results of the two methods, uniformly distributed loads with different intensities were applied on the internal beams in a non-linear static analysis. After applying the uniform load on the structure with the central column in place, the column support was released, and the vertical reaction of the central column was measured, see Figure 4.43. The decrease in the reaction of the central column represents the load that is undertaken by the beams. The amount of initial gravity load was varied so that on the initial structure the axial compression force in the central column would be 33%, 66% and respectively 100% of the maximum vertical force applied on the model (PL method). The models are detailed in Table 4.2:

Table 4.2. Static models for the ANS-M specimen

Model name	UDL on main beams	Equivalent surface load
PL (Point load)		
UDL-1	42kN/m	28 kN/m^2
UDL-2	83kN/m	56 kN/m^2
UDL-3	125kN/m	84 kN/m^2

Figure 4.43.c shows the vertical reaction force vs. vertical displacement curves obtained using the two methods. In what concerns the UDL curves, initial reaction forces are always negative as a result of applied distributed loads on beams. If the ultimate force is beyond zero, this indicates the applied UDL is less than the capacity and the structure does not fail and additional point load is required to reach failure. If the ultimate force does not reach zero value, this indicates the applied UDL is larger than the capacity, and the structure fails before redistributing all load. Therefore, the determination of the exact value of UDL corresponding to the attainment of failure requires several iterations. To compare the results of PL and UDL methods, reaction forces obtained using UDL (Figure 4.43.c) were offset to start from zero force, see Figure 4.43.d. A uniform distributed load of 33% from the maximum column point load (UDL-1) does not substantially change the response, and its influence may be neglected. In the case of UDL-2, the ductility of the system is reduced by 25%. A uniform distributed load that produces a central column reaction equal to its maximum capacity in the reference loading system (UDL-3) will reduce the vertical force capacity and vertical displacement by 40%, and also the yielding force by 17%. The different ultimate capacities obtained by varying the intensity of the UDL are resulting as the effects of different moment distribution before failure, see Figure 4.44. To note the M_N represents the maximum bending moment corrected due of the presence of the axial force (M-N interaction). ([177])

a) Load step 1   b) Load step 2

c) Vertical reaction vs. vertical displacement   d) Vertical force vs. vertical displacement
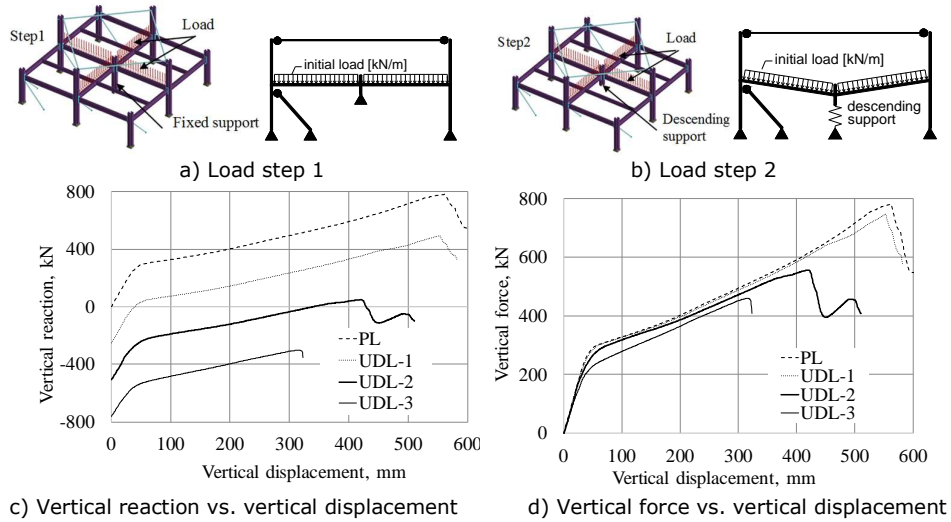
Figure 4.43. Uniformly distributed load method [177]

a) UDL-1   b) UDL-2   c) UDL-3
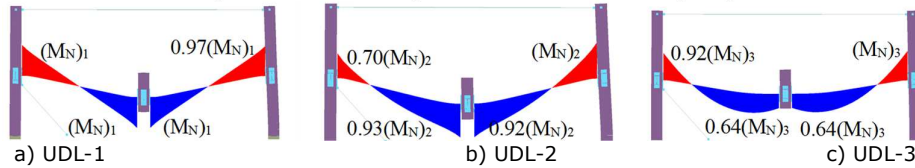
Figure 4.44. Moment distribution before failure for UDL [177]

Several iterations are required to determine the exact value of UDL corresponding to the attainment of failure. A direct method to obtain the complete path of the force-displacement curve under gravity load can employ a pushdown analysis, where the column is removed and the distributed load is incremented up to the attainment of failure. The advantage of the pushdown analysis is the possibility to directly compare the point load results with all UDL at zero reaction force. Figure 4.45.a shows the numerical model and distribution of loads in the pushdown analysis. To compare the results of the pushdown simulation with the point load test, the total vertical reaction (sum of total applied loads) needs to be allocated to each column based on their tributary zone. For the central column, the corresponding vertical force was 1/4 of the total reaction. Figure 4.45.b shows the vertical force - vertical displacement curves comparison for the reference model (validated against experimental test) and the pushdown analysis. For comparison, the equivalent uniformly distributed load on the floor is also shown on the secondary vertical axis. As seen from the two curves, the initial stiffness, and post-yielding behavior are almost identical until the vertical force reaches 380 kN. After this, the model with UDL exhibits an almost constant stiffness, until the failure is attained at a force of 510 kN (or an equivalent UDL of 62 kN/m^2). The ultimate displacement amounted 410 mm. Comparatively, the ultimate resistance and deformation capacity of the model loaded with a point load at the missing column location were much higher, i.e. 773 kN and 564 mm, respectively. As the case with distributed gravity loads on the floors represents a more realistic loading scenario, the prediction of the structural capacity using point load method requires further calibrations to improve the consistency. When compared with the discrete UDL

analysis (see Figure 4.43.c), it may be seen the ultimate capacity is very close to the UDL-2 (56kN/m^2). [177]
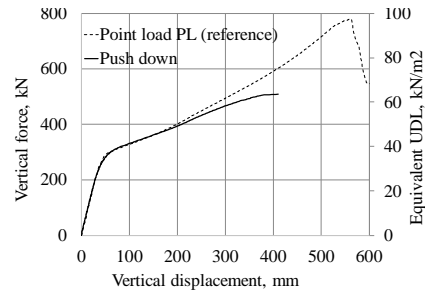
a) Distribution of UDL   b) Force-displacement curve

Figure 4.45. Pushdown analysis [177]

The ultimate strength and the ductility are very much affected by the distribution of loading. The reduction in capacity is caused by the difference between the maximum force that can be resisted as a point load in the middle of the span vs. a uniformly distributed load causing the same bending moment at the beam ends. Point load implies moments are equal in the both external and internal beams ends/ sagging and hogging. Uniformly distributed load results in higher bending moment values at the external ends (hogging) than at the internal ends (sagging). Pure bending failure load is reached at the same moment capacity in the external beam ends, but at different equivalent loading, respectively a 25% reduction from the point load distribution maximum capacity should be applied to reach the UDL maximum load capacity. The reduction in strength influences and limits the ductility as well. Therefore, a reduction in deformation capacity of at least 25% may be expected depending on the loading conditions.

4.3.3   DIF estimation based on AEM results

In the event of a sudden column loss, the total force acting on the floor is the summation of directly applied gravity loads and inertial forces developed during the dynamic response of the structure. For the study, the model was loaded with a uniformly distributed gravity load (UDL) and then the central column was instantaneously removed, thus exposing the structure to a dynamic effect. The analysis was done for UDL of increasing intensity, up to failure. Figure 4.46.a shows the history of vertical displacement for different levels of UDL. The ultimate load before failure amounted 40 kN/m^2, at a maximum vertical displacement of 321 mm. The vertical force - vertical displacement envelope obtained in the incremental dynamic analysis is presented in Figure 4.46.b and compared with the static pushdown curve. The maximum loading in the dynamic analysis is less than that 2/3 of the static pushdown capacity. To quantify the dynamic effect in the structure, either the force or displacement response may be used. The two dynamic factors, DIF, are defined in Figure 4.46.b. The force-based dynamic factor, DIF$_F$, and displacement-based dynamic factor, DIF$_D$, which were calculated based on the numerical analysis results, are presented in Figure 4.47. The values are compared with DIF calculated using formulas proposed in [25] and [100]. Due to the contribution of post-yield stiffness (increased due to the development of catenary action), the force-based amplification factor DIF$_F$ is underestimated for normalized rotations larger than 2

when UFC formula [25] is adopted. A better estimation is given by analytical formula proposed in [100]. The results obtained for DIF_D are also in good agreement with the results obtained with the relation proposed in [100].
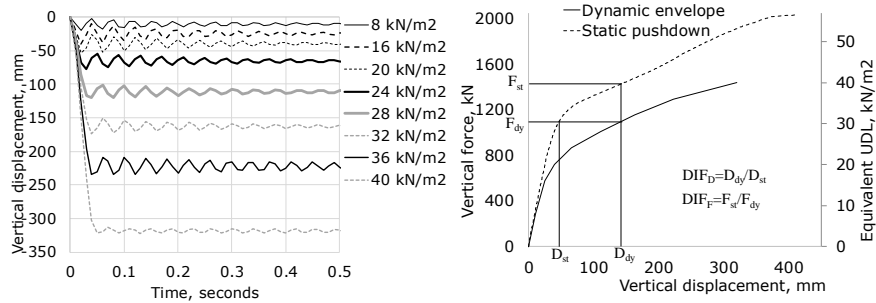
a) Vertical displacement vs time   b) Static vs dynamic force-displacement curves

Figure 4.46. Dynamic analysis results [177]
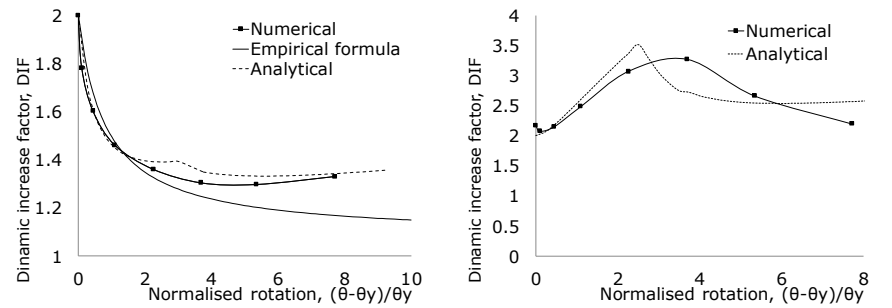
a) Force-based factor DIFF   b) displacement-based factor DIFD

Figure 4.47. Comparison of dynamic increase factors and [177]

The dynamic response of steel frame structures due to a sudden removal of a column using numerical simulations can also be evaluated using empirical and analytical formulas. The lower limit of force-based DIF appears to be higher than empirical based results [25]. Similar observations were reported in [100]. This increase may be explained by the increase of post-yield stiffness under large deformations as a result of catenary action development. The displacement-based DIF increases with the increase of the plastic deformation, until reaches a maximum value of 3.25 for a normalized rotation of 3.6 ([177]).

4.4   Case studies

4.4.1   Selection of case study structures

The performance of four type of connections under column loss was investigated through experimental testing and numerical simulations. The conclusions that were drawn are limited to the specific conditions of the tests, and cannot be used to describe in general the performance of the beam-to-column connections of similar configurations. Therefore, it is of interest to investigate what are the main parameters that might affect the performance of connections. Full-scale numerical tests are first used but with configurations selected from real structural configuration. These numerical investigations aim at evaluating the performance and vulnerability of full-scale beam-to-column connections of steel frames subjected to internal forces corresponding to large displacements derived from column loss events. One parameter is the level of seismic intensity used in design. Therefore, buildings are designed for different seismic zones but keeping the same configuration, number of bays, and number of stories. A layout plan with four bays and four spans is considered. The lateral load resisting system consists of moment resisting frames MRF on both directions. Since the MRF structures are not feasible for large number of stories, the structures are limited to six storey height.
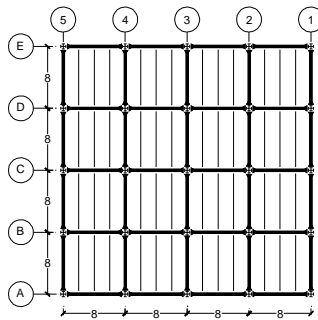
Figure 4.48. Plan layout of the case study structures

4.4.2   Design of case study structures

4.4.2.1 Design of moment resisting frames taking into account beam-to-column typology

MRF structures have been designed in three different locations, with different seismic conditions both for design ground acceleration and for ground type (given by corner period). The locations are Cluj-Napoca (low intensity seismic zone LSZ), Craiova (medium intensity seismic zone MSZ) and Bucharest (high intensity seismic zone HSZ). The structures have 4 spans of 8m in each direction and 6 stories of 4 m. Intensity of dead and live loads is 4kN/m^2. The very high seismic intensity location (Focsani) was no longer chosen as MRF with semi-rigid joints cannot be designed due to seismic drift conditions (see remarks in section 3.2.1).

Seismic loads are computed in accordance with the Romanian Seismic Code provisions, P100-1 (2013) [120]. The design is based on standards mentioned in section 3.2.1.

The 3D model of the structure was built using SAP2000 software [121] (see Figure 4.49.a), including the strength and stability checks. Steel grade S355 was considered for all structural elements.

The details of the connections were also modeled in the SAP2000 software, considering the overlap of beam elements.

- For CWP, the strengthened part of the beam was considered by modeling a beam element with the length of the cover plate having the supplementary cover plates added to the cross-section of the beam. Detailing was performed according to FEMA 350 [146].
- For the EPH connection, the haunch was modeled considering a tapered beam section with the height of the haunch height added to the beam height at the face of the column, and the height of the beam at the end of the haunch. The length of the tapered section is equal to the haunch length (see Figure 4.49.b). The stiffness of the bolted connection at the end-plate – column interface was calculated with *STeel CONnection* [148] and introduced in the model. Requirements from EN 1998-1 [117] and EN 1993-1-8 [147] were verified.
- For RBS connection, the reduced zone of the beam was modeled as a beam with the lengths of the reduction and the section of the beam with the maximum of flange reduction (see Figure 4.49.c). Dimensions resulted from ANSI/AISC 358-10 [149] recommendations.
- For EP, like in the case of EPH, after determining the stiffness of the bolted connection at the end-plate – column interface with *STeel CONnection* [148], the value was introduced as rotational stiffness in SAP2000 model. EN 1998-1 [117] and EN 1993-1-8 [147] provisions were used for detailing the EP connection.
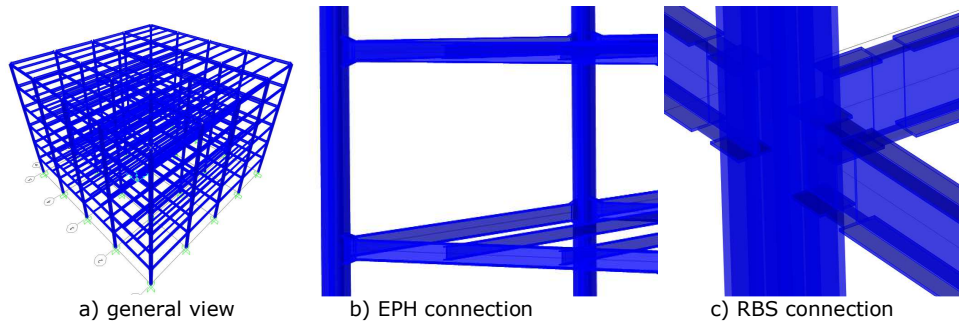
a) general view   b) EPH connection   c) RBS connection
Figure 4.49. 3D model of the case study structure in SAP2000

The seismic requirements for the three locations and the section of elements based on the design considering each type of connections are presented in Table 4.3. The maximum bending moment in beams is obtained from seismic design situation for MSZ and HSZ and from fundamental design combination for LSZ. Therefore, seismic requirements for the LSZ structure does not influence the size of the elements.

The beams in case of structures with CWP & EPH connections are slightly smaller than the beams of structures with RBS & EP connections for all seismic zones, since the maximum bending moment is at the end of the beam, where CWP & EPH connections are strengthened and RBS & EP connections have less resistance with respect to the beam capacity (RBS due to the section reduction and EP due to partial

strength), see Table 4.3. The EP connection has a resistance of 0.8 with respect to the resistance of the beam.

Table 4.3 Case study structures

Name	Location	T_c	a_g	Column	Beams RBS & EP	Beams CWP & EPH
LSZ	Cluj-Napoca	0.7	0.1	2X HEB450	IPE450	IPE400
MSZ	Craiova	1.0	0.2	2X HEB550	IPE550	IPE500
HSZ	Bucharest	1.6	0.3	2X HEB900	IPE750X137	IPE600

4.4.2.2 Details of beam-to-column connections

The connections have been designed using the same design guidelines as in the case of the experimental specimens (see details in 3.4.2).

The length (L_p) of the additional flange cover plate of the CWP connection is equal to the length of the haunch of the EPH connections the for each seismic zone. The dimensions are given in Table 4.4, along with the ones for the width and the thickness of the cover plate. Bolts in EPH and EP connections are class 10.9. The height of the haunch is labeled H_h, see Table 4.4, where a, b, and c are the dimensions of the reduced beam section as defined in ANSI/AISC 358-10 [149]. The plates and profile part of the connections are from S355 structural steel.

Table 4.4. Connection dimensions (in mm)

	CWP			EPH			RBS			EP	
	L_p	B_p	t_p	bolt	end-plate	Hh	a	b	c	bolt	end-plate
LSZ	230	220	18	M24	30	185	100	360	30	M24	25
MSZ	240	240	24	M27	30	200	110	450	32	M27	28
HSZ	350	260	28	M30	35	320	150	600	40	M27	30

4.4.3   Response of moment resisting frame structures under column loss scenario. Influence of beam-to-column joint

The validated numerical model detailed in section 4.2.6 was used to assess the performance of full-scale connections of MRF subjected to column loss. Numerical models were built in Abaqus considering all parameters, meshing procedures, and analysis settings determined in the calibration. Structural steel S355 with nominal values was used for all elements, with all material properties considered in the calibration models.

2D frames have been extracted from the designed structures presented in section 4.4.2. The frames are perimeter frames from the ground floor, see Figure 4.50. The middle column (A3) is considered to be removed. To consider the effect of the secondary beams, an out-of-plane system with no friction are placed at the location of the secondary beams (see Figure 4.50.b).

The three intermediate columns and the two beams between them are modeled with solid elements, detailing all plates and bolts of the connections (Figure 4.51). The other columns and beams are modeled with beam elements for a faster analysis time, but to maintain the in-plane stiffness of the system.
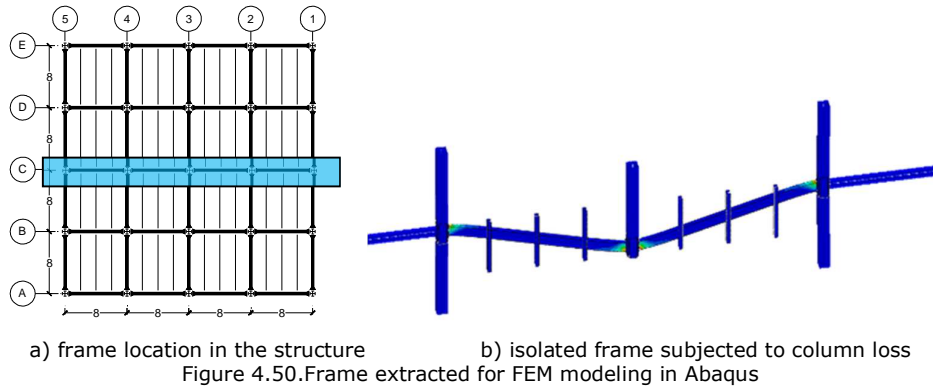
a) frame location in the structure   b) isolated frame subjected to column loss
Figure 4.50.Frame extracted for FEM modeling in Abaqus

The loading protocol followed the experimental one, i.e. imposing a vertical displacement on top of the middle column in a monotonic and quasi-static loading regime.

Figure 4.53.a shows the force-displacement curves for all connection typologies for the full-scale frames. From the zones where plastic hinges formed in the beam ends, based on the nodal forces of the finite elements in the section, axial force and bending moment were computed (Figure 4.53.b and Figure 4.53.c). The forces were normalized with respect to N_{pl} and M_{pl}. Failure modes are presented in Figure 4.52. As expected, the highest yielding forces and ultimate resistance occurs for the structures designed for the highest seismic requirements. This trend is similar for all connection typologies with increasing forces at the same vertical displacement for structures located in high seismic zone.
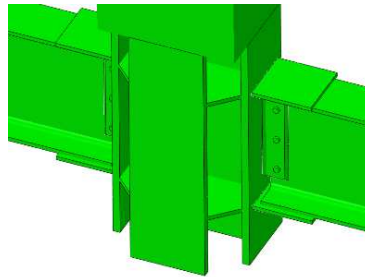
Figure 4.51. Detail modeling of the central column

a) CWP   b) EPH   c) RBS   d) EP
Figure 4.52. Failure mode of connection

a) vertical force vs. vertical displacement

b) normalized bending moment vs. vertical displacement

c) normalized axial force vs. vertical displacement

Figure 4.53. Vertical force, bending moment, and axial force vs. vertical displacement
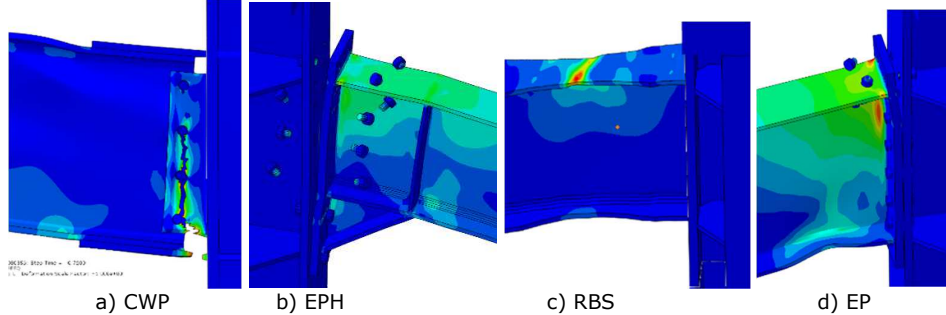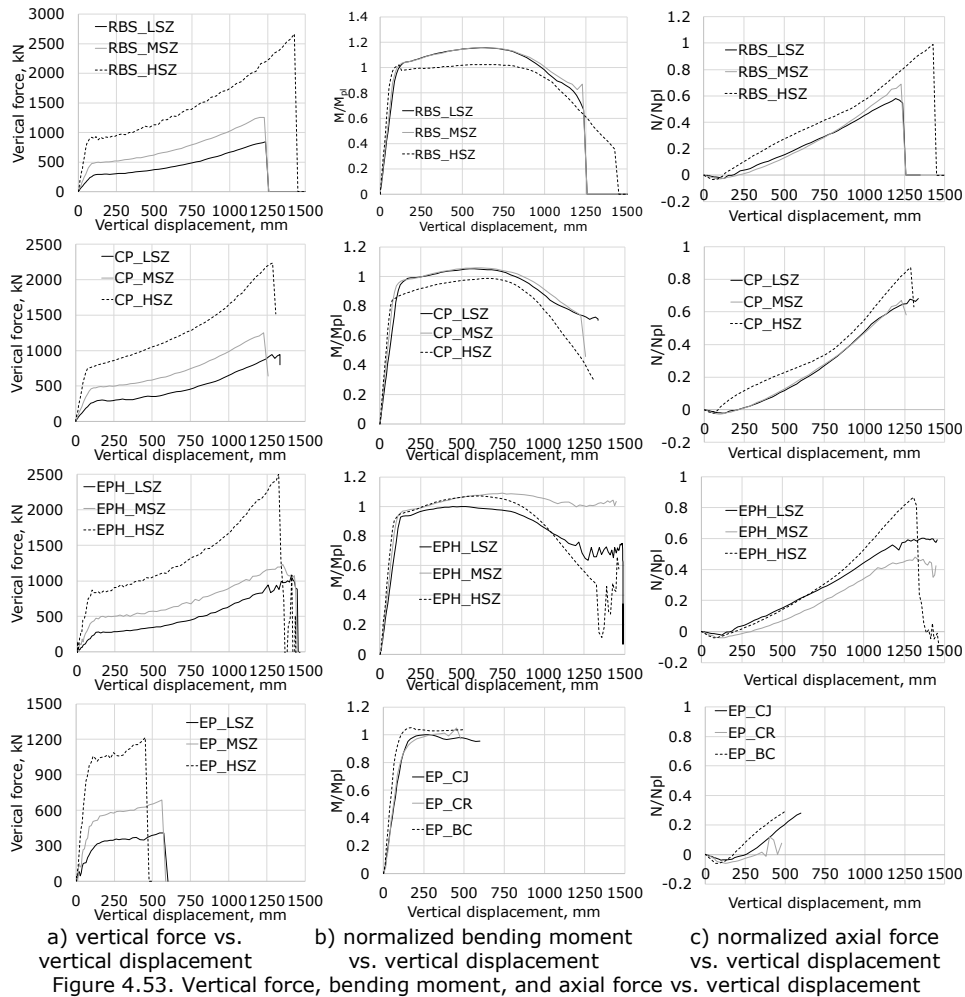
The failure mode for CWP full-scale model is similar to the CWP experimental specimen, namely the cover plate welded on the top of the tensioned flange fractures in tension in the clearance zone between the beam profile and the column in the same time with the failure of the shear tab in the net area.

As in the case of the experimental EPH specimen, the full-scale model failed due to fracture of two bolt rows near the unstiffened beam flange in tension.

The frames with the RBS connection failed by tearing in tension of the flange in the reduced beam section, similar to the failure recorded during testing.

The EP connections of the full-scale structure failed due to bolt fracture in tension at very limited vertical displacements with respect to the other connection typologies (CWP, EPH, and RBS).

The axial forces for the most stressed bolts are normalized with respect the capacity and presented in Figure 4.54. The variation of force demand in bolts is the same for all ranges of beams in relation with the displacement, indicating that the

performance of this connection typology is not very dependent on the geometric characteristic of the beam (height).

Figure 4.55 shows the vertical force vs. vertical displacement curves for the four typologies of connections, and for each seismic zone. The end of the elastic stage in colum loss scenarios is directly dependent on the seismic design requirements, without significant influence of connection typology. For instance, the RBS-LSZ frame reaches a maximum capacity of 800 kN in static column removal at a vertical displacement of 1250 mm. If the same structure is designed for a HSZ, with EP connection, for the same 800 kN static force, no yielding would occure and the vertical displacement would reach 65 mm (about L/250 for the double span lenth). Thus the seismic conditions imposing higher beam sections have a large impact on the capacity of the system under column loss, especially for the initial stiffness and force at yielding. The yielding force increased with 64% from LSZ to MSZ frames and with with 96% from MSZ to HSZ structures, respectivelly.
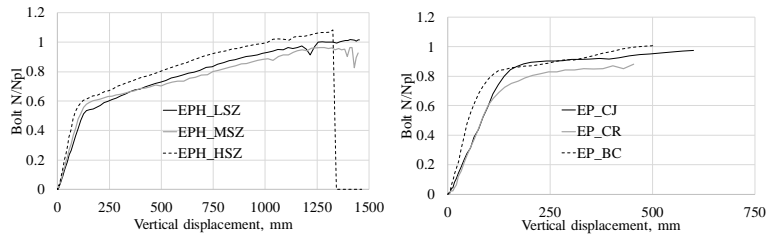
Figure 4.54.Normalized bolt axial force for the most loaded bolt rows
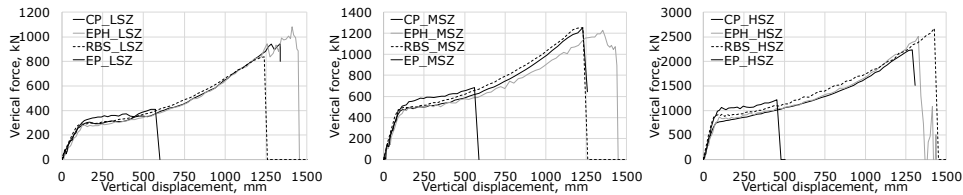
Figure 4.55. Vertical force vs vertical displacement for structures designed for the same level of seismic intensity

All failure modes are consistent with the ones identified in the experimental tests. Therefore, their performance is based on the specific detailing resulting from seismic codes, leaving some components vulnerable to the bending moment-axial force interaction. The result of strengthening the components beyond the seismic requirements is the focus of the next section.

4.4.4 Connection enhancements to reduce the risk of progressive collapse

In this sections, proposal to enhance the response of steel frames under column loss scenarios are proposed. The main aim is to obtain beam-to-column connections with improved resistance to axial force and bending moment that are developing at large deformation stage induced by column loss scenarios. The four typologies of connections proposed for study are CWP, EPH, RB, and EP.

4.4.4.1 CWP connection

Based, on the CWP model validated against experimental data (section 4.2.6), three new models were constructed, one for each level of seismic intensity (LSZ, MSZ, and HSZ). Numerical models were built in Abaqus considering all parameters, meshing procedures, and analysis settings determined in the calibration. Structural steel S355 with nominal values was used for all elements, with all material properties considered in the calibration models. The loading protocol followed the experimental one, i.e. imposing a vertical displacement on top of the middle column in a monotonic and quasi-static loading regime.

For each model, the cover plate thickness was increased until the failure took place due to fracture of the beam flange and not in the cover plate (see Figure 4.56). Table 4.4 presents the increase of the cover plate thickness for the connections of the three case study structures. The failure mode is the fracture of the beam flange in tension for all full-scale frame CWP connection models. Large plastic deformations are concentrated immediately after the end of the cover plate, as there is an important jump regarding strength and rigidity. Changing the failure mode from the cover plate to the beam flange enhances the ductility on average by 19%, having the same elastic and post-yielding rigidity, as seen in Figure 4.56.a.

Table 4.5. Changes proposed for CWP connections

	CWP	
	Seismic	**Robustness (column loss)**
	Cover plate thickness	
LSZ	18	24
MSZ	24	28
HSZ	28	35
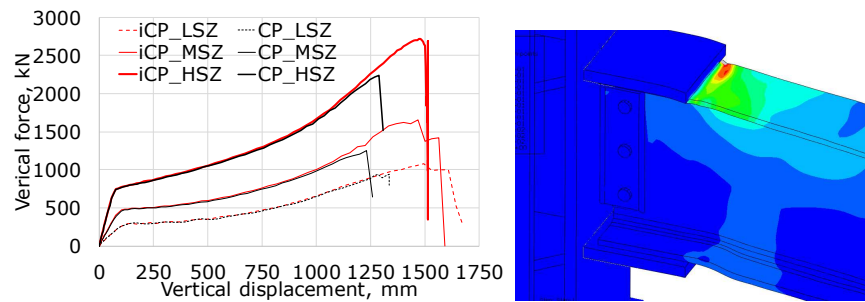
a) vertical force vs. vertical displacement   b) failure mode

Figure 4.56. Strengthened CWP to improve robustness performance

4.4.4.2 EPH connection

To improve the connection, the upper two bolt rows were increased in diameter, using the same 10.9 bolt class. Calculations performed using *STeel CONnection* [148] indicated that the weakest component of the T-stub is the end-plate. Therefore, the thickness of the end-plate was also increased to resist forces close to the capacity of the bolts. The contour geometry of the end-plate, the haunch, and the position of bolts remained the same as presented in section 4.4.2.2. The full-scale frame models with improved EPH connection were modified according to Table 4.5. Numerical tests were performed following the same protocol. The result of the modified versions of connections are presented in Figure 4.57.a.

The failure mode of the strengthened EPH connection, see Figure 4.57.b, consists in fracture of the bottom beam flange in tension near the strengthened zone. Connections under hogging bending showed an adequate performance, preventing failure in bolts, see Figure 4.58. This occurred in all cases in the connection near the middle column, as for these connections the flange in tension is stiffened by the haunch, and the two flanges in tension (flange of the haunch and flange of the beam) transfer all the force in the unstiffened part of the beam flange.

The strengthening of the two bolt rows and the end-plate resulted in significant increase in capacity and ductility, see Figure 4.57.a. The highest relative increase is in the case of the LSZ structure, which actually has the lowest capacity, therefore is the most vulnerable in the event of column loss scenarios.

Table 4.6. Changes proposed for EPH connections

	EPH			
	Seismic		**Robustness (column loss)**	
	bolt	end-plate	bolt	end-plate
LSZ	M24	30	M27	35
MSZ	M27	30	M30	35
HSZ	M30	35	M36	40
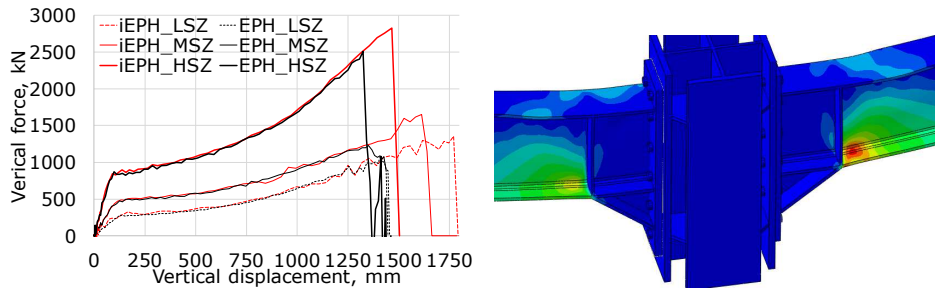
a) vertical force vs. vertical displacement   b) failure mode

Figure 4.57. Strengthened EPH to improve robustness performance
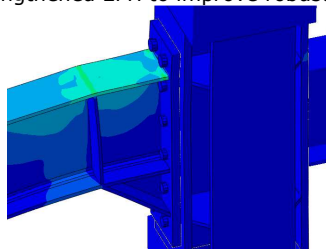
Figure 4.58. Strengthened EPH connection under hogging moment

4.4.4.3 RBS connection

For RBS connection, no strengthening or optimization method was adopted, as previous results showed good ductility and strength to allow the development of full catenary action in beams. More details and discussions are presented in section 5.2.2.3.

4.4.4.4 EP connection

The full-scale frame models with EP connections were modified according to Table 4.6, which presents the increase of the end-plate thickness and bolt diameter in the connections for the three case study structures.

Numerical tests were performed following the same protocol. The result of the modified versions of connections presented in Figure 4.59.a. The failure mode of the strengthened EP connection, see Figure 4.59.b, consists in fracture of the beam flange in tension. Due to symmetry, the failure can take place also near the marginal column.

The strengthening of the bolts and the end-plate resulted in a large increase in ultimate strength and ductility (see Figure 4.59.a), as the system reached the largest vertical displacement. This can be explained by the fact that the frame with this type of connection is more flexible than the system with haunches or cover plates.

Table 4.7. Changes proposed for EP connections

	EP			
	Seismic		**Robustness (column loss)**	
	bolt	end-plate	bolt	end-plate
LSZ	M24	25	M30	35
MSZ	M27	28	M36	35
HSZ	M27	30	M36	40

a) vertical force vs. vertical displacement   b) failure mode
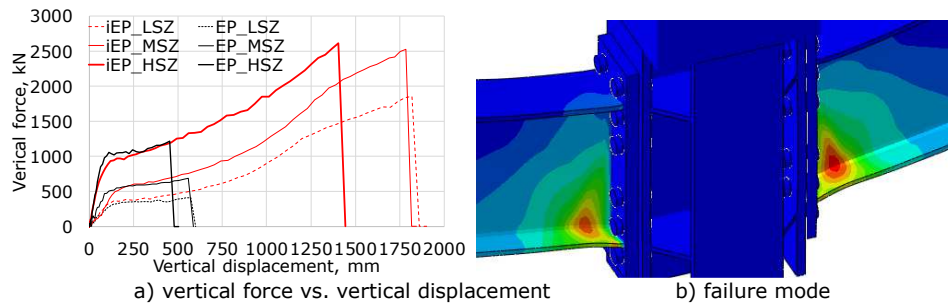
Figure 4.59. Strengthened EP to improve robustness performance

4.4.4.5 Comments regarding strengthening of connection

All four connection typologies were investigated using numerical simulations to find some improvements in the overall performance of the frame in case of column loss. The highest improvement (relative to initial configuration) was obtained for the EP connection. By increasing the bolt diameter and end-plate thickness such that it becomes full strength and rigid connection, the connection provides the capacity that is necessary for full development of catenary action in beams.

The effect of such improvements should be also investigated regarding global structural performance, and considering also loading distribution and dynamic effects. This will be performed in the next section.

4.4.5   AEM investigations on global structural response in case of column loss

Column loss is in many cases a dynamic event, and a full understanding of the phenomenon must take into consideration the dynamic effects. First, the

amplification of the gravity loading due to inertial effects (dynamic load amplification) and second, the changes in the mechanical properties of materials (strain rate). However, as indicated in section 4.2.2.5, the loss of a column does not affect significantly the behavior of the materials and therefore strain rate effect will be neglected in this study.

Starting from AEM models validated against experimental test in quasi-static conditions, the response after the loss of a column is investigated and compared with the quasi - static one.

The improvements proposed and tested in the previous section (section 4.4.4) will be also verified using this methodology to see if they are still valid or require further adjustments. Therefore, the structure with connections designed for the seismic requirements is compared with the ones with connections designed with robustness requirements (over-strength for axial force – bending moment interaction) in the case of column loss scenarios.

4.4.5.1 AEM model calibration

The procedure indicated in section 4.1.3 was followed to determine the global performance of the structure in column loss situations. The calibration of the FEM model presented in section 4.2 was used to get the data for full-scale frame assemblies that were isolated, modeled numerically, and subjected to column loss by imposing a vertical deformation on the middle column. This was performed in section 4.4.3, and Figure 4.53.a shows the vertical force vs vertical displacement curves for the pushdown column test under displacement control. Figure 4.59.a shows the same curves for the enhanced EP connections and for the same frames.

The same models were replicated for EP frame connections designed for LSZ and HSZ, before and after strengthening the connections. Figure 4.60 presents the model in ELS for the AEM simulations that are identic to the FEM simulations in section 4.4.3.
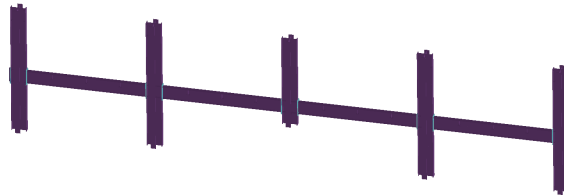
Figure 4.60. EP connection frames modeled in ELS

ELS models were tested using the same loading procedure (imposed displacement of the column) as in the models. Figure 4.61 shows a very good correlation between the response of the FEM and AEM models, with the same initial stiffness, yield force, post-elastic behavior, and ultimate force and displacement.
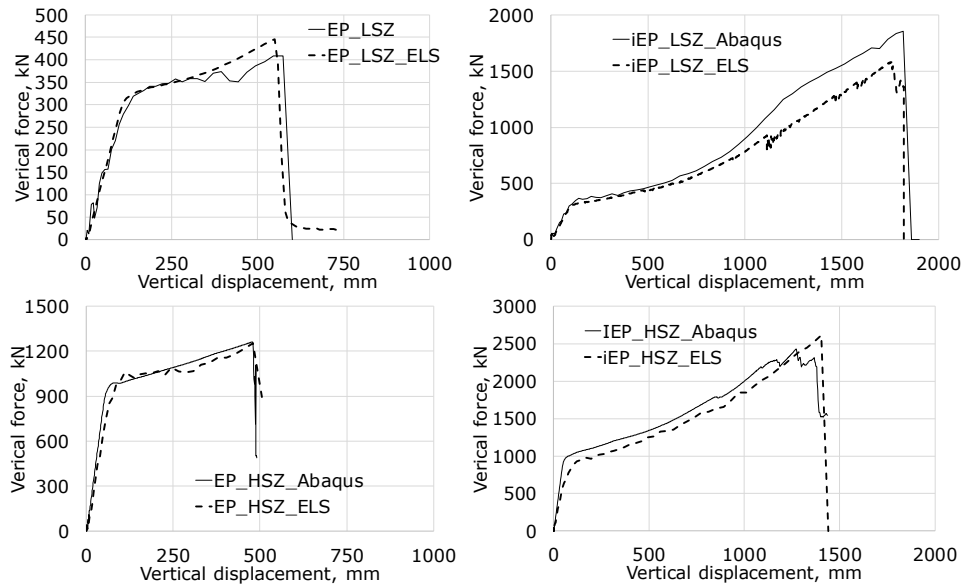
Figure 4.61. ELS model calibration based on FEM results

       Calibration was performed on several parameters in order to obtain the same results. One issue is the discretization of the end-plate and the ultimate strength and elongation (ultimate strain) of materials, since it would affect the yield point, the peak force and deformation capacity. In order to get realistic material degradation, the elements of the mesh have to be very small (4 mm or less). Locally, in single or few individual elements the maximum strain accepted before failure can reach plastic strains of 0.6 or beyond (see Figure 4.12 which presents also VIC 3D experimental data). This high strain is valid only for the development of local plastic deformations that occur during necking. ELS does not model this phenomenon but can model the consequences of this effect. Therefore, the ultimate strain and mesh sizing for elements influence their allowable ductility so adjustments to the material ultimate strain are necesasary.

       Since bolts in ELS were modeled as a single spring between centroid elements of the end-plate and respectively the elements in the face of the column, their length differ from the true length of the bolt, therefore the stiffness is compensated by modifying the axial stiffness of the bolt (Young modulus E of the bolt material). The change of E-modulus does not affect the shear modulus G, which has an independent definition. Calibration provides verification of the validity of these amendments in material properties.

4.4.5.2 Static response of moment frames under column loss scenario

       The model of each structure was created with the same element meshing, material properties, and adjustments that were undertaken for specific connections in order to calibrate the AEM models against the FEM results.

       The AEM model of the entire structure is shown in Figure 4.62.a, while the position of the lost column (C2) is marked in Figure 4.62.b.

In static analysis, the lower elements of the column are removed before loading the structure. The load is applied on the transverse girders (including secondary beams) using a nonlinear incremental analysis.

The vertical displacement of the column above the removed elements is measured in function of the load applied to the structure. The load is normalized in relation with the floor load corresponding to (1.2DL+0.5LL) load combination and denoted as λ – overload factor. For the nominal load combination 1.2DL+0.5LL, λ equals to 1. Figure 4.63 plots the vertical displacement of the column versus the overload factor. The capacity to resist central column loss for the structure designed for high seismic action is about three times larger than for the one designed for low seismic action. The configurations with improved robustness (connections) have larger overload factors (by 25% in both cases). This increase in capacity is especially important for LSH structure, as the capacity of the structure with initial connections is 1.74 λ.

a) 3D view   b) first floor view with removed column
Figure 4.62. Frame structure model with EP connection
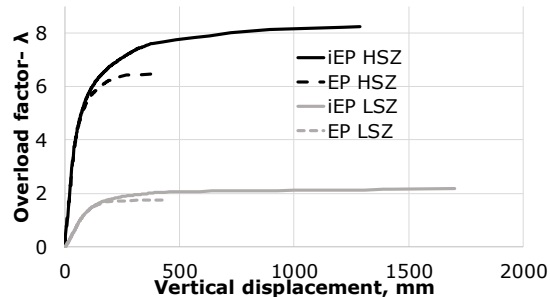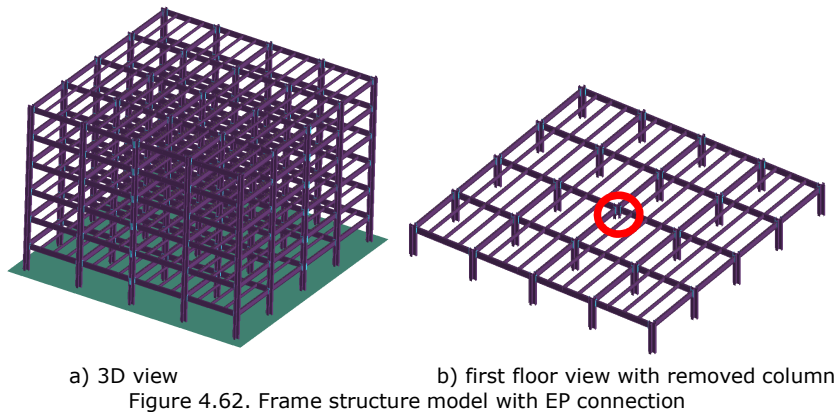
Figure 4.63. Static capacity of the structure with EP connection in case of column loss

4.4.5.3 Dynamic response of steel frames under column loss scenario

Because progressive collapse is a dynamic process, it is important to evaluate in what extent the loads are amplified and how much the response is affected. The dynamic analysis is performed in two steps. First the gravity load (with different intensities) is applied on the structure in a static analysis is run. Then, the column is removed almost instantaneously (0.001 seconds) and the dynamic analysis starts from the end of the static analysis.

Figure 4.64.a displays the time history of the vertical displacement under the removed column for structures with initial connections (without any strengthening). The initial velocity (first 0.02 seconds) of the LSH structure is significantly higher than the one of the HSZ structure. The same difference can be also seen for the maximum displacement. The neutral displacement is the displacement at which the system stabilizes. This displacement is lower than maximum displacement, as inertia also influences the maximum displacement.

Figure 4.64.b displays the time history for the LSZ structures with initial and strengthened EP connections. Although up to 0.6 seconds there are no differences in velocity between the two structures, there is a slight difference in maximum displacements.

The static capacity (section 4.4.5.2) is defined as the response of the structure to static loading, without considering inertial effects. *The dynamic capacity* is the response of a structure for various load factors (λ) in terms of maximum displacement. *The neutral capacity* [102] is the response of a structure for multiple load factors (λ) in terms of permanent displacements. The dynamic capacity considers the full effect (maximum) of the inertia, while neutral capacity only the permanent effects. From Figure 4.64, studying the response of LSZ structure with the initial connections, the maximum displacement is 150 mm, a point that will be represented in the static capacity as a displacement of 150 and λ=1. The permanent displacement is approximately 111 mm, a point used in the neutral capacity curve as a displacement of 150 mm and λ=1.
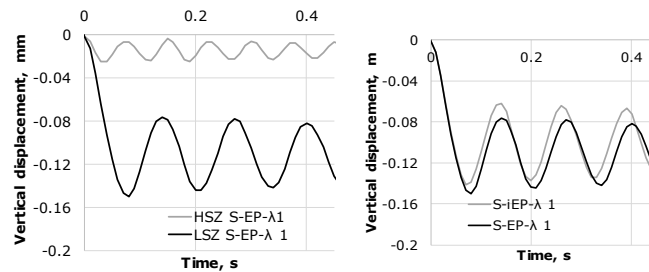
a) seismic design of EP   b) robustness improved design EP

Figure 4.64. Static, dynamic and neutral column loss capacity for EP-LSZ structure

Figure 4.65 plots the static, dynamic, and neutral capacity curves for the EP-LSZ structure. In the elastic range, the displacement for the same overload factor of the static capacity is half that for the case of dynamic capacity, but equal to the displacement from the neutral capacity. Because no plastic deformations occur, after the initial dynamic effect is consumed, the permanent response of the system loaded dynamically is the same to the static response.

The increase of the dynamic capacity of the LSZ structure due to connection strengthening is about 50% (from 1.26λ to 1.9λ), although the strength of the connection is increased with more than 100%. On the other hand, the ductility increase due to connection strengthening can also be seen in the performance of the structure in case of column removal.

Figure 4.66 shows the static, dynamic, and neutral capacity curves for the EP-HSZ structure. A ductility improvement due to connection strengthening can be seen, but the increase in ultimate resistance is reduced. Although the structure with strengthened EP connection doubles its resistance to vertical loads, in the case of point load evaluation, the maximum overload factor increases with only 36%.

a) seismic design of EP

b) robustness improved design EP

Figure 4.65. Static, dynamic and neutral column loss capacity for EP-LSZ structure

a) seismic design of EP

b) robustness improved design EP

Figure 4.66. Static, dynamic and neutral column loss capacity for EP-HSZ structure
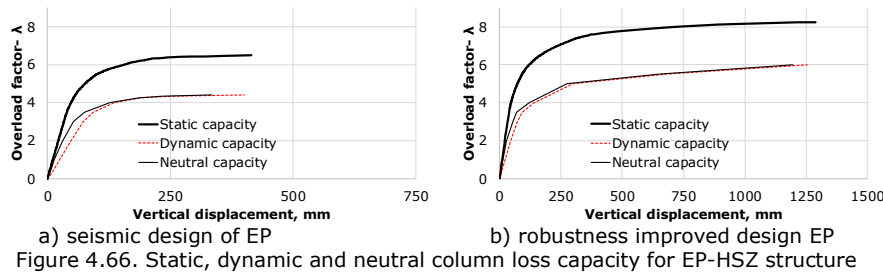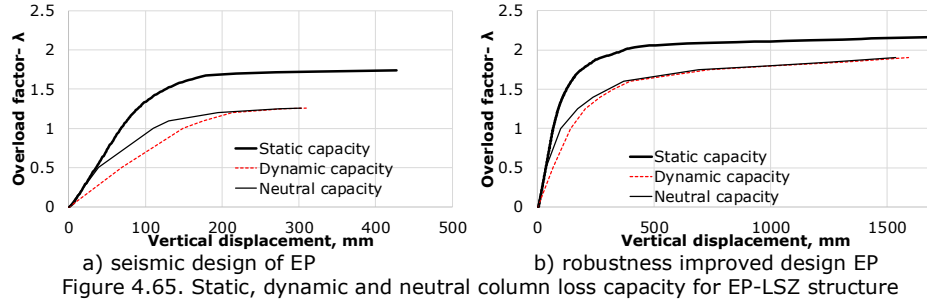
The maximum overload factor for LSZ structure with initial connections is $\lambda=1.26$ for central column loss. This indicates a limited robustness and high risk of progressive collapse.

4.4.5.4 Dynamic increase factor

Figure 4.67 shows the force and displacement based dynamic increase factors (DIF) for EP-LSZ structure. Force based DIF ranges from 2 to 1.14., while the displacement based DIF reaches even values of 6 in the case of the EP-LSZ structure. For similar overloading factors, the DIF of the two structures is similar up to an overload factor of 1.25.

a) seismic design

b) robustness improved design

Figure 4.67. Force based and displacement based dynamic increase factors for EP-LSZ
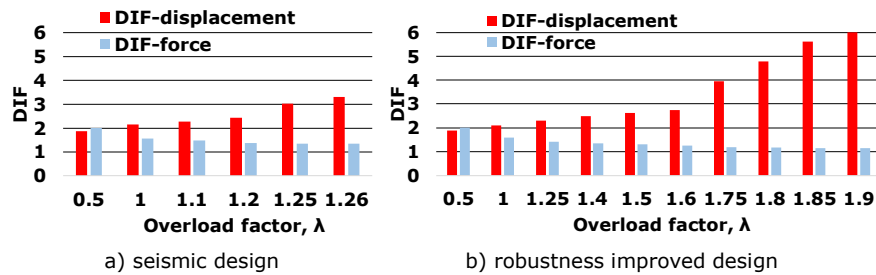
4.4.6   Comments regarding on case study results

The performance of connections tested experimentally have been also evaluated in case of full-scale structures subjected to column removal. Structures were designed for three different seismic zones. The strength of frames design for

high seismic forces is considerable higher than in the case of frames designed for low seismic forces.

By strengthening the connections, failure of the frames changed from connections to beams, attaining larger ultimate displacements and resistance, without significant changes in the initial stiffness and post-yield (flexural) response. The largest response improvement was obtained for the EP specimen, where the ductility and ultimate strength increased with more 100%.

The AEM investigation of EP connection structures designed for LSZ and HSZ follows the FEM-AEM combined analysis presented in section 4.1.3. Inertia forces reduces the capacity of frames to resist column loss in terms of force, and especially displacement. The capacity of the system subjected to internal column loss, can be significantly reduced if uniform distributed load is applied rather than column point load.

4.5   Concluding remarks

The models used in the numerical program were all validated against experimental data obtained from connection macro-components, 2D, and 3D assembly frame tests. Due to different scale and level of details, two different numerical environments were employed. First, for small-scale components and steel frames (2D and 3D), FEM using Abaqus has been used and validated with great accuracy. FEM models can accurately simulate the complex material behavior (e.g. necking, degradation, strain rate) and stress and plastic behavior of complex geometric configurations undergoing local plastic deformations. Based on the experimental data obtained using the DIC system, it was possible to compare with high accuracy the distributions of the strains from yielding to large deformation stage and even complete fracture.

For large scale models however, the analyses require generally large computational expense, which result in longer time and less efficiency. In such cases, a second environment showed better performances, i.e. AEM simulation using ELS. Such method provided high accuracy and increased computational efficiency compared to FEM for large (full-scale) structures. As several analysis options are available in the program, it can be also used in practice for simulating such complex problems.

A method for combining the advantages of the two numerical methods is proposed in order to obtain reliable results with reasonable computational cost for evaluating global structural performance of structures in case of sudden column removal. The behavior of the joint in case of axial forces–bending moment interaction due to large displacements following column loss in AEM can be verified using the results obtained by FEM. After such calibrations, the model of the entire structure can be created in ELS to perform global analyses. The AEM solver can be further used for evaluation of structures in case of direct effects of accidental actions (e.g. blast, or impact). This method was used in the evaluation of the response for case study structures.

FEM: Material properties from coupon tests
The models of coupon tests are calibrated against the experimental results using the engineering stress-strain curve. In order to capture the correct behavior beyond the maximum strength from the engineering curve, mesh size should be defined in relation with the material degradation parameters. As a result, the mesh size used in the tensile test models was based on the properties of the material in the

critical zones, where the material reaches plastic strains those corresponding to the maximum stress point in the engineering curve.

FEM: Effects of strain rate on the connection macro-components

The tests performed on connection macro-components showed that the strain-rate effect significantly affect the material properties in the reduced zones of the bolted T-stub but the effect on the overall performance is reduced. Two methods have been used to simulate the effect of strain rate; first method is recommended for simpler models while the second method is more appropriate for large scale models. Simulations of strain rate influence on the performance of T-stubs showed that the ultimate resistance and deformation depends on the configuration (failure mode). For T-stubs designed for mode 1, the failure is ultimately due to fracture of the bolts due to additional prying force and due to bending of the bolts. Thus, forces developed in bolts can increase by more than 100% compared to the external force applied on the T-stub due to prying effects. The bending in the bolts has also a detrimental effect but is significantly lower than prying.

For detailed validations, FEM surface strain maps were directly compared with experimental strain maps obtained from DIC measurement. This direct validation using strains on large areas of the models confirms the FEM models replicate the behavior of the experimental specimens with high accuracy (not just the force-displacement curve or failure mode).

FEM: assemblies tested for column removal (2D and 3D structures)

To calibrate the 2D and 3D assembly models, the test set-up was modeled in detail. Numerical results are very close to experimental ones, both in terms of force-displacements curves and strain development. For each model, the behavior until failure was in very good agreement with the experimental testing.

In 2D frame test, the columns remain essentially elastic, without plastic deformation of the columns web panel or flanges. The continuity plates are very important for transferring the axial forces developed in beams due to catenary action. Free edge columns in the 3D assembly tests, which represent perimeter columns in real building structures, undergo plastic deformations due to catenary action developed in beams. Integrated internal forces in the main beams of the 3D system indicate a very similar behavior on the two perpendicular direction up to the point of the first failure in beam.

The extended end-plate numerical study on 3D and 2D column loss scenarios indicate that boundary conditions derived from the rest of the structure restraining have a great impact on the performance of the frame, and that 3D analyses give more accurate results than 2D analyses frames, as more complex state of deformations can be simulated.

AEM: 3D assembly frame tested for column removal

The ELS numerical model was developed and validated against the experimental data, with very good agreement. Distribution of axial forces in the connection bolt rows revealed that the bolts experiencing the largest tension forces are from the second bolt row. First bolt row may fail first, however, owing to the combined effects of the applied tensile load, prying action and bending effects.

The validated model was used to determine the influence of loading pattern on the response of the specimen in case of column loss. Uniformly distributed load changes the bending moment distribution on the girders, concentrating the flexural effect at the exterior end of the beams, and causing failure at a lower value of an

equivalent point load. The dynamic increase load factors show different trends (DIF_F and DIF_D) and require further studies especially for large deformation stage associated with the catenary action.

Case studies

The performance under column loss scenarios of different building structures was assessed for the same geometry, but designed for three different levels of seismic intensity and with the four types of studied connections. FEM point load simulation of column removal on frames extracted from the structures indicated the same failure pattern as in the case of the experimental tests. For CWP, welded cover plate failed in tension near the column weld. For EPH, bolt fractured near the unstiffened beam flange in tension. For RBS, beam flange fractured in tension in the reduced section zone. For EP, bolt failed at low levels of beam rotations (less than half compared with the other systems), before initiation of catenary action.

Except for the RBS connections, which exhibited a full catenary stage failure, the other three connections have been strengthened to improve the behavior under column loss. The simulations confirmed the efficiency of the strengthening strategies. In the next section, the effects of these strategies on the robustness of steel frames will be discussed in detail. Also, recommendations will be given for assessing the capacity of such configurations to transfer internal forces developed in column loss scenarios.

The AEM investigation of full-scale frames extracted from case study structures indicated that the load factor for structures designed for LSZ with external end-plate connections, and therefore the coresponding robustness, has the lowest value. Strengthening of connections can reduce this vulnerability.

The capacity to resist a column removal is very much dependent on the reserve of capacity against gravity loads. For structures that are designed from seismic requirements, this reserve can increase depending on the seismic intensity level. A procedure to estimate if strengthening strategies should be applied for steel connections will be discussed in the next chapter. This procedure can be applied to steel moment frames depending on the level of over strength against gravity loads and type of connection.

5 RECOMMENDATIONS FOR ROBUST DESIGN OF MOMENT STEEL FRAMES

5.1 Introduction

Design of buildings should ensure adequate performance when subjected to exceptional loading. The development of design recommendations and procedures suitable for assessment and improvement of seismic steel beam-to-column connections in the event of loss of a structural member is required and represent the third major objective of the thesis. In order to improve the structural robustness, design optimizations and verifications which enhance the connection robustness will be given for specific configurations of steel beam-to-column connections.

In general, building failure can result from overall damages to the structure, e.g. due to seismic ground motion, or due to local damages that extend and progress at entire structure (or large part of it), e.g. removal of a column due to a blast. In the second case, which is of interest for the present studies, the reduction of risk associated with the various accidental actions is based on three main type of measures, as described by eq.(5.1) [175]:

$$P(PC) = \Sigma\, P[PC|DH_i]\, P[D|H_i]\, P[H_i] \qquad\qquad (5.1)$$

Where:

P(PC) is the probability of collapse

$P[PC|DH_i]$ = probability of collapse, given that hazard and local damage both occur

$P[D|H_i]$ = probability of local damage, D, given that H_i occurs

$P[H_i]$ is the probability of hazard H_i (source of abnormal load)

The strategies that are necessary to reduce the probability of collapse should therefore look at reducing the hazard, strengthening individual elements and improve the overall system, see Figure 5.1. Actually, with little difference between several documents and codes, the following approaches are recommended for reducing the risk of progressive collapse: (a) Design of key elements to resist accidental load (threat dependent, intensity of the action is required); (b) Design of structure to resist the loss of a member, or alternate load path method (threat independent, intensity of the action not required); (c) providing acceptable structural robustness by applying prescriptive design detailing rules (tying force method). The selection of the methods depend on the consequence classes (or level of protection) for structures. In EN1990 [8], there are three such classes: CC1 - Low consequences of failure; CC2 - Medium consequences of failure; CC3 High consequences of failure. With these definitions and general information for risk analyses (see Figure 5.2) and acceptance criteria ("Acceptance criteria may be expressed qualitatively or numerically"), the code gives the framework for robustness performance based design. Excepting the last method, guidance provided in EN 1991-1-7 for first two methods are very limited, as it does not provide the verifications and requirements that enable engineers to assess or improve the structural robustness of steel structures and implicitly the steel beam-to-column connections.

Impact forces (vehicle impact) for key element design are given function of direction of impact, adjacent roadway category and vehicle type. Besides roadway, railway and sailing vessels are also considered. For explosions, only internal gas explosions are included. No provisions for external explosions or intentional attacks using explosives.

Current design of steel connections for seismic moment resisting frame structures are based on EN 1993-1-8 [147] *Eurocode 3: Design of steel structures - Part 1-8: General rules - Design of joints* for the main design issues and on EN 1998-1 [117] *Eurocode 8: Design of structures for earthquake resistance-part 1: general rules, seismic actions and rules for buildings* for specific details regarding seismic requirements, like overstrength. The overstrength and performance offered by these standards are limited to bending moment resistance and do not secure an adequate performance for bending moment – axial force interaction which is specific for column loss situations. In addition, guidance for robustness provided in EN 1991-1-7 [3] refers to all types of structures and does not provide explicit recommendations for steel frame structures, in general, and beam to column connections in particular.
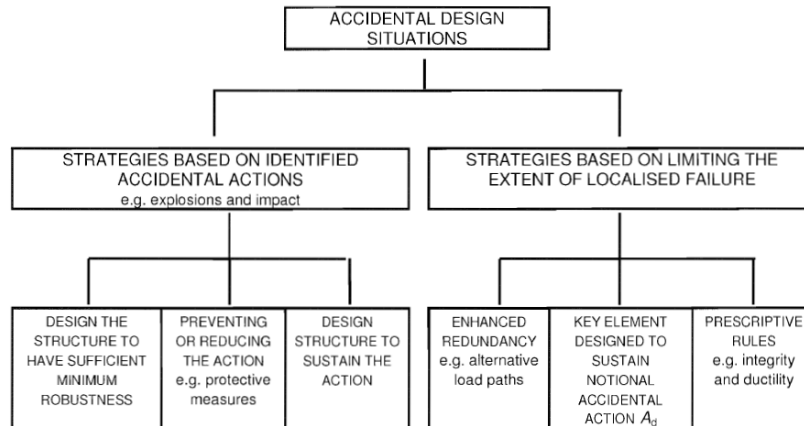
Figure 5.1. Strategies for accidental design situations [3]

The application of the tying method (alone) is limited to ordinary buildings (normal importance), while the first two methods (key element method and alternate load path method, respectively) can be used, alone or combined, for important buildings. The control of collapse mechanism by a combination of these two methods allows us to obtain higher performance with adequate structural interventions, i.e.:

- Takes advantage of residual capacity of key elements, which can be improved and taken into account in the structural analysis without complete removal. As an example, damages to the columns under the effect of explosion, impact or high temperatures (fire).

- Use/adjustment of elements capacity to comply with the demands. One such example is the increase of beam deformation capacity to allow to development of catenary stage (beyond flexural stage) or use of composite floor systems to take advantage of the steel beam - concrete floor interaction.

In the following, the main recommendations for the improvement of progressive collapse requirements and design methodologies are presented. They are structured on several categories and are based on the results of the experimental and numerical study presented in Chapter 3 and Chapter 4.
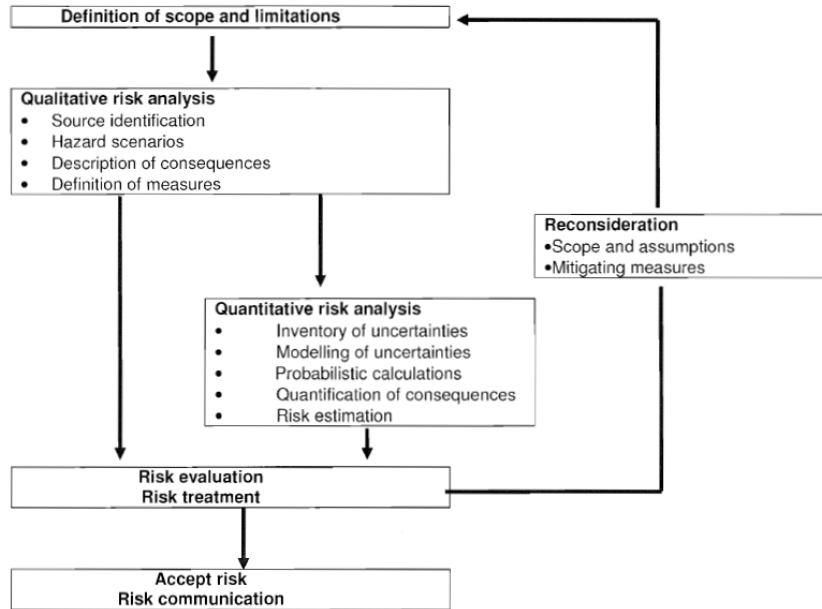
Figure 5.2. Overview of risk analysis [3]

5.2   Analysis recommendations

5.2.1   *Methodology for robustness analysis of steel frames*

The concept of collapse control design can be considered an appropriate approach for preventing the progressive collapse in case of extreme load events. The collapse control design method assesses and improves the redundancy of buildings by: (1) assuming the loss of structural members such as columns and beams due to extreme accidental loads, (2) assessing the numbers of members that might be lost until the entire collapse of the building [4].

An analysis procedure is proposed for robustness evaluation and improvement of moment resisting steel frames, see Figure 5.3. The initial structural design takes into consideration the load combinations for permanent and design situations, given its type of structure, functionality, and location. The structural design has as outputs the size of structural elements and the connections.

After the detailed design, first new analysis (compared to conventional design procedure) that should be performed is detail modelling of a structural assembly consisting of at least 2 frames (see section 5.2.1.1 for details and justification) subjected to column loss. In plane restraining should be provided as in the structure. The numerical model has to be calibrated on similar experimental tests and to be sensitive on any configuration change. In the second new analyses the results are used for calibrating the same subassembly using a simplified model which requires reasonable computational time to perform full structure analyses. If the structure has several connection configurations, these two analyses have to be performed for each configuration. The third new analysis is performed on the entire structure with the real loading patterns. The element definition from the previous step is used to model

the entire structure, adding all the simplified calibrated models. Notional removal is performed in an incremented dynamic analysis manner (separate analyses for different loading factors) to assess the ultimate overload factor for each considered column loss scenario. In some situations, (performance based robustness analysis), the overload factor for yielding or a certain vertical deformation should be evaluated with this simplified model dynamic analysis on the entire structure. These three steps are also described in section 4.1.3.

The selection of scenarios and selection of acceptable overload factors is not the focus of this thesis. Further studies are necessary for defining column loss probable scenarios depending on the exposure and functionality of the building. Vulnerability assesments should also be performed for recomanding acceptable overload factors for different performance levels.

If the output of the numerical analyses (overload factor) is higher than the accepted value for each specific performance demand (e.g. yielding; collapse prevention- ultimate capacity), than no further verifications should be performed, and the design of elements and connections is complete. Otherwise, strengthening of the structure must be performed.
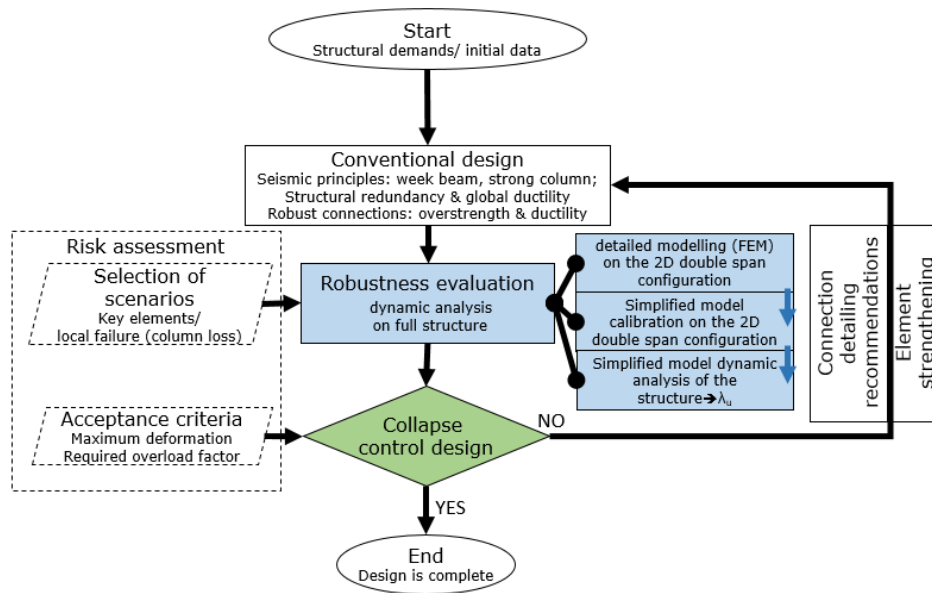
Figure 5.3. General methodology for robustness design of MRF structures and connections

If robustness is necessary to be enhanced, improvement of connection performance should firstly be discussed, as it would be the most cost-efficient solution. This strengthening strategy is functional if the desired robustness is not reached due to connection failure. Recommendations from sections 5.2.2 should be taken into consideration. The new connection configuration must respect seismic requirements. The 3 stage robustness assessment analysis is repeated for the new configuration.

If failure occurs in the elements for loads that are less than the required loading factor, then the strength of the elements must be improved, solution with a

high economic impact. The overall design process and verifications have to be performed for the structure with the new sections. Connections are also designed for the new sections, and the 3 stage analysis in order to assess the behavior of the structure is adequate.

The aplication of this analysis procedure is reccomended only for consequence class CC2 (Medium consequences of failure) in LSZ, as these are more vulnerable, and for consequence class CC3 (High consequences of failure).

5.2.1.1 Numerical modeling for column removal analysis methods

Several experimental studies available in the literature are based on simplified set-ups "beam-column-beam" that consider "zero" bending moment in the middle of the beam span and extract the specimen for testing. The advantage is that only two half beams and two connections are constructed and tested. This arrangement (see Figure 5.4) would correspond to a MRF structure where gravity loads are applied only on the columns beams, and there are no loads acting directly on the beam. The bending moment developed in the connections has the same diagram and value corresponding to double span specimen for the same load. However, this testing system does not give appropriate results for beams with asymmetric connections, as it evaluates the connection performance either to hogging or sagging bending moment. In continuous frames, the "zero" bending moment point shifts due to first plastic hinge development in the weakest (hogging or sagging) connection beam end. Therefore, the simple superposition of sagging and hogging results for frame behavior assessment is not entirely accurate. This is also valid for composite connections, which have a high unsymmetrical behavior.

Uniform load distribution (see Figure 5.4) can be a realistic loading pattern. In order to get the same results (displacements and moments) when comparing distributed load to point load in double hinge testing set-ups, the point load is distributed just to half of the spans, actually ¼ of the real span length for each beam. This is due to the fact that the vertical reactions in the hinges is artificial and not really present in the full frame. The distributed load on the full frames gives a bending moment distribution with higher bending moment values in hogging than in sagging. Also the "zero" bending moment is not at the middle of the beam, and will shift after plastic hinge development in the hogging ends. The maximum equivalent value for reaching yielding in the distributed load pattern is 25% less than in the point load pattern. Point load patterns (secondary beams supported on the main beam) would have consequences between the two loading patterns. Thus, robustness assessment on full frames should be corrected to take into account the real loading pattern.

It must be said also that the evaluation of the structural performance should take into account the real load distribution. Analysis on simplified loading conditions can lead to unconservative assumptions. For instance, in the case of Ans-M specimen (section 4.3.2), the ultimate strength and deformation capacity decrease by 37% and 40%, respectively, when the load changes from point load to uniformly distributed load.

In addition, the response should be corrected due to dynamic effects. This can be done either through energy balance methods to obtain the pseudo-static response, or by dynamic analysis, in which case the results are more accurate, as there is a significant reduction of capacity due to inertia forces.

From initial analyses, it was shown that the activation of catenary action was different from floor to floor, with largest development at first floor (over the removed column). Consequently, assessment of structural behavior should be done considering the real distribution of forces and deformations in the structure.
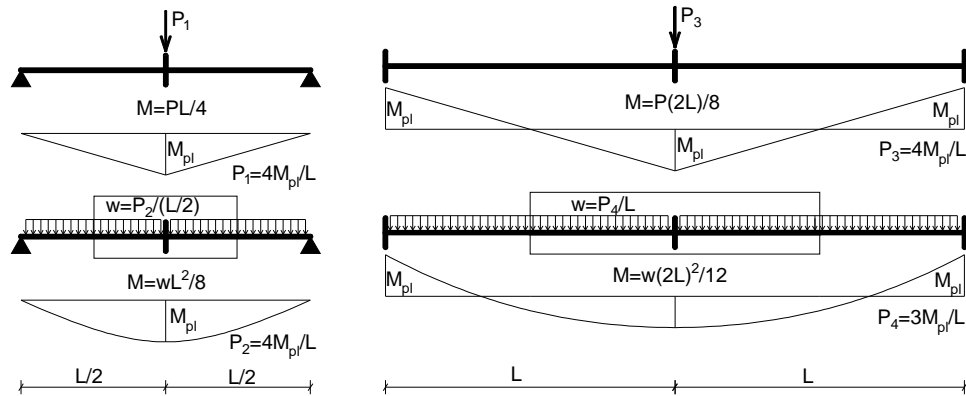
Figure 5.4. Load distribution influences on system capacity

5.2.2   Specific robustness requirements for CWP, EPH, RBS, and EP

Although beam-to-column connections that were investigated were designed according to seismic design requirements, the expected performance was not fully confirmed, due to failure in the connection components due to axial force – bending moment interaction. Strengthening of the connections led finally to improved response and robustness, after development of large deformations in beams and significant increase of capacity due to catenary action. A robustness capacity design philosophy was therefore adopted to provide connection integrity to forces developed in column loss scenarios. In the following sections, proposals for each type of connection (i.e. CWP, EPH, RBS, and EP) are made and compared with the actual design procedures.

If the connection design is taken as defined in the NSSS document [178] "The design of bolts, welds, cleats, plates and fittings required to provide an adequate load path between the end of a member and the component it connects to", the connection capacity can be improved by providing the load paths that are required for internal forces developed following column loss. Each connection typology requires particular solutions for improving the performance.

5.2.2.1 CWP connections

The failure of CWP connections in the experimental test and numerical simulations on full-scale frame structures is due to almost simultaneous fracture of the cover plate in tension near the column face and tearing of the shear tab in the net area. As the connection is symmetrical, the fracture can develop at each of the beam ends (near the lost column or near the adjacent column).

In order to prevent the failure of the cover plate, the resistance is increased by increasing the plate thickness (length and width remain unchanged). Table 4.5 shows the increase of the cover plate thickness for the connections used in the case study structures. The design strategy is to provide sufficient axial capacity to the cover plate ($N_{rd,wpl}$) such that it would be larger than the maximum force that can be transferred by the beam ($N_{ed,wpl}$), see eq. (5.2). Equation (5.3) defines the axial capacity of the welded cover plate, where A_{wpl} is the area of the cover plate. Eq. (5.4) also takes into consideration de supply of beams from higher material strength than ordered, through an overstrength factor γ_{ov} of 1.25.

Table 5.1 presents the values of $N_{rd,wpl}/N_{ed,wpl}$ ratio for the initial and strengthened connections in case studies configurations, with an overstrength factor γ_{ov} of 1.0, because in the numerical analysis al structural steel components were modeled from S355 nominal steel. In the conventional seismic design, the ratio exceeds 1, and therefore do not comply with eq. (5.2) requirements, while strengthened connections satisfy this equation. To note that in the later cases, failure was due to fracture in tension of beam flange.

$$N_{Rd,wpl} > N_{Ed,wpl} \tag{5.2}$$

$$N_{Rd,wpl} = A_{wpl} \cdot f_{y,wpl} \tag{5.3}$$

$$N_{Ed,wpl} = \frac{A_{beam}}{2} f_{y,beam} \cdot \gamma_{ov} \tag{5.4}$$

Table 5.1. $N_{rd,wpl}/N_{ed,wpl}$ values for CWP case study configurations

	CWP	iCWP
LSZ	1.07	0.80
MSZ	1.02	0.86
HSZ	1.07	0.86

Another option is increase the cover plate width near the column face, but this increase may be limited due to maximum width of the column.

5.2.2.2 EPH connections

The experimental specimen and numerical models of full-scale frames with EPH connections designed for seismic action failed due to fracture of the bolts near the unstiffened beam flange in tension. This type of failure occurred in all cases at the connection opposite to the lost column. The reason is specific configuration of this type of connection with asymmetric configuration, as the haunch and flange in tension distribute the forces to more bolt rows than in the case of the unstiffened beam flange.

Since the vulnerability is present only for bolts near the unstiffened flange, a strengthening approach is to provide a higher capacity just to these components. Therefore, only these two bolt rows need to be strengthened first, see Figure 5.5. Stresngtened EP performance Bolt capacity can be increased by using larger diameters. As it resulted from the numerical simulations performed in Chapter 4, it is also expected that the capacity of the T-stub to be limited by the resistance of the end-plate. The capacity of the T-stub can be used to assess the end-plate thickness that is required to increase the capacity of the T-stub ($F_{rd,T-sub}$). The maximum force transferred to the T-stub, $F_{ed,T-stub}$, can be limited to the axial plastic capacity of the tributary area of the beam for the T-stub. Equation (5.6) gives an expression for $F_{ed,T-stub}$.

$$F_{Rd,T-stb} > F_{Ed,T-stb} \tag{5.5}$$

$$F_{Ed,T-stb} = \left(\frac{A_{beam}}{2} - \Delta h \cdot t_w \right) \cdot f_{u,beam} \tag{5.6}$$
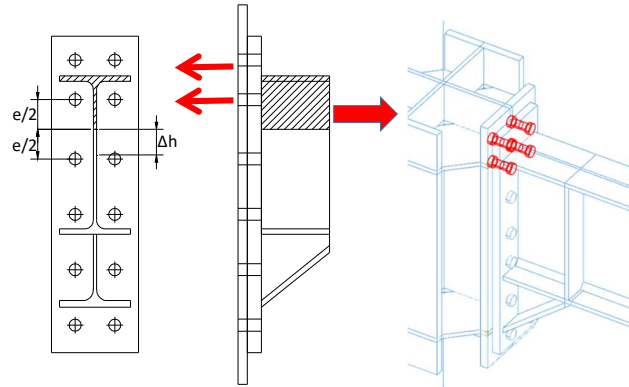
Figure 5.5. Stresngtened EP performance

The values of $F_{rd,T-sub}/F_{ed,T-stub}$ ratios are listed in Table 5.2. This proposal could be very conservative, due to the assumption that the force corresponding to ultimate capacity of the active area in tension (Figure 5.5) is transferred to the upper T-stub. Therefore, more studies are necessary to optimize the response and find the realistic distribution of forces at different bolt rows.

Table 5.2. $F_{rd,T-sub}/F_{ed,T-stub}$ values for EPH case study configurations

	EPH	iEPH
LSZ	1.08	0.83
MSZ	1.00	0.80
HSZ	1.03	0.71

5.2.2.3 RBS connection

The RBS connections provided adequate capacity to allow the development of full catenary action in beams (both in experimental 2D test and numerical simulations on case study frame structures). Since the failure of the connection always occurred in the flange in tension within the reduced zone, any strategy to increase the capacity against column loss should be limited to the increase of beam strength.

5.2.2.4 EP connection

Failure of partial strength EP connection (0.8 compared with the beam) in 2D frame test was due to bolt fracture near the flange in tension. The increase of the connection resistance (1.2 compared with the beam) allowed development of large deformations and catenary forces in beams in 3D frame test, see Figure 5.6. Note that the load for ANS-M represented in Figure 5.6 is divided by two, as there are two perpendicular frames that resist the applied load. The detailed study for the performance EP connections in 2D and 3D analyses with different boundary conditions (section 4.2.5) indicates that the general experimental conclusions specific for these connections regarding strength and ductility improvement for strengthened connection is not influenced by the test-set-up configuration.
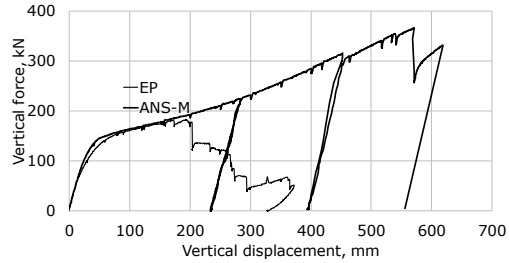
Figure 5.6. Experimental curves for EP connection

Table 5.3 presents the ratio of the connection resistance, calculated using the component method of EN 1993-1-8, to the beam resistance, for case study structures investigated in Chapter 4. EP are the initial connections, while iEP are the improved connections, strenghtened to avoid bolt fracture. As may be seen, the increase of connection capacity to bending moment also increases the axial resistance load. For all improved configurations, the failure developed in the beams and not in the connection. On the other hand, design of connection for full axial capacity of beam is too conservative.

Table 5.3. Beam/connection resistance ratios for EP connections case study configurations

F_{con}/ F_{beam}	EP		iEP	
	M	N	M	N
LSZ	0.79	0.67	1.28	0.89
MSZ	0.83	0.72	1.29	0.89
HSZ	0.84	0.77	1.26	0.94

5.3   Concluding remarks

A methodology for robustness evaluation of multi-storey steel frame structures was proposed. The approach utilizes the conventional seismic design rules for selection of structural system, types and properties of members and connections, but includes additional analysis sequences and verifications that are specific for column loss event. The response after a column loss is evaluated using a dynamic analysis and modelling parameters for members and connections, which are validated against experimental data. When the capacity to resist the loss of a column is not verified due to premature failure of connection, strengthening is done using improved detailing or new configurations. Element strengthening is necessary is structural capacity is limited by member resistance. The process is continued until progressive collapse requirements are met, without disregarding seismic design rules and principles. The following four connection typologies were studied and reconfigured to meet higher levels of deformation and axial strength capacity:

- CWP: welded cover plate thickness increase to resist the axial load transferred from the beam in tension
- EPH: strengthening of end-plate and bolt rows near the unstiffened beam flange in tension (T-stub capacity increase)
- RBS: no strengthening strategy is considered to be applied, excepting the design for seismic demands
- EP: end-plate and bolts are strengthened to allow the development of full catenary action in beam.

In order to include the effect of seismic sizing of elements, beam height, and span length, a parametric study has been performed and the effectiveness of the proposed methodology verified.

Further studies are needed to include other factors, e.g. static vs dynamic analysis, notional column removal vs direct blast effect, one-way vs two-way system, composite beam vs pure steel beam, and selection of column loss scenarios.

6 CONCLUSIONS, PERSONAL CONTRIBUTIONS, AND FUTURE RESEARCH DIRECTIONS

6.1   General conclusions remarks

Started after the collapse of Ronan Point building due to an accidental gas explosion, in 1968, the progressive collapse research gained more attention in the recent years, with large number of studies developed in the last two decades aiming to develop new/improved design guidelines and recommendations. Extensive experimental and numerical studies were used to identify the critical points and to find the structural issues that are required to contain the damage and to prevent the collapse propagation. Previous experimental research in progressive collapse resistance of structures include experimental tests on connection details, structural assemblies or full-scale structures. However, due to the large variety of structural systems that are currently employed, conditions used in design and operation, and diversity of hazards, the development of comprehensive design guidelines and recommendations are still needed. Seismic resistant systems are considered robust systems, and, with varying degrees, appropriate to provide resistance to progressive collapse in case of column loss. However, there are not enough results to support this assumptions, especially at the level of connection design and detailing, where large deformations are expected after a column removal. As a result, a large experimental and numerical program has been developed to evaluate the capacity of steel frames to resist progressive collapse after the loss of a column, including experimental tests on connection macro-components as well as 2D and 3D frame systems and numerical investigations covering also full scale structures.

The main strategies to avoid progressive collapse in case of extreme events are divided into two major categories, i.e. the accidental load is identified and the structure is designed to resist the action (key element design), or the damage is limited and loads are redistributed to undamaged members (alternate load path). The research developed in the thesis is based on enhancing the structural robustness by assuring adequate capacity of beam-to-column connections to redistribute the loads after a column removal. The conventional design process does not evaluate, nor guarantee an adequate performance of moment resistant frame structures to extreme events causing the loss of a column.

Static and dynamic column loss analyses on full scale structures showed that high seismic design requirements have a major influence on capacity increase of moment resisting frame structures to resist column loss events. Improved detailing also had significant contribution to structural performance. Experimental and numerical tests on 3D subassemblies subjected to column loss indicated that the ultimate capacity of the MRF structural system is dependent on the distribution of gravity loads. The tested loading system (point load) has a favorable bending moment distribution compared to the realistic case of uniform distributed load. The stability of the unrestrained laterally on both directions perimetral column, impacts the structural capacity to resist penultimate column loss, but concrete slab provides lateral restraint. Composite action of slab leads increases the stiffness, reaching the higher ultimate load compared to the pure steel specimen, but reduces the connections ductility. The

capacity of the structure to resist progressive collapse can be improved by element strengthening and by adequate detailing that would ensure continuity of the joint at large deformations.

In order to benefit from the maximum strength and ductility of the structural elements, connection should ensure the integrity of the structure and have sufficient capacity to allow failure to develop in the beams. Specific recommendations for robustness improvement of connections are based on experimental tests on 2D frames subjected to column loss and parametric numerical investigations on study case structures. The CWP connection, failing due to cover plate fracture in tension, requires cover plate thickness increase to assure sufficient capacity of the cover plate to transfer the forces from the beam to the column. The improvement strategy for EPH connection performance, failing due to fracture of bolt rows near the unstiffened beam flange, is the strengthening of the end-plate and of the two bolts rows near the unstiffened beam flange. RBS connection exhibited a good behavior, failure initiating in the reduced section of the beam by tensioned flange fracture. The capacity of the partial-strength EP system to reach catenary action is low, less than half than in the other cases. Therefore, significant improvements can be made in both ductility and strength regards, if bolts and end-plate are strengthened. Any optimization process should stay in the limit of seismic requirements and recommendations.

Connections capacity to provide strength and ductility of the system to axial force – bending moment interaction associated to column loss deformation state, is limited to the capacity of connection components to provide adequate strength and respectively to confine large plastic deformations in ductile components. Experimental and numerical tests on connection macro-components have been performed to determine the ultimate strength and deformation capacity under static and dynamic loading. The results showed no important influence of loading rate. If properly manufactured and checked, welds provide adequate response and failure is prevented. For bolted T-stubs, the failure was due to bolt fracture in all configurations, even designed for mode 1 or 2, owing to additional forces due to prying and bending effects in bolts. The capacity of the T-stub can be enhanced by strengthening the bolts (diameter or class) and of end-plate (thickness, material strength, bolt distance) such that failure takes place in the beam flange – the case of the tested pure steel 3D specimen showed that the improved configuration allowed the connection to resist the combined bending moment – axial force effect up to failure of beam flange in tension.

The presented procedure for robust assessment of seismic multi-storey steel frames is supplementary to conventional seismic design, adding several verifications based on alternate load path principles. The initial structure resulted from seismic design must be modelled in a 3D environment sensitive for the particular connection details performance, with connections calibrated for axial force – bending moment interaction. The load-bearing structural capacity for column loss scenarios results from dynamic column removal with actual loading patterns. 3D modelling is necessary as 2D evaluations can be unconservative. A time-efficient analysis procedure was developed to combine AEM-FEM numerical modeling to fulfill these analyses requirements. The procedure is based on selecting relevant assemblies from the structure to be assessed, modelling them in detail (geometry, bolts, welds, contacts, material degradation and failure) and calibration on identic simplified model substructures from which the full structure model is created for dynamic analyses. For a correct evaluation of structural capacity to mitigate progressive collapse, selected subassembly and boundary conditions must replicate the development of internal forces in the entire structure. The restraint given by the rest of the structure is crucial for representative development of internal loads and accurate evaluation of

system strength and capacity. If the structural performance is lower than required and failure is related to the connection, its capacity can be enhanced, while if failure is due to insufficient element capacity, their strength can be increased. The improved structural configuration (elements and connection detailing) must be checked to fulfill seismic requirements prior to another robustness evaluation. The structural configuration is suitable when the structure fulfils also the robustness criteria. Connection improvements address the need to prevent failure in the beam-column interface connection components, and attain failure in the tensioned beam web flange. Connection details verifications are proposed based on capacity of vulnerable components to transfer the capable force from other components.

Conclusions derived from this study are limited to the studied types of connections and type of structural elements, further studies being required for generalizations. Further parametric studies are necessary to confirm the conclusions for a broader range of structural solutions and to assess the influence of concrete slab on connection demands during column loss.

6.2   Specific conclusions

Main conclusions regarding specific stages in the design process of multi-storey frame buildings related to robustness of structures are given bellow, function of general analysis, performance of beam-to-column joints and connection components.

a) Modeling structural robustness scenarios and global analysis: Principles and recommendation

Alternate load path method should be used to assess the robustness of a multi-storey frame structure. Adequate capacity of beam-to-column connections to redistribute the loads after a column removal would enhance progressive collapse resistance, as well as strengthened elements.

Capacity reserve of elements in gravity combinations, given by high seismic requirements ensures a higher level of robustness if properly connected.

3D dynamic modelling of full structure with corresponding loading patterns gives most accurate results. 2D analysis can give unconservative results.

The model must incorporate the specific behavior of axial force - bending moment interaction for the given detailing of the connections.

Calibration of the connection behavior should be performed by investigating: (1) column loss relevant experimental evaluation of the specific connection typology and (2) relevant selected subassembly with adequate boundary conditions and detailed modeling of connection configuration.

Design and detailing should respect seismic requirements and principles also for improved structural and detail configurations.

b) Robustness conceptual design and assessment of beam-to-column moment joints

Beam-to-column connections should provide the integrity of the structure and have sufficient capacity to allow failure to develop in the beams.

Vulnerability of some details are identified and specific verifications can be performed to increase the robustness co the beam-to-column connections, function of their typology:

(1) CWP - cover plate to resist in tension the forces transferred by the beam. Conventional design of cover plate provides bending moment overstrength, and not axial force overstrength as well.

(2) EPH – upper (unstiffened by haunch) T stub should resist tension transferred by beam flange and part of the web. The unsymmetrical configuration is more vulnerable at hogging bending moment

(3) EP – connection should be designed with overstrength, as partial strength end-plate bolted connections are not suited to ensure catenary action development in case of column loss.

No verifications/ strengthening recommendations have been found necessary for RBS connections.

c) Design of components of robust beam-to-column moment joint

Resistance and strength of components should be designed in such a way that large connection rotations can be attained beyond seismic ductility requirements.

Components with brittle failure must possess overstrength with regards to components that are recommended to undergo large plastic deformations.

Ultimate failure mode consisting in bolt fracture should be avoided. This failure is frequent even for failure mode 1 and 2 T-stubs because of prying forces development at large displacements.

Ductility to the entire system can be achieved if failure of T-stub components (bolt, end-plate) is prevented. Failure is recommended to occur in the beam, namely by beam flange fracture in tension. Such a failure is ductile, even if failure mode 3 T-stubs, considered brittle configurations, are used.

T-stub capacity can increase by bolt strengthening (higher steel class or larger bolt diameters) or by end-plate strengthening (distance between bolts, plate thickness or steel quality).

6.3   Contributions of the author

Based on the studies undertaken in the thesis, particularly on the conclusions of the previous sections, the following results can be presented as contributions and achievements of the author:

• Based on detailed preliminary column loss assessment of several structures designed for low seismicity conditions, and considering selected literature recommendations for future research, the experimental testing framework was developed. Selection, design, and calibration of the **experimental specimens** is performed for connection macro-components, 2D frame assemblies with four types of seismic beam-to-column connections, and two 3D frame assemblies with different floor systems. Pioneering experimental tests in Romania on column loss subassemblies models have been performed on seismic typologies of connections. The design of the **test set-up configurations** replicated the boundary conditions present in the full structure to ensure adequate development of internal forces in column removal situations. Preliminary AEM analysis provided the required calibration of the restraining system, resulting an original 3D test set-up.

- The sets of **experimental results** on connection macro-components, 2D frame assemblies subjected to column loss with different types of beam-to-column connections, 3D structures subjected to column loss with and without reinforced concrete slab, used state of art instrumentation, i.e. displacement transducers, strain-gauges, and digital image correlation techniques. The obtained sets of experimental results supplements existing investigations regarding column loss structural resistance of frames, with substantial contributions related to seismic configurations which are less approached in research studies.
- **Validation of numerical models in AEM and FEM** is based on the experimental framework results. Test results have been used to increase the accuracy of the FEM analyses tools and to validate the ELS model. The numerical models provide further data related to the investigations and allows the expansion of experimental results dataset. The testing and numerical framework interconnections allow comparisons between tests of different categories, and for its complexity extent, can be a reference for further research.
- The developed **analysis procedure combining AEM-FEM** enables evaluating the performance of full-scale structures to different column loss scenarios considering dynamic effects and realistic loading patterns. The analysis procedure, based on the calibrated FEM and AEM models, can also be applied for global structural evaluation of direct effect of accidental action, modelling blast, impact, or similar effects.
- The results of the **parametric study** on performance of structures designed for different seismic requirements was used for defining a methodology for robustness evaluation and improvement of steel frame structures. Specific vulnerabilities have been identified and confirmed for different beam-to-column connections typologies. **Recommendations** for assessment and enhancement of structural resistance against progressive collapse have been presented raging from global analysis, to connections and components detailing, further research allowing them to be a basis for future code provisions. The proposed solutions deal with the prescriptive lack of guidance regarding robustness of seismic designed multi-storey frames.
- The integrated experimental work and numerical program was extensively disseminated through presentation in scientific events, workshops, seminars, technical committees of professional associations (TC10, TC13 of ECCS) and dedicated journals.

6.4 Research impact and dissemination of results

The presented results represent the core of the CODEC research project and have been made publicly available through research reports in the frame of the project at http://www.ct.upt.ro/centre/cemsig/codec.htm.

Some research results and conclusions have been presented and published in several conferences and journals. Most important papers are provided below:

ISI journals

Dinu, F, Dubina, D and **Marginean, I**, Improving the structural robustness of multistory steel-frame buildings, Structure and Infrastructure Engineering: Maintenance, Management, Life-Cycle Design and Performance: http://dx.doi.org/10.1080/15732479.2014.927509

Cited by Cassiano, D, D'Aniello, M, Rebelo, C, Landolfo, R and da Silva, LS, "Influence of seismic design rules on the robustness of steel moment resisting frames". Steel and Composite Structures, 21 (3), 479-500, 2016 *and* Charmpis, DC and Kontogiannis, A, "The cost of satisfying design requirements on

progressive collapse resistance–Investigation based on structural optimisation". Structure and Infrastructure Engineering, 12 (6), 695-713, 2016

Dinu, F, **Marginean, I**, Dubina, D and Petran, I, Experimental testing and numerical analysis of 3D steel frame system under column loss. Engineering Structures, 113 59-70, 2016 http://dx.doi.org/10.1016/j.engstruct.2016.01.022

Dinu, F, **Marginean, I**, Dubina, D, Experimental testing and numerical modeling of steel moment-frame connections under column loss – Engineering Structures (in review)

ISI conference proceedings

Dinu, F, Sigauan, A, **Marginean, I**, Kovacs, A and Ghicioi, E. Structural response of multistorey steel building frames to external blast loading. in 5th International Conference INTEGRITY - RELIABILITY - FAILURE. 2016.

Dinu, F, **Mărginean, I**, Sigauan, A, Dubina, D, Influence of composite slabs and beams on the progressive collapse resistance of steel frame buildings, in 5th International Conference INTEGRITY - RELIABILITY – FAILURE, 2016, Porto, Portugal

BDI journals

Dinu, F, Dubina, D, **Marginean, I**, Neagu, C, Petran, I, Structural Connections of Steel Building Frames under Extreme Loading, Advanced Materials Research, Volume 1111, DOI 10.4028/www.scientific.net/AMR.1111.223 ISSN: 1022-6680, 2015 (1 citare)

Both, I,. **Mărginean, I**, Neagu, C, Dinu, F, Dubina, D, Zaharia, R,. Experimental research on T-stubs under elevated temperatures. in Proceedings of the International Conference in Dubrovnik, 15-16 October 2015 in edition of Applications of Structural Fire Engineering. 2015. 153-158, 2015

Mărginean, I, Dubină, D, Dinu, F, Numerical Modeling of Beam-to-Column Connections Under Column Loss Scenarios, INTERSECTII/INTERSECTIONS, 13 (1), 58-68, 2016

Inernational conferences

Dinu, F, Dubina, D, **Marginean, I**. Effect of connection between R.C. slab and steel beams in multistory frames subjected to different column loss scenarios, Proc. of. 4th International Conference on Integrity, Reliability & Failure, Portugal, 23-27 June 2013, Ed. Inegi, ISBN 978-972-8826-27-7, pp. 41-42.

Dubina, D, Dinu, F, **Marginean,I**, Petran, I. Collapse prevention design criteria for moment connections in multistory steel frames under extreme actions, , Proc. of. 4th International Conference on Integrity, Reliability & Failure, Portugal, 23-27 June 2013, Ed. Inegi, ISBN 978-972-8826-27-7, pp. 215-216.

Dinu, F, Dubina, D, **Marginean, I**, Petran, I. Ultimate capacity of beam-to-column connections under bending and axial stresses, Italian conference on Steel Structure XXIV CTA, Torino 30 sept.-2 oct. 2013.

Dinu, F, Dubina, D, **Marginean, I**, Neagu, C. Experimental tests of steel beam-to-column joints under column loss scenarios, Napoli, Italy, ISBN 978-92-9147-121-8, 2014, 275, 276, 7th Europeean Conference on Steel and Composite Structures.

Dinu, F, **Marginean, I**, Dubina, D, Petran, I. Experimental Study of Seismic Resistant Steel Frames in Case of Column Loss, Eight International Conference on Advances in Steel Structures (ICASS'2015), July 2015, Lisabona, Portugalia, Proceedings of the Eighth International Conference on ADVANCES IN STEEL STRUCTURES, Lisbon, Portugal, July 22-24, 2015 (on CD, Paper ID 142).

Dinu, F, Dubina, D, **Marginean, I**, Neagu, C and Petran, I. Axial strength and deformation demands for t-stub connection components at catenary stage in the beams, 8th International Conference on Behavior of Steel Structures in Seismic Areas 1 July 2015 Shanghai, China.

Crisan, A, Dubina, D and **Marginean, I**. Numerical simulation of pallet rack systems failure under seismic actions, 8th International Conference on Behavior of Steel Structures in Seismic Areas 1 July 2015 Shanghai, China.

Marginean, I, Dinu, F, Dubina, D, Petran, I, Senila, M and Szilagyi, H. Numerical modeling of dynamic response of steel moment frames following sudden column loss. in The International Colloquium on Stability and Ductility of Steel Structures. 2016. ECCS – European Convention for Constructional Steelwork, 717-724, 2016.

Dinu, F, **Marginean, I**, Sigauan, A, Kovacs, A, Ghicioi, E and Vasilescu, D. Effects of close range blasts on steel frames. Experimental testing and numerical validation. in The International Colloquium on Stability and Ductility of Steel Structures. 2016. ECCS – European Convention for Constructional Steelwork, 699-708, 2016.

Dinu, F, **Mărginean, I**, Dubina, D, Neagu, C. Experimental evaluation of progressive collapse resistance of steel moment frame connections. in The International Colloquium on Stability and Ductility of Steel Structures. 2016. ECCS – European Convention for Constructional Steelwork, 681-690, 2016.

Both, I, **Mărginean, I**, Neagu, C, Dinu, F, Dubina, D, Zaharia, R. T-stubs response to extreme loading, The International Colloquium on Stability and Ductility of Steel Structures. 2016. ECCS – European Convention for Constructional Steelwork, 673-680, 2016.

Dinu, F, **Marginean, I**, Dubina, D, Petran, I, Pastrav, M, Sigauan, A, Ciutina, A. Experimental testing of 3D steel frame with composite beams under column loss. in The International Colloquium on Stability and Ductility of Steel Structures. 2016. ECCS – European Convention for Constructional Steelwork, 691-698, 2016.

Dinu, F, **Mărginean, I**, Dubina, D, Sigauan, A, Petran, I. Experimental research on the behavior of steel moment frame connections under column loss scenario, in Proceedings of the Eigth International Workshop on Connections in Steel Structures, Boston, USA.

Several papers have been published in Romania journals and conferences, one of which received the best research paper award for young researchers' papers presented at the XIV-th National Conference on Steel Structures:

Marginean, I, Dinu, F, Dubina, D, Neagu, C, Petran, I. Îmbinări grinda-stâlp pentru structuri în cadre metalice cu rezistență ridicată la colaps progresiv, the 14th National Conference on Steel Structures, 19-20 Novemver 2015, Cluj-Napoca, Romania, Ed. Mediamira, ISBN 978-973-713-334-2.

Two presentations have been made in the technical committee TC 10 of the European Convention for Constructional Steelwork- ECCS. The committee is a forum for investigation and debating problems of structural steel connections. The objectives of the forum are recommendations and consulting for design and execution of steel connections, drafting design guidelines and providing support for design codification in the field [179]:

I. Marginean, F. Dinu, D. Dubina Behaviour of beam- to-column connections under strong axial forces in the catenary phase of robustness scenarios, TC10 Reunion, ECCS, Papendrecht, 16-17 April 2015

I. Marginean, F. Dinu, D. Dubina, Recommendations for collapse prevention design of moment steel beam-to-column connections, TC10 Reunion, ECCS, London, 29 September 2016

6.5   Further research directions

Several research needs and opportunities have been identified during the activities within this thesis. The most important future personal research directions are presented as short-term and long-term perspectives.

6.5.1   Short-term perspectives

Unpublished results obtained within this thesis should be prepared for publishing in peer-reviewed scientific papers, such that through the reviewers' direct feedback, ideas and concepts are improved. Also, argumentation is consolidated in this process. Publishing the results in journal articles is very effective in terms of result dissemination, with an enhanced visibility potential compared to the thesis.

The 2nd generation of Eurocodes would be available approximately in 2020, with drafts appearing in the next years. The structural Eurocodes would contain robustness provisions, mostly in the form of verifications which can be performed by the designers. Conclusions from the thesis should be processed and extended in order to be applicable in some extent in the design verifications for structural robustness.

Column removal scenario is an effective, but simplistic scenario, as the direct effect of actions that may lead to column loss, besides fully or partially damaging the column, can also damage other structural elements. Unintended (domestic or industrial) and deliberate detonations can severely affect the integrity of a structure. The study of the direct effect of blast action on structures will be performed in *Experimental Development Projects* call project implemented by UPT (CMMC department) and INSEMEX Petrosani. The PN-III-P2-2.1-PED-2016-0962 project, *Experimental validation of the response of a full-scale frame building subjected to blast load* (FRAMEBLAST 2017-2018), is supported by research data from CODEC project and financed by UEFISCDI through the *Experimental Development Projects* financial instrument. The project objectives are:

• The experimental and numerical validation of blast load models and structural response of a typical frame building system under blast loading
• The development of a procedure to apply structural identification to components of a full-scale building structure with structural deterioration resulting from an internal or external blast
• The integration of structural detailing for mitigation of progressive collapse in case of a blast loading in a general methodology for protection against extreme actions that can cause the loss of a structural building member (e.g. earthquakes).

6.5.2   Long-term perspectives

The effect of the slab regarding capacity and ductility demand of the structures in case of column loss or partial loss scenarios needs to be studied. For many slab systems, even if the composite effect is not taken into account in the design, the floor solution allows significant beam-slab interaction that affects the overall performance of the connection. The influence of a variation of floor systems

on progressive collapse mitigation should be assessed. Also, seismic provisions (e.g. lack of connectors in the plastic hinge zone) should be studied.

With data obtained from the FRAMEBLAST project, regarding the direct effect of blast on the structure and elements, the potential post-blast remaining strength of the bearing element should be evaluated, in order to assess the structural capacity to resist blast actions considering the residual capacity of the damaged element.

The development of benchmark failure scenarios for multi-storey moment resisting frame structures performing vulnerability analyses to obtain fragility curves would be of great use for designers, owners, assurance companies, and public institutions with policy creating authority. Defining a statistical method to assess the probability of exceeding a given damage state (acceptance criteria) for loading demands, geometry and configuration structural properties requires extensive research activities that would span over a series of research projects and collaboration with several research teams. A multihazard aproch related to structural robustness should also be considered.

6.6   Acknowledgement

REFERENCES

[1]   Qian, K, Li, B and Tian, Y, "Recent Progress in Understanding of Load Resisting Mechanisms for Mitigating Progressive Collapse"*. Special Publication*, 309 1-18, 2016

[2]   Wang, H, Zhang, A, Li, Y and Yan, W, "A Review on Progressive Collapse of Building Structures"*. Open Civil Engineering Journal*, 8 183-192, 2014

[3]   CEN. EN 1991-1-7 Eurocode 1: Actions on structures - Part 1-7: Accidental actions 2006, Brussels

[4]   Dubina, D and Dinu, F. *Collapse prevention design of multistorey steel building frames under extreme action*. in *Proceedings of the Nordic steel construction conference*. 2012. 5-7, 2012

[5]   Management Association, IR, *Civil and Environmental Engineering: Concepts, Methodologies, Tools, and Applications: Concepts, Methodologies, Tools, and Applications*. 2016: IGI Global.

[6]   CODEC 2012, Structural conception and collapse control performance based design of multistory structures under accidental actions CODEC, Executive Agency for Higher Education, Research, Development and Innovation Funding (UEFISCDI) (2012-2016) Partnerships Program Joint Applied Research Projects grant number PN II PCCA 55/2012

[7]   CODEC. *Structural conception and collapse control performance based design of multistory structures under accidental actions*. 2016; Available from: http://www.ct.upt.ro/centre/cemsig/codec.htm.

[8]   CEN. EN 1990 Eurocode - Basis of structural design, 2002, Brussels

[9]   Corley, W, Sozen, M, Thornton, C and Mlakar, P, The Oklahoma City bombing: improving building performance through multi-hazard mitigation"*. Federal Emergency Management Agency Mitigation Directorate, FEMA Report*,FEMA, 1996

[10]   Dinu, F, Dubina, D and Marginean, I, "Improving the structural robustness of multi-story steel-frame buildings"*. Structure and Infrastructure Engineering*, 11 (8), 1028-1041, 2015

[11]   DoD. UFC 4-023-03 Unified facilities criteria: design of buildings to resist progressive collapse, 2009, Washington (DC), US

[12]   Ellingwood, BR, Smilowitz, R, Dusenberry, DO, Duthinh, D, Lew, H and Carino, NJ, NISTIR 7396"Best practices for reducing the potential for progressive collapse in buildings"*. US Department of Commerce, National Institute of Standards and Technology, 2007

[13]   HMSO. Building and Buildings Statutory Instrument No. 1676, 1976, London

[14]   Moore, D. *The UK and European regulations for accidental actions*. in *National Workshop on Prevention of Progressive Collapse in Rosemont, III, Multihazard Mitigation Council of the National Institute of Building Sciences, Washington, DC*. 2002. 2002

[15]   HMSO. Approved Document A Structure, 1992 Edition 1992, London

[16]   The Daily Telegraph, *Ronan Point*. 1968: London Over the Border, historical website

[17] Granstrom, S, "Stability of Buildings after Accidental Damage. Forces in Element Joint - Model Tests". *Swedish Building Research Report R20*, 4 (3), 1971

[18] Hanson, K and Olesen, SO, Failure Load and Failure Mechanism of Keyed Shear Joints". *Academy of Engineering, Building Department Report 69/22*, 1969

[19] ANSI. A58. 1 Building Code Requirements for Minimum Design Loads in Buildings and Other Structures, 1972,

[20] TM 5-1300 Structures to Resist the Effects of Accidental Explosions, 1990, Departments of the Army, The Navy, The Air force, USA

[21] DoD. UFC 3-340-02 Unified facilities criteria: Structures to resist the effects of accidental explosions, 2008, Washington (DC), US

[22] DoD. UFC 4-023-03 Unified facilities criteria: design of buildings to resist progressive collapse, 2005, Washington (DC), US

[23] Stevens, D, *PC UFC Design Strategies-- Tie Forces and Alternate Path*, in *PC UFC Breifing*. 2004.

[24] DoD. UFC 4-023-03 with Change 1 Unified facilities criteria: design of buildings to resist progressive collapse, 2010, Washington (DC), US

[25] DoD. UFC 4-023-03 with Change 2 Unified facilities criteria: design of buildings to resist progressive collapse, 2013, Washington (DC), US

[26] DoD. UFC 4-023-03-with Change 1 Unified facilities criteria: design of buildings to resist progressive collapse, 2016, Washington (DC), US

[27] ASCE. ASCE/SEI 41-13 Seismic evaluation and retrofit of existing buildings, 2013,

[28] Grecea, D, Dinu, F and Dubină, D, "Performance criteria for MR steel frames in seismic zones". *Journal of Constructional Steel Research*, 60 (3), 739-749, 2004

[29] GSA, "Progressive collapse analysis and design guidelines for new federal office buildings and major modernization projects". *Washington, DC (US)*, 2003

[30] GSA, "Alternate Path Analysis and Design Guidelines for Progressive Collapse Resistance". *Washington, DC (US)*, 2013

[31] Demonceau, J, Huvelle, C, Comeliau, L, Hoang, L, Jaspart, J and Fang, C, Robustness of car parks against localised fire (Robustfire)". *Grant Agreement Number RFSR-CT-2008-00036, Final report, EUR*,European Commission,, 2013

[32] Hoffmann, N, Kuhlmann, U, Demonceau, J-F, Jaspart, J-P, Colomer, C, Hoffmeister, B, Zandonini, R, Hjiaj, M and Mohler, C. *Robust Impact Design of Steel and Composite Buildings*. in *IABSE Symposium Report*. 2015. International Association for Bridge and Structural Engineering, 38-45, 2015

[33] Korndörfer, J, Hoffmeister, B, Feldmann, M, Heng, P and Hijaj, M. *Robust impact design of steel and composite buildings Advances in the Residual Strength Method*. International Association for Bridge and Structural Engineering, 54-61,

[34] Kuhlmann, U, Jaspart, J, Vassart, O, Weynand, K and Zandonini, R, Robust structures by joint ductility. RFCS Publishable Report Contract-No RFS-CR-04046". 2008

[35] Bursi, O, et al., Design and integrity assessment of high strength tubular structures for extreme loading conditions". EUROPEAN COMMISSION, 2012

[36] Hoffmeister, B, et al., ADBLAST–Advanced design methods for blast loaded steel structures. RFCS-Projekt Nr". *RFSR-CT-2010-00 030, 2010-2013, 2015*

[37]   Summaries of RFCS Projects 2003 – 2014". *Full list of projects co-financed by the Research Fund for Coal and Steel of the European Commission*,European Commission, 2015

[38]   Hauke, B, et al., COSIMB - Composite Column and Wall Systems for Impact and Blast Resistance". *RFCS Contract-Number RFS-CR-04047, Forschungsbericht*, 2008

[39]   Mazzolani, FM, *Front Matter*, in *Urban Habitat Constructions Under Catastrophic Events*. 2010, CRC Press.

[40]   Canisius, TG, Structural robustness design for practising engineers". *COST Action TU0601*, 2011

[41]   Xu, G and Ellingwood, BR, "Disproportionate collapse performance of partially restrained steel frames with bolted T-stub connections". *Engineering Structures*, 33 (1), 32-43, 2011

[42]   Gong, Y, "Ultimate tensile deformation and strength capacities of bolted-angle connections". *Journal of Constructional Steel Research*, 100 50-59, 2014

[43]   Dinu, F, Marginean, I, Dubina, D and Petran, I, "Experimental testing and numerical analysis of 3D steel frame system under column loss". *Engineering Structures*, 113 59-70, 2016

[44]   Abidelah, A, Bouchaïr, A and Kerdal, DE, "Influence of the flexural rigidity of the bolt on the behavior of the T-stub steel connection". *Engineering Structures*, 81 181-194, 2014

[45]   Ribeiro, J, Santiago, A, Rigueiro, C and da Silva, LS, "Analytical model for the response of T-stub joint component under impact loading". *Journal of Constructional Steel Research*, 106 23-34, 2015

[46]   Dinu, F, Dubina, D, Marginean, I, Neagu, C and Petran, I. *Axial strength and deformation demands for t-stub connection components at catenary stage in the beams*. in *8th International Conference on Behavior of Steel Structures in Seismic Areas*. 2015. 623-630, 2015

[47]   Yang, B and Tan, KH, "Robustness of bolted-angle connections against progressive collapse: Mechanical modelling of bolted-angle connections under tension". *Engineering Structures*, 57 153-168, 2013

[48]   Baldassino, N, Bernardi, M and Zandonini, R. *Strain rate influence on T-stub response*. in *Proceedings of the Eigth International Workshop on Connections in Steel Structures*. 2016. Boston, US, 2016

[49]   Rahbari, R, Tyas, A, Buick Davison, J and Stoddart, EP, "Web shear failure of angle-cleat connections loaded at high rates". *Journal of Constructional Steel Research*, 103 37-48, 2014

[50]   Astaneh-Asl, A, Madsen, EA, Noble, C, Jung, R, McCallen, DB, Hoehler, MS, Li, W and Hwa, R, "Use of catenary cables to prevent progressive collapse of buildings". *Report No.: UCB/CEE-STEEL-2001/02*, 2001

[51]   Tan, S and Astaneh-Asl, A, "Cable-based retrofit of steel building floors to prevent progressive collapse". *Berkeley: University of California*, 2003

[52]   Yu, M, Zha, X and Ye, J, "The influence of joints and composite floor slabs on effective tying of steel structures in preventing progressive collapse". *Journal of Constructional Steel Research*, 66 (3), 442-451, 2010

[53]   Sadek, F, El-Tawil, S and Lew, H, "Robustness of composite floor systems with shear connections: Modeling, simulation, and evaluation". *Journal of Structural Engineering*, 134 (11), 1717-1725, 2008

[54]   Alashker, Y and El-Tawil, S, "A design-oriented model for the collapse resistance of composite floors subjected to column loss". *Journal of Constructional Steel Research*, 67 (1), 84-92, 2011

[55] Demonceau, J-F and Jaspart, J-P, "Experimental test simulating a column loss in a composite frame". *Advanced steel construction*, 6 (3), 891-913, 2010

[56] Guo, L, Gao, S, Fu, F and Wang, Y, "Experimental study and numerical analysis of progressive collapse resistance of composite frames". *Journal of Constructional Steel Research*, 89 236-251, 2013

[57] Lew, HS, Main, JA, Robert, SD, Sadek, F and Chiarito, VP, "Performance of Steel Moment Connections under a Column Removal Scenario. I: Experiments". *Journal of Structural Engineering*, 139 (1), 98-107, 2013

[58] Sherif, E-T, Lew, HS, Joseph, AM and Fahim, S, "Performance of Steel Moment Connections under a Column Removal Scenario. II: Analysis". 2013

[59] Li, L, Wang, W, Chen, Y and Lu, Y, "Experimental investigation of beam-to-tubular column moment connections under column removal scenario". *Journal of Constructional Steel Research*, 88 244-255, 2013

[60] Li, L, Wang, W, Chen, Y and Lu, Y, "Effect of beam web bolt arrangement on catenary behaviour of moment connections". *Journal of Constructional Steel Research*, 104 22-36, 2015

[61] Li, L, Wang, W, Chen, Y and Teh, LH, "Column-wall failure mode of steel moment connection with inner diaphragm and catenary mechanism". *Engineering Structures*, 2016

[62] Wang, W, Fang, C, Qin, X, Chen, Y and Li, L, "Performance of practical beam-to-SHS column connections against progressive collapse". *Engineering Structures*, 106 332-347, 2016

[63] Qin, X, Wang, W, Chen, Y and Bao, Y, "A special reinforcing technique to improve resistance of beam-to-tubular column connections for progressive collapse prevention". *Engineering Structures*, 117 26-39, 2016

[64] Wang, W, Wang, J, Sun, X and Bao, Y, "Slab effect of composite subassemblies under a column removal scenario". *Journal of Constructional Steel Research*, 129 141-155, 2017

[65] Yang, B and Tan, KH, "Numerical analyses of steel beam–column joints subjected to catenary action". *Journal of Constructional Steel Research*, 70 1-11, 2012

[66] Yang, B and Tan, KH, "Experimental tests of different types of bolted steel beam–column joints under a central-column-removal scenario". *Engineering Structures*, 54 112-130, 2013

[67] Yang, B and Tan, KH, "Robustness of Bolted-Angle Connections against Progressive Collapse: Experimental Tests of Beam-Column Joints and Development of Component-Based Models". *Journal of Structural Engineering*, 139 (9), 2013

[68] Liu, C, Tan, KH and Fung, TC, "Dynamic behaviour of web cleat connections subjected to sudden column removal scenario". *Journal of Constructional Steel Research*, 86 92-106, 2013

[69] Marais, S, Tait, R, Cloete, T and Nurick, G, "Material testing at high strain rate using the split Hopkinson pressure bar". *Latin American Journal of Solids and Structures, an ABCM Journal*, 1 (3), 219-339, 2004

[70] Yang, B and Tan, KH, "Behavior of composite beam-column joints in a middle-column-removal scenario: Experimental tests". *Journal of Structural Engineering*, 140 (2), 04013045, 2013

[71] Hayes, ME, Raebel, CH and Foley, CM, *EXPERIMENTAL EVALUATION OF THE ROBUSTNESS OF WT CONNECTIONS UNDER QUASI-DYNAMIC LOAD*, in *RESILIENT INFRASTRUCTURE*. 2016: London.

[72]   Hoffmann, N and kuhlmann, U, *Experimental investigations of composite joints and their behaviour during the loss of a column*, in *Eighth International Workshop on Connections in Steel Structures* 2016: Boston, US.

[73]   Lew, HS, Bao, Y, Sadek, F, Main, JA, Pujol, S and Sozen, MA, "An experimental and computational study of reinforced concrete assemblies under a column removal scenario". *NIST technical note*, 1720, 2011

[74]   Kozłowski, A, Giżejowski, M, Ślęczka, L, Pisarek, Z and Saleh, B. *EXPERIMENTAL INVESTIGATIONS OF THE JOINT BEHAVIOR*. in *EUROSTEEL*. 2011. Budapest, HU, 2011

[75]   Kai, Q and Li, B, "Dynamic performance of RC beam-column substructures under the scenario of the loss of a corner column—Experimental results". *Engineering Structures*, 42 154-167, 2012

[76]   Chen, J, Huang, X, Ma, R and He, M, "Experimental Study on the Progressive Collapse Resistance of a Two-Story Steel Moment Frame". *Journal of Performance of Constructed Facilities*, 26 (5), 567-575, 2012

[77]   Hoffmann, N, Kuhlmann, U, Demonceau, J-F, Jaspart, J-P, Baldassino, N, Freddi, F and Zandonini, R. *Robust impact design of steel and composite building structures: the alternate load path approach*. in *Proceeding of the IABSE Workshop-Safety, Robustness and Condition Assessments of Structures*. 2015. 46-53, 2015

[78]   Xuan Dat, P and Tan, KH, "Experimental study of beam–slab substructures subjected to a penultimate-internal column loss". *Engineering Structures*, 55 2-15, 2013

[79]   Dat, PX and Tan, KH, "Experimental Response of Beam-Slab Substructures Subject to Penultimate-External Column Removal". *Journal of Structural Engineering*, 141 (7), 04014170, 2015

[80]   Dat, PX and Hai, TK, "Membrane actions of RC slabs in mitigating progressive collapse of building structures". *Engineering Structures*, 55 107-115, 2013

[81]   Ren, P, Li, Y, Lu, X, Guan, H and Zhou, Y, "Experimental investigation of progressive collapse resistance of one-way reinforced concrete beam–slab substructures under a middle-column-removal scenario". *Engineering Structures*, 118 28-40, 2016

[82]   Lu, X, Lin, K, Li, Y, Guan, H, Ren, P and Zhou, Y, "Experimental investigation of RC beam-slab substructures against progressive collapse subject to an edge-column-removal scenario". *Engineering Structures*, 2016

[83]   Wang, T, Chen, Q, Zhao, H and Zhang, L, "Experimental study on progressive collapse performance of frame with specially shaped columns subjected to middle column removal". *Shock and Vibration*, 2016, 2015

[84]   Hull, LA, *Experimental testing of a steel gravity frame with a composite floor under interior column loss*. 2013.

[85]   Johnson, ES, Meissner, JE and Fahnestock, LA, "Experimental Behavior of a Half-Scale Steel Concrete Composite Floor System Subjected To Column Removal Scenarios". *Journal of Structural Engineering*, 142 (2), 04015133, 2016

[86]   Kai, H, Sanlin, Q, Ge, Q, Li, J, Zheng, L and Shengsheng, Y, "Application of Progressive Collapse Analysis in a High-Rise Frame-Core Tube Structure". *American Journal of Civil Engineering*, 4 (3), 111-116, 2016

[87]   Baciu, C, "Efficient Measures to Mitigate Effects of Terrorist Bomb Attacks on Buildings". *National Strategies Observer No*, 2, 2015

[88]   Song, BI, *Experimental and analytical assessment on the progressive collapse potential of existing buildings*. 2010, The Ohio State University.

[89]   Song, BI, Giriunas, KA and Sezen, H, "Progressive collapse testing and analysis of a steel frame building"*. Journal of Constructional Steel Research*, 94 76-83, 2014

[90]   Serkan, S and Mehrdad, S, "Progressive Collapse Resistance of Hotel San Diego"*.* 2008

[91]   Scott, F, Serkan, S, Ali, K and Mehrdad, S, "Progressive Collapse Resistance of an Actual 11-Story Structure Subjected to Severe Initial Damage"*.* 2011

[92]   Song, BI and Sezen, H, "Experimental and analytical progressive collapse assessment of a steel frame building"*. Engineering Structures*, 56 664-672, 2013

[93]   Botez, M, *Acurateţe şi eficienţă în analiza la colaps progresiv a structurilor multietajate din beton armat*. 2014: UTCN.

[94]   Bredean, L, *Mecanisme de rezistenţă la colaps progresiv ale structurilor în cadre din beton armat*. 2015: UTCN.

[95]   Izzuddin, BA, Vlassis, AG, Elghazouli, AY and Nethercot, DA, "Progressive collapse of multi-storey buildings due to sudden column loss — Part I: Simplified assessment framework"*. Engineering Structures*, 30 (5), 1308-1318, 2008

[96]   Vlassis, AG, Izzuddin, BA, Elghazouli, AY and Nethercot, DA, "Progressive collapse of multi-storey buildings due to sudden column loss—Part II: Application"*. Engineering Structures*, 30 (5), 1424-1438, 2008

[97]   Izzuddin, BA, "Robustness by design - Simplified progressive collapse assessment of building structures"*. Stahlbau*, 79 (8), 556-564, 2010

[98]   Yang, B, Tan, KH and Xiong, G, "Behaviour of composite beam–column joints under a middle-column-removal scenario: Component-based modelling"*. Journal of Constructional Steel Research*, 104 137-154, 2015

[99]   Liu, C, Fung, TC and Tan, KH, "Dynamic Performance of Flush End-Plate Beam-Column Connections and Design Applications in Progressive Collapse"*. Journal of Structural Engineering*, 142 (1), 04015074, 2016

[100]   Tsai, M-H, "An analytical methodology for the dynamic amplification factor in progressive collapse evaluation of building structures"*. Mechanics Research Communications*, 37 (1), 61-66, 2010

[101]   Tsai, M-H, "Assessment of analytical load and dynamic increase factors for progressive collapse analysis of building frames"*. Advances in Structural Engineering*, 15 (1), 41-54, 2012

[102]   Tsai, M-H and Shyu, W-S, "A proper estimation of inelastic dynamic increase factor in support-loss experiments"*. Journal of the Chinese Institute of Engineers*, 38 (3), 372-381, 2014

[103]   Huvelle, C, Hoang, V-L, Jaspart, J-P and Demonceau, J-F, "Complete analytical procedure to assess the response of a frame submitted to a column loss"*. Engineering Structures*, 86 33-42, 2015

[104]   Chen, CH, Zhu, YF, Yao, Y, Huang, Y and Long, X, "An evaluation method to predict progressive collapse resistance of steel frame structures"*. Journal of Constructional Steel Research*, 122 238-250, 2016

[105]   Gerasimidis, S and Sideri, J, "A new partial-distributed damage method for progressive collapse analysis of steel frames"*. Journal of Constructional Steel Research*, 119 233-245, 2016

[106]   Mazurkiewicz, L, Malachowski, J and Baranowski, P, "Blast loading influence on load carrying capacity of I-column"*. Engineering Structures*, 104 107-115, 2015

[107] Zolghadr Jahromi, H, et al., "Robustness Assessment of Building Structures under Explosion". *Buildings*, 2 (4), 497-518, 2012

[108] Dinu, F, Marginean, I, Sigauan, A, Kovacs, A, Ghicioi, E and Vasilescu, D. *Effects of close range blasts on steel frames. Experimental testing and numerical validation*. in *The International Colloquium on Stability and Ductility of Steel Structures*. 2016. ECCS – European Convention for Constructional Steelwork, 699-708, 2016

[109] Dinu, F, Sigauan, A, Marginean, I, Kovacs, A and Ghicioi, E. *Structural response of multistorey steel building frames to external blast loading*. in *5th International Conference INTEGRITY - RELIABILITY - FAILURE*. 2016. 2016

[110] Tsai, M-H and You, Z-K, "Experimental evaluation of inelastic dynamic amplification factors for progressive collapse analysis under sudden support loss". *Mechanics Research Communications*, 40 56-62, 2012

[111] SELVARAJAH, J, *ROBUSTNESS ANALYSIS AND DESIGN OF STEEL-CONCRETE COMPOSITE BUILDINGS*. 2014.

[112] Demonceau, J-F, *Steel and composite building frames: sway response under conventional loading and developmet of membrane effects in beams further to an exceptional action*. 2008, Université de Liège.

[113] Weigand, JM, *The integrity of steel gravity framing system connections subjected to column removal loading*. 2014.

[114] Vidalis, CA, *Improving the resistance to progressive collapse of steel and composite frames*. 2014.

[115] El-Tawil, S, Li, H and Kunnath, S, "Computational Simulation of Gravity-Induced Progressive Collapse of Steel-Frame Buildings: Current Trends and Future Research Needs". *Journal of Structural Engineering*, 140 (8), A2513001, 2014

[116] CEN. EN 1991-1-1 Eurocode 1: Actions on structures - Part 1-1: General actions 2002, Brussels

[117] CEN. EN 1998-1 Eurocode 8: Design of structures for earthquake resistance-part 1: general rules, seismic actions and rules for buildings, 2005, Brussels

[118] MDRT. CR 1-1-4/2012 CR 1-1-4/2012 Cod de proiectare. Evaluarea actiunii vântului asupra constructiilor, 2012, INCERC, Bucharest (in Romanian)

[119] MDRT. CR 1-1-3/2012 CR 1-1-3/2012 Cod de proiectare. Evaluarea actiunii zapezii asupra constructiilor, 2012, INCERC, Bucharest (in Romanian)

[120] MDRAP. P100-1 P100-1/2013. Seismic Design Code. Part 1: Earthquake Resistant Design of buildings., 2013, Bucharest (in Romanian)

[121] Computers and Structures, Inc. (CSI): *SAP 2000 Advanced Structural Analysis Program, Version 12*. 2010, Berkeley, CA

[122] CEN. EN 1993-1-8 Eurocode 3: Design of steel structures - Part 1-8: Design of joints, 2011, Brussels

[123] Dinu, F, Dubina, D and Marginean, I. *Effect of connection between reinforced concrete slab and steel beams in multi-story frames subjected to different column loss scenarios*. in *4th International Conference on INTEGRITY, RELIABILITY & FAILURE*. 2013. 2013

[124] ELS, Applied Science International: *Extreme loading for structures*,3.1. 2010, Durham, NC

[125] Da Silva, LS, de Lima, LR, da SVellasco, P and de Andrade, SA, "Behaviour of flush end-plate beam-to-column joints under bending and axial force". *Steel and Composite structures*, 4 (2), 77-94, 2004

[126] Dubina, D, Dinu, F, Marginean, I and Petran, I. *Collapse prevention design criteria for moment connections in multi-story steel frames under extreme*

actions. in *4th Int. Conf. on Integrity, Reliability and Failure, Funchal, Portugal*. 2013. 23-27, 2013

[127] Khandelwal, K and El-Tawil, S, "Pushdown resistance as a measure of robustness in progressive collapse analysis"*. Engineering Structures*, 33 (9), 2653-2661, 2011

[128] Ruth, P, Marchand, KA and Williamson, EB, "Static equivalency in progressive collapse alternate path analysis: reducing conservatism while retaining structural integrity"*. Journal of Performance of Constructed Facilities*, 20 (4), 349-364, 2006

[129] Foley, CM, Barnes, K and Schneeman, C, "Quantifying and Enhancing Robustness in Steel Structures: Part 2--Floor Framing Systems"*. Engineering journal*, 45 (4), 267, 2008

[130] Dinu, F, Dubina, D and Ciutina, A. *Robustness performance of seismic resistant building frames under abnormal loads*. in *Structures & Architecture: ICSA 2010-1st International Conference on Structures & Architecture, July 21-23 July, 2010 in Guimaraes, Portugal*. 2010. CRC Press, 171, 2010

[131] Kaneko, H, Influence of strain-rate on yield ratio. Kobe Earthquake Damage to Steel Moment Connections and Suggested Improvement"*. JSSC Technical Report, 1997

[132] Jaspart, JP, "General report: session on connections"*. Journal of Constructional Steel Research*, 55 (1–3), 69-89, 2000

[133] BCSA, *Steel Buildings*. 2013.

[134] Roeder, CW, "Connection Performance for Seismic Design of Steel Moment Frames"*. Journal of Structural Engineering*, 128 (4), 517-525, 2002

[135] Dinu, F, Dubina, D, Marginean, IM and Petran, I. *Ultimate capacity of beam-to-column connections under bending and axial stresses*. in *XXIV Giornate italiane della Costruzione in Acciaio*. 2013. Torino, 2013

[136] CEN. EN ISO6892-1: 2009, Metallic materials-tensile testing-part 2009,

[137] Both, I, Mărginean, I, Neagu, C, Dinu, F, Dubina, D and Zaharia, R. *Experimental research on T-stubs under elevated temperatures*. in *Proceedings of the International Conference in Dubrovnik, 15-16 October 2015 in edition of Applications of Structural Fire Engineering*. 2015. 153-158, 2015

[138] Both, I, Mărginean, I, Neagu, C, Dinu, F, Dubina, D and Zaharia, R. *T-stubs response to extreme loading*. in *The International Colloquium on Stability and Ductility of Steel Structures*. 2016. ECCS – European Convention for Constructional Steelwork, 673-680, 2016

[139] Correlated Solutions, inc: *Vic-3D digital image correlation software,* ,7.2.4. 2016, Columbia, USA

[140] Schreier, H, Orteu, J-J and Sutton, MA, *Image correlation for shape, motion and deformation measurements*. 2009: Springer US.

[141] Dinu, F, Dubina, D, Marginean, I and Neagu, C. *Experimental tests of steel beam-to-column joints under column loss scenarios*. in *7th European Conference on Steel and Composite Structures*. 2014. 2014

[142] Dinu, F, Dubina, D, Marginean, I, Neagu, C and Petran, I, "Structural Connections of Steel Building Frames under Extreme Loading"*. Advanced Materials Research*, 1111 223-228, 2015

[143] Simonsen, M. *Strain Tensors in Vic*. 2015; Available from: www.correlatedsolutions.com/support/index.php?/Knowledgebase/Article/View/2/1/strain-tensors-in-vic.

[144] Dinu, F, Petran, I, Pastrav, M, Kovacs, A, Aschilean, D, Dubina, D and Marginean, I, CODEC Research report: research stage 2- 2013". UPT, 2013

[145] Dřevěný, Z, *Behaviour of beam-to-column joints under large vertical displacements following the loss of a column*, in *Department of Steel Structures and Structural Mechanics*. 2014, Politehnica University of Timisoara.

[146] Federal Emergency Management Agency. FEMA-350 FEMA-350 Recommended Seismic Design Criteria for New Steel Moment-Frame Buildings 2000,

[147] CEN. EN 1993-1-8 Eurocode 3: Design of steel structures - Part 1-8: General rules - Design of joints, 2005, Brussels

[148] FIDES DV-Partner *STeel CONnection 2015.355 - program for the design of bolted and welded steel connections*,2015.355. 2015, Munich, Germany

[149] ANSI/AISC. 358-10 Prequalified connections for special and intermediate steel moment frames for seismic applications, 2014, Chicago, USA

[150] Dinu, F, Mărginean, I, Dubina, D and Neagu, C. *Experimental evaluation of progressive collapse resistance of steel moment frame connections*. in *The International Colloquium on Stability and Ductility of Steel Structures*. 2016. ECCS – European Convention for Constructional Steelwork, 681-690, 2016

[151] Novotechnik, *Position Transducers Linotast, induktive Series F 200 g*, Novotechnik, Editor. 2010: Postfach, Germany.

[152] Dinu, F, Marginean, I, Dubina, D, Sigauan, A and Petran, I. *Experimental research on the behavior of steel moment frame connections under column loss scenario* in *Proceedings of the Eigth International Workshop on Connections in Steel Structures*. 2016. Boston, US, 2016

[153] Dinu, F, Marginean, I, Dubina, D, Petran, I, Pastrav, M, Sigauan, A and Ciutina, A. *Experimental testing of 3D steel frame with composite beams under column loss*. in *The International Colloquium on Stability and Ductility of Steel Structures*. 2016. ECCS – European Convention for Constructional Steelwork, 691-698, 2016

[154] Kövecsi, T, *Membrane action of slabs in framed structures in case of accidental column loss*, in *Department of Steel Structures and Structural Mechanics*. 2014, Politehnica University of Timisoara.

[155] Florea, D, Dubina, D, Petran, I, Ciutina, A and Kovecsi, T. *Numerical simulation of 3D assembly models under large deformation conditions*. in *7th European Conference on Steel and Composite Structures(EUROSTEEL 2014)*. 2014. 2014

[156] ECCS, *Recommended testing procedure for assessing the behaviour of structural steel elements under cyclic loads{ECCS, 1986 #1450}*, ed. S.S.L.T.W.G. Technical Committee 1, Seismic Design. 1986: ECCS.

[157] Hamburger, R and Whittaker, A, "Design of steel structures for blast-related progressive collapse resistance"*. Modern steel construction*, 44 (3), 45-51, 2004

[158] Kim, J and Hwang, J-S, *Effect of catenary action on collapse of steel frames*, in *EUROSTEEL 2008*. 2008: Graz, Austria.

[159] Dassault Systèmes Simulia Corp.: *Abaqus 6.14-4* 2014, Providence, RI

[160] Dinu, F, Petran, I, Pastrav, M, Kovacs, A, Aschilean, D, Dubina, D and Marginean, I, CODEC Final research report: 2012-2016". UPT, 2016

[161] Hughes, TJ, *The finite element method: linear static and dynamic finite element analysis*. 2012: Courier Corporation.

[162] Systèmes, D. *ABAQUS*. 2016; Available from: http://www.3ds.com/products-services/simulia/products/abaqus.

[163] Abdullah, R, Paton-Cole, VP and Easterling, WS, "Quasi-static analysis of composite slab"*. Malaysian Journal of Civil Engineering*, 19 (2), 91-103, 2007

[164] Meguro, K and Tagel-Din, H, "Applied element simulation of RC structures under cyclic loading"*. Journal of structural engineering*, 127 (11), 1295-1305, 2001

[165] Tagel-Din, H and Meguro, K, "Applied Element Method for simulation of nonlinear materials: theory and application for RC structures"*. Structural Eng./Earthquake Eng., JSCE*, 17 (2), 2000

[166] Meguro, K and Tagel-Din, H, "Applied element method for structural analysis: Theory and application for linear materials"*. Structural Engineering Earthquake Engineering*, 17 (1), 21s-35s, 2000

[167] Applied Science International. *Extreme Loading® for Structures Software (ELS)* 2016; Available from: http://www.extremeloading.com/.

[168] Jaini, Z and Feng, Y. *Computational modelling of damage behaviour of reinforced concrete slabs subjected to blast loading*. in *Proceeding of the 8th International Conference on Structural Dynamics, Leuven*. 2011. 2011

[169] Applied Science International, *Extreme Loading for Structures Theoretical Manual*. 2015: Durham, NC.

[170] CEN. EN 1993-1-5 Eurocode 3: Design of steel structures - Part 1-5: General rules - Plated structural elements, 2006, Brussels

[171] Arasaratnam, P, Sivakumaran, K and Tait, M, "True stress-true strain models for structural steel elements"*. ISRN Civil Engineering*, 2011, 2011

[172] Mărginean, I, Dubină, D and Dinu, F. *Numerical modelling of beam-to-column connections under column loss scenarios*. in *"Computational Civil Engineering 2015", International Symposium*. 2015. Editura Societatii Academice "Matei - Teiu Botez", 121-132, 2015

[173] Al Hallak, MI, *Response of T-stub macro components under high speed loading caused by column loss*, in *Department of Steel Structures and Structural Mechanics*. 2015, Politehnica University of Timisoara.

[174] DoD. UFC 3-340-01 Design and analysis of hardened structures to conventional weapons effects, 2002, Washington (DC)

[175] Al Hallak, MI: *Dynamic Material generator*,1.0.0. 2015, Timisoara, Romania

[176] Dinu, F, Marginean, I, Dubina, D and Petran, I. *Experimental study of seismic resistant steel frames in case of column loss*. in *Eighth International Conference on ADVANCES IN STEEL STRUCTURES*. 2015. 2015

[177] Marginean, I, Dinu, F, Dubina, D, Petran, I, Senila, M and Szilagyi, H. *Numerical modeling of dynamic response of steel moment frames following sudden column loss*. in *The International Colloquium on Stability and Ductility of Steel Structures*. 2016. ECCS – European Convention for Constructional Steelwork, 717-724, 2016

[178] BCSA, *National Structural Steelwork Specification for Building Construction 5th edition (CE Marking Version)* 2010.

[179] ECCS. *TC 10 - Structural Connections*. 2012; Available from: https://www.steelconstruct.com/site/.

ANNEX A Specific definitions

Abnormal Loads　　　or extreme loads, or accidental loads; low frequency load type or amplitude not taken into consideration in conventional design

Alternate path method　evaluation method for the ability of the structure to bridge over vertical load-bearing elements that are notionally removed one at a time at specific plan and elevation locations

Column loss　　　or notional column removal; scenario for which the column is removed from analysis, on the consideration that it has no bearing capacity

Corner column　　　column in the corner of the structure

DIC　　　　　　Digital image correlation - an optical method that employs tracking and image registration techniques for 2D and 3D accurate measurements of displacements within images

DIF$_D$　　　　　Displacement based dynamic increase factor - dimensionless number describing the amplification of static force in relation to the dynamic force such that the same displacements are obtained

DIF$_F$　　　　　Force based dynamic increase factor - dimensionless number describing the amplification of deflections caused by the application of dynamic load compared to the same displacement caused by the same load applied static

Hazard　　　　any source of potential damage, harm or adverse effects on the structural system

Internal column　　column in the interior of the structure, not in the façade

Near penultimate column interior column adjacent to a penultimate column

Penultimate column　column adjacent to the corner column

Perimeter column　　or free edge column, or façade column, or external column; is the column in the perimetral line of the structure

Free edge column　　Perimetral column adjacent to removed internal column

Progressive collapse　or disproportionate collapse, is a situation where local failure of a primary structural component leads to the collapse of adjoining members which, in turn, leads to additional collapse. Hence, the total damage is disproportionate to the original cause. [29]

*Structural redundancy*　the ability of a structural system to redistribute loads among its undamaged elements

Structural reliability   the probability that structural failure will not occur or that a specified criterion will not be exceeded

Structural resilience   the capacity to recover quickly from difficulties, to return to the original structural form/ functionality

Structural robustness the ability of a structure to withstand events like fire, explosions, impact or the consequences of human error, without being damaged to an extent disproportionate to the original cause [3]
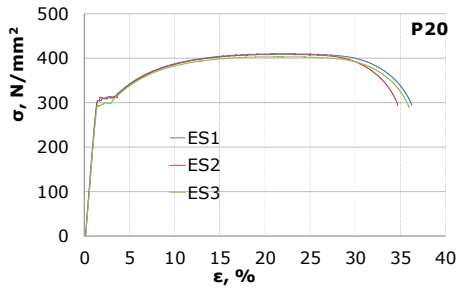
ANNEX B Engineering σ-ε curves for material
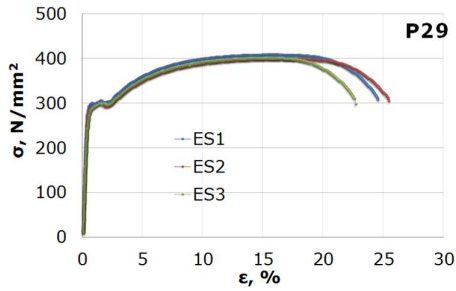
P29- Welded T-stub web, t = 15 mm
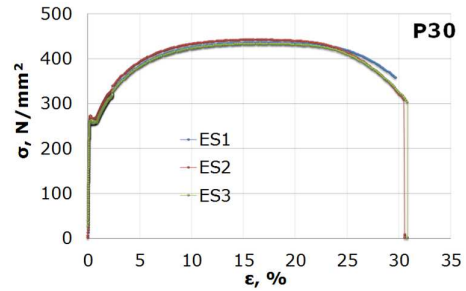
P30 - Welded T-stub end-plate, t = 25 mm

P20- bolted T-stub end-plate, t = 10 mm
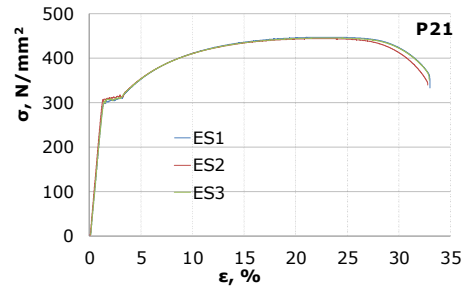
P21- bolted T-stub end-plate, t = 10 mm
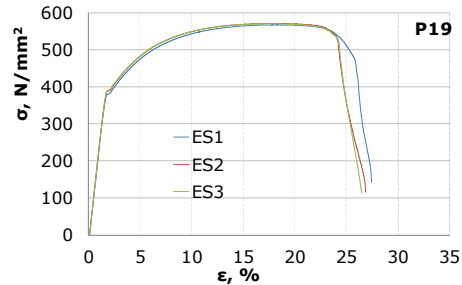
P19 - Bolted T-stub web, t = 10 mm
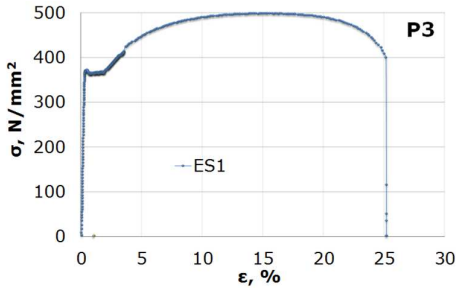
P3- Beam web IPE220, t = 5.9 mm
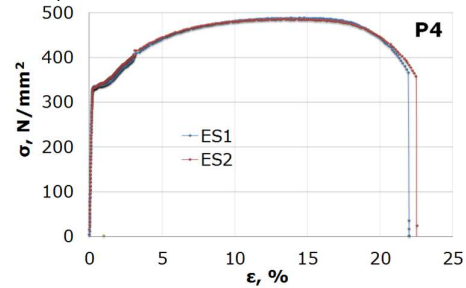
P4- Beam flange IPE220, t = 9.2 mm
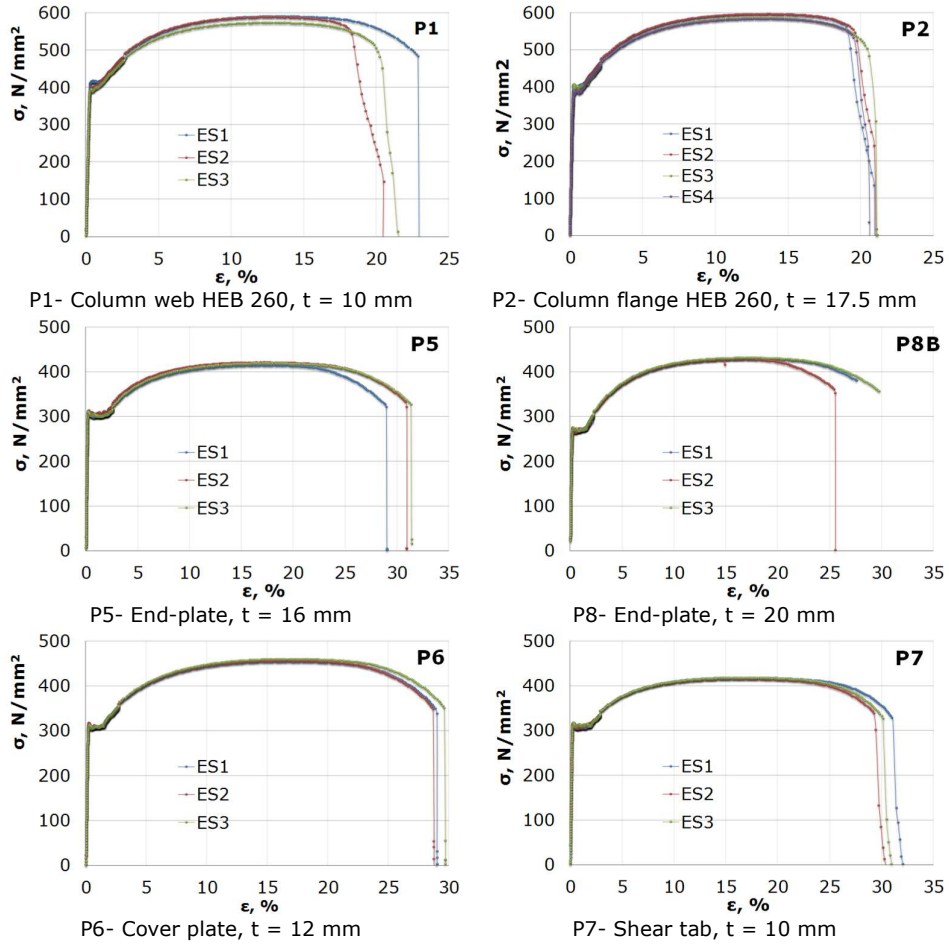
Figure B.1 Engineering stress-strain curves for coupon tests

ANNEX C Measurements of T-stubs

Table C.1 Bolted T-stubs dimensions measured before test

Specimen	Dimensions, Figure 3.29					
	t_p	b_p	L_p	c	e	m_x
T-10-16-100C	9.6	88.9	160	99.9	30.3	43.7
	9.6	89.2	160	100.5	30.5	43.6
T-10-16-100CS	9.7	89.1	160	99.8	30.5	43.8
	9.7	89.4	160	99.8	30.2	43.9
T-10-16-120C	9.7	89	180	120.3	30.5	44.4
	9.7	89.5	180	120.9	30.2	44.4
T-10-16-120CS	9.7	89.3	180	102.7	30.2	44.4
	9.7	89.3	180	102.9	30.3	44.4
T-10-16-140C	9.7	89.3	200	141.3	30.2	44.8
	9.7	89.37	200	141.9	30.2	45.9
T-10-16-140CS	9.7	89.7	200	141.7	29.4	46.1
	9.7	89.5	200	142.5	29.4	46.3
T-12-16-100C	11.8	88.6	160	101.3	29.6	44.8
	11.8	89.2	160	101.4	28.6	43.5
T-12-16-100CS	11.8	88.9	160	102.7	27.9	44.7
	11.8	89.2	160	101.5	29	44.8
T-12-16-120C	11.8	89.7	180	121.5	29.6	46.0
	11.8	89.9	180	121.0	29.5	45.8
T-12-16-120CS	11.8	88.9	180	120.9	30.2	43.5
	11.8	89.8	180	120.8	29.7	43.8
T-12-16-140C	11.8	89.4	200	139.9	30.6	45.0
	11.8	89.5	200	140.4	30.5	43.2
T-12-16-140CS	11.8	90.0	200	140.7	30.8	45.2
	11.8	89.4	200	140.4	28.7	43.4

Table C.2. Welded T-stubs dimensions measured before test

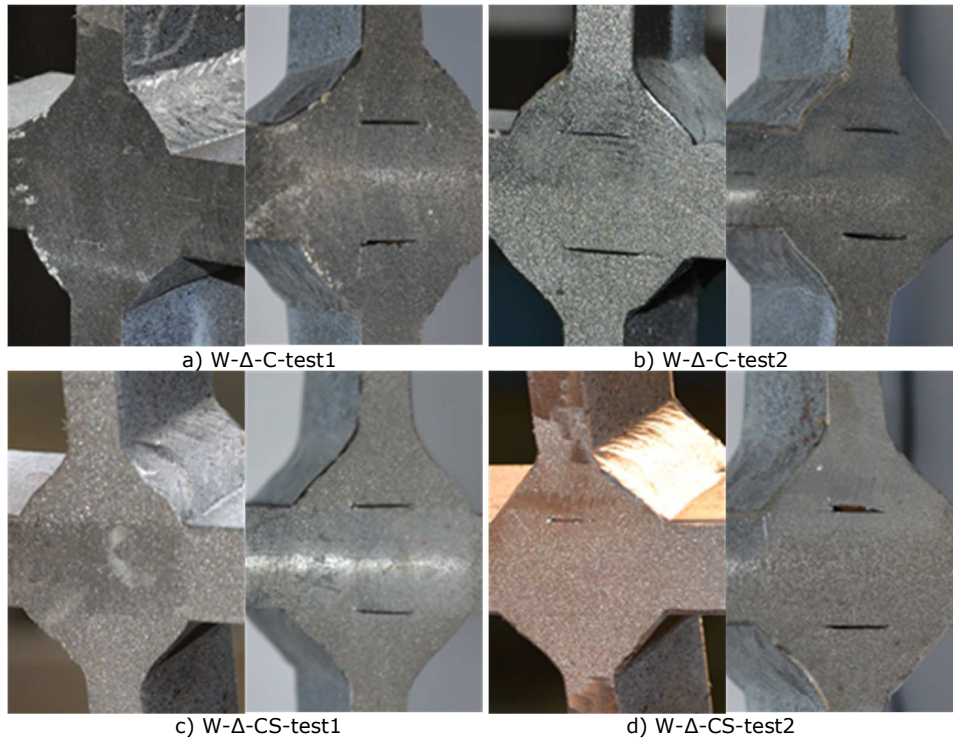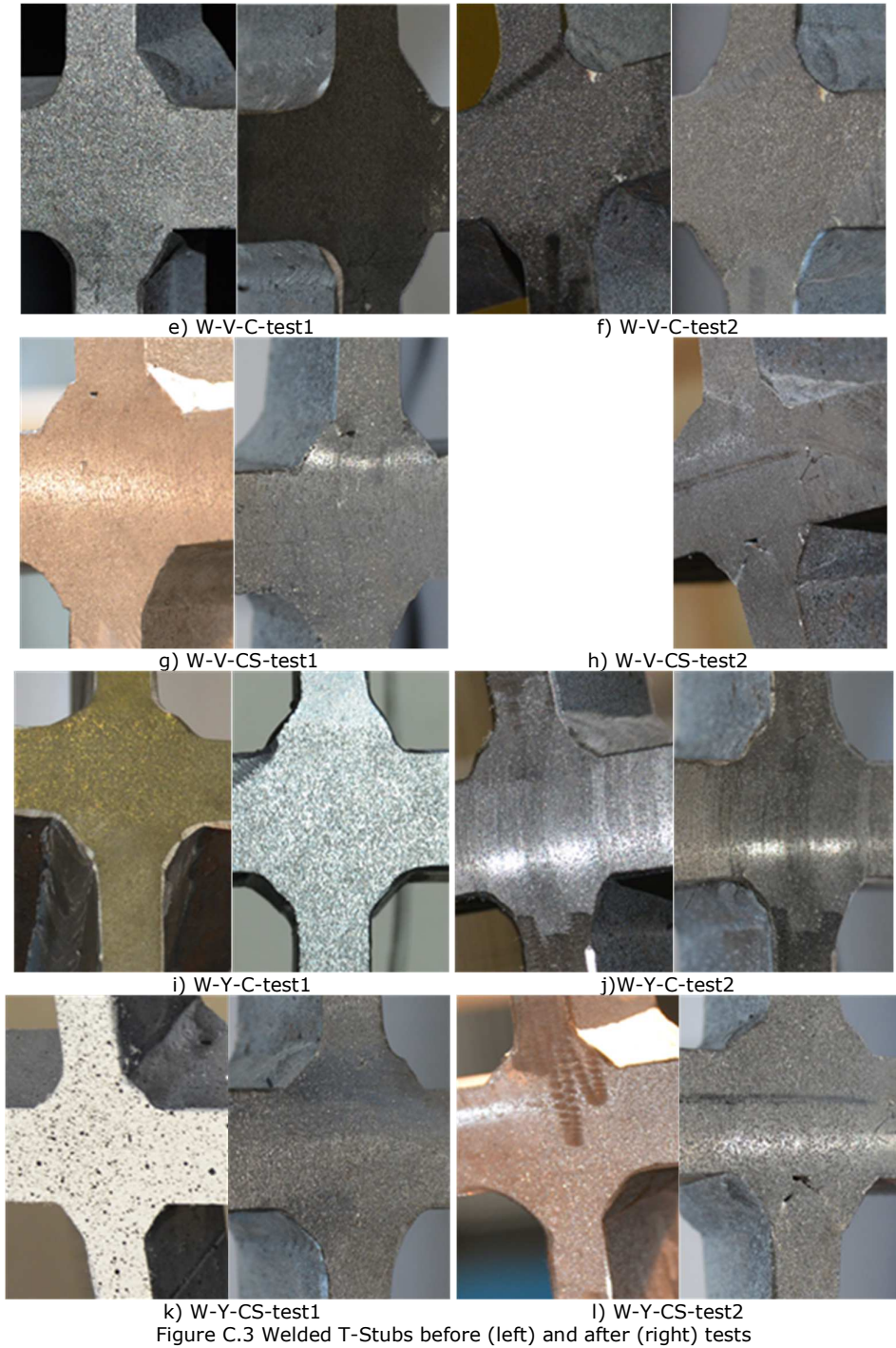| parameters	H	bt	bb	tf	tt	tb	mt	mb	L1	H1	L2	H2	L3	H3	L4	H4
W-Y-C-test1	215	60	60.1	25.5	15.5	15.8	15.1	15.7	7.47	12.48	8.53	12.15	10.31	9.17	10.93	8.45
W-Y-C-test2	217	60.78	60.83	26.07	14.78	16.25	14.52	15.66	5.58	10.41	8.36	12.24	6.56	11.06	7.46	8.09
W-Y-CS-test1	214	60	60.08	25.23	15.82	15.93	15.41	15.7	8.85	9.26	7.9	8.47	5.8	10.03	7.34	9.48
W-Y-CS-test2	217	60.76	61.42	25.31	15.79	15.21	15.28	14.76	8.53	9.51	7.7	8.76	10.93	10.62	8.11	10.19
W-Δ-C-test1	216	62.81	63.24	25.89	15.38	15.84	-	-	14.73	15.46	13.22	17.18	14.86	13.91	16.58	14.8
W-Δ-C-test2	216	61.45	61.88	25.56	15.83	16.08	-	-	15.39	16.85	13.63	16.27	17.64	14.77	17.61	15.39
W-Δ-CS-test1	216	60.21	60.56	25.14	15.94	16.46	-	-	15.17	16.31	16.14	16.34	18.11	15.38	18.09	18.69
W-Δ-CS-test2	215	60.26	60.7	25.45	15.78	15.89	-	-	18.09	17.6	16.28	15.82	15.97	15.51	19.62	15.47
W-V-C-test1	214	59.78	60.18	25.35	15	16.03	14.78	15.91	6.72	14.31	8.72	12.37	5.52	9.81	8.47	10.54
W-V-C-test2	215	60	60.49	25.12	15.85	15.84	15.55	15.69	9.07	8.62	8.88	9.71	6.4	11.29	8.25	11.14
W-V-CS-test1	210	60.23	60.12	25.35	15.27	15.91	15.09	15.74	7.72	10.21	9.83	9.2	7.87	10.14	8.18	11.66
W-V-CS-test2	216	59.53	59.69	25.12	16.01	15.96	15.56	15.67	9.89	8.31	7.33	8.11	7.19	9.2	9.36	9.81
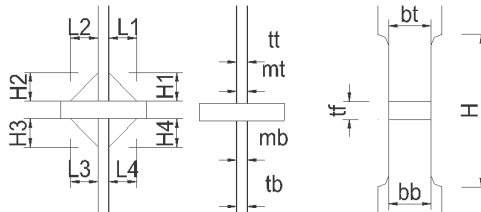
Figure C.2 Welded T-stub notations of geometrical lengths

Table C.3. Welded T-stubs dimensions measured after test

parameters	bt	bb	mt	mb	H
W-Y-C-test1	42.51	54.63	11.63	14.51	269
W-Y-C-test2	45.34	54.45	10.03	14.45	265
W-Y-CS-test1	43.88	55.04	10.16	14.81	264
W-Y-CS-test2	54.91	41.6	14.7	11.22	265
W-Δ-C-test1	53.13	46.11	12.93	10.56	273
W-Δ-C-test2	46.04	56.4	9.85	14.55	268
W-Δ-CS-test1	44.46	55.3	11.95	14.4	260
W-Δ-CS-test2	44.83	54.21	10.09	13.92	262
W-V-C-test1	45.89	56.18	10.7	14.63	262
W-V-C-test2	55.15	42.99	14.26	9.75	268
W-V-CS-test1	43.98	56.25	10.16	14.75	256
W-V-CS-test2	53.85	43.13	14.64	11.41	263

a) W-Δ-C-test1

b) W-Δ-C-test2

c) W-Δ-CS-test1

d) W-Δ-CS-test2

e) W-V-C-test1   f) W-V-C-test2

g) W-V-CS-test1   h) W-V-CS-test2

i) W-Y-C-test1   j)W-Y-C-test2

k) W-Y-CS-test1   l) W-Y-CS-test2

Figure C.3 Welded T-Stubs before (left) and after (right) tests
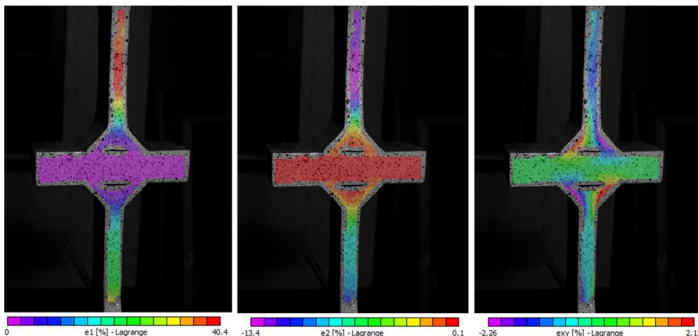
Figure C.6 W-Δ-CS-test1
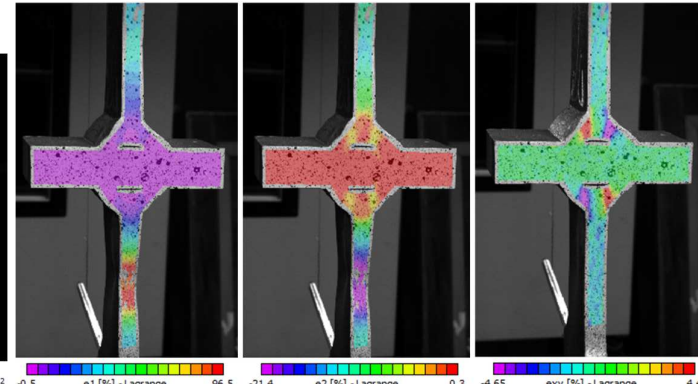
Figure C.4 W-Δ-C-test1
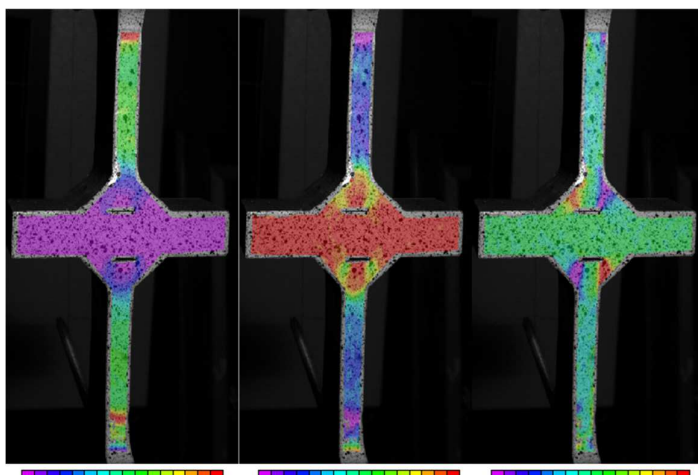
Figure C.7 W-Δ-CS-test2
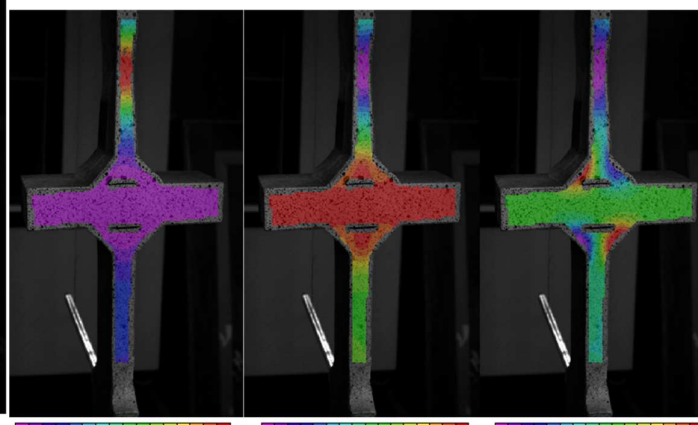
Figure C.5 W-Δ-C-test2
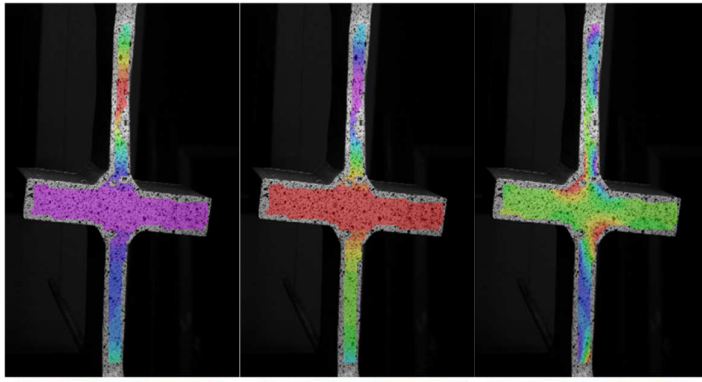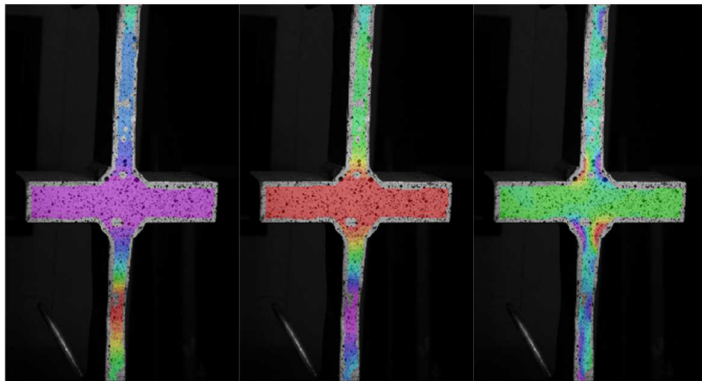
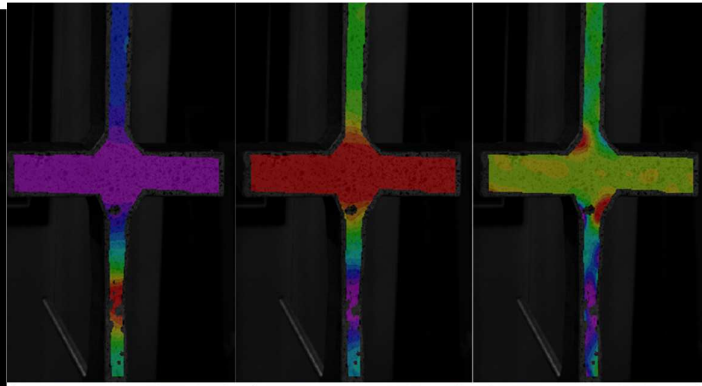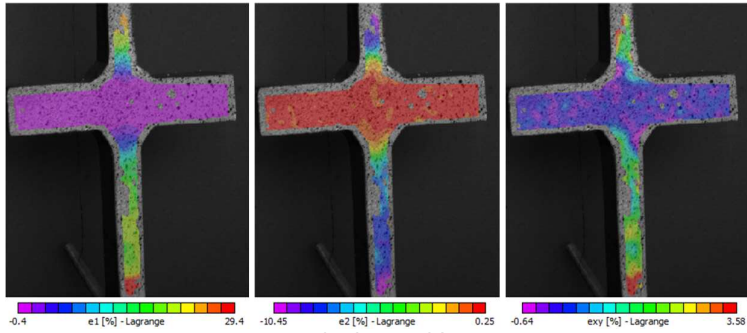Figure C.10 W-V-CS-test1
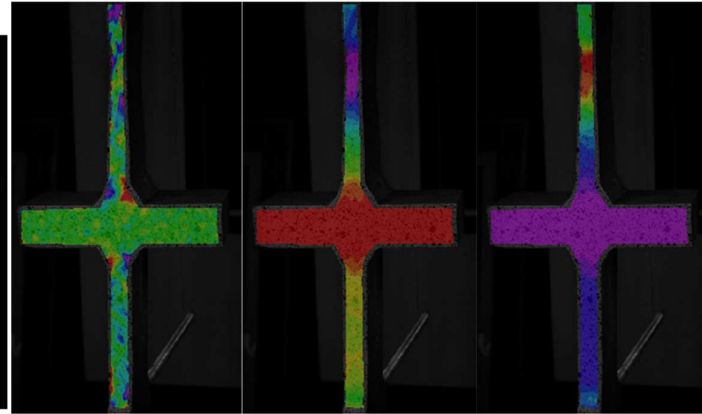
Figure C.8 W-V-C-test1

Figure C.11 W-V-CS-test2

Figure C.9 W-V-C-test2

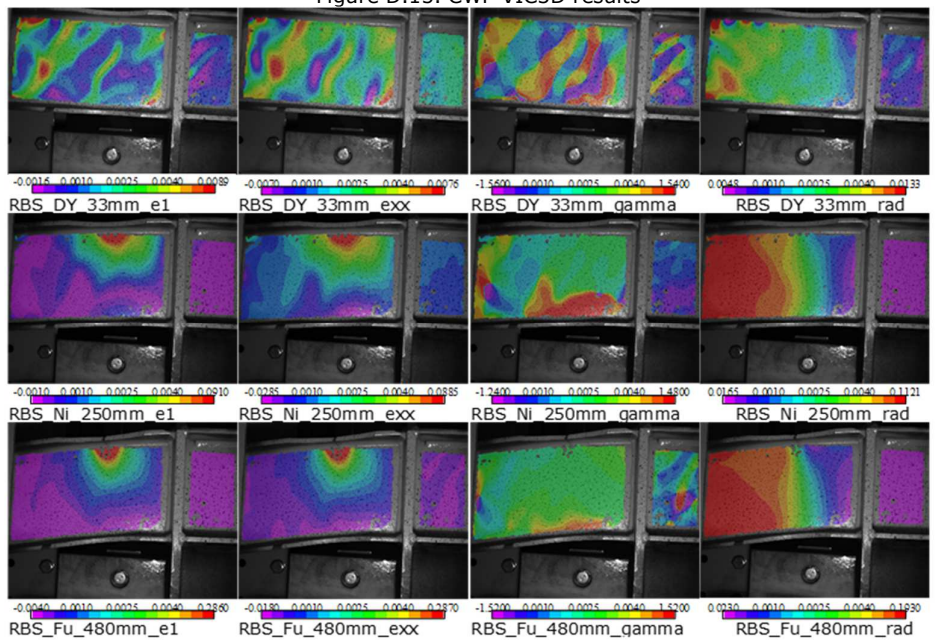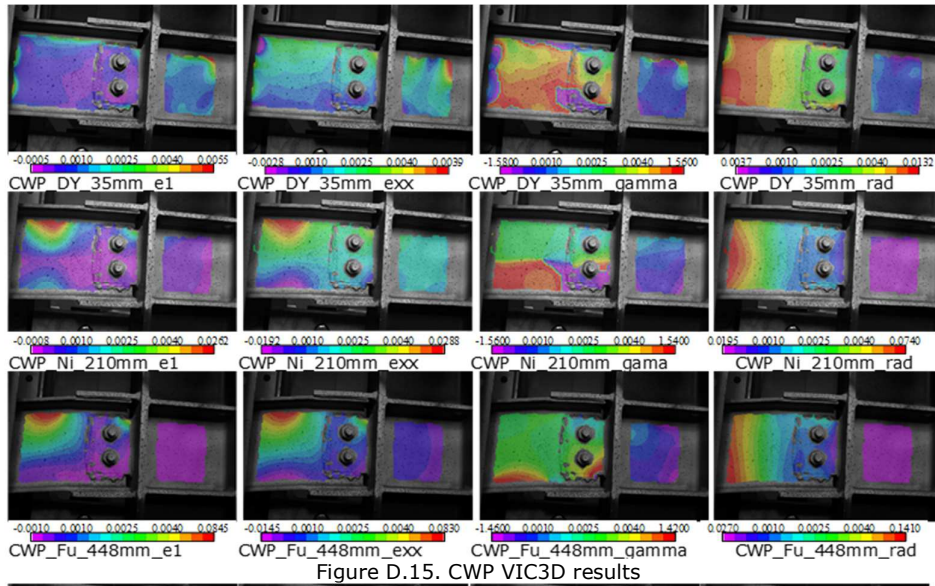Figure C.13 W-Y-CS-test1

No data available for W-Y-C-test1
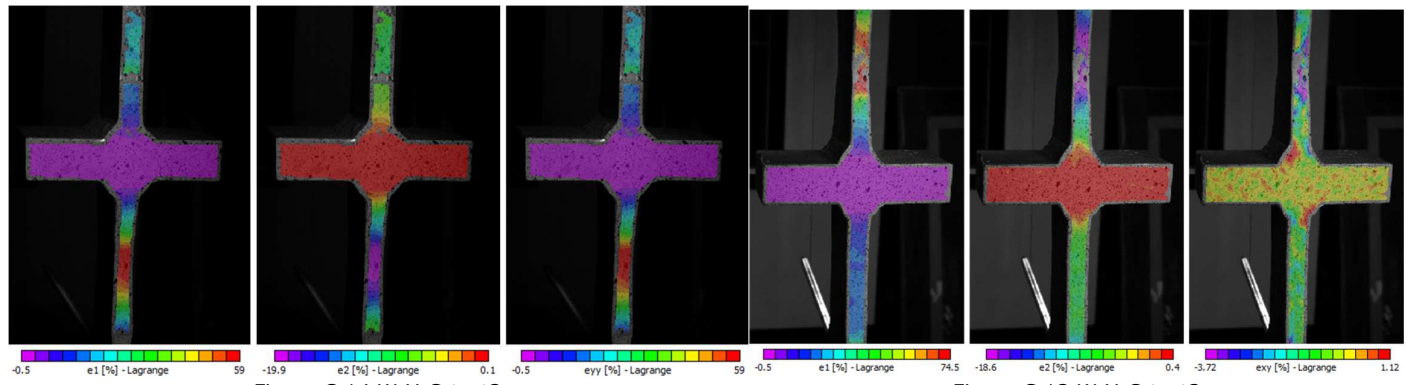
Figure C.14 W-Y-C-test2

Figure C.12 W-Y-C-test2

ANNEX D 2D assembly connection VIC results

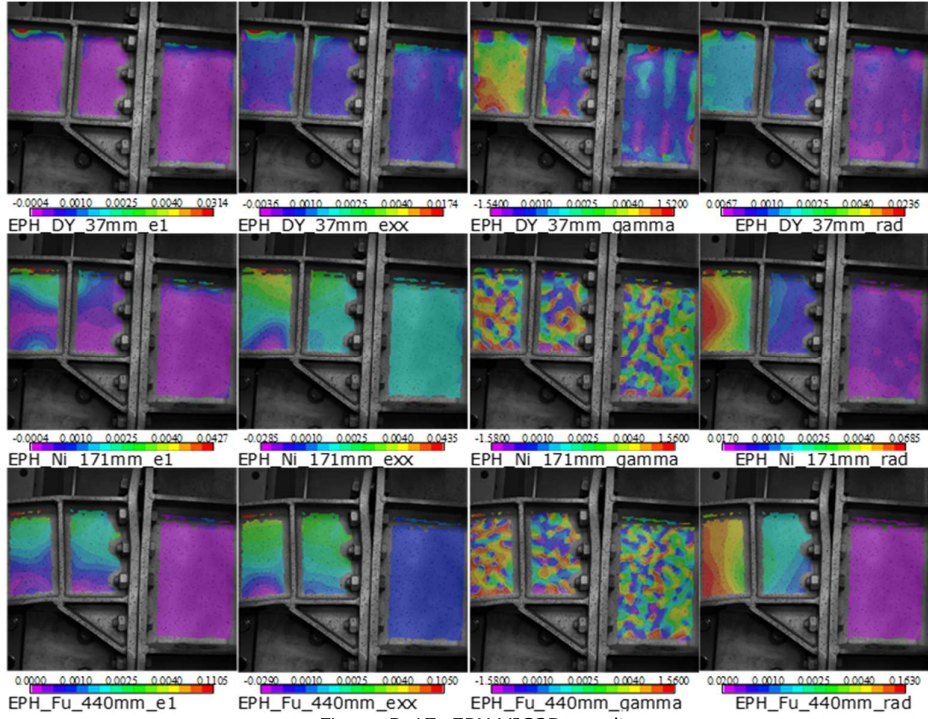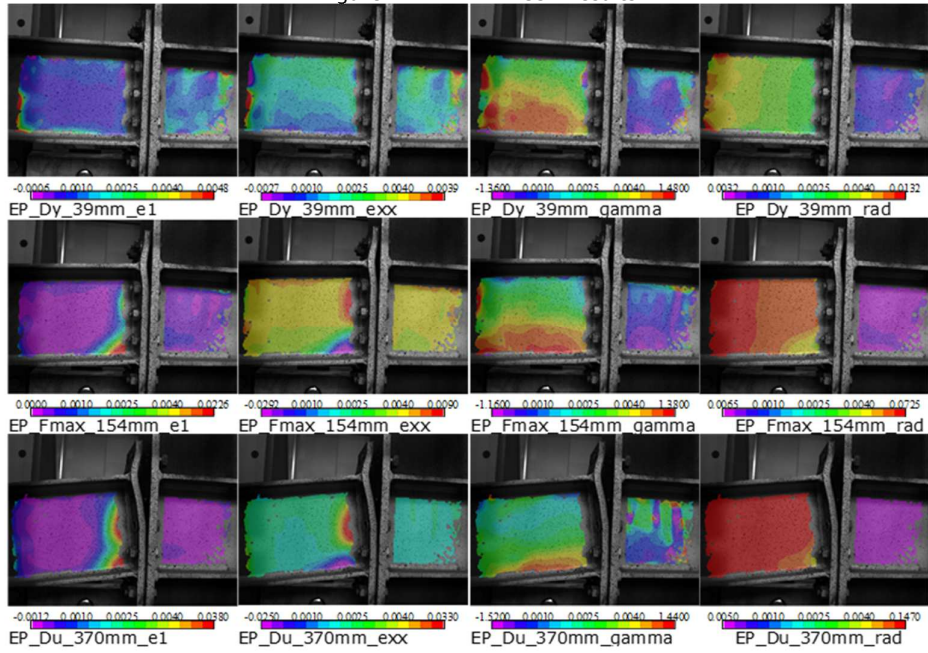Figure D.15. CWP VIC3D results

Figure D.16. RBS VIC3D results

Figure D.17. EPH VIC3D results

Figure D.18. EP VIC3D results